TECHNISCHE UNIVERSITÄT WIEN
Vienna University of Technology

D I S S E R T A T I O N

Supercritical Carbon Dioxide -

Advanced Applications

in Flow Chemistry and Biomass Valorization

ausgeführt zum Zwecke der Erlangung des akademischen Grades eines

Doktors der technischen Wissenschaften unter der Leitung von

Univ.Prof.[in] **Dipl.-Ing.**[in] **Dr.**[in] **techn. Katharina Schröder**

und Mitbetreuung von

Assoc. Prof. Dipl.-Ing. Dr. techn. Michael Schnürch

eingereicht an der Technischen Universität Wien

Fakultät für Technische Chemie

Institut für Angewandte Synthesechemie (E163)

von

Dipl.-Ing. Philipp Mikšovsky

Matrikelnummer: e01128996

Wien, am 8. Jänner 2024

Table of Contents

Danksagung

Zuallererst möchte ich mich bei Prof. Katharina Schröder bedanken, für die Möglichkeit diese Dissertation in ihrer Forschungsgruppe durchführen zu dürfen. Vielen Dank für all die hilfreichen Gespräche, Tipps, Hinweise während den Seminaren und in persönlichen Gesprächen sowie die Ermöglichung der Teilnahme an nationalen und internationalen Konferenzen. Vielen Dank!

Mein Dank gilt ebenso Prof. Michael Schnürch für die Mitbetreuung dieser Arbeit. Vielen Dank für Deine Betreuung und Inputs aller Art während den Seminaren sowie in persönlichen Gesprächen!

Weiters möchte ich mich bei allen Gutachtern dieser Dissertation bedanken, für Ihre Zeit zur Erstellung der Gutachten sowie ihre Verfügbarkeit als Prüfer und Prüferin beim Rigorosum.

Vielen Dank an meine Kooperationspartner und Kollegen, Prof. Heidi Halbwirth, Prof. Thomas Konegger, Prof. Dominik Eder, Dr. Christoph Kornpointner, Katharina Rauchenwald und Dr. Shaghayegh Naghdi für die gelungene Zusammenarbeit und die daraus resultierenden Publikationen.

An dieser Stelle möchte ich mich ebenso bei allen Laborkollegen, Fabian, Lisa, Aitor, Kristof, Julia, Adam, Alina, Michi, Dario, Bletë, Jasmina, Prasad, Connie, Thomas, Flo und Apurba bedanken. Vielen Dank für all das Erlebte innerhalb und außerhalb des Labors, für all die Hilfen, Tipps und Tricks, Gespräche, etc. die wir während dieser Zeit untereinander austauschen konnten und die uns gegenseitig weitergebracht haben und die jedenfalls zu einer sehr guten Atmosphäre und zu einem effektiven und angenehmen Arbeitsklima beigetragen haben!

Vielen Dank auch an all meine Studenten, die ich während meiner Zeit als Dissertant betreuen durfte und auch als Betreuer von euch lernen durfte. Es war mir eine Ehre mit euch zusammenarbeiten zu dürfen. Danke für euren Beitrag, Isi, Elias, Zahra, Maria, Flo, Elma und Julia! Viel Erfolg euch weiterhin!

Vielen Dank ebenso an Irena, UFlo, Walter, Martin, Andrea, Emylia, Simone, Isolde, Thomas, Sabine, Dagmar, Danko, Niklas, Andreas, Johannes, Manuel und viele viele mehr für euren Beitrag zu Fragen und Problemlösungen technischer Natur, finanzieller Natur, chemischer Natur und administrativer Natur sowie für den möglichst reibungsfreien Ablauf am Institut.

Danke an dieser Stelle an das gesamte Institut für angewandte Synthesechemie sowie deren Forschungsgruppen für all die gewinnbringenden Begegnungen, Gespräche und vieles mehr.

An letzter Stelle möchte ich mich bei meiner Familie sowie bei Freunden und all jenen bedanken, die ich noch nicht in dieser Danksagung erwähnt habe, die aber trotzdem meinen Dank verdienen:

VIELEN HERZLICHEN DANK !!!

Abstract

This dissertation deals with the application of carbon dioxide in its supercritical state. Initially, it was used for the enzyme-assisted extraction of flavonoids from apple pomace. Furthermore, the unique and opposite properties of supercritical carbon dioxide and ionic liquids were combined to use these two neoteric solvents in catalysis. Thus, supercritical carbon dioxide was applied to the batch-wise and continuous production of bio-based cyclic carbonates using supported ionic liquid phases (SILPs) as heterogeneous catalysts.

At first, an enzyme-assisted supercritical carbon dioxide extraction of flavonoid aglycones from apple pomace was developed. The commercially available enzyme mix snailase was employed for the hydrolysis of the flavonoid glycosides to enable a facilitated subsequent supercritical fluid extraction of the aglycones, with apolar carbon dioxide and a minimum amount of polar cosolvent. Ultimately, a scalable simultaneous process was developed, showing high activity of snailase, even under pressurized conditions with wet and dry apple pomace.

To expand the application of supercritical carbon dioxide to catalysis, a continuous-flow method for the production of bio-based cyclic limonene carbonates, starting from limonene oxides and supercritical carbon dioxide as reagent and sole solvent, was investigated, employing ionic liquids as catalysts. For continuous flow, ionic liquids were physisorbed on silica as commonly used support. After elaborate optimization in short-term experiments, the catalyst's long-term stability was investigated for 48 h.

Furthermore, silicon oxycarbides were investigated as alternative supports to silica for SILPs. Silicon oxycarbides and silicon oxycarbide-based SILPs were analyzed *via* infrared spectroscopy, thermogravimetric analysis, nitrogen adsorption, microscopy, X-ray photoelectron spectroscopy, and solvent adsorption. The application of silicon oxycarbide-based SILPs under batch-wise conditions resulted in higher selectivities and yields for the production of limonene and linseed oil-derived cyclic carbonates. Ultimately, macroporous monolithic silicon oxycarbide-based SILPs were successfully applied to the continuous production of limonene carbonate.

Kurzfassung

Diese Dissertation beschäftigt sich mit der Anwendung von Kohlenstoffdioxid im überkritischen Zustand. Zunächst wurde es für die enzymunterstützte Extraktion von Flavonoiden aus Apfeltrester verwendet. Des Weiteren wurden die einzigartigen und gegensätzlichen Eigenschaften von superkritischem Kohlenstoffdioxid und ionischen Flüssigkeiten kombiniert, um diese zwei modernen Lösungsmittel in der Katalyse zu verwenden. Demzufolge wurde superkritisches Kohlenstoffdioxid für die chargenweise und kontinuierliche Herstellung von biobasierten cyclischen Carbonaten unter Verwendung von immobilisierten ionischen Flüssigphasen (SILPs) als heterogene Katalysatoren angewendet.

Zuallererst wurde die enzymunterstützte überkritische Kohlenstoffdioxidextraktion von Flavonoidaglykonen aus Apfeltrester untersucht. Dabei wurde die kommerziell erhältliche Enzymmischung Snailase zur Hydrolyse der Flavonoidglykoside eingesetzt, um anschließend eine erleichterte überkritische Fluidextraktion der Aglykone mit unpolarem Kohlenstoffdioxid und einer geringen Menge an polarem Co-Lösungsmittel zu ermöglichen. Abschließend wurde ein skalierbarer simultaner Prozess entwickelt, der eine hohe Aktivität von Snailase selbst unter Druckbedingungen mit feuchtem und trockenem Apfeltrester aufwies.

Um die Anwendung von superkritischem Kohlenstoffdioxid auf den Bereich der Katalyse auszuweiten, wurde eine kontinuierliche Flussmethode zur Herstellung von biobasierten cyclischen Limonencarbonaten aus Limonenoxiden und überkritischem Kohlenstoffdioxid als Reagenz und alleinigem Lösungsmittel untersucht, wobei ionische Flüssigkeiten als Katalysatoren eingesetzt wurden. Für den kontinuierlichen Fluss wurden die ionischen Flüssigkeiten auf Silica, einem häufig verwendeten Trägermaterial, physisorbiert. Nach umfassender Optimierung in Kurzzeitversuchen wurde die Langzeitstabilität des Katalysators für einen Zeitraum von 48 Stunden untersucht.

Des Weiteren wurden Siliciumoxycarbide als alternative Trägermaterialien zu Silica für SILPs untersucht. Siliciumoxycarbide und Siliciumoxycarbid-basierte SILPs wurden mittels Infrarotspektroskopie, thermogravimetrischer Analyse, Stickstoffadsorption, Mikroskopie, Röntgenphotoelektronenspektroskopie und Lösungsmitteladsorption analysiert. Die Anwendung von Siliciumoxycarbid-basierten SILPs unter chargenweisen Bedingungen führte zu erhöhten Selektivitäten und Ausbeuten bei der Herstellung von cyclischen Carbonaten, die von Limonen und Leinsamenöl stammen. Schließlich wurden makroporöse monolithische Siliciumoxycarbid-basierte SILPs erfolgreich für die kontinuierliche Produktion von Limonencarbonat eingesetzt.

A   List of Abbreviations

[C_2mim]Br	1-ethyl-3-methyl imidazolium bromide
[C_2mim]Cl	1-ethyl-3-methyl imidazolium chloride
[C_2mim]I	1-ethyl-3-methyl imidazolium iodide
[C_2mim]X	1-ethyl-3-methyl imidazolium halide
[C_2mim]NTf$_2$	1-ethyl-3-methyl imidazolium bistriflimide
[C_4mim]NTf$_2$	1-butyl-3-methyl imidazolium bistriflimide
[C_4tma]NTf$_2$	butyltrimethylammonium bistriflimide
[C_{18}tma]NTf$_2$	octadecyltrimethylammonium bistriflimide
C_4-SiO$_2$	silica modified with butyl chains
BET	Brunauer–Emmett–Teller (surface area)
BJH	Barret–Joyner– Halenda (pore size distribution)
CALB	*Candida antarctica* lipase B
CDCl$_3$	deuterated chloroform
CE	capillary electrophoresis
DRIFTS	diffuse reflectance infrared Fourier transform spectroscopy
DVB	divinylbenzene
EA-SFE	enzyme-assisted supercritical fluid extraction
ee	enantiomeric excess
ESI	electrospray ionization
EtOAc	ethyl acetate
EtOH	ethanol
FEG-SEM	field emission gun – scanning electron microscopy
FRP-SiO$_2$	fluorous reverse phase silica
FTIR	Fourier transform infrared spectroscopy
GC	gas chromatography
GC/MS	gas chromatography / mass spectrometry
HPLC	high-performance liquid chromatography
ICP-OES	inductively coupled plasma optical emission spectrometry
IL	ionic liquid
IUPAC	international union of pure and applied chemistry
J	coupling constant (NMR)
LP	light petroleum (boiling point 40 - 60 °C)
MeOH	methanol
NMR	nuclear magnetic resonance (spectroscopy)
p_c	critical pressure

PDC	polymer-derived ceramic
PIL	polymerized ionic liquid
poly-SILP	polymerized supported ionic liquid phase
pH	quantity of hydrogen
ppm	parts per million
PSO	polysiloxane
PTFE	polytetrafluorethylene (teflon)
qTOF-MS	quadrupole time of flight – mass spectrometry
rpm	revolutions per minute
$scCO_2$	supercritical carbon dioxide
SCF	supercritical fluid
SFE	supercritical fluid extraction
SILP	supported ionic liquid phase
SiO_2	silica
SiOC	silicon oxycarbide
TBAB	tetrabutylammonium bromide
TBAC	tetrabutylammonium chloride
TBAI	tetrabutylammonium iodide
TBAX	tetrabutylammonium halide
t-BuOH	*tert*-butanol
T_c	critical temperature
TGA	thermogravimetric analysis
UHPLC	ultra-high-performance liquid chromatography
UV	ultraviolet
VBC	4-vinylbenzyl chloride
wt%	weight percent
δ	chemical shift (NMR)

B   Introduction

B.1   Supercritical Fluids

B.1.1   Definition of Supercritical Fluids

"A supercritical fluid is a compound, mixture, or element
above its critical pressure (p_c) and critical temperature (T_c)
but below the pressure required to condense it into a solid." [1]

Philip G. Jessop and Walter Leitner state this definition for supercritical fluids (SCFs) being a slight modification of the definition from IUPAC:

"Supercritical fluid: The defined state of a compound, mixture, or element above its critical pressure
(p_c) and critical temperature (T_c).[2]

The fact that a supercritical fluid can also be transformed again to its solid state by further increasing the pressure is often ignored, since required pressures are usually high but not impractically as shown in **Scheme 1**.
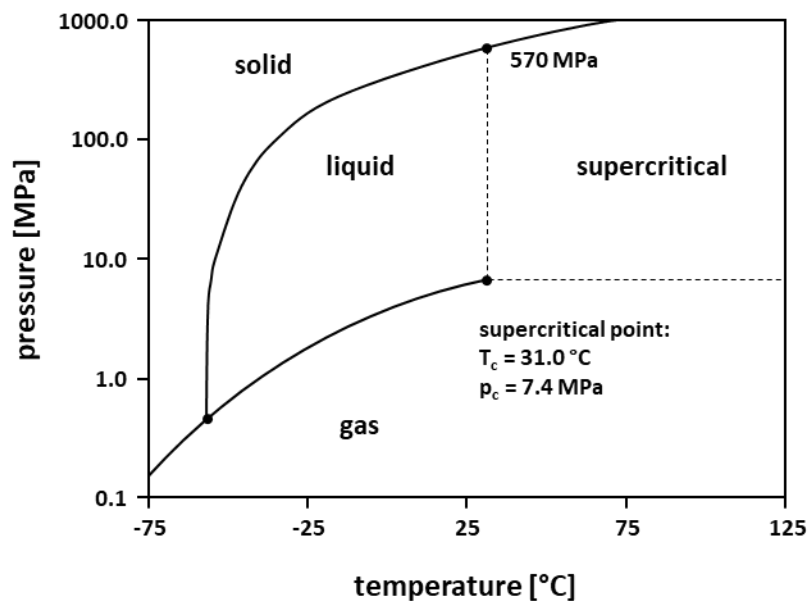
Scheme 1: Phase diagram of carbon dioxide.

8

B.1.2 Properties of Supercritical Fluids

Critical pressures and temperatures are substance-specific parameters, and the values for selected compounds and elements are listed in **Table 1**. Furthermore, some additional properties that must be considered regarding the feasibility of a process are shown. Wirth regard to organic reactions and biomass extractions with supercritical fluids, it is worth mentioning that if the supercritical state can only be reached at temperatures where organic matter starts to decompose due to limited thermal stability, this particular supercritical fluid can be considered as not suitable.

Table 1: Critical pressures and temperatures of selected compounds and elements. Modified from reference[3, 4].

compound / element	name	T_c [°C]	p_c [MPa]	other properties
C_2H_4	ethene	9.3	5.0	highly flammable
Xe	xenon	16.6	5.8	expensive
$\underline{CO_2}$	carbon dioxide	31.0	7.4	low polarity
C_2H_6	ethane	32.2	4.9	highly flammable
N_2O	dinitrogen monoxide	36.5	7.2	oxidizing
C_3H_8	propane	96.7	4.3	highly flammable
NH_3	ammonia	132.5	11.3	toxic, corrosive
C_4H_{10}	*n*-butane	152.0	3.8	highly flammable
C_5H_{12}	*n*-pentane	196.6	3.4	highly flammable, high T_c
C_3H_7OH	1-propanol	235.2	4.8	highly flammable, high T_c
CH_3OH	methanol	239.5	8.1	highly flammable, high T_c
C_2H_5OH	ethanol	242.9	6.4	highly flammable, high T_c
C_6H_6	benzene	289.5	4.9	toxic, high T_c
C_7H_8	toluene	318.6	4.2	highly flammable, high T_c
H_2O	water	374.2	22.1	corrosive, high T_c

Above these critical pressure and temperature, the phase separation between the liquid and gaseous phase disappears, resulting in unique properties. For example, supercritical fluids feature densities between 0.1-1 g/cm^3, which can be tuned by adjusting the pressure and temperature, making them more "gas-like" or "liquid-like" regarding their solvation power, as shown in **Scheme 2** for carbon dioxide. From there, it is visible that higher pressures lead to higher densities and, thus, greater solubilities. In contrast, higher temperatures lead to a decrease in density. However, the solubility of compounds is not only dependent on the density of the supercritical fluid (decreases with temperature) but also on the vapor pressure of the solute (increases with temperature). Thus, a crossover pressure exists.

Below this pressure, the solubility decreases with temperature since density is decreasing with temperature. On the other hand, above the crossover pressure, the solubility increases due to a higher volatility of the solute. Furthermore, below the critical temperature of carbon dioxide, the density changes are negligible. Thus, tunability of the density and further the solubility is only possible in the supercritical state.
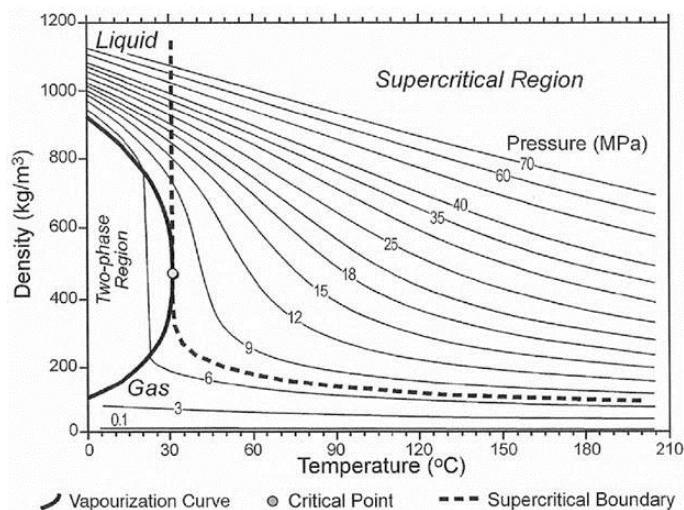
Scheme 2: Influence of pressure and temperature on the density of supercritical carbon dioxide.[5]

Apart from the tunability of densities ($0.1 - 1$ g/cm^3), supercritical fluids also possess lower viscosities ($10^{-4} - 10^{-5}$ Pa·s) and, thus, higher diffusivities (10^{-3} cm^2/s) and no surface tension, compared with the liquid state, which is beneficial in terms of mass transfer. These unique properties (**Table 2**)[6] make supercritical fluids perfectly suitable for many applications, as shown in the next chapter.

Table 2: Typical physicochemical parameters of liquids, supercritical fluids, and gases. Modified from reference [6].

parameter	liquid	supercritical	gas
density [g/cm^3]	1	0.1 - 1	10^{-3}
viscosity [Pa·s]	10^{-3}	10^{-4} - 10^{-5}	10^{-5}
diffusivity [cm^2/s]	10^{-5}	10^{-3}	10^{-1}
surface tension [dyn/cm]	20 - 50	0	0

B.1.3 Historical and Current Applications of Supercritical Fluids

An early and very well-known application of supercritical fluids in industry is the synthesis of ammonia (T_c: 132.5 °C, p_c: 11.3 MPa). However, this process might not be considered a typical application of supercritical fluids, at first, because the employed temperatures (400-530 °C) are much higher than the supercritical one.[1] The process (**Scheme 3**), developed by Fritz Haber and Carl Bosch,[7] is based on Henry Le Chatelier's patent and was further commercialized by BASF in 1913.[8]

$$N_2 \ + \ 3\,H_2 \quad \xrightarrow[\substack{10\ -\ 35\ MPa \\ 400\ -\ 530\ °C}]{\text{Fe - catalyst}} \quad 2\,NH_3$$
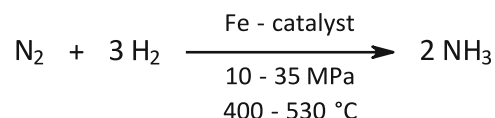
Scheme 3: Haber-Bosch synthesis of ammonia commercialized by BASF in 1913.

Today, the Haber-Bosch process can be considered one of the most energy-demanding and carbon dioxide-emitting processes since natural gas (50%), oil (31%), or coal (19%) are used for the production of hydrogen. Thereof, the methane-based processes showing the highest energy efficiency and lower carbon emissions. In these processes, methane is converted via steam reforming to carbon monoxide and hydrogen followed by a water-gas shift reaction to transform carbon monoxide and water into carbon dioxide and hydrogen.[9] Nowadays, much effort is put into the investigation of alternatives to the Haber-Bosch process, such as the electrochemical synthesis of ammonia.[10]

Apart from this historical example of the use of supercritical fluids, today, they are commonly applied for various extraction processes,[11] which will be discussed in the following chapters in more detail. Further applications of supercritical fluids are summarized in **Table 3**.

Table 3: Applications of supercritical fluids.

application	supercritical fluid	reference
supercritical drying of food	$scCO_2$ + EtOH	[12]
supercritical cleaning	$scCO_2$	[13]
impregantion of biocides into wood	$scCO_2$ + MeOH	[14]
impregnation of dyes in textiles	$scCO_2$ + H_2O/acetone/DMSO etc.	[15]
supercritical chromatography (e.g., natural products, pharmaceuticals, forensics, bioanalysis)	$scCO_2$ + MeOH/EtOH etc.	[16]
polymer synthesis	$scCO_2$ + H_2O/EtOH	[17]
synthesis of nanostructured materials	$scCO_2$, scH_2O, scC_6H_{14}, scC_3H_7OH etc.	[18]
supercritical fluid extractions	$scCO_2$ + MeOH/EtOH	see chapter B.2

Supercritical fluids are employed in supercritical drying, supercritical cleaning, and impregnation of biocides into wood or dyes in textiles, and in the field of supercritical chromatography, e.g., for natural products, pharmaceuticals, forensics or bioanalysis. Moreover, supercritical fluids are employed in the synthesis of polymers or nanostructured materials.

Carbon dioxide is by far the most used supercritical fluid due to its relatively low and, for this reason, technically easily reachable critical temperature (T_c: 31.0 °C) and critical pressure (p_c: 7.4 MPa)[19] (**Scheme 1**). Furthermore, carbon dioxide is considered a non-toxic, non-flammable, and inexpensive chemical, available from industrial processes, such as the synthesis of ammonia[9], as discussed before, or the production of cement.[20] Moreover, carbon dioxide is a relatively inert chemical, which is beneficial for many applications, such as extractions or chromatography. On the other hand, highly active catalysts have to be developed in case carbon dioxide needs to be incorporated into a chemical compound.

In this thesis, supercritical carbon dioxide was used for enzyme-assisted supercritical fluid extractions and was also used as solvent and reagent to form cyclic carbonates, in batch mode and continuous flow, using supported ionic liquids as heterogeneous catalysts.
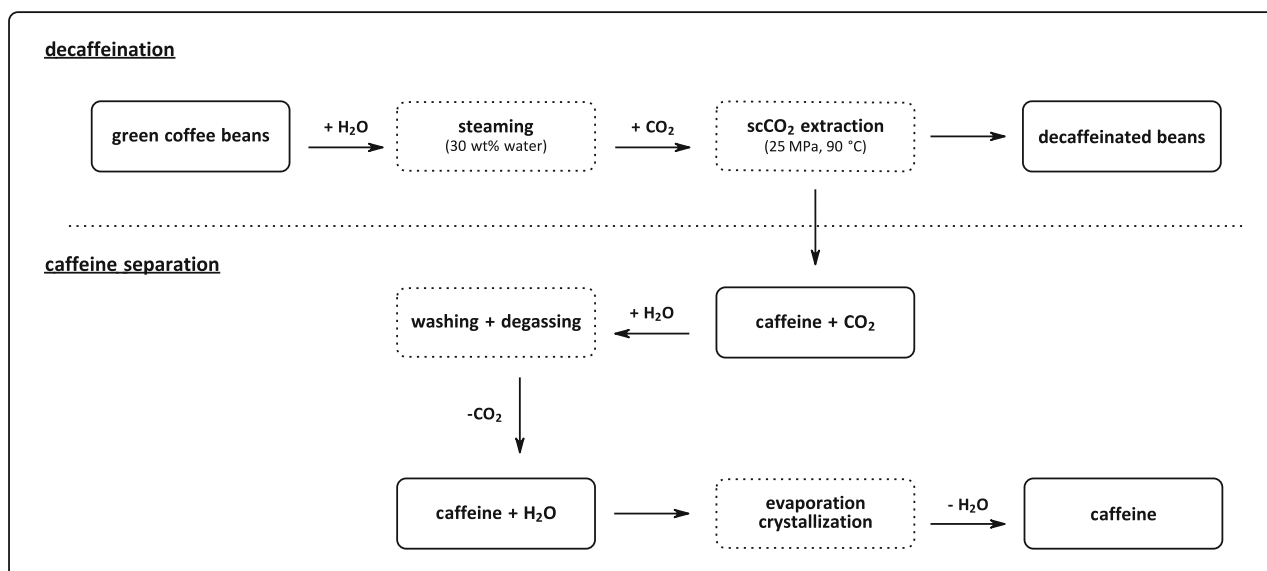
B.2 Supercritical Fluid Extractions

B.2.1 Supercritical Fluid Extractions on an Industrial Scale

The most famous supercritical fluid extraction on an industrial scale is the decaffeination of coffee with the aid of supercritical carbon dioxide. In 1974, the recovery of caffeine from green coffee beans was patented by Kurt Zosel.[21] The actual application for the decaffeination of green coffee beans was specified in a patent in 1981 again by Kurt Zosel.[22]

However, the first extraction of caffeine on an industrial scale was already implemented by Hag in Germany and was later transferred to General Foods in the United States.[1] Dichloromethane was employed in this process due to satisfactory extraction efficiency. Health risks, especially the carcinogenicity of dichloromethane, led to the use of ethyl acetate as a less hazardous alternative to dichloromethane. Nevertheless, ethyl acetate brought its own drawbacks into the process: the high flammability and the flavor-changing fruity aroma, typical for many esters.[23]

Another alternative was brought up by the Swiss Water Process,[24] where water as a sustainable and nonhazardous solvent was employed for decaffeination. However, in this process, water has to be enriched with all water-soluble solids found in green coffee except caffeine since water is not selective for the extraction of caffeine and would result in a change of flavor of the decaffeinated coffee.[23]

With the development of the decaffeination process using supercritical carbon dioxide, an alternative solvent was found that was nontoxic, nonflammable, selective, and, thus, did not affect the taste and quality of coffee.[23]

Scheme 4: Overview of the decaffeination process using supercritical carbon dioxide as extractant. Modified from reference [23].

As shown in **Scheme 4**, the extraction process starts from green, unroasted coffee beans, which get swollen in water. Thus, extraction of caffeine with supercritical carbon dioxide is facilitated by enhanced mass transfer. The carbon dioxide which is enriched with caffeine during the extraction exits the extractor for further processing. After washing the caffeine/carbon dioxide mixture with water, caffeine is mostly dissolved in water due to its better solubility in water, thus the caffeine-free carbon dioxide is released and, subsequently, recycled. After concentration of the extract *via* evaporation, caffeine can be crystallized and employed in the beverage industry or as an active pharmaceutical ingredient.

Apart from coffee, tea is also decaffeinated using supercritical carbon dioxide, starting from tea leaves.[25] Other applications of supercritical fluid extractions in food industry are the extraction of bittering agents from hops[26] and the extraction of nutraceuticals, flavors, and essential oils from different sources, such as spices or herbs.[27, 28] Moreover, supercritical fluid extraction is commonly used in the pharmaceutical industry for the extraction of various bioactive compounds with antioxidant, antiviral, antibacterial or anti-inflammatory properties. This part will be discussed in the following chapter, where a selection of examples is provided (**Table 4**).

Furthermore, supercritical fluid extraction is commonly used in the oil industry, specifically in deasphalting processes. The most famous process in this regard is the so-called ROSE process (Residuum Oil Supercritical Extraction). Many modifications of the ROSE process exist which differ in feedstock and used solvent.[29] Depending on the process, solvents containing $C_3 - C_6$ are employed near their supercritical conditions to separate the heavy fraction of the petroleum feedstock into deasphalted oil, asphalt, and resins. Separation of metal-containing, highly viscous asphalt and resins from the rest of the oil is crucial for ideal transport properties, suppression of equipment corrosion, and low levels of catalyst coking in subsequent processes. Thus, the deasphalted oil is a perfect feedstock, for example, for hydrocracking, lube oil blending or catalytic cracking.[30]

B.2.2   Supercritical Fluid Extraction of Bioactive Compounds

The extraction of bioactive compounds from various natural sources has gained a lot of interest in the past years since these compounds feature several desirable properties, such as antimicrobial, antibacterial, antiviral, antifungal, antioxidant, anti-inflammatory and antitumor.[31] For this reason, supercritical fluid extraction is applied in food industry and pharmaceutical industry.[32] Furthermore, different bioactive compounds, such as alkaloids, terpenoids, fatty acids, or phenolics, are of primary interest due to their polarity and featured properties.[11] A selection of bioactive compounds obtained *via* supercritical fluid extraction is presented in **Table 4**.

Table 3 gives an overview of the range carbon dioxide applications. Carbon dioxide is the most used supercritical fluid applied for extractions due to the aforementioned advantages of low toxicity and low critical temperature, amongst others. The fact that the used solvent features no or low toxicity is of high interest. For conventional extraction, remaining toxic solvent traces can be problematic when the extracted products are applied as food additives, in cosmetics, or as pharmaceutical ingredients. However, the final purification of desired products would be challenging. In the case of supercritical carbon dioxide, it is entirely removed by simple pressure expansion, and no further purification of the product is required. Furthermore, separated carbon dioxide can be recycled easily, which is especially important for applications on an industrial scale.

Moreover, the low critical temperature of 31.0 °C of carbon dioxide is crucial since it allows extractions at relatively low temperatures of 40-60 °C, thus preventing decomposition and loss of bioactivity during the extraction process. Furthermore, usually relatively high pressures are applied because density and, thus, solubility increases with higher pressures and leads to improved extraction yields.

The drawback of applying carbon dioxide as supercritical fluid for extraction is mainly its low polarity. For this reason, the extraction of polar compounds, such as phenolics, can be rather challenging with pure supercritical carbon dioxide. To circumvent this problem, small amounts of polar solvents,[34] typically alcohols or water, are usually added to enable and enhance the extraction of polar compounds.

Another issue that has to be considered is that these compounds are often contained in a matrix and, therefore, are not always easily accessible and extractable. The extraction can be facilitated by addition of enzymes during the extraction process, which will be discussed in the following chapter.

Table 4: Examples of supercritical fluid extractions of bioactive compounds from plant materials. Modified from references [11, 31].

| source	compound class	solvent	temperature [°C]	pressure [MPa]	bioactivity	reference
spearmint leaves	flavonoids	CO_2 + 17% EtOH	60	20	antioxidant	[33]
blackberries	flavonoids	CO_2 + 5-10% EtOH/water	40 - 60	15 - 25	antioxidant	[34]
seabuckthorn leaves	flavonoids	CO_2 + 20% EtOH	50	20	anti-inflammatory	[35]
haskap berries	flavonoids, terpenes, lipids	CO_2 + 1-50 v% EtOH	50	30	antioxidative, antimicrobial	[36]
chinaberries	fatty acids	CO_2 + 30% EtOH	50	30	antiviral	[37]
pink shrimp residues	fatty acids, terpenes	CO_2	60	30	anti-obesity, hypolipidemic	[38]
black pepper	terpenes	CO_2	40	30	antioxidant	[39]
Eupatorium intermedium flower	terpenes, polyphenols	CO_2 / C_3H_8 (subcritical)	30 - 80 / 20 - 60	15 - 25 / 3 - 100	antibacterial, antioxidant	[40]
black sage leaves	terpenes	CO_2	50	30	antitumor	[41]
sage leaves	terpenes	CO_2	40	10 - 30	anti-inflammatory	[42]
industrial hemp	cannabinoids	CO_2 pretreatment: [C_2mim][OAc] or [Ch][OAc] in H_2O (1:3)	70	20	anti-inflammatory, anti-epileptic, anticonvulsive	[43]
pepper elder leaves	alkaloids	CO_2 + 5% EtOH or MeOH	40 - 60	15 - 25	antifungal	[44]
periwinkle	alkaloids	CO_2 + 2-10% EtOH	40 - 60	30	anticancer	[45]

B.2.3 Enzyme-Assisted Extraction Techniques for Bioactive Compounds

As shown before, many bioactive compounds are located in plants and more specifically in their cells which are surrounded by cell walls to impart stability and protect against mechanical and osmotic stress.[46] The cell walls consist of robust networks of lignin, pectin, cellulose, and hemicelluloses amongst others. Furthermore, some bioactive compounds such as phenolics are bound via hydrogen bonds. The robustness of the cell wall and the additional interactions of the desired bioactive compounds with the matrix making it challenging to extract them and, thus, leading to low extraction efficiency.[47]
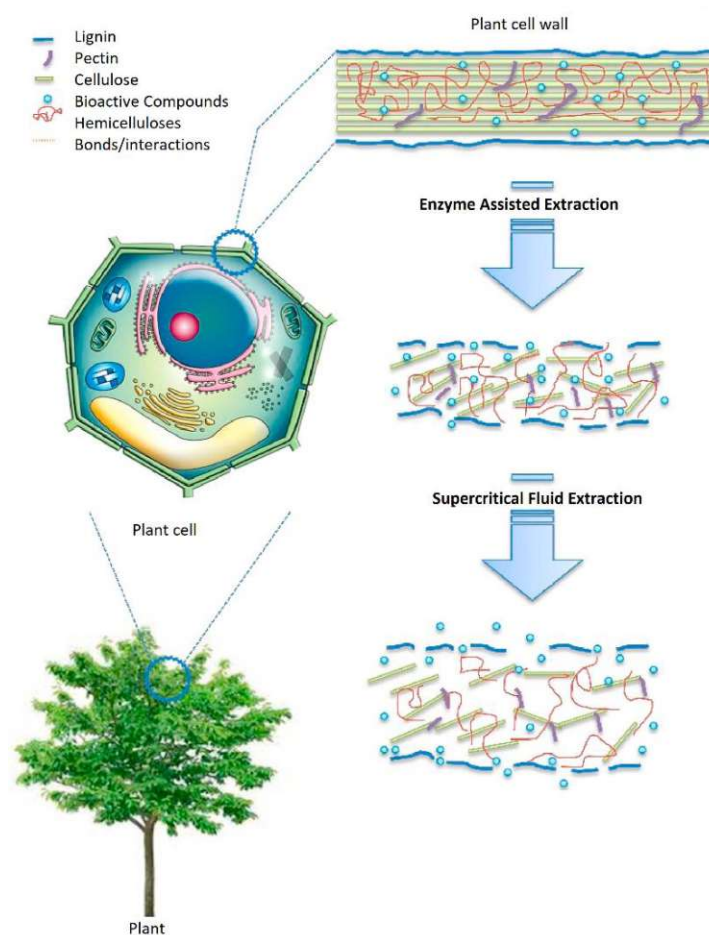

Scheme 5: Schematic representation of bioactive compounds located in the plant cell wall and released *via* enzyme-assisted supercritical fluid extraction. Modified from reference [47].

In a first step of the extraction process, the raw material is typically dried and ground to provide a high surface area and to ensure an optimal diffusion and mass transport of supercritical fluid through the matrix. A promising approach to further ensure this is the use of hydrolytic enzymes to distort and deform the cell walls and, thereby, to enhance and enable the release of bioactive compounds by cleaving the bonds between them and the matrix (**Scheme 5**). Thus, combining the enzyme-assisted extraction with supercritical fluid extraction has the added benefit of the facilitated release of bioactive compounds. Enzymatic hydrolysis and supercritical fluid extraction can either be performed separately or simultaneously (**Scheme 6**). Whether a simultaneous process is possible, mostly depends on the kind of enzyme, the water content, the employed cosolvent and the operating temperature and pressure for supercritical fluid extraction, since the structure of enzymes can significantly change and differ under such extreme conditions.[47, 48]
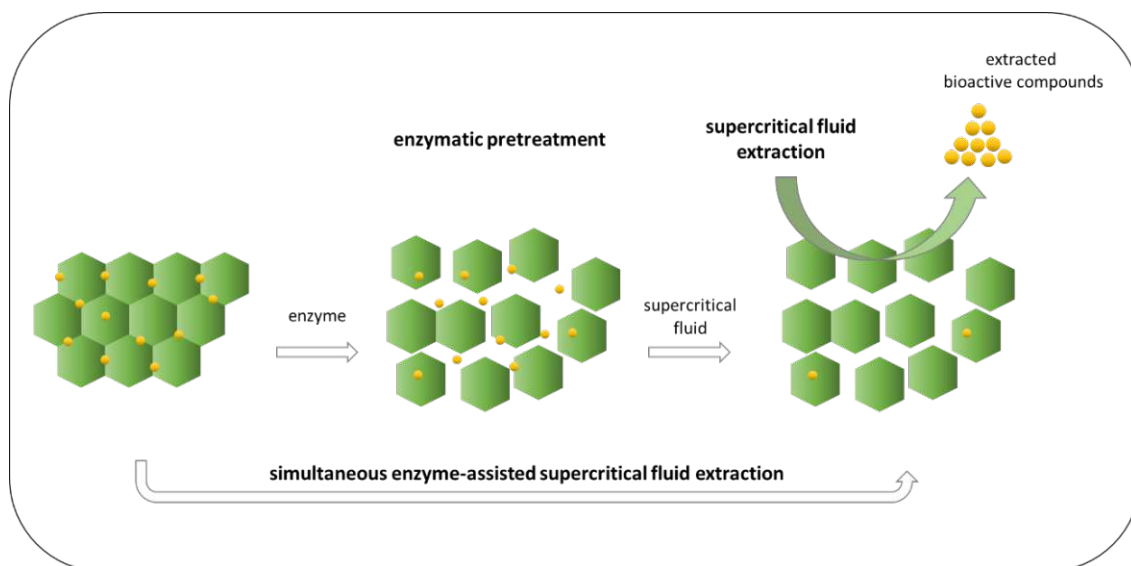
Scheme 6: Subsequent and simultaneous enzyme-assisted supercritical fluid extraction process.

 Apart from enzymes, also ionic liquids were found to be highly suitable for the dissolution of biomass. In this regard, ionic liquids with basic and hydrogen bond acceptor properties were found to dissolve for example cellulose, one of the most abundant biopolymers on earth. Thus, the extraction efficiency is increased compared to the extraction with conventional solvents as shown in **Scheme 7**.[49, 50]
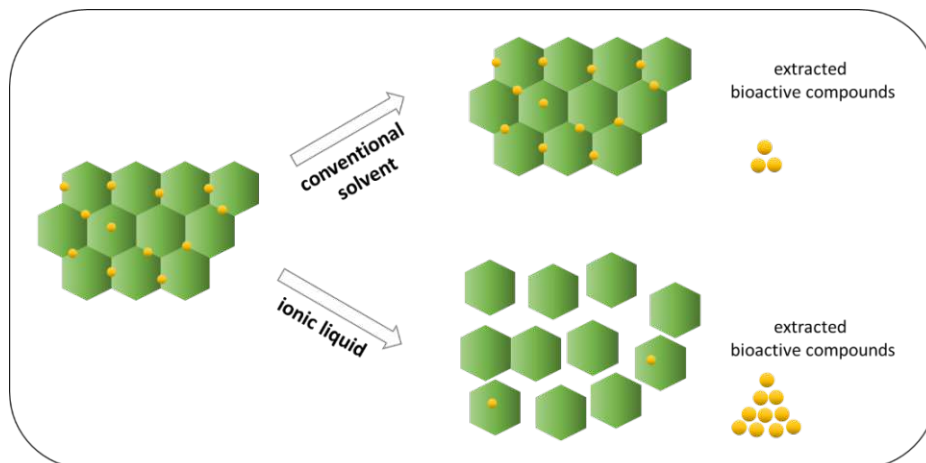
Scheme 7: Comparison of conventional extraction and ionic liquid-based extraction of bioactive compounds from biomass. Modified from reference [50].

In this thesis, the enzyme-assisted extraction approach was combined with the benefits of supercritical carbon dioxide extraction for the extraction of flavonoids from apple pomace. Although the field of enzyme-assisted supercritical fluid extraction is a relatively new one, some examples already exist in literature and are partly covered in a review by Patil *et al*.[47] from 2021. A summary of reviewed and recently published examples is given in **Table 5**.

Nevertheless, supercritical carbon dioxide was also combined with ionic liquids and employed as catalysts for the continuous production of bio-based cyclic carbonates; results are discussed in a separate chapter.

Table 5: Reported enzyme-assisted supercritical fluid extractions.

entry	source	compound class	enzyme	supercritical fluid extraction			process type	ref
				solvent	T [°C]	p [MPa]		
1	blackcurrant pomace	fatty acids, tocopherols, polyphenols	Viscozyme	CO_2	60	45	1. SFE 2. enzymatic treatment of residue	[51]
2	sea buckthorn	tocopherols, sugar acids, phenolics, triterpenes	Viscozyme CeluStar	CO_2	20	10	1. SFE 2. enzymatic treatment of residue	[52]
3	black tea leftover	polyphenols	Kemzyme, Alcalase, Viscozyme, Pektinex, acid cellulase	CO_2 + 9% EtOH	45	30	1. enzymatic treatment 2. SFE	[53]
4	alfalfa leaves	flavonoids, phenolic acids	Kemzyme	CO_2 + 16% EtOH	68	21	1. enzymatic treatment 2. SFE	[54]
5	alfalfa leaves	flavonoids, phenolic acids	Kemzyme	CO_2 + 19% EtOH	50	22	1. enzymatic treatment 2. SFE	[55]
6	pomegranate peel	phenolic acids	acid cellulase, Kemzyme, Pectinex, Alcalase	CO_2 + 9% EtOH	55	30	1. enzymatic treatment 2. SFE	[56]
7	guarana seeds	phenolics, alkaloids	Celluclast, Pectinex	CO_2 + 50% EtOH	50	10	1. enzymatic treatment 2. SFE	[57]
8	tomato peels	pigment lycopene	Celluclast, Novozyme, Viscozyme	CO_2	86	50	1. enzymatic treatment 2. SFE	[58]
9	blue bean plant seeds	phytosterols, tocopherols, fatty acids	alcalase, pectinase	CO_2	40	30	1. enzymatic treatment 2. SFE	[59]
10	prickly pear cactus	flavonoids	Rapidase maxi fruit	CO_2 + 20% EtOH	60	10	simultaneous	[60]
11	black pepper	essential oil	α-amylase	CO_2	60	30	simultaneous	[61]
12	cardamon	essential oil	α-amylase	CO_2	50	20	simultaneous	[62]

As shown in **Table 5**, different plant and waste materials have already been employed for enzyme-assisted supercritical fluid extraction, such as leaves, peels, seeds, hulls, spicery, leftovers, and pomace. Depending on the biomass and the chosen conditions, different compound classes, such as fatty acids, alkaloids, essential oils, terpenes, but also more polar compounds, such as flavonoids or other phenolics, can be extracted. In the case of the extraction of more polar compounds, ethanol was the cosolvent of choice to increase the polarity of apolar carbon dioxide.

In the first examples (**Table 5,** entries 1-2), supercritical fluid extraction was performed with pure carbon dioxide to extract apolar compounds, such as fatty acids and tocopherols. In a separate step, the residue was treated with pressurized ethanol or directly employed in enzymatic extraction to extract more polar compounds. However, in the majority of the examples the biomass is treated with enzymes prior to supercritical fluid extraction to release the bioactive compounds by digestion of the plant tissue (**Table 5,** entries 3-9). Nevertheless, three examples of simultaneous enzymatic treatment and supercritical fluid extraction are also reported (**Table 5,** entry 10-12). In these cases, the enzyme is applied under supercritical conditions, and a static extraction for a particular amount of time is followed by a dynamic extraction with supercritical fluid and optionally cosolvent.

Extraction temperatures are generally in the lower range (20-86 °C) due to the thermal sensitivity of bioactive compounds. Furthermore, the density of supercritical carbon dioxide and, thus, the solubility decreases at higher temperatures (**Scheme 2**). However, density can be increased with pressure; for this reason, enzyme-assisted extractions of bioactive compounds are performed usually at pressures between 10-50 MPa.
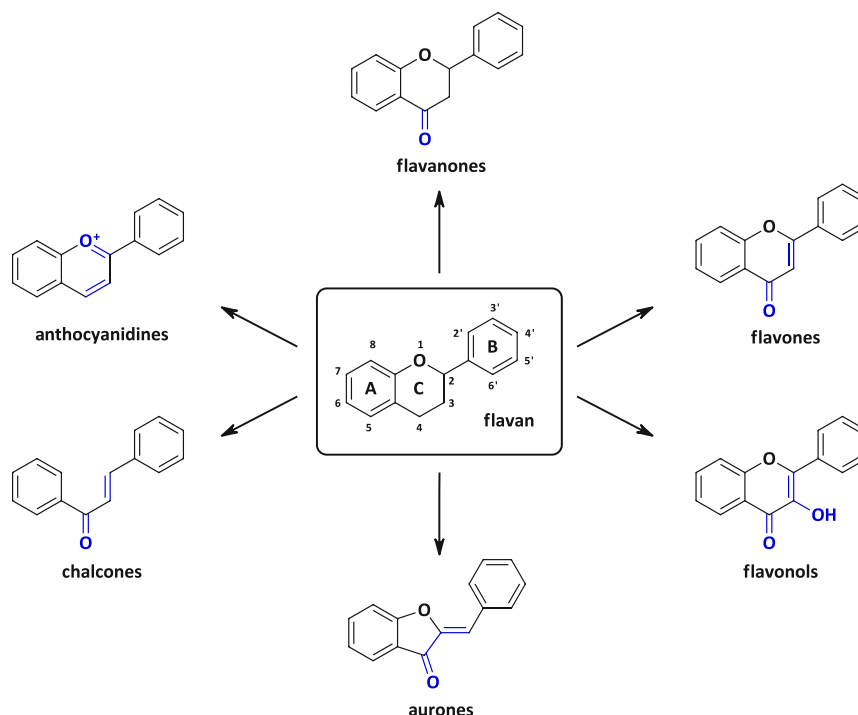
**Scheme 8: Chosen flavonoid subgroups based on flavan's skeletal structure.**

One important group of bioactive compounds are flavonoids, which were also extracted in the first project of this thesis. Flavonoids were discovered in 1930 by Albert Szent-Györgyi[63] and were proposed to be named "vitamin P" at first.

Today, more than 8000 different flavonoids are described.[64] They are characterized by a skeletal structure, the flavan, consisting of three connected rings (A, B, C). They are further divided into subclasses dependent on the position of hydroxyl groups, carbonyl groups, and double bonds, as well as if the C-ring is closed or if the flavonoid is present in its open-chained form, which is dependent on the biosynthetic pathway.[65, 66] A selection of flavonoid subclasses is illustrated in **Scheme 8**.

Furthermore, most of the flavonoids in nature are present in their water soluble glycosylated form,[67] which makes them ideal candidates for enzyme-assisted extraction. The polarity of flavonoid aglycones is lower, rendering them even more attractive for extraction with apolar carbon dioxide.

B.3 Combination of Ionic Liquids and Supercritical Carbon Dioxide

As shown before, ionic liquids can be employed for the distortion and deformation of biomass (**Scheme 7**) and therefore used to enhance the release of bioactive compounds further extracted with supercritical carbon dioxide. These two neoteric solvents were further combined in catalytic processes due to their fundamentally different properties as shown in **Scheme 9**.
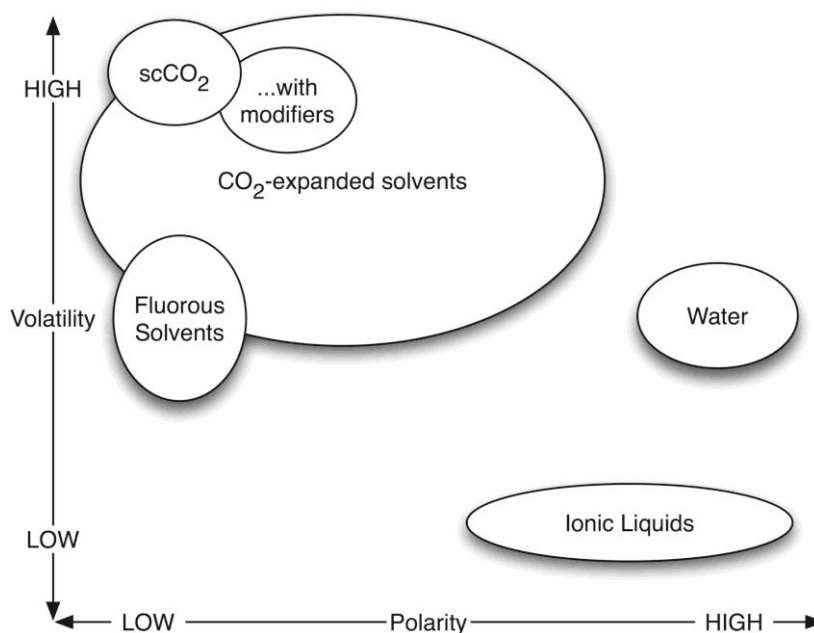

Scheme 9: Volatility and polarity of different solvent classes.[68]

On the one hand, supercritical carbon dioxide is highly volatile and apolar. The polarity can be further increased by the addition of polar cosolvents, the modifiers, such as ethanol or methanol, being crucial for extractions. On the other hand, ionic liquids have very low vapor pressures and show a much lower polarity. These differences and the resulting solubility properties, described in chapter B.3.3, making them ideal candidates for their combined application in catalysis. For this reason, a short introduction to ionic liquids is given in the following before their use in catalytic processes is described.

B.3.1 Ionic Liquids and their Applications

Ionic liquids are salts with glass-transition temperatures or melting points below 100 °C. They were first described in literature in 1888 by Gabriel, who discovered ethanolammonium nitrate with a melting point of 52-55 °C.[69, 70] In 1914, Walden described ethylammonium nitrate with a melting point of 12 °C, the most famous earliest example of a room temperature ionic liquid.[71]

Ionic liquids consist of specially shaped and bulky cations or bulky anions, which contribute to their low melting points due to the low lattice energy, which has to be overcome to transfer the compound to its liquid state. Furthermore, ionic liquids are often considered as sustainable solvents due to their very low vapor pressures (e.g., 1-butyl-3-methyl imidazolium bistriflimide [C_4mim]NTf$_2$: 1.2 Pa at 120 °C)[72] compared to commonly used organic solvents (e.g., acetone: 25 kPa at 20 °C)[73] and their non-flammability under ambient conditions. They also possess electric conductivity, a broad liquid range, are primarily hydrophilic, and are known to be a highly tunable substance class in terms of their acidity, basicity, melting point, hygroscopic properties, and miscibility, enabled by the combination of different anions and cations.[74, 75] Commonly used cations and anions are shown in **Scheme 10**.
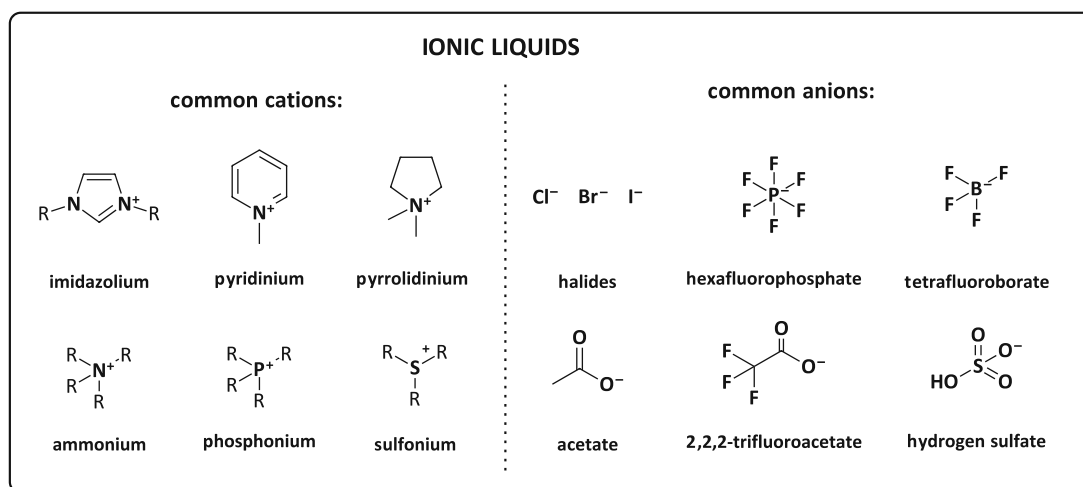
Scheme 10: Common cations and anions used in ionic liquids.

Furthermore, ionic liquids are easy to prepare *via* protonation of the cation or *via* quaternization with a haloalkane. An anion exchange can follow *via* treatment with a Lewis acid or a metathesis reaction.[76] Different synthesis pathways, such as classical conventional heating and microwave irradiation, ultrasound irradiation, or simultaneous ultrasound and microwave irradiation, are described in literature.[75] Nowadays, many ionic liquids are commercially available in large quantities, which renders them also attractive for industrial applications.[77] One of the most famous industrial applications of ionic liquids is the BASIL process[78] (**Scheme 11**), established in 2002 by BASF. It is employed for the intermediate synthesis of diethoxy phenylphosphine starting from dichlorophenylphosphine and ethanol and further converted to photoinitiators used in coatings and printing inks.
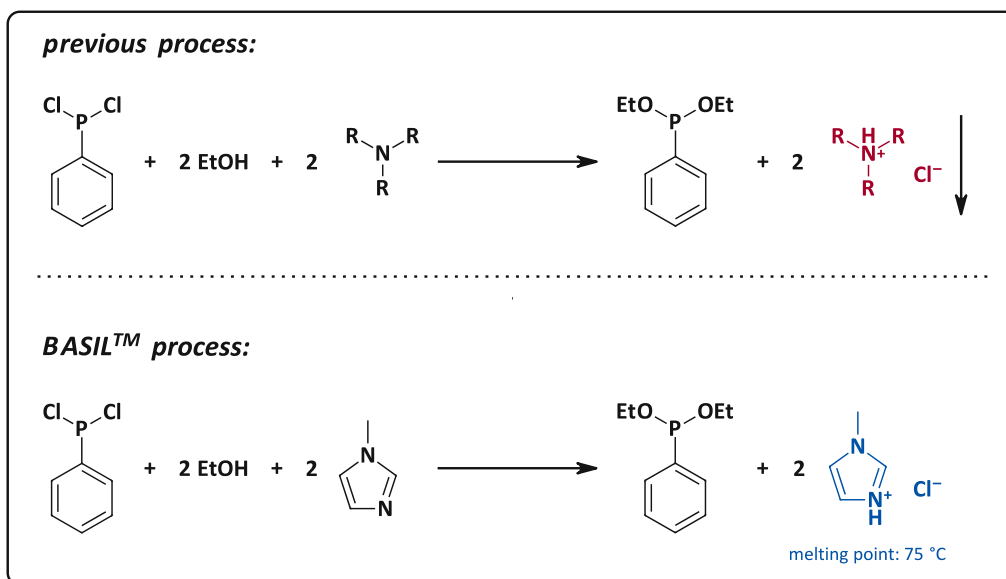
Scheme 11: Development of the synthesis of diethoxy phenylphosphine with trialkylamine used as a base for the more advanced BASIL™ process, where an ionic liquid acts as an acid scavenger.

In this reaction, hydrogen chloride is formed. Thus, an acid scavenger is required. Usually, tertiary amines are used for this purpose to form the corresponding ammonium salt. In many cases, a non-stirrable slurry is formed, leading to limited heat transfer and highly viscous solutions. Alternatively, higher amounts of solvent were required, followed by the necessity to separate the product *via* filtration. This problem was circumvented by using 1-methylimidazole instead of a trialkylamine, which formed 1-methyl imidazolium chloride during the reaction with hydrogen chloride. The formed protic salt has a melting point of 75 °C, thus making reaction temperatures of 80 °C possible without the need for solvent. Furthermore, a liquid-liquid biphasic reaction is ongoing since the product and ionic liquid are non-miscible and can be easily separated after the reaction. Moreover, the ionic liquid can be easily recycled by deprotonation using sodium hydroxide.

Besides the BASIL™ process, ionic liquids are used for many other industrial applications, such as entrainers for extractive distillation, as catalysts, e.g., for the cleavage of ethers, for fluorination or for oligomerization processes, as electrolytes for electropolishing and electroplating, as antistatic additives for cleaning fluids, as liquid support for gas storage, and as stabilizers for pigment pastes.[77]

Besides the industrial applications of ionic liquids, they have gained much interest in different fields of research and development, visible in the increasing numbers of publications entered in SciFinder; from up to 90 publications per year in the 1990s to around 8000 publications per year in the past five years (2018-2022, keyword "ionic liquid"). A summary of their applications is illustrated in **Scheme 12**.
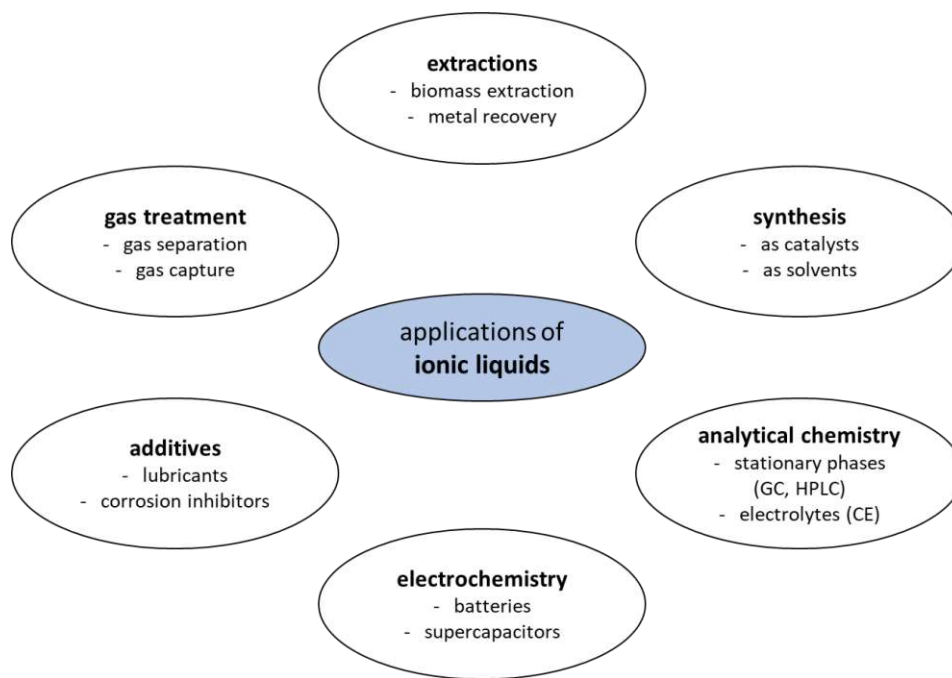
Scheme 12: Summary of applications of ionic liquids.

As shown in **Scheme 12**, ionic liquids are applied in extraction processes, in synthesis, in analytical chemistry, in electrochemistry, as additives and in industry.

For this thesis, the application of ionic liquids in organic synthesis is of primary interest, more specifically, their application as heterogeneous catalysts, where the ionic liquid is either immobilized on a solid support or is polymerized.

B.3.2 Supported Ionic Liquids as Heterogeneous Catalysts

Ionic liquids are extensively used in homogeneous catalysis. However, their application in biphasic ionic liquid–liquid systems can be limited by mass transfer problems if diffusion rates are low.[79] This problem can be circumvented by immobilizing a thin film of ionic liquids on, primarily, inorganic or polymer-based porous supports to prepare supported ionic liquids, which have gained much interest in the past years.[80] Their use is not limited to catalysis[81-87] but they are also applied to, e.g., gas purification and storage[88-91] as well as metal recovery.[92-94]

In catalysis, supported ionic liquids combine the previously mentioned advantageous properties of ionic liquids, such as their very low vapor pressure, non-flammability and tunability in terms of solubility, basicity, acidity, and (catalytic) activity, by simple variation of anions and cations, with the advantages arising from heterogeneous systems, such as the improved mass transfer compared to liquid-liquid biphasic systems. Furthermore, heterogeneous catalyst systems benefit from easier recovery and recycling as well as the easy feasibility for the application in continuous flow processes.[95]

There are numerous classes of supported ionic liquids used in the field of catalysis described in literature.[80, 96] A brief selection is illustrated in **Scheme 13**.
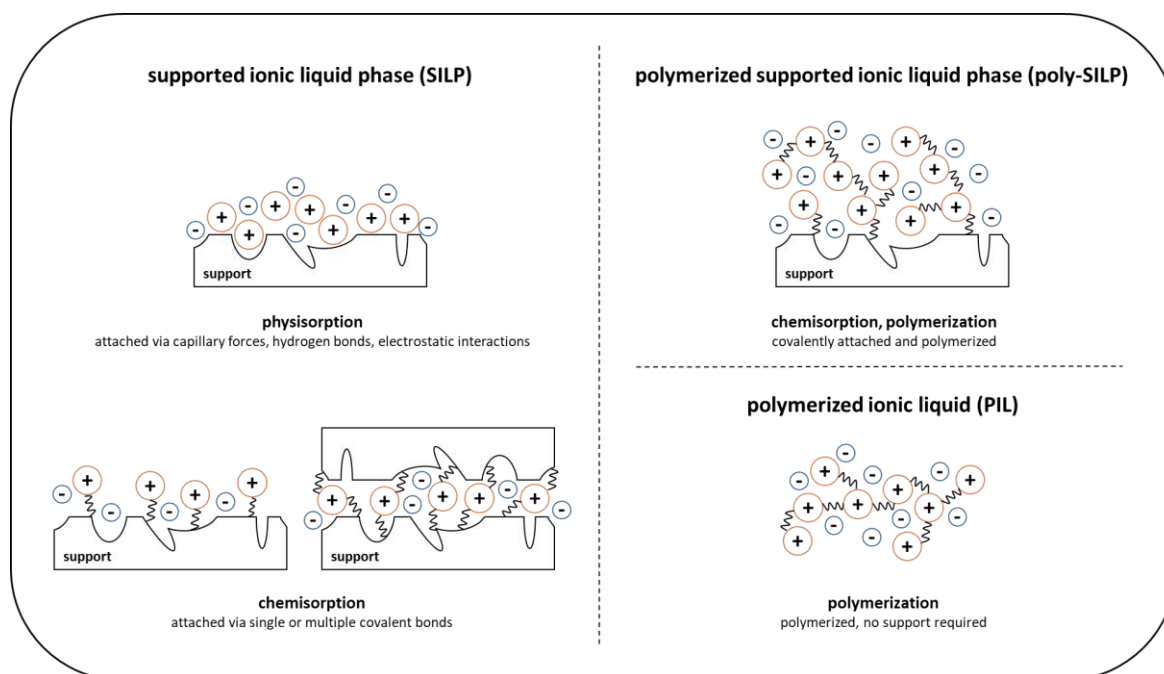
Scheme 13: Selection of different classes of supported ionic liquids applied as heterogeneous catalysts.

As shown in **Scheme 13**, the ionic liquid is either attached to the solid support *via* capillary forces, hydrogen bonds, electrostatic interactions, or covalent bonding in case of supported ionic liquid phases (SILPs). Furthermore, either the ionic liquid can be catalytically active by itself, or a catalyst, such as a metal-organic compound or an enzyme, can be dissolved in the ionic liquid phase. [95, 97, 98] Apart from these classic supported ionic liquid phases (SILPs), other versions of supported ionic liquids exist, such as polymerized supported ionic liquid phases (poly-SILPs),[99, 100] where ionic liquid monomers are attached covalently to a solid support and polymerized.
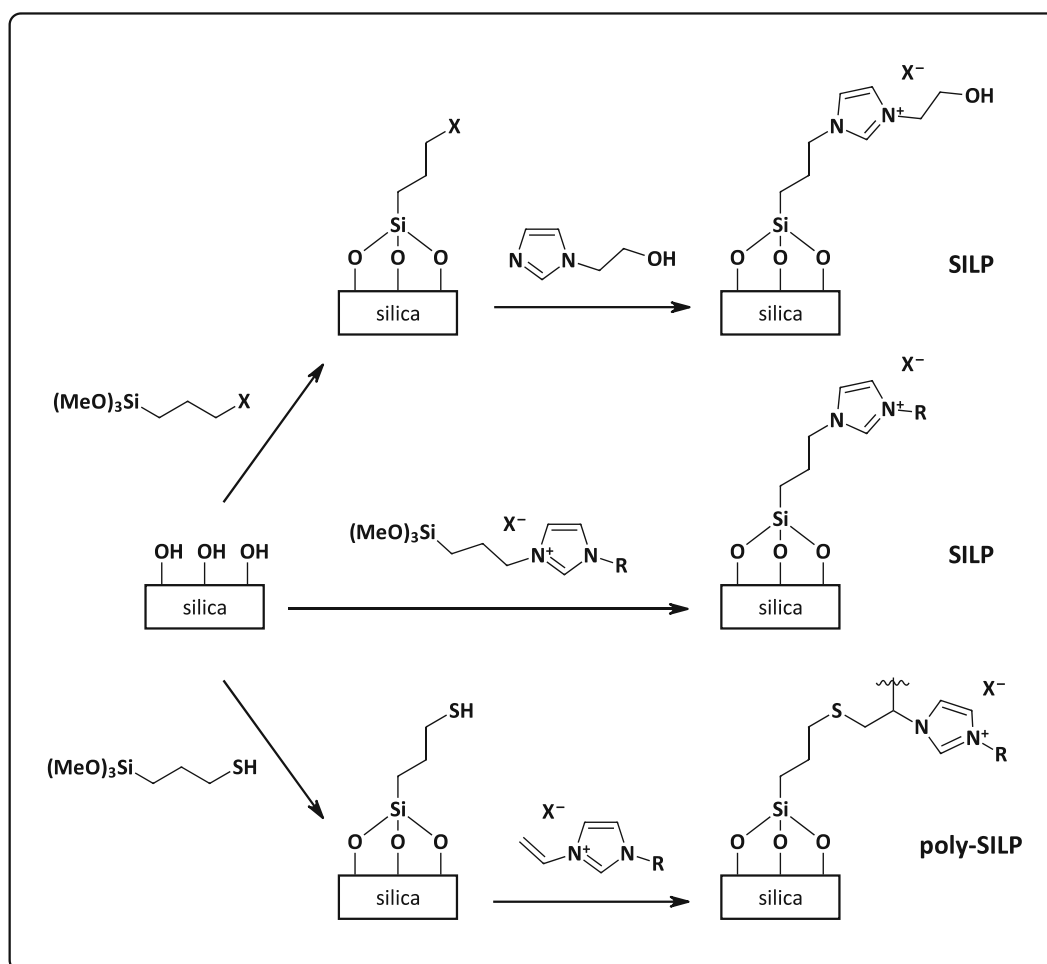
Scheme 14: Covalent binding of imidazolium-based ionic liquids to silica as solid support (X = halide).
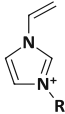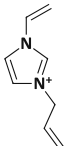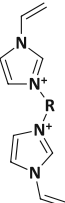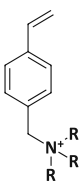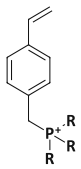
In general, covalent binding of ionic liquid to the solid supports occurs in most cases *via* a silane linker,[101] if the surface contains hydroxy groups, or *via* a sulfur linker,[100] if the surface is equipped with a thiol functionality (**Scheme 14**) . Supports for (polymerized) supported ionic liquid phases (SILP, poly-SILP) are mainly based on silica, but also other inorganic oxides, carbides, polymers, or bio-based materials are employed. A brief selection of used supports is presented in **Table 6**.

Table 6: Selection of supports for (polymerized) supported ionic liquid phases (SILP, poly-SILP).

support	type of SILP	reference
silica-60, silica-100	SILP (physisorption)	93, 101-103
silica-60, silica-100, SBA-15	SILP (chemisorption)	97, 98, 101, 104, 105
silica-60, SBA-15	poly-SILP	93, 100, 106
calcined silica	SILP (physisorption)	107, 108
magnesium/calcium oxide silicates	SILP (chemisorption)	109
silicon carbide	SILP (physisorption)	110
polyethylene	SILP (chemisorption)	111
polystyrene	SILP (chemisorption)	112
γ-alumina	SILP (physisorption)	113, 114
carbon nanotubes	SILP (chemisorption)	115-118
Fe_3O_4 nanoparticle	SILP (chemisorption)	119, 120
chitosan	SILP (chemisorption)	121

Polymeric ionic liquids (PILs) represent the class of heterogeneous ionic liquid-based catalysts where no support is required. In these systems, ionic liquid-based monomers are polymerized.[122, 123] Polymeric ionic liquids (PILs) are prepared mainly by radical polymerization of ionic liquid-containing monomers, employing primarily AIBN as a radical starter. However, examples with photoinitiators such as benzoin ethyl ether have also been reported.[124] As shown in **Table 7**, different imidazolium-, ammonium- and phosphonium-based precursors can be polymerized, and, e.g., styrene, divinylbenzene, or acrylonitrile are used as spacers and additional crosslinkers.[124, 125] Ionic liquid-based monomers can contain one double bond to obtain linear polymers, but also examples with two polymerizable ends are known in literature.[100] Furthermore, different chain lengths, as well as different anions, are described for ionic liquid-based monomers.

Table 7: Examples of ionic liquid-based monomers for the synthesis of polymeric ionic liquids (PILs).

cation	R =	anion	reference
	C_2-C_{18}	Br^-, HCO_3^-, PF_6^-	[123-127]
	-	Br^-	[124]
	C_1, C_2, C_4, C_8	Br^-, I^-, BF_4^-	[100, 123, 127]
	C_1-C_4	Cl^-, BF_4^-, OTf^-, NTf_2^-	[128]
	C_1-C_4	Cl^-, BF_4^-, OTf^-, NTf_2^-	[128]

The differences between ionic liquids and supercritical carbon dioxide render supported ionic liquids very attractive for the application as heterogeneous catalysts in supercritical carbon dioxide. Ionic liquids feature very high vapor pressures and high polarities, whereas supercritical carbon dioxide is characterized by high volatility and low polarity. Furthermore, supercritical carbon dioxide is known to be highly soluble in ionic liquid, but the ionic liquid itself rarely dissolves in supercritical carbon dioxide, which is beneficial if solutes need to be extracted from an ionic-liquid phase using supercritical carbon dioxide.[129] On the other hand, this difference in solubility also leads to the suppression of leaching of ionic liquid from the solid support, which is advantageous for continuous flow-application where leaching can be problematic.[86] This unique behavior of ionic liquid / supercritical carbon dioxide systems will be discussed in more detail in the following chapter.

B.3.3 Behavior of Ionic Liquids and Carbon Dioxide under High-Pressure Conditions

As discussed in previous chapters, ionic liquids are widely used as solvents and, mainly due to their very low vapor pressure, are often considered as sustainable solvents. Thus, recovery of solutes from ionic liquids after reactions is highly interesting. Volatile solutes can be recovered by evaporation or distillation. Non-volatile or thermally labile but polar solutes can be recovered *via* extraction with water, in case the ionic liquid is hydrophobic. For water-miscible ionic liquids, apolar extractants are required. Unlike, e.g., hexane or heptane, which are unfavorable from a sustainable chemistry point of view, (supercritical) carbon dioxide is a well-studied alternative.[130]

The system $[C_4mim]PF_6$ in carbon dioxide is one of the most studied due to the very high solubility of carbon dioxide in this particular ionic liquid that is also easy to synthesize.[130, 131] Brennecke *et al.*[132, 133] observed an increase in solubility of ionic liquid with higher pressures (up to 9.3 MPa) and a slight decrease in solubility with higher temperatures (40-60 °C). Furthermore, the influence of water was investigated. Due to the low solubility of water in carbon dioxide and *vice versa*, a decrease of solubility of carbon dioxide in $[C_4mim]PF_6$ saturated with water (2.3 wt%) was observed compared to dried samples (0.54 *vs.* 0.13 mole fraction CO_2, at 5.7 MPa, at 40 °C). Moreover, the formation of carboxylic acid from water and carbon dioxide and the accompanied decrease in pH value were suggested as possible reasons for the difference in solubility behavior. Studies of the influence of different cations and anions ($[C_4mim]PF_6 \approx [C_8mim]PF_6 \approx [C_8mim]BF_4 > [N-bupy]BF_4 > [C_4mim]NO_3 > [C_2mim]EtSO_4$ at 9.3 MPa) showed that ionic liquids containing fluorinated anions exhibit a higher solubilizing capacity for carbon dioxide due to the hydrophilic nature of their fluorine substituents.

Moreover, Peters *et al.*[134] compared the solubility of carbon dioxide in $[C_2mim]PF_6$ and $[C_4mim]PF_6$ and observed that the solubility is much lower in $[C_2mim]PF_6$ (approximately 0.6 mole fraction of CO_2 at 9.6 MPa) than in $[C_4mim]PF_6$ (approximately 0.6 mole fraction of CO_2 at 1.0 MPa). This was primarily attributed to the increased bulkiness of the butyl chain compared to the ethyl chain and, thus, the higher density of $[C_2mim]PF_6$. Furthermore, the solubility of ionic liquid in carbon dioxide was investigated, by preparing a mixture of a low amount of $[C_2mim]PF_6$ (0.3 mol%) in carbon dioxide (99.7 mol%). Measurements were further performed under supercritical conditions of carbon dioxide (40-90 °C, up to 10 MPa). No ionic liquid was detected in the supercritical carbon dioxide, demonstrating the suitability of supercritical carbon dioxide for the extraction of organic solutes without cross-contamination with ionic liquids.

One of the first studies of extraction of low volatile solutes from ionic liquids with supercritical carbon dioxide was carried out by Brennecke and coworkers[131] using naphthalene as a model substrate in a [C_4mim]PF_6 / carbon dioxide system. They were able to extract naphthalene with high recoveries of 94-96% at supercritical conditions (40 °C, 13.8 MPa) without detectable contamination of the extract with ionic liquid. Studies of the [C_4mim]PF_6 / carbon dioxide system were further expanded to other organic solutes, such as aniline, anisole, benzoic acid, or 1,4-butanediol, always resulting in recoveries higher than 95%.[135]

Based on these excellent extraction properties of different solutes from ionic liquids, a combined ionic liquid and supercritical carbon dioxide extraction of cannabinoids from industrial hemp was recently developed in our group.[43] Therein, different ionic liquids, namely [C_2mim]OAc, [Ch]OAc, and [C_2mim]DMP, were chosen for pretreatment of the biomass and subsequent supercritical extraction. Especially acetate anions are known to enhance the dissolution of cellulose,[136] thus leading to a better penetration of supercritical carbon dioxide into the plant tissue and further resulting in higher yields than using other anions, such as dimethylphosphate (DMP). Furthermore, the addition of water leads to a decrease in the viscosity of the ionic liquids and a decrease in solubility of cannabinoids in the ionic liquid-water phase and, therefore, a further increase in extraction yield.

Cross-contamination can become an issue if the addition of (organic) cosolvents to supercritical carbon dioxide becomes necessary to increase the solvation power of the supercritical carbon dioxide phase. Wu *et al*.[137, 138] reported the influence of *n*-hexane, acetone, and ethanol on the solubility of [C_4mim]PF_6 in carbon dioxide at 40-55 °C and 12-15 MPa. The solubility of the chosen ionic liquid in pure carbon dioxide of $3.2 \cdot 10^{-7}$ mole fraction (40 °C, 15 MPa) was determined. While *n*-hexane shows no effect on the solubility of the ionic liquid in supercritical carbon dioxide, the solubility increases significantly when 10 mol% of acetone or ethanol is added, as shown in **Scheme 15**. Furthermore, it is evident that solubility increases with pressure and dipole moment of the solvent (hexane < ethanol < acetone), whereas the influence of temperature is negligible.
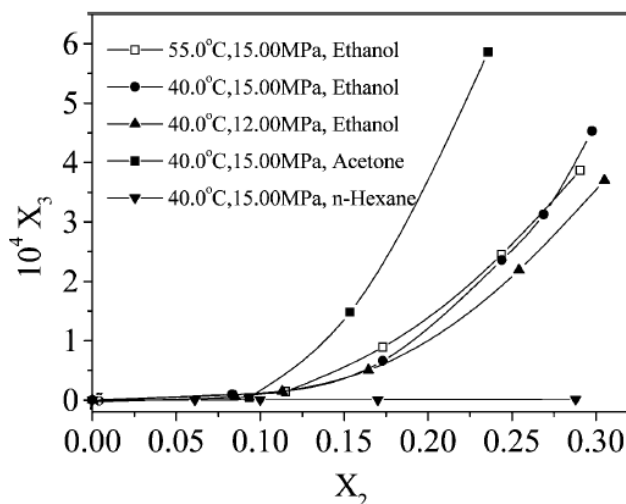
Scheme 15: Solubility of [C$_4$mim]PF$_6$ (X$_3$) in solvent/carbon dioxide mixtures (X$_2$).[137]

The solubility of ionic liquid in supercritical carbon dioxide in the presence of organic solvents is of crucial importance, especially when supported ionic liquids are employed as heterogeneous catalysts, in batch or continuous-flow reactions. Leaching of ionic liquid over time can be an issue for the long-term stability of the heterogenous systems, which is more probable if the ionic liquid is physisorbed and not chemically bound to the porous support material.[101]

High-pressure continuous flow set-ups and examples of supported ionic liquids employed as heterogeneous catalysts in supercritical environment are presented in the following chapters. Further, the impact of catalyst leaching on the long-term stability of the chosen reaction systems is demonstrated.

B.3.4 Equipment for Continuous-Flow Reactions in Supercritical Fluids

There are different in-house constructed or modified commercial equipment currently available for continuous reactions, which are suitable for the high pressures required to reach the supercritical state.[102, 139, 140] A system originally developed for supercritical fluid extraction by Jasco (Jasco Corporation, Tokyo, Japan)[102,139] was used for the projects herein presented. It was modified by exchanging the extraction vessels with empty HPLC columns, which were used as cartridges for powdered heterogeneous catalysts or impregnated monoliths.

A general set-up used for continuous reactions in supercritical fluids based on Poliakoff *et al*. and our experience has been described in the litereture.[102, 141, 142] Carbon dioxide is delivered from a gas cylinder with an ascending pipe. Since carbon dioxide cannot be pumped easily at room temperature due to its high compressibility, it has to be cooled using e.g., cooled pump heads, where a cooling

agent, delivered by a chiller, can circulate. Liquid substrates are delivered by HPLC pumps, either in neat form or mixed with solvent. Alternatively, gaseous starting materials can be delivered *via* mass-flow controllers. Static mixers or simple t- or v-pieces can be used to ensure complete mixing of starting materials and solvents before they enter the reactor unit.

Catalysts, in most cases ionic liquids and metal-organic species or enzymes, can be employed as a homogeneous mixture through which substrates and supercritical fluid are bubbled.[143] Herein, the focus will be on the employment of heterogeneous systems, where the catalyst is immobilized on a solid support and can be filled into a tube reactor (**Scheme 16**). For analysis, techniques such as gas chromatography[144] or UV-Vis (with diode-array detectors) coupled with mass spectrometry[145] can be employed online. The products can also be analyzed off-line after their collection and the release of carbon dioxide.
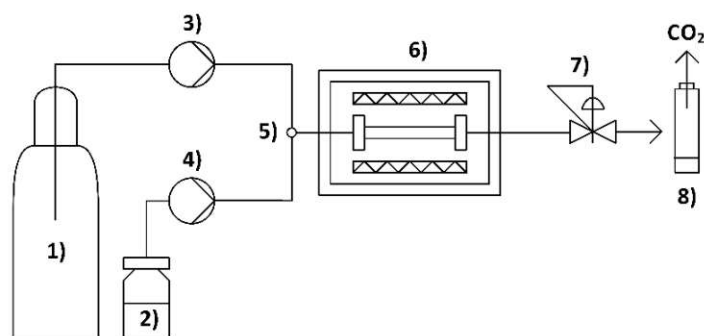
Scheme 16: Schematic representation of a set-up employed for heterogeneous catalysis in supercritical fluids.
(1) carbon dioxide cylinder, (2) substrate (+ solvent), (3) carbon dioxide pump, (4) substrate pump, (5) mixer, (6) tubular reactor in oven, (7) back-pressure regulator, (8) product collector

Continuous reactions catalyzed by supported ionic liquids using supercritical fluids, either as solvent or reactant, are presented in the following chapter. In these cases, metal-organic species, enzymes, or solely the ionic liquid acted as catalytically active species. These reactions are partly covered in a 2015 review by Garcia-Verdugo *et al*.[143] and further presented in the following chapter.

B.3.5 Continuous Reactions: Supported Ionic Liquids and Supercritical Fluids

The adsorption of ionic liquid on a porous solid support combines the advantageous properties of ionic liquid-based homogeneous systems with them of heterogenous ones, for examples higher mass transfer, easier recyclability and the simpler application in continuous flow. Different examples with supercritical carbon dioxide as solvent or reactant and supported ionic liquids as catalysts employed in continuous flow are summarized in the following.

B.3.5.1 Metal-Organic Species as Catalysts
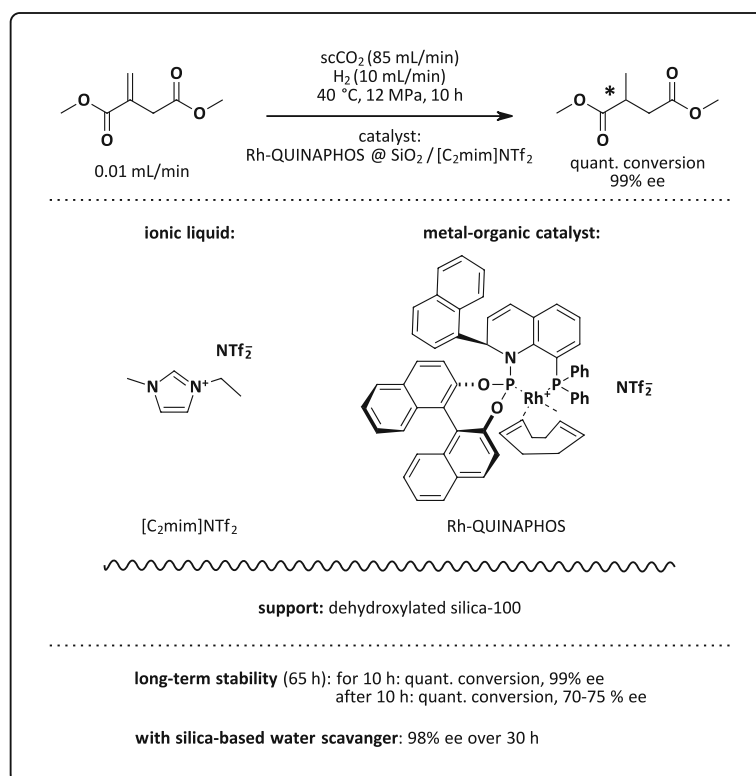
Scheme 17: Continuous rhodium-catalyzed enantioselective hydrogenation in scCO$_2$.[146, 147]

Leitner *et al.*[146] performed an enantioselective hydrogenation of dimethyl itaconate in continuous flow, employing a chiral rhodium complex with QUINAPHOS ligands, immobilized on dehydroxylated silical-100 with 1-ethyl-3-methylimidazolium bistriflimide ([C$_2$mim]NTf$_2$) as ionic liquid (**Scheme 17**). The flow of carbon dioxide was set to 85 mL/min, the flow of hydrogen was set to 10 mL/min, and both were delivered *via* mass-flow controllers. The reaction was carried out in supercritical carbon dioxide at 40 °C and 12 MPa. Enantioselective hydrogenation resulted in full conversion over 65 h and > 99% ee for 10 h. After 10 h, enantioselectivity dropped to 70-75% ee, which was ascribed to a partial decomposition of the QUINAPHOS ligand over time. The unfavorable influence of water on the long-term stability of the catalyst, when silica-based supports are used for immobilization of the metal-organic species, was further demonstrated in a follow-up project.[147] Therein, a water scavenger based on dehydroxylated silica was employed and resulted in 98% ee over 30 h on stream.
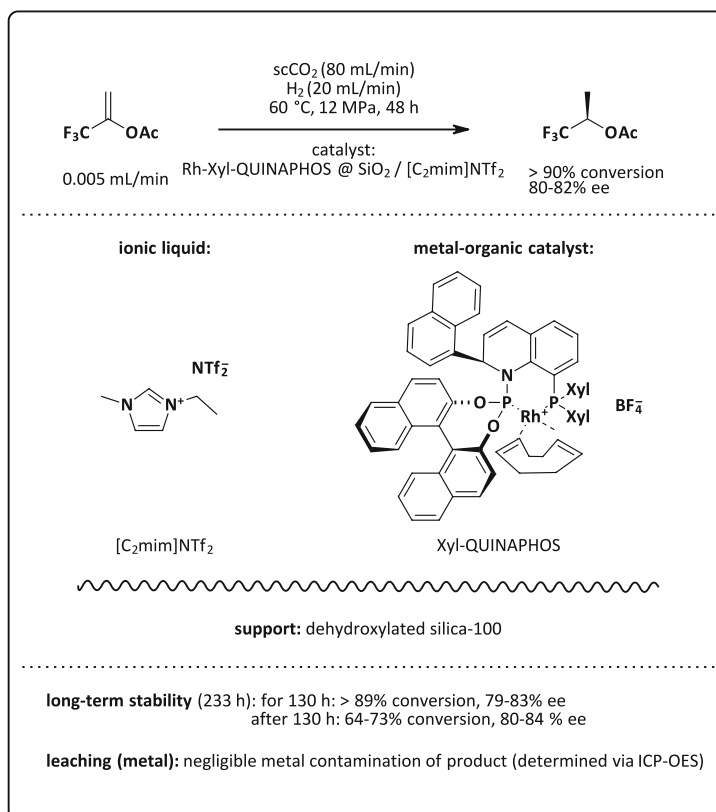
Scheme 18: Continuous rhodium-catalyzed enantioselective hydrogenation in scCO$_2$.[148]

Leitner and Franciò *et al*.[148] also reported the continuous hydrogenation of 1-(trifluoromethyl)vinyl acetate employing slightly different Xyl-QUINAPHOS ligands for rhodium catalyst, which was immobilized on dehydroxylated silica coated with 1-ethyl-3-methylimidazolium bistriflimide ([C$_2$mim]NTf$_2$) (**Scheme 18**). For the first 130 h on stream, conversions of > 89% and 79-83% ee were achieved. Flow rates were doubled, resulting in a reduction of residence time and, consequently, lower conversions of around 70%, whereas enantiomeric excess remained stable and reached a maximum when flow rates were set again to the initial values after 211 h on stream. Furthermore, just negligible amounts of leached metal catalyst were detected *via* inductively coupled plasma optical emission spectrometry (ICP-OES). Especially enantiomeric excess could be improved in this particular hydrogenation. In this regard, it was shown in the next example that different supports can drastically change the performance of a hydrogenation.
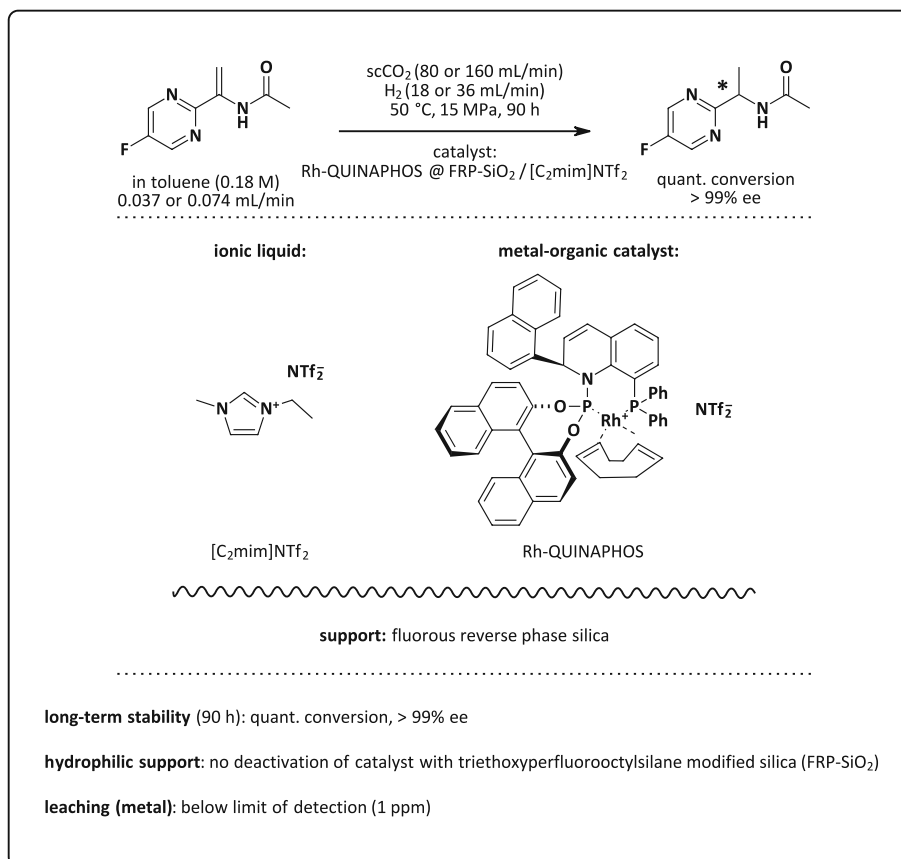
Scheme 19: Further developments in the continuous rhodium-catalyzed enantioselective hydrogenation in scCO$_2$.[149]

Based on the developed rhodium-QUINAPHOS supported system, Franciò and Leitner *et al.*[149] (**Scheme 19**) investigated the continuous-flow hydrogenation of an heteroaromatic enamide, known as a key intermediate of an active pharmaceutical ingredient (API). Toluene was found to be a suitable cosolvent in order to enable the synthesis of nonvolatile and poorly soluble substrates in pure supercritical carbon dioxide. Furthermore, hydrophobic fluorous reverse-phase silica, prepared by modification of the surface with triethoxy perfluorooctylsilane, replaced the previously used dehydroxylated silica as support and resulted in a stabilization of conversion over time. Quantitative conversion and > 99% ee for a period of 90 h were achieved. Furthermore, no leaching of the metal catalyst was observed, which is also required for the long-term stability of the system.
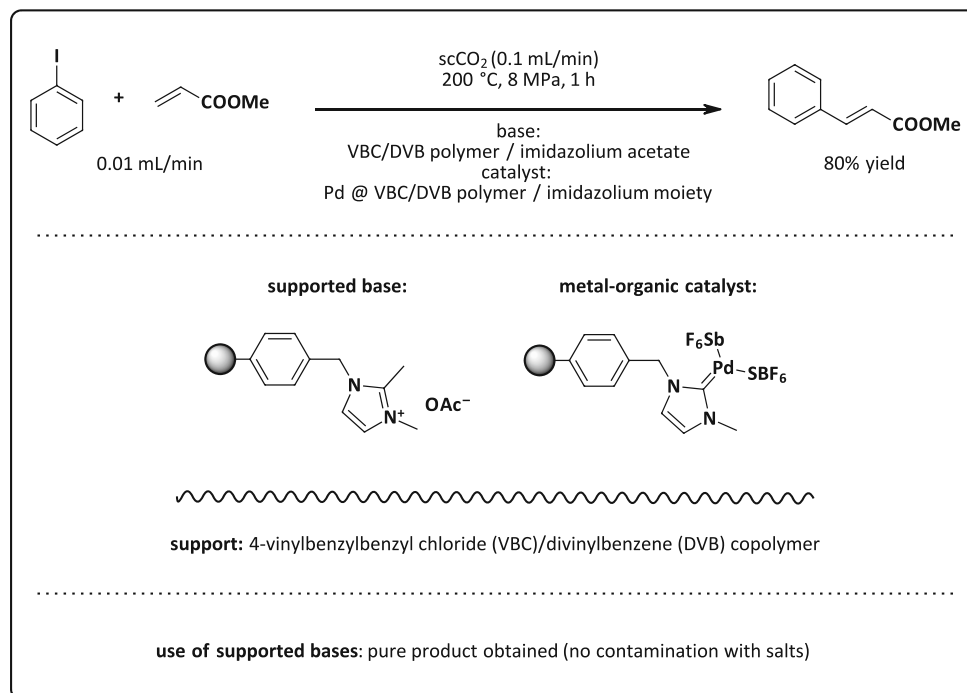
Scheme 20: Continuous palladium-catalyzed Heck reaction in scCO$_2$.[150]

Luis *et al.*[150] performed a Heck reaction in continuous flow using supercritical carbon dioxide as the sole solvent. They started from iodobenzene and methyl acrylate and employed polymer-supported imidazolium-based palladium catalyst for the C-C coupling (**Scheme 20**). Supported imidazolium acetate was used as a base to avoid contamination of the product with formed salt, as this was observed when triethylamine was used as a base. The reaction was performed at 8 MPa and 200 °C and resulted in a constant 80% yield for 1 h. After 1 h, the conversion dropped significantly. The ongoing consumption of the base was assumed to be the reason. Furthermore, it was stated that optimization will push the process to quantitative yields, whereas no further purification of the product will be necessary, which is beneficial in terms of sustainable chemistry.

B.3.5.2 Enzymes as Catalysts
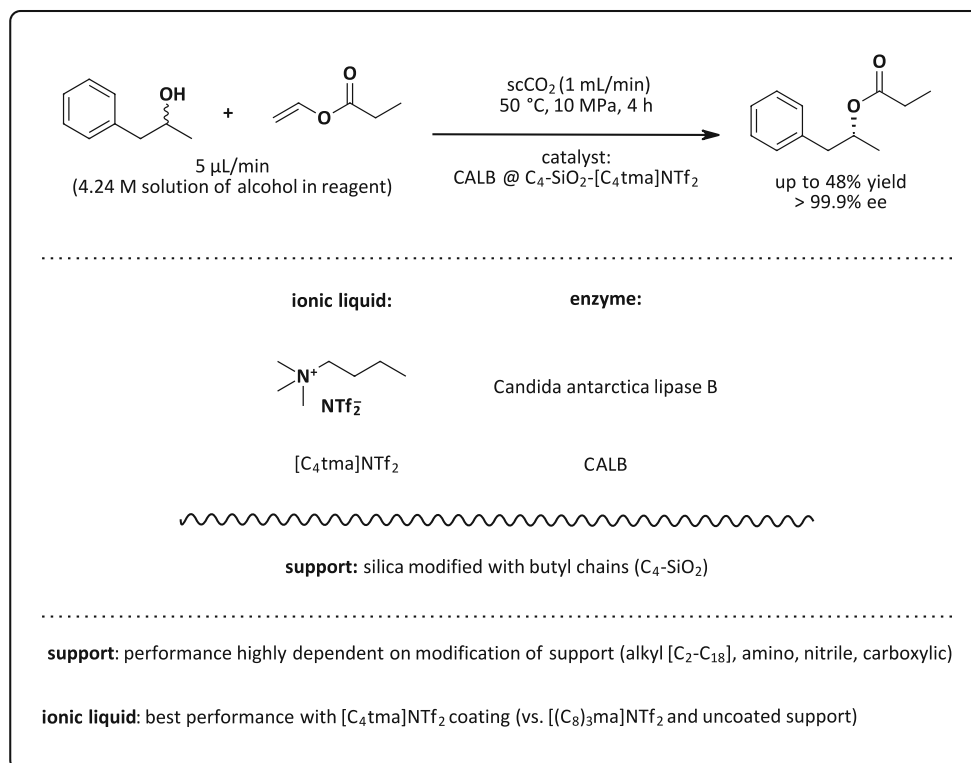
Scheme 21: Continuous lipase-catalyzed kinetic resolution in scCO$_2$.[151]

Iborra et al.[151] immobilized *Candida antarctica* lipase B (CALB) on different silica supports modified with different side chains (alkyl, amino, nitrile, carboxylic) to investigate the influence of different supports on the activity of enzyme employed to the kinetic resolution of 1-phenyl ethanol in ionic liquid / supercritical carbon dioxide systems (**Scheme 21**). Enzyme immobilized on butyl-modified silica coated with butyltrimethylammonium bistriflimide ([C$_4$tma]NTf$_2$) resulted in the highest yields up to 48%, representing an almost full conversion of the desired enantiomer (max. 50%) and > 99.9% ee. Furthermore, it was shown that functionalization of silica had a clear positive impact on the reaction performance, since enzyme supported on non-functionalized silica coated with ionic liquid showed very low activity. Moreover, reactions were carried out at moderate temperatures of 50 °C, at 10 MPa, but high enough to reach the supercritical state of carbon dioxide, demonstrating once again the advantage of reaching the supercritical state at low temperatures.
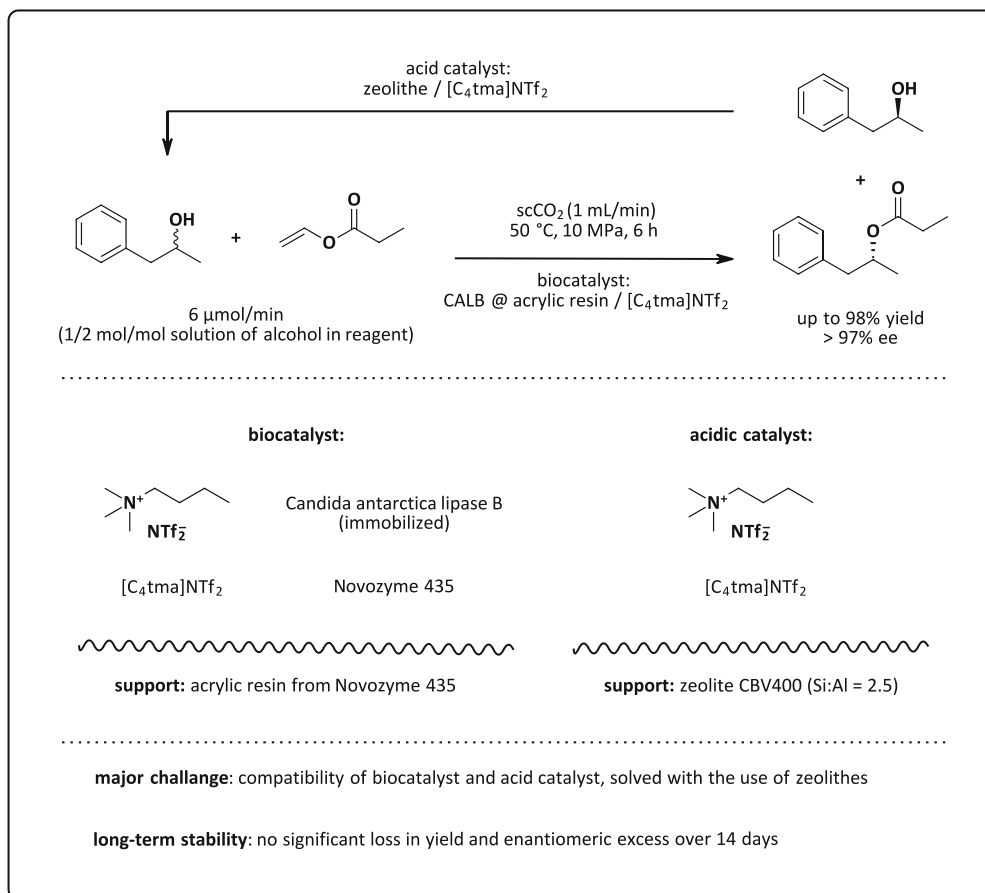
Scheme 22: Continuous lipase-catalyzed dynamic kinetic resolution in scCO₂.[152]

As a next step, the dynamic enzymatic kinetic resolution of 1-phenyl ethanol was reported by Iborra *et al*.[152, 153] (**Scheme 22**). For this purpose, 1-phenyl ethanol had to be racemized by continuously employing an acidic catalyst. Herein, the major challenge was the compatibility of biocatalyst and acidic catalyst to avoid deactivation of enzyme over time. This should be limited by the application of the SILP concept, whereas a minimum interaction of both heterogeneous catalytic systems should be guaranteed compared to a homogeneous system. However, a first attempt, where a mixture of immobilized biocatalyst Novozym 435 and benzenesulfonic acid-modified silica was used, resulted in a rapid loss of activity. In a second attempt, heterogeneous acid catalyst was placed on two ends of the catalyst cartridge, and biocatalyst was located in the middle. All three catalytically active zones were separated using glass wool. This attempt resulted in yields up to 75% and 91-98% ee.[153] In a follow-up project (**Scheme 22**), ionic liquid-coated zeolites featuring a decreased acidity compared to benzenesulfonic acid-modified silica were found to be suitable for the successful resolution without the need to separate the two catalysts from each other. Yields of 98% and 97% ee were achieved, showing excellent long-term stability over 14 days.[152]
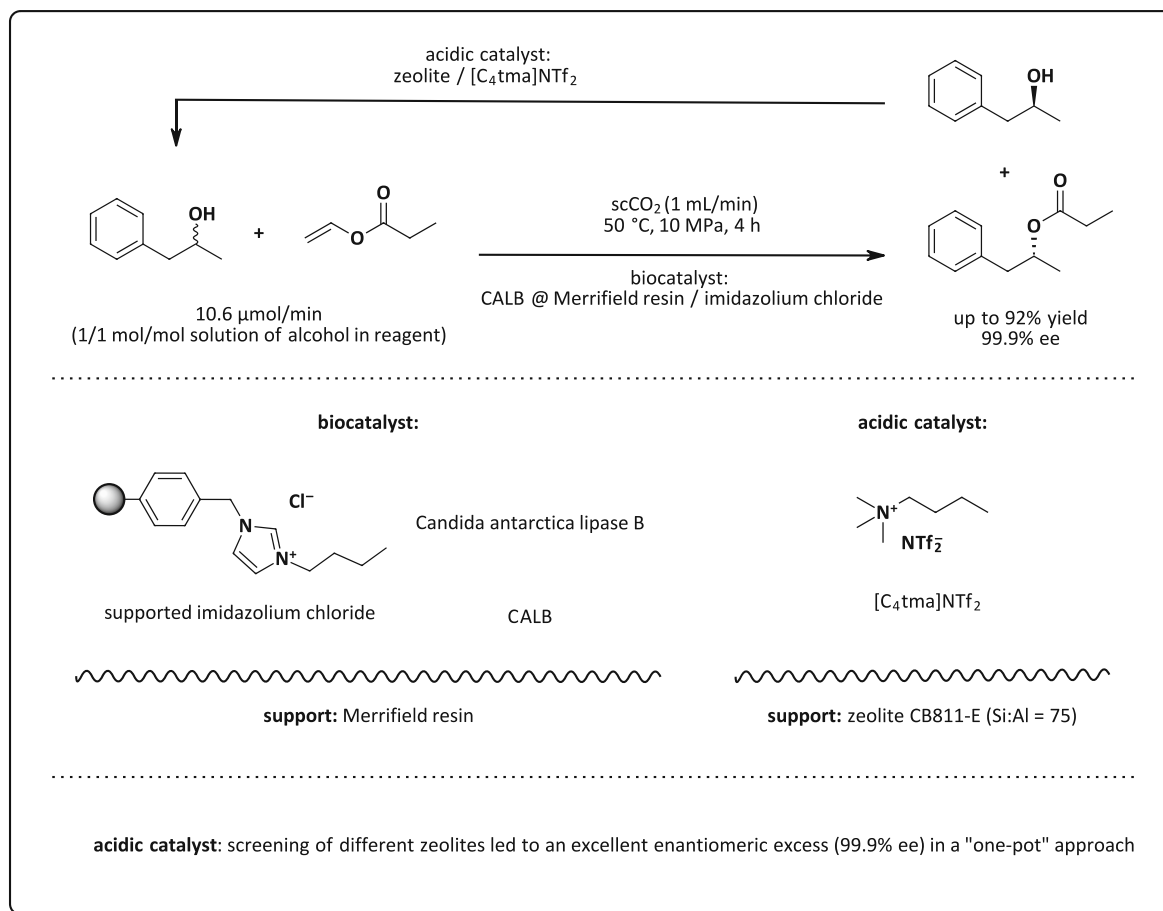
Scheme 23: Further improvement of the continuous lipase-catalyzed dynamic kinetic resolution in scCO$_2$.[154]

Luis *et al.*[154] also reported ionic-liquid modified Merrifield resins for the immobilization of *Candida antarctica* lipase B applied for the dynamic enzymatic kinetic resolution of 1-phenyl ethanol (**Scheme 23**). Imidazolium chloride-based ionic liquids were chemisorbed on Merrifield resins with different amounts of divinyl benzene as crosslinker to demonstrate the impact of porosity of support on the catalytic activity. Macroporous supports were preferred in terms of yield and enantioselectivity. Furthermore, zeolite coated with butyltrimethylammonium bistriflimide ([C$_4$tma]NTf$_2$) was employed as acidic catalyst for continuous racemization of the alcohol. This reaction system resulted in yields of 92% and again in excellent enantioselectivities of > 99.9% ee.
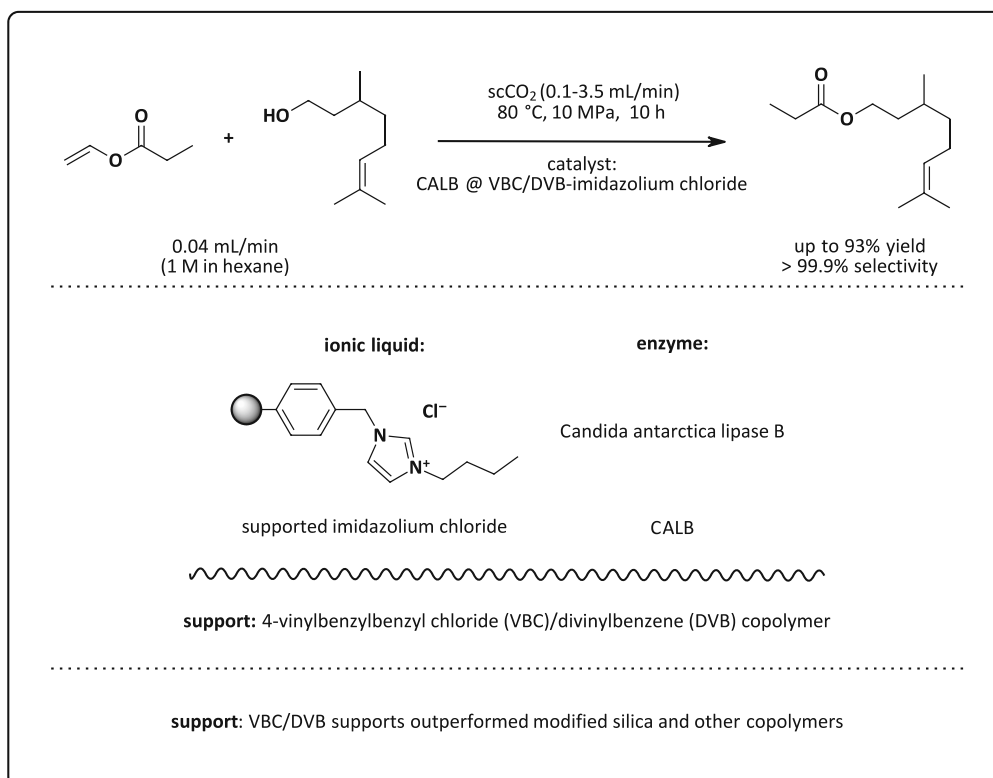
Scheme 24: Continuous lipase-catalyzed production of citronellyl propionate in scCO₂.[155]

Instead of polymeric beads based on Merrifield resin, Iborra *et al.*[155] reported macroporous monolithic imidazolium-supported polymers where the enzyme was adsorbed and applied for the production of citronellyl propionate, a terpene ester used as flavor and fragrance (**Scheme 24**). *Candida antarctica* lipase B was employed as a biocatalyst, and butylimidazolium chloride-based ionic liquid was immobilized on vinylbenzylchloride–divinylbenzene copolymers and outperformed 2-hydroxyethyl methacrylate–ethylene dimethacrylate polymers and butyl-modified silica. Reactions were performed at 80 °C and 10 MPa and resulted in yields of up to 93% and selectivity higher than 99.9%.
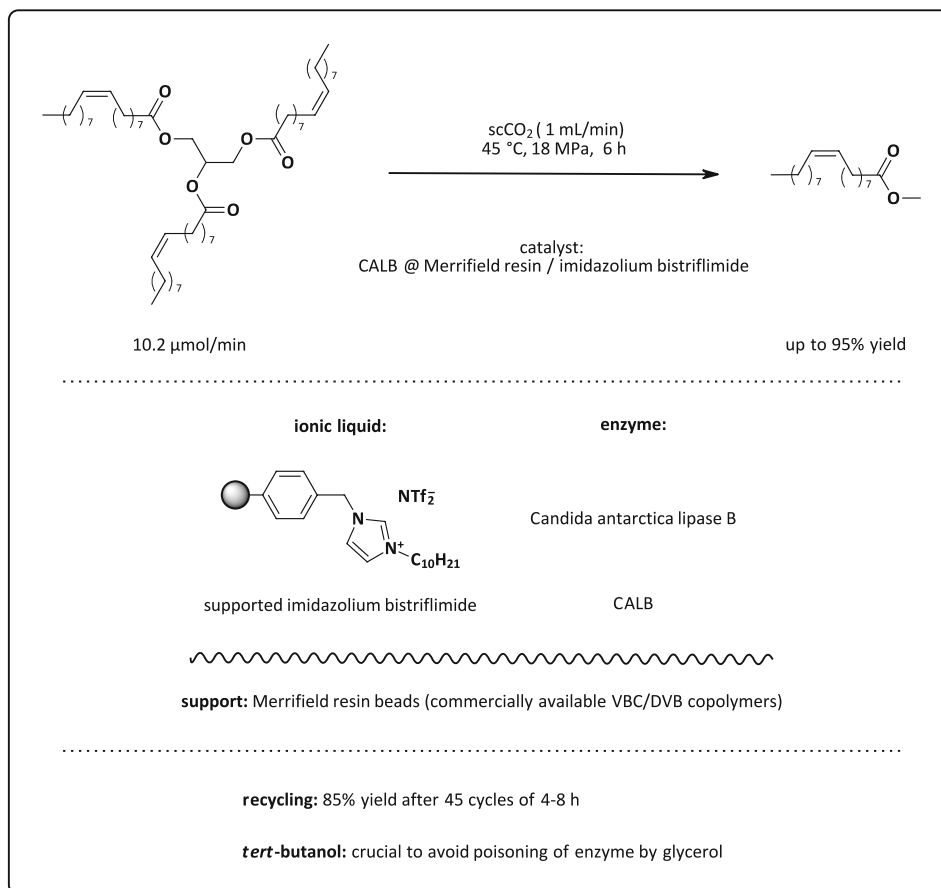
Scheme 25: Continuous lipase-catalyzed biodiesel production in scCO₂.[156]

Luis *et al.*[156] established an enzyme-catalyzed continuous methanolysis for the production of methyl oleate (biodiesel) in supercritical carbon dioxide starting from triolein (**Scheme 25**). Enzyme *Candida antarctica* lipase B (CALB) was immobilized on divinylbenzene-polystyrol polymeric matrices of different porosity, prepared from commercially available Merrifield resins, where 1-decyl-2-methylimidazolium-based ionic liquids were chemisorbed. Reactions were performed at relatively moderate temperatures of 45 °C at 18 MPa, nevertheless, reaching the supercritical state of carbon dioxide and yielding up to 95% of product. Furthermore, this system showed good stability of 85% yield after 45 cycles of 4-8 h. Additionally, *tert*-butanol as co-solvent in supercritical carbon dioxide turned out to be crucial to avoid poisoning of the enzyme over time by the blockage of catalytically-active sites by glycerol formed during the reaction.
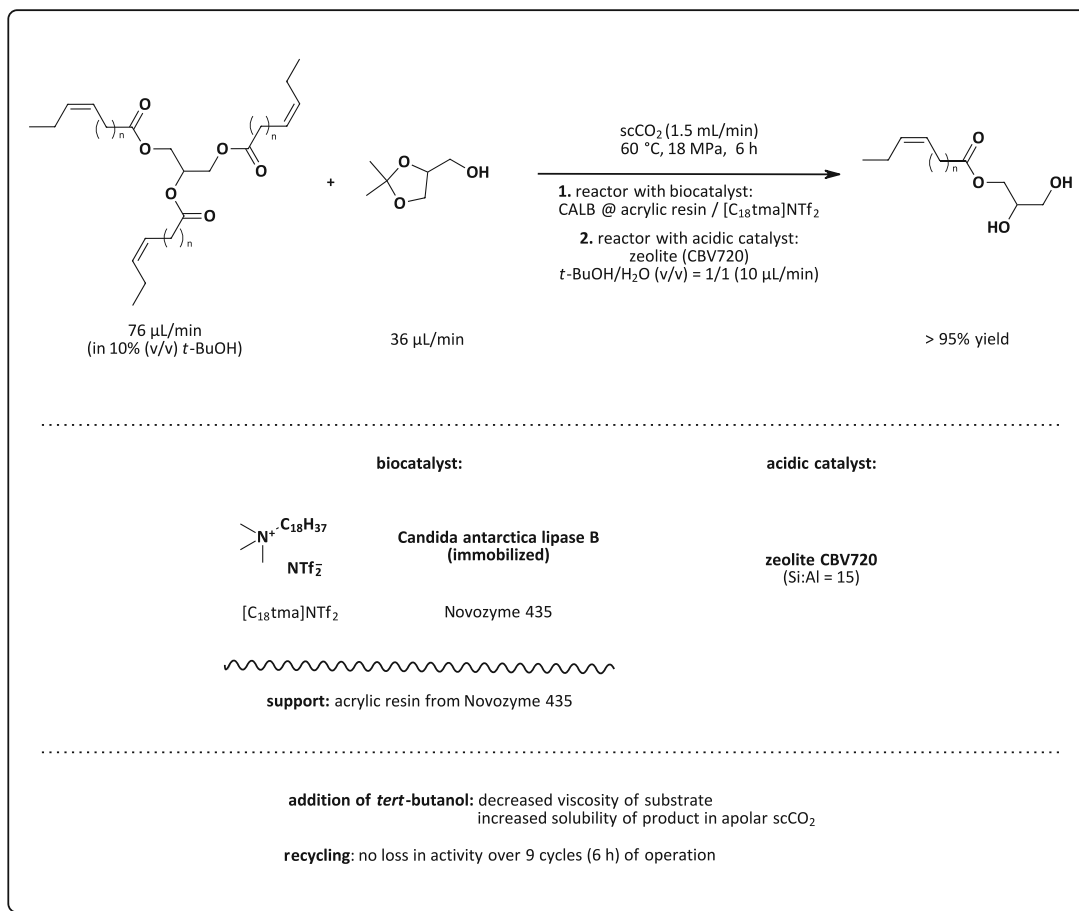
Scheme 26: Continuous lipase-catalyzed production of omega-3 monoacylglycerides in scCO$_2$.[157]

Lozano *et al.*[157] investigated a continuous two-step synthesis of omega-3 monoacylglycerides, starting from fish oil or linseed oil dissolved in *tert*-butanol in order to reduce the viscosity and facilitate mass transfer (**Scheme 26**). In a first step, the immobilized enzyme *Candida antarctica* lipase B was employed for transesterification, and in a second step, the solketal moieties were hydrolyzed employing zeolites as solid acid catalysts. While no cosolvent was employed for the transesterification (1st step), a mixture of water and *tert*-butanol was used for the hydrolysis (2nd step) in order to guarantee the transport of hydrophilic fatty acid solketal ester intermediate in apolar supercritical carbon dioxide phase, without blocking the reactor during the reaction. Yields of more than 95% monoglyceride were achieved in 9 cycles of operation for a period of 6 h.

B.3.5.3   Ionic Liquids as Sole Catalysts
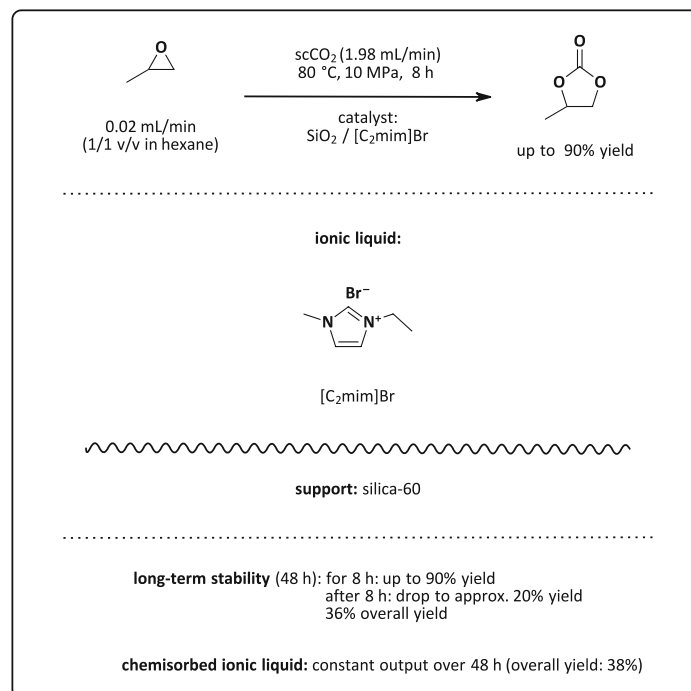
Scheme 27: Continuous imidazolium bromide-catalyzed production of propylene carbonate in scCO$_2$.[101]

In our group, Schröder *et al.*[101] investigated the continuous production of propylene carbonate employing silica-supported 1-ethyl-3-methylimidazolium bromide ([C$_2$mim]Br) as the sole catalyst without the need for additional catalysts, such as enzymes or metals (**Scheme 27**).

Additionally, supercritical dioxide acted in this case not only as solvent (together with hexane) but also as a reactant, since carbon dioxide had to be incorporated into propylene oxide to form propylene carbonate. Two different catalyst-immobilization approaches were studied; for the first approach, [C$_2$mim]Br was simply physisorbed on silica. This catalytic system resulted in a maximum yield of around 90% for 8 h but led to a rapid decrease due to leaching of ionic liquid from the support and the deposition of formed by-products, such as oligomers and polymers, on the catalytically-active surface. This process was triggered by free hydroxyl groups on the surface of silica and led to an overall yield of 36% over 48 h. For this reason, imidazolium bromide based ionic liquids were chemisorbed on silica using the free hydroxyl groups as an attachment point for a silane linker. With this approach, a constant output of 38% of pure propylene carbonate over a period of 48 h was achieved.

This publication served as the basis for the continuous flow-related projects presented in this thesis, where neat starting material and supercritical carbon dioxide as sole solvent were employed to prevent catalyst leaching in the production of bio-based cyclic carbonates. Furthermore, alternative support materials were studied to achieve selective conversion to cyclic carbonates.

C Aim of this Thesis

Supercritical carbon dioxide is well established for the application as solvent for supercritical fluid extractions. Many bioactive compounds of different classes such as flavonoids, terpenes, lipids, fatty acids, cannabinoids, and alkaloids were extracted from various sources. To enhance the release of bioactive compounds from plant material, hydrolytic enzymes can be employed for the distortion and deformation of the matrix to enhance the release of bioactive compounds.

This thesis, dealing with biomass valorization, focuses on the development of an enzyme-assisted supercritical carbon dioxide extraction process employing the enzyme mix snailase for the deformation of the plant matrix of apple pomace and the hydrolysis of the contained polar flavonoid glycosides to less polar flavonoid aglycones to facilitate their extraction process. Finally, this work aims for a simultaneous process of the enzymatic hydrolysis and the supercritical fluid extraction.

Due to contrary solubility properties of supercritical carbon dioxide and ionic liquids, a highly tunable compound class, these two neoteric solvents were combined in heterogeneous catalytic processes for the continuous production of bio-based cyclic carbonates using supercritical carbon dioxide as reagent and sole solvent. Supported ionic liquids were employed as heterogeneous catalyst. A focus was further put on the investigation and development of different support materials to achieve higher yields and selectivities.
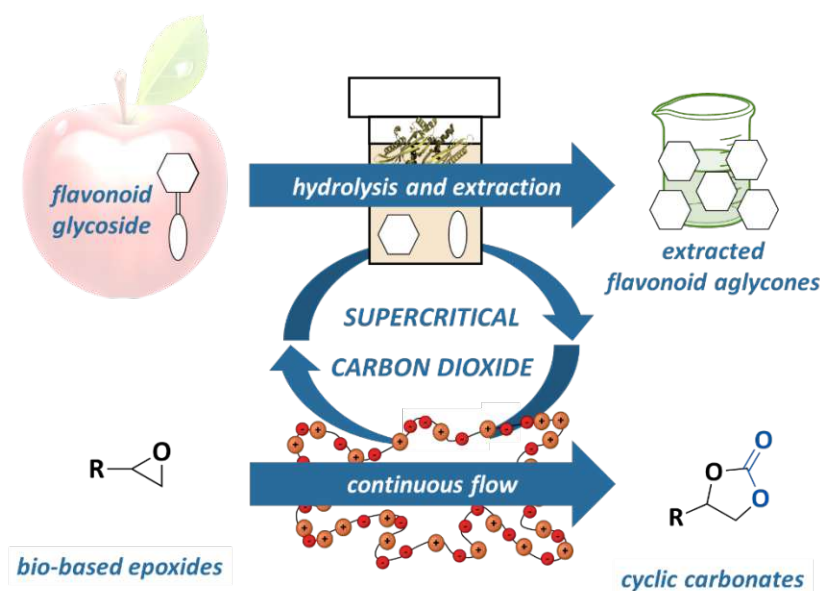
Scheme 28: Aim of this thesis - Application of supercritical dioxide in biomass valorization and in continuous flow.

D Enzyme-Assisted Supercritical Fluid Extraction of Flavonoids from Apple Pomace (*Malus × domestica*)

Enzyme assisted-supercritical fluid extraction has been employed on different plant materials to facilitate or even enable the extraction of bioactive compounds by the digestion and deformation of plant tissue.[47] Bioactive compounds, such as flavonoids,[64] feature, for example, antioxidative, antiaging, cardioprotective, or anti-inflammatory effects and are, therefore, applied in the pharmaceutical and food industry as well as in cosmetics. Many flavonoids remain in apple pomace after juice, jam, cider, or vinegar production,[158] but apple pomace has never been employed for enzyme-assisted supercritical fluid extraction to the best of our knowledge.
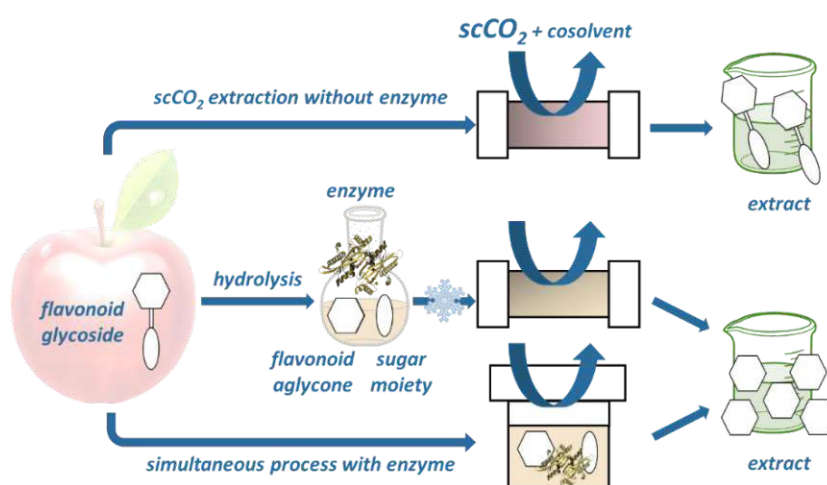
Scheme 29: Supercritical fluid extraction of flavonoids from apple pomace and enzyme-assisted supercritical fluid extractions in a subsequent and a simultaneous process.

An enzyme-assisted supercritical carbon dioxide extraction of flavonoids from apple pomace was investigated and compared to a supercritical carbon dioxide extraction without enzyme of dried and milled biomass (**Scheme 29**). This study focused on the four most prominent flavonoid glycosides in apple pomace and the enzymatic hydrolysis products, the flavonoid aglycones quercetin, kaempferol, phloretin, and 3-hydroxyphloretin. For successful enzymatic hydrolysis, the commercially available enzyme mix snailase was employed. Optimization of enzymatic hydrolysis focused on the influence of the amount of snailase, pre-treatment of apple pomace, and the time for enzymatic hydrolysis. After lyophilization of hydrolyzed samples, they were transferred into a flow reactor for subsequent supercritical fluid extraction, where the amount and kind of polar cosolvent, as well as the time for the extraction, were investigated. Ultimately, the enzymatic hydrolysis and supercritical fluid extraction were performed in a one-pot, simultaneous process, which demonstrated the potential of snailase for a scalable process under pressurized conditions with dry and milled but also wet apple pomace.

In the following, the below-mentioned publication is presented:

Mikšovsky, P.; Kornpointner, C.; Parandeh, Z.; Goessinger, M.; Bica-Schröder, K.; Halbwirth, H., Enzyme-Assisted Supercritical Fluid Extraction of Flavonoids from Apple Pomace (Malus × domestica). *ChemSusChem* **2023**, https://doi.org/10.1002/cssc.202301094.

As a main author, together with Christoph Kornpointner, I contributed to the investigation, conceptualization, methodology, visualization, writing of the original draft, and review of the manuscript.

Enzyme-Assisted Supercritical Fluid Extraction of Flavonoids from Apple Pomace (Malus × domestica)

Philipp Mikšovsky[a],†, Christoph Kornpointner[b],†, Zahra Parandeh[a], Manfred Goessinger[c], Katharina Bica-Schröder*[a] and Heidi Halbwirth*[b]

[a] P. Mikšovsky, Z. Parandeh, Prof. Dr. K. Bica-Schröder
TU Wien
Institute of Applied Synthetic Chemistry (E163)
Getreidemarkt 9, 1060 Vienna, Austria
E-mail: katharina.schroeder@tuwien.ac.at

[b] Dr. C. Kornpointner, Prof. Dr. H. Halbwirth
TU Wien
Institute of Chemical, Environmental and Bioscience Engineering (E166)
Getreidemarkt 9, 1060 Vienna, Austria
E-mail: heidrun.halbwirth@tuwien.ac.at

[c] Dr. M. Goessinger
Department of Fruit Processing
Federal College and Institute for Viticulture and Pomology
Wiener Strasse 74, 3400 Klosterneuburg, Austria

Supporting information for this article is given via a link at the end of the document.

Abstract: Herein an enzyme-assisted supercritical fluid extraction (EA-SFE) was developed using the enzyme mix snailase to obtain flavonols and dihydrochalcones, subgroups of flavonoids, from globally abundant waste product apple pomace. Snailase, a commercially available mix of 20—30 enzymes, was successfully used to remove the sugar moieties from quercetin glycosides, kaempferol glycosides, phloridzin and 3-hydroxyphloridzin. The resulting flavonoid aglycones quercetin, kaempferol, phloretin and 3-hydroxyphloretin were extracted using supercritical carbon dioxide ($scCO_2$) and minimum amounts of polar cosolvents. A sequential process of enzymatic hydrolysis and supercritical fluid extraction was developed, and the influence of the amount of snailase, pre-treatment of apple pomace, the time for enzymatic hydrolysis, the amount and type of cosolvent and the time for extraction, was studied. This revealed that even small amounts of snailase (0.25%) provide a successful cleavage of sugar moieties up to 96% after 2 h of enzymatic hydrolysis followed by supercritical fluid extraction with small amounts of methanol as cosolvent, leading up to 90% of the total extraction yields after 1 h extraction time. Ultimately, a simultaneous process of EA-SFE successfully demonstrates the potential of snailase in scalable $scCO_2$ extraction processes for dry and wet apple pomace with satisfactory enzyme activity, even under pressurized conditions.

Introduction

Recent studies[1] revealed the potential of the relatively new field of enzyme-assisted supercritical fluid extraction (EA-SFE) of various bioactive compounds from different plant materials, such as leaves[1a, 2] (*Medicago sativa*), peels[3] (*Punica granatum*, *Ananas comosus*, *Solanum lycopersicum*), seeds[1b, 4] (*Paullinia cupana*, *Hippophae rhamnoides* L., *Decaisnea insignis*, *Vitis vinifera* L.), hulls[5] (*Fagopyrum escalentum*), cladodes[6] (*Opuntia fiscus-indica* (L.) Miller), spicery[7] (*Piper nigrum*, *Elettaria cardamomum*), leftovers[8] (*Camellia sinensis*) and pomace[4b, 9] (*Ribes nigrum*, *Hippophae rhamnoides* L.). The enzymes α-amylase, cellulase, pectinase, protease and xylanolytic enzyme, as well as commercially available enzyme mixtures Alcalase®, Celluclast®, CeluStar®, Flavourzyme®, Kemzyme®, Novozyme®, Pectinex®, Rapidase Maxi Fruit® and Viscozyme® were all employed with the same goal: the digestion and deformation of plant tissue, namely the polysaccharide network[1c], constructed from cellulose, hemicellulose, lignin and pectin, in order to enable, facilitate or even improve the release of various valuable bioactive compounds for further supercritical fluid extraction (SFE) due to an enhanced penetration of supercritical fluid into the plant material.[10]

In context of the extraction of valuable bioactive compounds from plant material, flavonoids[11] are well known as polyphenolic and therefore antioxidative secondary plant metabolites. They exhibit antiaging effects[12], are anti-inflammatory[13], cardioprotective[14], immunomodulatory[15] and feature antiviral[11b, 16], antibacterial[17] and antifungal[18] activities. For these reasons, flavonoids are commonly applied in cosmetics, the food industry and the pharmaceutical sector.

Flavonoids mostly appear in their glycosylated form in nature[19], increasing their polarity, and thus their water solubility. In contrast, nonpolar supercritical carbon dioxide is primarily suitable for the extraction of compounds with lower polarity such as the corresponding aglycons which furthermore exhibit an increase in antioxidant capacity.[20]

Recently snailase was reported as a promising tool for the efficient enzymatic hydrolysis of flavonoid glycosides from plant extracts[21],

49

RESEARCH ARTICLE

resulting in a decrease of their polarity and thus facilitating supercritical carbon dioxide extraction. Snailase, obtained from the digestive tracts of snails (genus *Limax*)[22], is a mixture of 20—30 enzymes used for hydrolysis and digestion purposes and contains for instance, cellulase, invertase, polygalacturonase, hemicellulose, protease and pectinase[23].

Flavonoid glycosides of seven subclasses, namely aurones, chalcones, dihydroflavonols, flavanones, flavones, flavonols and isoflavones, from nine flower and leaf extracts were efficiently hydrolyzed. The hydrolysis by snailase led to highest yields of all investigated flavonoids, independently of type of plant and flavonoid, when compared with other enzymes (cellobiase, cellulase, β-glucosidase or pectinase) and acidic hydrolysis.[21]

Concerning waste valorization, many valuable flavonoids in apples, with worldwide production increasing from 83 Mt/year to 93 Mt/year (2017—2021)[24], remain in the pomace after juice, cider, jam and vinegar production[25].

Currently, apple pomace, a mixture of seeds, skin, flesh and stem, is used for further fermentation to ethanol[26], butanol[27], hydrogen[28], pectin[29], acrylic acid[21], propionic acid[30] and vitamin B12[30], to name a few, but is also subjected to numerous extraction techniques such as enzyme-assisted[31], microwave[32], ultrasound[32b, 33], radiofrequency-assisted[34] or supercritical fluid extractions[35].

Sole enzyme assisted extractions (EAE) feature the previously mentioned benefits of digestion and deformation of plant tissue, which facilitates the extraction of target compounds due to a better solvent penetration. However, plant tissue, enzyme and products are not separated and thus increasing the effort for further purification and solvent recycling. This can be circumvented by combining the enzymatic treatment with supercritical fluid extraction using supercritical carbon dioxide as extractant.
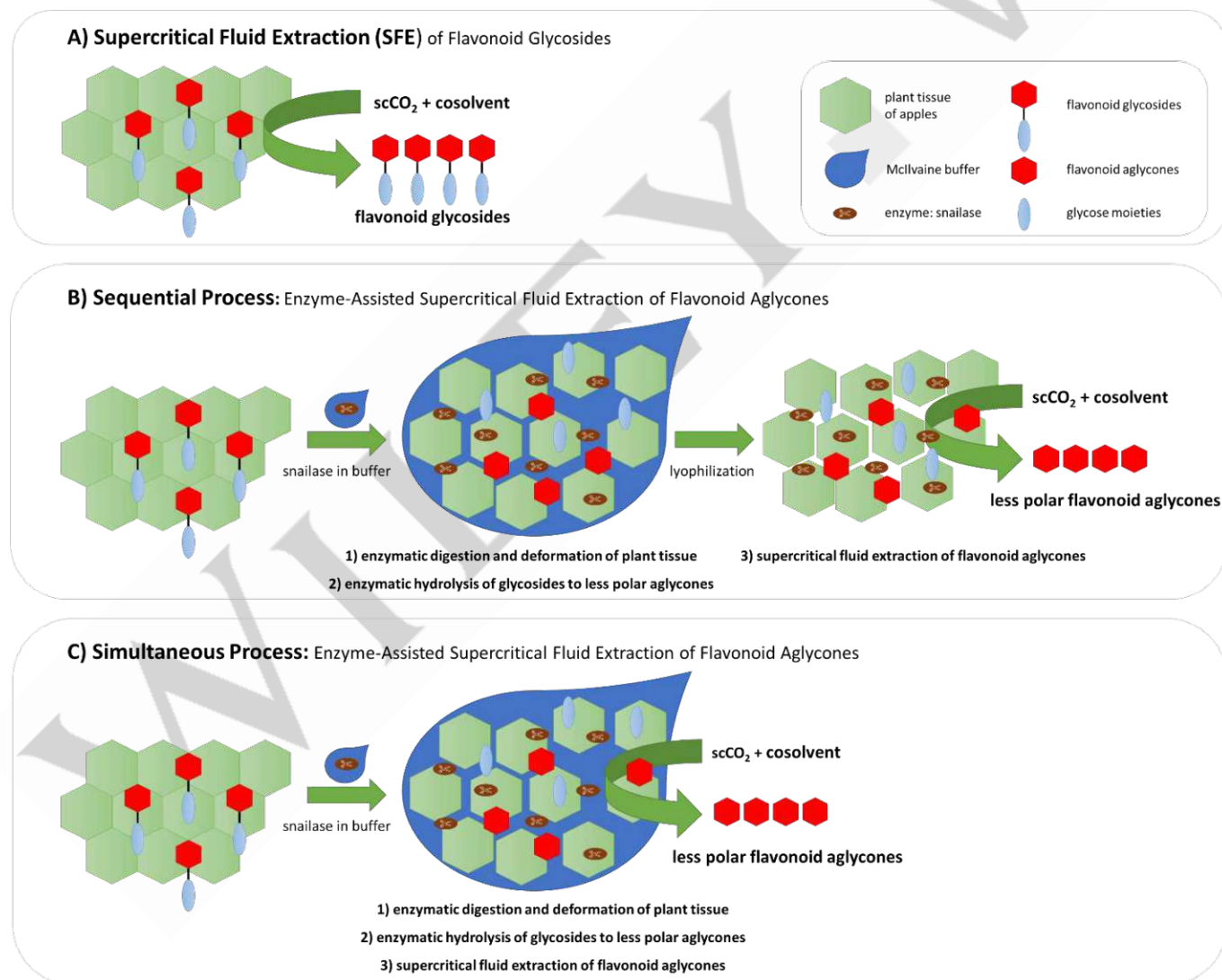
Figure 1: Scheme of different SFE techniques carried out in this work: A) Supercritical fluid extraction of flavonoid glycosides **2a-d** from enzymatically untreated apple pomace. B) Enhancement of snailase-assisted supercritical fluid extraction of less polar flavonoid aglycones **1a-d** conducted in a sequential manner. C) Development of a simultaneous process for the snailase-assisted supercritical fluid extraction of flavonoid aglycones **1a-d** from apple pomace.

RESEARCH ARTICLE

Carbon dioxide is simply separated by expansion directly after the extraction process. Furthermore, it is an abundant chemical with a relatively low critical temperature (31 °C) and critical pressure (7.38 MPa)[36], featuring favorable properties in terms of toxicity and flammability. Thus, it is an ideal replacement for organic solvents being used for conventional extractions. Furthermore, no remaining solvent traces are present in the extracts due to simple gas-liquid separation via expansion of carbon dioxide after extraction, which is in turn a crucial factor in cosmetics, food and pharmaceutical industries.

Moreover, the polarity of supercritical carbon dioxide can be tuned by the addition of small amounts of polar sustainable cosolvents[37], such as ethanol or methanol, in order to enhance the extraction performance.

To the best of our knowledge, snailase with its high efficiency for enzymatic hydrolysis of flavonoid glycosides in combination with apple pomace as valuable waste material, has never been employed for enzyme-assisted supercritical fluid extraction.

In this work (**Figure 1**) we present the enhancement of an enzyme-assisted supercritical carbon dioxide extraction of less polar flavonoid aglycones (kaempferol **1a**, quercetin **1b**, phloretin **1c** and 3-hydroxyphloretin **1d**) from globally abundant apple pomace using snailase for the digestion of plant tissue to facilitate the penetration of carbon dioxide in the matrix[10], and to hydrolyze polar flavonoid glycosides **2a-d** to less polar flavonoid aglycones **1a-d**. Ultimately, a simultaneous process for enzymatic hydrolysis and supercritical fluid extraction was developed under the considerations of pressure- and pH-dependent enzyme activity[38], revealing the potential for an up-scaled industrial process for various waste materials in the future.
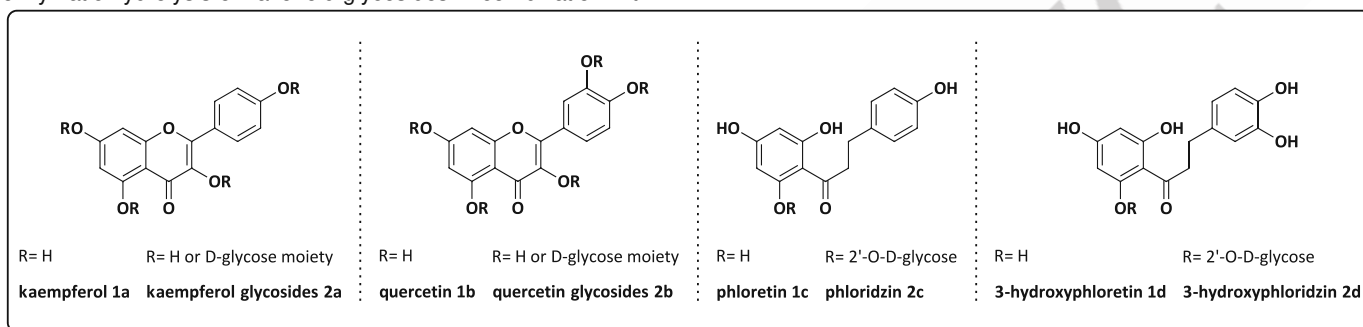
Figure 2: Most abundant flavonoids extracted from apple pomace (cultivar Topaz) in this work: Flavonoid aglycones **1a-d** obtained via enzymatic hydrolysis of flavonoid glycosides **2a-d** and supercritical fluid extraction. Quantification was performed via high-performance liquid chromatography (HPLC).

Results and Discussion

The Way to a Simultaneous Snailase-Assisted Supercritical Fluid Extraction: Overview of the Concept

As illustrated in **Figure 1**, this work is separated in three main parts: A) The supercritical fluid extraction of primarily flavonoid glycosides **2a-d** from apple pomace, B) the enhancement of enzymatic hydrolysis and supercritical fluid extraction of primarily flavonoid aglycones from apple pomace in a sequential process, and ultimately, C) the simultaneous enzyme-assisted supercritical fluid extraction of primarily flavonoid aglycones from apple pomace.

Initial supercritical fluid extractions of flavonoid glycosides **2a-d** (**Figure 1A**) show the limitations of extracting polar glycosylated compounds with nonpolar supercritical carbon dioxide compared to their aglycone species **1a-d**. The penetration depth of carbon dioxide into the plant tissue, and thus the efficiency of the extraction is limited due to the fact that the bioactive compounds are embedded into a robust matrix, the plant tissue.[1c] For this reason, the enzyme mix snailase was introduced to the extraction process to digest the apple pomace and to enzymatically hydrolyze the targeted flavonoid glycosides before supercritical fluid extraction. This sequential process is depicted in **Figure 1B**. With the aid of snailase, it was possible to enzymatically digest and deform the plant tissue in order to enhance the supercritical fluid extraction due to an easier penetration[10] of carbon dioxide,

and therefore, a facilitated release of flavonoids. At the same time, the polar flavonoid glycosides were enzymatically hydrolyzed to less polar flavonoid aglycones, improving the extractability with nonpolar supercritical carbon dioxide containing small amounts of polar cosolvent. Furthermore, the separation of water-soluble snailase, plant tissue, flavonoid glycosides and the remaining sugar moieties is triggered. However, we mainly focused on studying the ratio of glycosides **2a-d** to aglycones **1a-d,** as well as the total yields under different conditions. An energy demanding and interruptive lyophilization step was necessary in the sequential process, because a flow extraction vessel (**Figure S1**, (**6**)) was used for supercritical fluid extraction.

For this reason, a simultaneous process (**Figure 1C**) for EA-SFE was carried out after investigating the influence of the amount of snailase, grinding the apple pomace, the time of hydrolysis and the influence of cosolvent. For this purpose, enzymatic hydrolysis, digestion of plant tissue and supercritical fluid extraction were performed at the same time in a batch extraction vessel without lyophilizing the enzymatically treated apple pomace beforehand. The successful application of enzyme during the simultaneous process revealed the potential of using snailase under pressurized conditions and the influence of pH-lowering supercritical carbon dioxide in a scalable industrial process.

3

51

RESEARCH ARTICLE

A) Supercritical Fluid Extractions of Flavonoid Glycosides 2a-d from Enzymatically Untreated Apple Pomace

We commenced our studies with the supercritical carbon dioxide extraction of flavonoids from enzymatically untreated, dried and ground apple pomace using ethanol as polar cosolvent (**Figure 3**). The cultivar Topaz[39], which is commonly less susceptible to scab and therefore popular in organic orchards, was chosen as feed material, due to favorable flavonoid concentrations compared with other apple varieties found by preliminary conventional ethanolic extraction. Quantification via HPLC revealed that flavonols (**2a-b**) and dihydrochalcones (**2c-d**) are the predominant flavonoid glycosides present in apple pomace (**Figure 2**).

For the initial supercritical carbon dioxide extractions, dried and ground apple pomace was loaded into a flow extraction vessel (**Figure S1**, (**6**)). Extraction conditions were modified according to literature[40]. Ethanol as a polar and sustainable organic cosolvent[37] was required for extraction since preliminary extractions with pure supercritical carbon dioxide were not feasible.
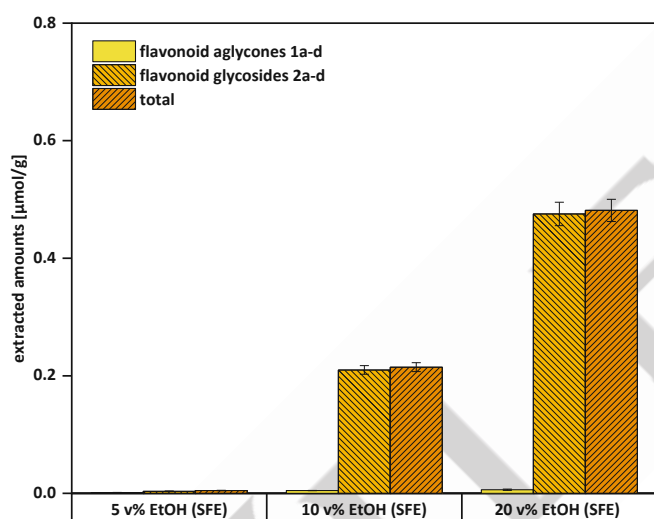
Figure 3: Results (µmol/g) of SFE of enzymatically untreated apple pomace: Conditions for SFE: 3.0 g apple pomace (dried and ground), 2 mL/min total flow, 5—20 v% EtOH, 60 °C, 25 MPa, 2 h. Experiments were performed in triplicate and results are reported as mean values.

Table 1: Composition of flavonoid glycosides and aglycones in % in extracts obtained by SFE illustrated in **Figure 3**.

	5 v% EtOH (SFE)	10 v% EtOH (SFE)	20 v% EtOH (SFE)
1a-d	28%	2%	1%
2a-d	72%	98%	99%

The results of supercritical fluid extraction of enzymatically untreated apple pomace (**Figure 3**) revealed that 5 v% of ethanol as cosolvent result in the extraction of a negligibly small amount of flavonoid glycosides **2a-d** (< 0.01 µmol/g). Yields increased with higher amounts of cosolvent, achieving 0.21 µmol/g with 10 v% EtOH and reaching 0.48 µmol/g at 20 v% EtOH. In total, one kaempferol glycoside **2a** (2%), five quercetin glycosides **2b** (84%), phloridzin **2c** (12%) and 3-hydroxyphloridzin **2d** (1%) were detected. Additionally, without enzymatic treatment, a small amount of < 1% of the extract (**Table 1**) referred to quercetin **1b**, the most abundant flavonoid aglycone in apple pomace found after performing snailase-assisted supercritical fluid extractions.

On the other hand, 0.82 µmol/g of flavonoid glycosides **2a-d** (flavonoid aglycones **1a-d**: 0.01 µmol/g) were achieved with conventional ethanolic extraction, indicating the importance of the efficient enzymatic hydrolysis of flavonoid glycosides by snailase[21]. In particular, releasing hydrolyzed less polar flavonoid aglycones **1a-d** from enzymatically digested plant tissue allows to use nonpolar, non-flammable and non-toxic carbon dioxide with a minimum amount of sustainable organic cosolvent due to a facilitated penetration of extractant into the matrix.[10] Hence, the consumption of volatile organic solvents and the consecutive evaporation can be minimized, while yields can be improved by snailase-assisted supercritical fluid extraction.

B) Enhancement of Snailase-Assisted Supercritical Carbon Dioxide Extraction of Flavonoids from Apple Pomace

To investigate the influence of enzymatic pre-treatment, the following optimization of EA-SFE was carried out in a sequential manner in order to exclude a pressure dependent activity of snailase, as well as the pH-lowering influence of carbon dioxide on the activity of enzyme[38]. Thus, the enzymatically treated samples were lyophilized and loaded into a flow extraction vessel for subsequent supercritical carbon dioxide extraction. For enzymatic hydrolysis, snailase buffer (0—20%) and dried apple pomace were suspended in McIlvaine buffer and shaken for variable times (0.5 h, 1 h, 2 h) in an incubator at 37 °C. Supercritical fluid extractions were carried out as described in chapter A for untreated apple pomace (**Figure 3**; 2 mL/min total flow, 20 v% EtOH, 60 °C, 25 MPa, 2 h).

Our previous study[21] revealed that the optimized temperature and pH-value for snailase-assisted hydrolysis of flavonoids are T = 37 °C and pH = 5.5. Thus, we focused on studying other parameters (chapter B1—3) relevant for extracting supercritically herein, namely, the amount of snailase to digest the plant material and hydrolyze the flavonoid glycosides (**Figure 4**), the relevance of grinding the dried biomass (**Table 3**, **Figure S2**), as well as the incubation time for enzymatic hydrolysis (**Figure 5**). In a last step, the optimal amount and type of cosolvent were investigated (**Figure 6**).
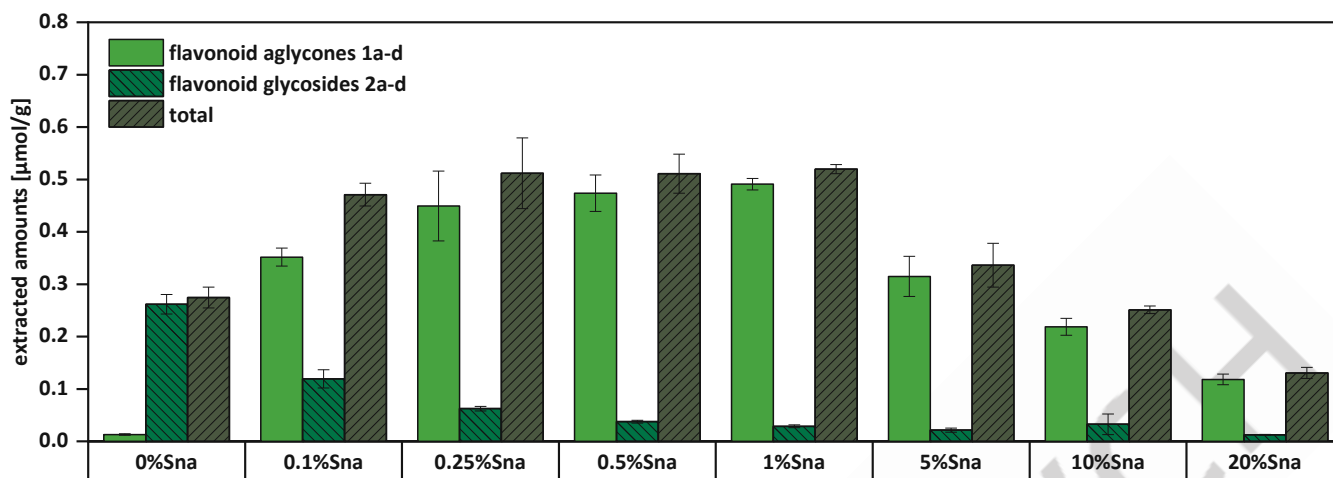
Figure 4: Results (µmol/g) of varying the amount of snailase for EA-SFE. Conditions for enzymatic hydrolysis: 3 g apple pomace (dried and ground), snailase (0—20%, 0—3.0 g/15 mL), 15 mL 0.1 M McIlvaine buffer (pH = 5.5), shaken for 1 h (37 °C, 180 rpm), lyophilized for 48 h; conditions for SFE: 2 mL/min total flow, 20 v% EtOH, 60 °C, 25 MPa, 2 h. Experiments were performed in triplicate and results are reported as mean values. Sna: Snailase.

Table 2: Composition of flavonoid glycosides and aglycones in % in the extracts obtained by EA-SFE illustrated in **Figure 4**.

	0%Sna	0.1%Sna	0.25%Sna	0.5%Sna	1%Sna	5%Sna	10%Sna	20%Sna
1a-d	5%	75%	88%	93%	94%	94%	87%	90%
2a-d	95%	25%	12%	7%	6%	6%	13%	10%

B1) Influence of Amount of Snailase and Relevance of Grinding Apple Pomace

As shown in **Figure 4,** when incubating apple pomace with enzyme-free buffer (**0%Sna**), low amounts of flavonoid aglycones **1a-d** (0.01 µmol/g), already present in the untreated raw material (**Table 1**), were extracted. Thereby demonstrating that an increase in total yields, in particular of flavonoid aglycones **1a-d**, correlates with the addition of snailase. Variation of the enzyme amount (**Figure 4**) revealed that no more than 0.1 % of snailase lead to a high enzymatic hydrolysis yield of 75% (**Table 2**). This resulted in yields of 0.35 µmol/g of flavonoid aglycones **1a-d** and improved the total yields up to 0.47 µmol/g when compared to the enzyme-free experiment (0.27 µmol/g, **0%Sna**).

A further increase of snailase in buffer up to 0.25%, 0.5% and 1% resulted in an efficient removal of sugar moieties demonstrated by the content of flavonoid glycosides **2a-d** ranging from 6—12% in the extracts (**Table 2**). In these cases, comparable yields of 0.45—0.49 µmol/g of flavonoid aglycones **1a-d** ($p < 0.05$) were obtained, whereas only 0.03—0.06 µmol/g of flavonoid glycosides **2a-d** remained present.

In contrast, higher amounts of enzyme of 5—20% (**Figure 4, 5%Sna, 10%Sna, 20%Sna**) showed no further improvement in enzymatic hydrolysis as shown in **Table 2**. In addition, total yields of flavonoids decreased significantly to 0.34 µmol/g and lower, when applying 5—20% snailase for enzyme-assisted supercritical fluid extraction ($p < 0.05$).

This data indicates that higher concentrations (0.25—1%) of the digestive enzyme snailase leads, in accordance to its assigned role in nature, to a better release of bioactive compounds from the plant matrix and therefore to higher extraction yields, due to better solubility and accessibility of the targeted flavonoid aglycones in scCO$_2$. However, excessive amounts of enzyme (> 5%) seem to reduce flavonoid aglycone yields by further metabolizing the flavonoid aglycones. Further identification of these products proved to be difficult since, although snailase was already used for the hydrolysis of pure flavonoid glycosides to aglycones [21, 41], further metabolism products were not studied so far.

Table 3:Influence of grinding the apple pomace before enzymatic hydrolysis and supercritical fluid extraction on the yields of flavonoid glycosides and aglycones in µmol/g as well as the relative composition in %.[a] Pictures of ground and unground apple pomace are shown in **Figure S2**.

	flavonoid aglycones 1a-d [µmol/g]	flavonoid glycosides 2a-d [µmol/g]	total [µmol/g]
ground	0.47 ± 0.04 (93%)	0.038 ± 0.003 (7%)	0.51 ± 0.04
unground	0.26 ± 0.04 (58%)	0.19 ± 0.04 (42%)	0.46 ± 0.07

[a] Drying was performed at 60 °C for 48 h and grinding was carried out with a cutting mill using a 2 mm sieve. Conditions for enzymatic hydrolysis: 3 g apple pomace (dried; ground (average particle diameter: 0.3 ± 0.2 mm, **Figure S2**) or unground (average particle diameter: 11 ± 3 mm, **Figure S2**), snailase (0.5%, 0.075 g/15 mL), 15 mL 0.1 M McIlvaine buffer (pH = 5.5), shaken for 1 h (37 °C, 180 rpm), lyophilized for 48 h; conditions for SFE: 2 mL/min total flow, 20 v% EtOH, 60 °C, 25 MPa, 2 h. Experiments were performed in triplicate and results are reported as mean values.

RESEARCH ARTICLE

As a next step, we investigated if grinding the apple pomace has an impact on the efficiency of hydrolysis and supercritical fluid extraction. As shown in **Table 3,** the relative content of flavonoid aglycones **1a-d** increased from 58% (0.26 μmol/g) to 93% (0.47 μmol/g) when ground apple pomace was used. This indicates that the greater surface area has a beneficial effect on the efficiency of enzymatic hydrolysis. In contrast, the total amount of extracted flavonoid glycosides **2a-d** and flavonoid aglycones **1a-d** were comparable for both experiments, demonstrating that there is no significant influence of the grinding process on the efficiency of supercritical fluid extraction ($p < 0.05$). Further experiments were conducted with ground apple pomace and 0.25%, 0.5% and 1% of snailase, since these amounts resulted in an efficient cleavage of sugar moieties of 88—94%, which corresponds to the yields of flavonoid aglycones **1a-d** of 0.45—0.49 μmol/g gained SFE (**Figure 4**).
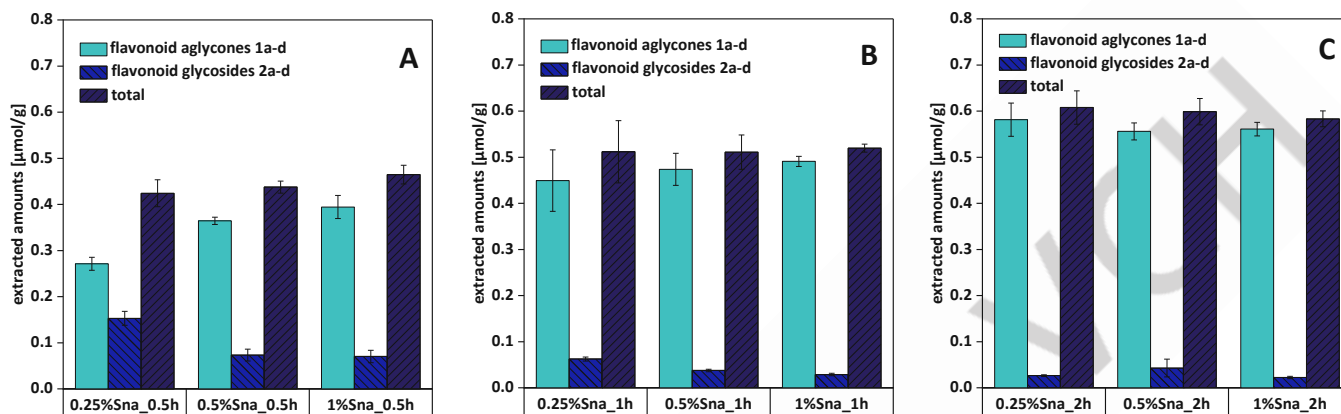
Figure 5: Results (μmol/g) of EA-SFE performed for 0.5 h (A), 1 h (B) and 2 h (C). Conditions for enzymatic hydrolysis: 3 g apple pomace (dried and ground), snailase (0.25—1%, 0.037—0.15 g/15 mL), 15 mL 0.1 M McIlvaine buffer (pH = 5.5), shaken for 0.5 h, 1 h or 2 h (37 °C, 180 rpm), lyophilized for 48 h; conditions for SFE: 2 mL/min total flow, 20 v% EtOH, 60 °C, 25 MPa, 2 h. Experiments were performed in triplicate and results are reported as mean values. Sna: Snailase.

Table 4: Composition of flavonoid glycosides and aglycones in % in extracts obtained by EA-SFE illustrated in **Figure 5A-C.**

	(A)			(B)			(C)		
	0.25%Sna 0.5h	0.5%Sna 0.5 h	1%Sna 0.5h	0.25%Sna 1h	0.5%Sna 1 h	1%Sna 1h	0.25%Sna 2h	0.5%Sna 2 h	1%Sna 2h
1a-d	64%	83%	85%	88%	93%	94%	96%	93%	96%
2a-d	36%	17%	15%	12%	7%	6%	4%	7%	4%

B2) Influence of Incubation Time During Enzymatic Hydrolysis

After investigating the amount of snailase (**Figure 4**) with a fixed reaction time of 1 h we extended our optimization studies by varying the time of enzymatic hydrolysis between 0.5—2 h (**Figure 5A**-**C**). Reducing the incubation time from 1 h to 0.5 h (**Figure 5A**) resulted, in case of 0.25% snailase (**Figure 5C, 0.25%Sna_0.5h**), in an threefold increase of flavonoid glycosides **2a-d** to 0.15 μmol/g (36% of the total composition). Thus, to a less efficient hydrolysis. Comparable behavior can be seen, when using 0.5% or 1% snailase buffer for 30 min (**Table 4**). In addition, no difference between the total yields of the conducted experiments at 30 min and 60 min for the three tested amounts of snailase can be reported ($p < 0.05$).

On the other hand, doubling the time to 2 h (**Figure 5C**) improved the efficiency of enzymatic hydrolysis arising in an increase of flavonoid aglycones **1a-d** of up to 96% when using 0.25% or 1% of snailase. Thus, leading to a better hydrolysis yield compared with the experiments performed for 1h or 30 min. Due to comparable yields at 2h between the three tested amounts of enzyme, the lower amounts of snailase (0.25-0.5%) and thus, the less expensive alternative was chosen for further experiments.

In addition to a more complete cleavage of flavonoid glycosides **2a-d** to their aglycones when performing enzymatic-assisted supercritical fluid extraction for 2 h (**Figure 5C**), the extension of time led, in case of 0.25% snailase, to significantly higher yields of flavonoid aglycones **1a-d** of 0.58 μmol/g, when compared to its respective one-hour experiment ($p < 0.05$). This can be explained by the improved digestion of cell walls in plant tissue, and thus leading to a better release of flavonoid glycosides **2a-d** for subsequent enzymatic cleavage.

The screening of time was not further extended to longer incubation times than 2h, because the total yields were not significantly improving between 1 h and 2 h ($p < 0.05$). Thus, no further improvement of the release of flavonoids by enzymatic digestion could be expected.

6

RESEARCH ARTICLE
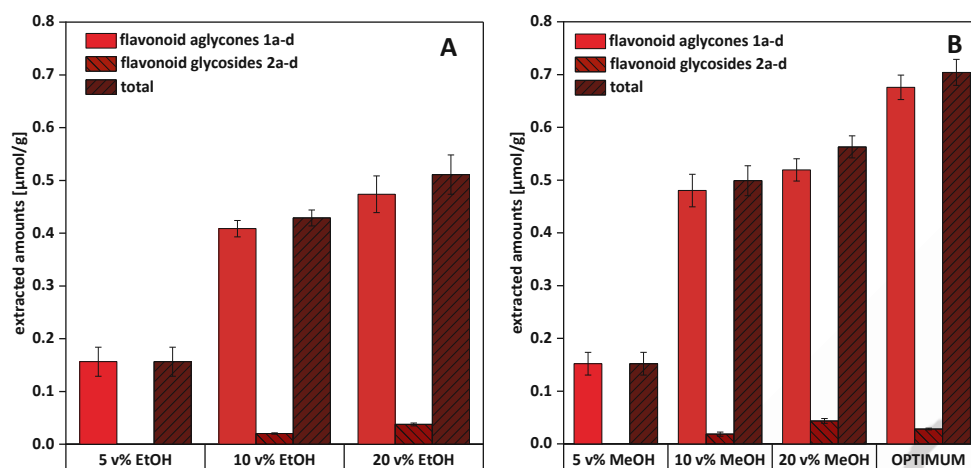
Figure 6: Results (µmol/g) of EA-SFE using ethanol (A) and methanol (B) as cosolvents of flavonoid aglycones 1a-d. Furthermore, results applying the optimum conditions for the sequential process (OPTIMUM – 0.25% snailase, 2 h incubation time, 20 v% MeOH) are illustrated (B). Conditions for enzymatic hydrolysis: 3 g apple pomace (dried and ground), snailase (0.5%, 0.075 g/15 mL; optimum conditions: 0.25%, 0.037 g/15 mL), 15 mL McIlvaine buffer (pH = 5.5), shaken for 1 h (finally optimized conditions: 2 h) (37 °C, 180 rpm), lyophilized for 48 h; conditions for SFE: 2 mL/min total flow, 5-20 v% EtOH or MeOH (optimum conditions: 20 v% MeOH), 60 °C, 25 MPa, 2 h. Experiments were performed in triplicate and results are reported as mean values

Table 5: Composition of flavonoid glycosides and aglycones in % in extracts obtained by EA-SFE illustrated in **Figure 6A-B**.

	(A)			(B)			
	5 v% EtOH	10 v% EtOH	20 v% EtOH	5 v% MeOH	10 v% MeOH	20 v% MeOH	OPTIMUM
1a-d	100%	95%	93%	100%	96%	92%	96%
2a-d	0%	5%	7%	0%	4%	8%	4%

B3) Influence of Type and Amount of Cosolvent

In parallel to the screening of the incubation time, the influence of the amount of polar cosolvents for supercritical fluid extractions, namely ethanol and methanol was investigated, using 0.5% of snailase for enzymatic hydrolysis (**Figure 6**).

While the influence of pressure and temperature on SFE of flavonoids from plant material is described in literature, less data exists on the influence of different organic cosolvents[35, 40a, 42]. For instance, water as cosolvent was not suitable for our process due to the expectable contamination of extract with water-soluble enzyme. These studies additionally revealed that temperatures up to 60—80 °C result in optimal extraction yields of flavonoids, but higher temperatures tend to degrade selected flavonoids. In addition, higher pressures of 25—30 MPa have been reported to be beneficial for extraction yields.

As illustrated in **Figure 6**, the total amount of extracted flavonoid aglycones **1a-d** and flavonoid glycosides **2a-d** increased with higher amounts of cosolvent, independently of applying ethanol or methanol. However, even at low amounts of cosolvent of 5 v%, substantial amounts of 0.15—0.16 µmol/g of flavonoid aglycones **1a-d** without detected traces of flavonoid glycosides were extracted. This result underlines the digestion power of snailase (0.5% of snailase, 0.075 g snailase /15 mL McIlvaine buffer) since 5 v% cosolvent turned out to be unfeasible when using enzymatically untreated apple pomace for sole supercritical fluid

extraction (**Figure 3**). It is noteworthy, that with 5 v% of cosolvent no flavonoid glycosides **2a-d** were extracted due to their higher polarity, thus providing the additional benefit of separating flavonoid glycosides **2a-d** from their respective flavonoid aglycones **1a-d.**

Furthermore, it was shown that the yields increased with 10—20 v% of cosolvent. The yields of flavonoid aglycones **1a-d** were slightly higher with methanol (**Figure 6B**, 10v%: 0.48 µmol/g; 20v%: 0.52 µmol/g) compared with ethanol (**Figure 6A**, 10v%: 0.41 µmol/g; 20v%: 0.47 µmol/g), due to the higher polarity of cosolvent.

Ultimately, the optimum conditions of all performed screenings (**Figure 6B**, OPTIMUM: 0.25% of snailase, 0.037 g snailase /15 mL McIlvaine buffer, ground apple pomace, , 2 h of enzymatic hydrolysis; 20 v% MeOH as cosolvent) were combined and resulted in an efficient sugar moiety removal of flavonoid glycosides **2a-d** and a beneficial digestion of cell walls in the plant material, even with a small amount of snailase. Thus, enabling a successful supercritical fluid extraction with a minimum amount of organic cosolvent. The extract obtained under optimized conditions (**Table 6**) contained 74% of quercetin **1b**, 12% of 3-hydroxyphloretin **1d**, 9% of phloretin **1c** and 2% of kaempferol **1a**. In total, 96% of the flavonoid composition is assigned to the desired flavonoid aglycones **1a-d**. The unconverted flavonoid glycosides **2a-d** primarily contained quercetin glycoside **2b** with a relative content of 3% in the extract.

RESEARCH ARTICLE

Moreover, 90% of the quantified compounds were extracted in the first hour, while the remaining 10% contain: 7% of quercetin **1b** and 1% of 3-hydroxyphloretin **1d**, whereas the amounts of the aglycones kaempferol **1a** and phloretin **1c,** as well as the flavonoid glycosides **2b** and **2d**, were below 1% or not detected as in case of kaempferol glycoside **2a** and phloridzin **2c**. This time dependent extraction does not only offer the potential for separating different flavonoids, but additionally allows a reduction of time, depending on the targeted flavonoids. Thus, the overall consumption of resources (e.g., organic solvent, carbon dioxide, electrical power) can be further minimized.

The yields of flavonoids achieved by the initial supercritical fluid extraction of untreated apple pomace (**Figure 3**) were successfully improved by enzymatic hydrolysis of glycoside moieties. This underlines the importance of lower polarity of flavonoid aglycones **1a-d** by enzymatic hydrolysis and the improved release of flavonoids by enzymatic digestion and deformation of the cell walls.

Table 6: Results (µmol/g) of the snailase-assisted supercritical carbon dioxide extraction of flavonoid aglycones **1a-d** and flavonoid glycosides **2a-d** from apple pomace applying the optimum conditions for the sequential process (**Figure 6B** - OPTIMUM).[a]

type of flavonoid	Yields after supercritical fluid extraction [µmol/g]					
	1st hour (fraction 1)		2nd hour (fraction 2)		total	
kaempferol **1a**	0.0139 ± 0.0003	2%	0.0011 ± 0.0001	<1%	0.0150 ± 0.0003	2%
quercetin **1b**	0.47 ± 0.02	66%	0.051 ± 0.001	7%	0.52 ± 0.02	74%
phloretin **1c**	0.056 ± 0.003	8%	0.0043 ± 0.0002	<1%	0.060 ± 0.003	9%
3-hydroxyphloretin **1d**	0.074 ± 0.006	11%	0.0083 ± 0.0004	1%	0.082 ± 0.006	12%
total amount of flavonoid aglycones **1a-d**	0.61 ± 0.02	87%	0.0650 ± 0.0009	9%	0.68 ± 0.02	96%
kaempferol glycoside **2a**	0.0007 ± 0.0001	<1%	n.d.	0%	0.0007 ± 0.0001	<1%
quercetin glycosides **2b**	0.019 ± 0.002	3%	0.0049 ± 0.0002	<1%	0.024 ± 0.002	3%
phloridzin **2c**	0.0014 ± 0.0001	<1%	n.d.	0%	0.0014 ± 0.0001	<1%
3-hydroxyphloridzin **2d**	0.00156 ± 0.00005	<1%	0.0009 ± 0.0002	<1%	0.0025 ± 0.0002	<1%
total amount of flavonoid glycosides **2a-d**	0.022 ± 0.002	3%	0.0058 ± 0.0002	<1%	0.028 ± 0.002	4%
total amounts	0.63 ± 0.03	90%	0.0708 ± 0.0008	10%	0.70 ± 0.03	100%

[a] Conditions for enzymatic hydrolysis: 3 g apple pomace (dried and ground), snailase (0.25%, 0.037 g/15 mL), 15 mL McIlvaine buffer (pH = 5.5), shaken for 2 h (37 °C, 180 rpm), lyophilized for 48 h; conditions for SFE: 2 mL/min total flow, 20 v% MeOH, 60 °C, 25 MPa, 2 h. Experiments were performed in triplicate and results are reported as mean values. n.d. = not detected.

C) Simultaneous Enzyme-Assisted Supercritical Fluid Extraction of Flavonoids

So far, enzymatic hydrolysis and supercritical fluid extraction were carried out sequentially, performing hydrolysis followed by lyophilization of the enzymatically treated apple pomace before subsequent SFE.

Ultimately, we applied the optimized conditions (**Figure 6B**) to a simultaneous process in a batch extraction vessel to provide an alternative and future perspective for a scalable industrial process (**Figure 7**).

For this reason, the following experiments (**Table 7**), were carried out in a batch extraction vessel in order to avoid the energy demanding lyophilization process. In accordance with the optimized conditions, a mixture of dried and ground apple pomace as well as snailase in McIlvaine buffer (0.25%) was loaded into the batch extraction vessel and stirred for 2 h without pressurizing the system in a first attempt (**entry 1**).

Yields of 0.25 µmol/g of flavonoid aglycones **1a-d** were achieved after two hours of supercritical fluid extraction (total flow: 5 mL/min)[43] with 20 v% of MeOH.

Successively (**entry 2**), wet biomass (15 g; approx. 80% of water) was applied to circumvent the initial drying and grinding process of apple pomace. Enzymatic hydrolysis and supercritical fluid extraction were carried out under the same conditions and resulted in yields of 0.08 µmol/g of flavonoid aglycones **1a-d**. The decrease in yield for wet apple pomace, as well as the uncomplete hydrolysis can be attributed to stirring issues of the voluminous wet biomass.
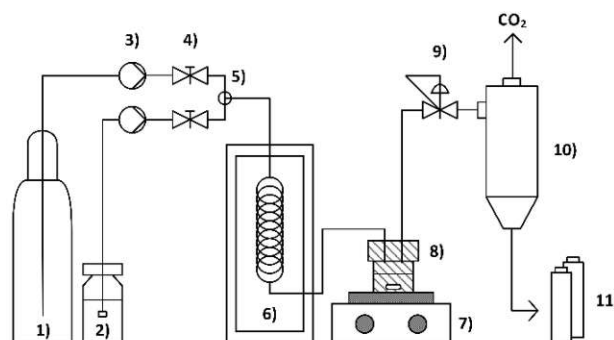
Figure 7: Schematic representation of the SFE set-up for the simultaneous process. (1) carbon dioxide cylinder with ascending pipe; (2) cosolvent supply; (3) HPLC pump; (4) hand operated valve; (5) t-piece; (6) oven with heating coil; (7) magnetic stirrer; (8) batch extraction vessel; (9) back-pressure regulator; (10) gas-liquid separator; (11) product collector

RESEARCH ARTICLE

Ultimately, a simultaneous process for enzymatic hydrolysis (0.25% snailase) and supercritical fluid extraction was conducted (**entry 3** and **entry 4**) for 4 h with a minimum amount of cosolvent (5 v% of MeOH or EtOH), thus pushing the process to the exclusive extraction of flavonoid aglycones **1a-d** (**Figure 6**) as much as possible. The selective extraction of less polar flavonoid aglycones **1a-d** is of crucial importance for the simultaneous process since the polar flavonoid glycosides **2a-d** have to remain in the batch extraction vessel in order to serve permanently as feed substance for enzymatic hydrolysis. The obtained yields of 0.07 µmol/g to 0.09 µmol/g of flavonoid aglycones **1a-d** with MeOH or EtOH as cosolvents (**entry 3** and **entry 4**) demonstrate the high potential of the simultaneous process for the efficient enzyme assisted extraction of valuable flavonoids from apple pomace without lyophilizing the sample in between. In addition, a small amount of snailase (0.25%) was sufficient under pressurized conditions and the pH-lowering effect of $scCO_2$ to extract the desired compounds. Additionally, no further separation of flavonoid aglycones **1a-d** from enzyme is required, as the water-soluble snailase remains in the reactor, thus rendering the process superior to solvent-based conventional extraction techniques.

pomace, snailase was employed in order to facilitate and enhance the extraction via deformation and digestion of plant tissue. Thus, increasing extraction yields due to the improved access and increased penetration depth of carbon dioxide into the pre-treated apple pomace. Flavonoid glycosides were hydrolyzed efficiently by snailase to their less polar flavonoid aglycones, enhancing the extractability with nonpolar supercritical carbon dioxide. After hydrolysis, quercetin **1b** has been identified as the predominant flavonoid aglycone in the extracts. Optimization showed that a small amount of enzyme (0.25% of snailase) is feasible for cleaving sugar moieties efficiently, which additionally, resulted in a further increase of extraction yields.

Moreover, the effect of grinding the apple pomace, the time of hydrolysis and the influence of cosolvents as well as extraction time during SFE were studied. Firstly, the results reveal that grinding is beneficial due to a greater surface area, leading to higher amounts of aglycones in the extracts. Secondly, two hours of enzymatic hydrolysis, in dependence of the amount of enzyme, result in an efficient hydrolysis of up to 96%. Thirdly, one hour of extraction is sufficient to obtain more than 90% of the targeted flavonoids for the optimized process. Finally, EA-SFE with 20 v% methanol as cosolvent led the highest extraction yields of flavonoid aglycones **1a-d** of 0.68 µmol/g.

Ultimately, the outstanding effect of the sole extraction of low polar flavonoid aglycones **1a-d** and thus the separation from feed glycosides **2a-d** with 5 v% of cosolvent was used for a simultaneous process combining enzymatic hydrolysis and supercritical carbon dioxide extraction, avoiding a process interruption by a lyophilization step. Furthermore, it was shown that enzymatic hydrolysis and supercritical carbon dioxide extraction can be successfully performed with dry but also wet apple pomace, avoiding further drying and milling. These experiments showed the potential for a scalable industrial process for snailase-assisted supercritical fluid extraction of flavonoids from apple pomace in the future. Moreover, the novel enzyme-assisted supercritical fluid extraction strategy developed herein is not limited to apple pomace as raw material, since the enzyme mix snailase and supercritical fluid extraction can be employed to numerous other plant materials.

Table 7: Results (µmol/g) of EA-SFE employing the batch extraction vessel.

entry	process parameter	flavonoid aglycones 1a-d [µmol/g]	flavonoid glycosides 2a-d [µmol/g]	total amounts [µmol/g]
1	sequential[a] 20 v% MeOH dried pomace	0.25 ± 0.02	0.09 ± 0.07	0.34 ± 0.05
2	sequential[a] 20 v% MeOH wet pomace	0.08 ± 0.04	0.07 ± 0.02	0.15 ± 0.06
3	simultaneous[b] 5 v% MeOH dried pomace	0.07 ± 0.04	0.02 ± 0.02	0.09 ± 0.05
4	simultaneous[b] 5 v% EtOH dried pomace	0.09 ± 0.07	0.004 ± 0.003	0.09 ± 0.07

[a] Conditions: 3 g dried and ground or 15 g wet apple pomace (approx. 80% water), snailase (0.25%, 0.037 g/15 mL), 15 mL 0.1 M McIlvaine buffer (pH = 5.5), stirred for 2 h at 37 °C in the batch extraction vessel; subsequent SFE with a total flow of 5 mL/min with 20 v% MeOH at 60 °C and 25 MPa for 2 h. [b] Conditions for the simultaneous process: 3 g apple pomace (dried and ground), snailase (0.25%, 0.037 g/15 mL), 15 mL McIlvaine buffer (pH=5.5), stirred at 60 °C in the batch extraction vessel, simultaneous SFE with a total flow of 5 mL/min with 5 v% MeOH or EtOH at 60 °C and 25 MPa for 4 h. Experiments were performed in triplicate and results are reported as mean values.

Conclusion

We investigated the sequential and simultaneous snailase-assisted supercritical carbon dioxide extraction of enzymatically hydrolyzed flavonoid aglycones **1a-d** (kaempferol **1a**, quercetin **1b**, phloretin **1c** and 3-hydroxyphloretin **1d**) and their glycosides **2a-d** from apple pomace. After initial SFE of primarily polar flavonoid glycosides **2a-d** from enzymatically untreated apple

Experimental Section

Biomass and Enzyme

Topaz apples were cultivated in Austria, 3400 Klosterneuburg. In total, 20 kg of apples were washed, sorted, crushed using a centrifugal grinder (Voran, 4632 Pichl bei Wels, Austria) and pressed with a hydraulic press (40 L, Speidel Tank- und Behälterbau GmbH, 72131 Ofterdingen, Germany). The pomace was dried in a drying cabinet (11 m², Kreuzmayr, 4702 Wallern an der Trattnach, Austria) at 65° C for 16 hours. The aw values of the pomace were determined (Novasina, LabTouch-aw, Zeller, 6845 Hohenems, Austria) (aw value: wet: 0.977, aw value dry: 0.349). Dry apple pomace was further ground with a Fritsch Universal Pulverisette 19 cutting mill (Oberstein, Germany) using a 2 mm sieve and stored in a desiccator over silica gel drying agent.

57

RESEARCH ARTICLE

Lyophilized snailase was purchased from Abbexa Limited (Art. No. abx082089).

Conventional Extraction

Conventional extraction was carried out with 15 mL of ethanol and 1 g of dried and ground apple pomace, the suspension was stirred at room temperature for 2 h.

Supercritical Fluid Extraction

Supercritical fluid extraction was carried out with an SFE-device from Jasco (Jasco Cooperation, Tokyo, Japan). Carbon dioxide (Messer Austria GmbH, > 99.995% purity, ascension pipe) was introduced by two HPLC pumps (PU-2086Plus), pump heads were cooled to -7 °C with a recirculating cooler (CF 40, JULABO GmbH). HPLC grade cosolvents were introduced by another HPLC pump (PU-2089Plus) and a t-piece served as a mixer. The samples for supercritical fluid extraction were loaded into a flow extraction vessel (high pressure vessel EV-2-10, Jasco Cooperation, Tokyo, Japan, 10 mL volume, 130 mm length, 10 mm ID, 32 mm OD, material SU316L, PEEK seals, 2 µm filter) and heated up in a column oven (CO-2060Plus; maximum temperature: 80 °C) to 60 °C. Pressure was released by a back-pressure regulator (BP-2080Plus, temperature set to 60 °C) and extracts were collected via a product collector (SCF-Vch-Bp) in 40 mL vials. All devices were connected with 1/16" stainless steel tubing (VICI Pre-Cut Tube-Kit, 1/16" OD x 0.030"/0.75mm ID, 5-100 cm length, material 316SS).

Supercritical Fluid Extraction of Flavonoid Glycosides 2a-d from Enzymatically Untreated Apple Pomace (Part A)

Supercritical fluid extraction was carried out according to a modified procedure gleaned from literature[40a].

For SFE, 3.0 g of dried and ground, but enzymatically untreated apple pomace, was loaded into the flow extraction vessel, pressurized to 25 MPa and heated up to 60 °C. The total flow of carbon dioxide and cosolvent was set to 2 mL/min (5—20 v% EtOH). Supercritical fluid extraction was carried out for 2 h, extracts were collected in 40 mL glass vials (1 h / fraction) and were further analyzed via HPLC (see chapter below). Experiments were performed in triplicate.

Sequential Enzymatic Hydrolysis and Supercritical Fluid Extraction of Flavonoid Aglycones 1a-d (Part B)

Snailase (e.g. 0.25%, 0.037 g / 15 mL buffer) and 3.0 g of dried apple pomace were suspended in 15 mL 0.1M McIlvaine buffer (for 200 mL buffer: 3.60 g Na_2HPO_4 2 H_2O, 0.80 g (+)-sodium L-ascorbate, adjustment of pH value to 5.5 with citric acid of a concentration of 0.6 g/mL). For enzymatic hydrolysis[21], the suspension was shaken at 180 rpm in an incubator (B. Braun Biotech International, Certomat BS-1) at 37 °C for 0.5 h, 1 h or 2 h. After incubation, the samples were shock frozen with liquid nitrogen and lyophilized (Flexi-Dry MP) for 48 h. The lyophilized samples were cooled and crushed in a mortar with liquid nitrogen and loaded into the flow extraction vessel. The vessel was pressurized to 25 MPa and heated up to 60 °C. The total flow of

carbon dioxide and cosolvent (5—20 v% EtOH or MeOH) was set to 2 mL/min. Supercritical fluid extraction was carried out for 2 h, the extracts were collected in 40 mL glass vials (1 h per fraction) and were further analyzed via HPLC. Experiments were performed in triplicate.

Simultaneous Enzymatic Hydrolysis and Supercritical Fluid Extraction of Flavonoid Aglycones 1a-d (Part C, Table 7, Entry 3 and Entry 4)

Buffer with snailase and apple pomace was prepared as described before, however, in a batch extraction vessel (EV-3, Jasco Cooperation, Tokyo, Japan, 40 mL volume) with 0.5 g glass wool on top of the solution. The vessel was pressurized to 25 MPa and heated up to 60 °C using a magnetic stirrer (**Figure 7**). The total flow of carbon dioxide and cosolvent (5 v% MeOH or EtOH) was set to 5 mL/min in accordance to a previous project[43], where the batch extraction vessel was used for SFE. Supercritical fluid extraction was carried out for 4 h, the extracts were collected in 40 mL glass vials (2 h per fraction) and were further analyzed via HPLC. Experiments were performed in triplicate.

Quantification via HPLC

For quantification, extracts were diluted with cosolvent (EtOH or MeOH) to 5 mL (5 v% cosolvent used for SFE) or 25 mL (10—20 v% cosolvent used for SFE). An aliquot of 200 µL was further diluted with 100 µL mobile phase (0.1 v% formic acid in acetonitrile) and centrifuged, 80 µL of the supernatant was used for HPLC measurements (4 µL injection volume). Quantification was carried out with a Dionex UltiMate RSLC System equipped with a Dionex AcclaimTM RSLC 120 C18 column (2.2 µm, 120 Å, 2.1 × 150 mm, Bonded Silica Products: no. 01425071) and a DAD-3000RS Photodiode Array Detector (Thermo Scientific, Germany). The temperature oven was heated up to 25 °C, and the flow rate was set to 0.2 mL/min. The following gradient of 0.1 v% formic acid in H_2O (A) and 0.1 v% formic acid in acetonitrile (B) was used for elution: 4 min equilibration at 7.5 v% (B), 22 min to 53 v% (B), 5 min to 95 v% (B), 5 min at 95 v% (B), 1 min to 7.5 v% (B) and 2 min at 7.5 v% (B). Calibration and quantification for flavonols **1a-b** and **2a-b** were performed with quercetin **1b** (≥99%, Extrasynthese, France) and for dihydrochalcones **1c-d** and **2c-d** with phloretin **1c** (≥99%, SigmaAldrich, USA). Additional information for the calibration is given in the supplement material (**Figure S3**, **Table S2**).

Identification of Flavonoids via UHPLC-ESI-qTOF-MS

The method was adapted from literature[21, 44]. Flavonoids were identified using a 1290 Infinity II LC System equipped with a ZORBAX Eclipse Plus C18 Rapid Resolution HD (1.8 µm, 2.1 × 150 mm) which was connected to a G7117C diode array detector and a 6545 LC/Q-TOF (Agilent, USA) with a Dual Agilent Jet Stream ESI ion source. Flow rate was set to 0.3 ml/min, the column oven was heated up to 35 °C. Mobile phase was used with the following gradients: 1 min at 5 v% (B), 4 min from 5 to 15 v% (B), 6 min to 53 v% (B), 4 min to 100 v% (B), 6.5 min at 100 v% (B), 0.5 min to 5 v%, and post run 4 min at 5 v% (B). The wavelength during analysis was set to 290 nm. All solvents were

58

of LC-MS grade. Mass spectrums were recorded in ESI-negative mode between m/z 100 and 1,000 Da (scan rate: 2 spectra/s) after a 5 min solvent cut. The mass spectrometer operated at the following conditions: gas temp.: 350 °C, gas flow: 10 l/min, nebulizer: 40 psig, sheathgas temp.: 350 °C, sheathgas flow: 12 L/min, VCap: 3.5 kV, nozzle: 0 V fragmentor: 180 V, skimmer: 75 V, octopoleRFpeak: 600 V.

Characterization of flavonoids was carried out by comparing retention times, substance specific UV absorbance as well as mass spectrometric data (molecular ion, fragments). Further details are provided in **Table S1**.

Statistical Analysis

Statistical tests were performed with OriginPro 2021b. For experiments conducted in triplicate, one-way ANOVA tests were carried out at significance level of 0.05 followed by Tukey's honestly significant difference (HSD) post-hoc tests.

[1] aA. Krakowska-Sieprawska, K. Rafinska, J. Walczak-Skierska, A. Kielbasa, B. Buszewski, *Materials* **2021**, *14*, 2724; bQ. Wang, J. Huang, H. Shao, Y. Zhou, K. Xia, F. Huang, H. Zhang, X. Yang, *Food Science and Technology Research* **2019**, *25*, 755-763; cP. D. Patil, S. P. Patil, R. K. Kelkar, N. P. Patil, P. V. Pise, S. S. Nadar, *Trends in Food Science & Technology* **2021**, *116*, 357-369.

[2] A. Krakowska, K. Rafinska, J. Walczak, B. Buszewski, *Industrial Crops and Products* **2018**, *124*, 931-940.

[3] aM. Mushtaq, B. Sultana, F. Anwar, A. Adnan, S. S. H. Rizvi, *J Supercrit Fluid* **2015**, *104*, 122-131; bN. Mohamad, N. Ramli, S. Abd-Aziz, M. F. Ibrahim, *3 Biotech* **2019**, *9*, 234; cM. S. Lenucci, M. De Caroli, P. P. Marrese, A. Iurlaro, L. Rescio, V. Bohm, G. Dalessandro, G. Piro, *Food Chem* **2015**, *170*, 193-202.

[4] aA. L. Santana, L. D. Queiros, J. Martinez, G. A. Macedo, *Food and Bioproducts Processing* **2019**, *117*, 194-202; bV. Kitrytė, D. Povilaitis, V. Kraujalienė, V. Šulniūtė, A. Pukalskas, P. R. Venskutonis, *LWT - Food Science and Technology* **2017**, *85*, 534-538; cC. P. Passos, R. M. Silva, F. A. Da Silva, M. A. Coimbra, C. M. Silva, *The Journal of Supercritical Fluids* **2009**, *48*, 225-229.

[5] I. Mackėla, T. Andriekus, P. R. Venskutonis, *Journal of Food Engineering* **2017**, *213*, 38-46.

[6] M. Antunes-Ricardo, J. A. Mendiola, T. Garcia-Cayuela, E. Ibanez, J. A. Gutierrez-Uribe, M. P. Cano, D. Guajardo-Flores, *J Supercrit Fluid* **2020**, *158*, 104713.

[7] aS. Dutta, P. Bhattacharjee, *Journal of Food Engineering* **2017**, *201*, 49-56; bS. Dutta, P. Bhattacharjee, *Journal of Food Measurement and Characterization* **2017**, *11*, 310-319; cS. Dutta, P. Bhattacharjee, *Journal of Bioscience and Bioengineering* **2015**, *120*, 17-23.

[8] M. Mushtaq, B. Sultana, S. Akram, F. Anwar, A. Adnan, S. S. H. Rizvi, *Analytical and Bioanalytical Chemistry* **2017**, *409*, 3645-3655.

[9] H. I. O. Basegmez, D. Povilaitis, V. Kitryte, V. Kraujaliene, V. Sulniute, C. Alasalvar, P. R. Venskutonis, *J Supercrit Fluid* **2017**, *124*, 10-19.

[10] A. R. C. Morais, A. M. da Costa Lopes, R. Bogel-Łukasik, *Chemical Reviews* **2015**, *115*, 3-27.

[11] aD. M. Kopustinskiene, V. Jakstas, A. Savickas, J. Bernatoniene, *Nutrients* **2020**, *12*, 457; bS. L. Badshah, S. Faisal, A. Muhammad, B. G. Poulson, A. H. Emwas, M. Jaremko, *Biomedicine & Pharmacotherapy* **2021**, *140*, 111596; cL. Ciumărnean, M. V. Milaciu, O. Runcan, Ș. C. Vesa, A. L. Răchișan, V. Negrean, M.-G. Perné, V. I. Donca, T.-G. Alexescu, I. Para, G. Dogaru, *Molecules* **2020**, *25*, 4320; dM. Russo, S. Moccia, C. Spagnuolo, I. Tedesco, G. L. Russo, *Chemico-Biological Interactions* **2020**, *328*, 109211; eK. Wen, X. Fang, J. Yang, Y. Yao, S. K. Nandakumar, L. M. Salem, K. Cheng, *Current Medicinal Chemistry* **2021**, *28*, 1042-1066; fM. M. Juca, F. M. S. Cysne Filho, J. C. de Almeida, D. D. S. Mesquita, J. R. M. Barriga, K. C. F. Dias, T. M. Barbosa, L. C. Vasconcelos, L. Leal, J. E. Ribeiro, S. M. M. Vasconcelos, *Nat Prod Res* **2020**, *34*, 692-705.

[12] D. Tungmunnithum, S. Drouet, C. Hano, *Molecules* **2022**, *27*, 1102.

[13] aJ. Ren, D. Su, L. Li, H. Cai, M. Zhang, J. Zhai, M. Li, X. Wu, K. Hu, *Toxicology and Applied Pharmacology* **2020**, *387*, 114846; bJ. M. Al-Khayri, G. R. Sahana, P. Nagella, B. V. Joseph, F. M. Alessa, M. Q. Al-Mssallem, *Molecules* **2022**, *27*, 2901.

[14] M.-n. Wang, Y.-g. Cao, Y.-x. Wei, Y.-j. Ren, Y.-l. Liu, X. Chen, C. He, X.-k. Zheng, W.-s. Feng, *Natural Product Research* **2022**, *36*, 3317-3323.

[15] L. Han, Q. Fu, C. Deng, L. Luo, T. Xiang, H. Zhao, *Scandinavian Journal of Immunology* **2022**, *95*.

[16] A. Di Petrillo, G. Orrù, A. Fais, M. C. Fantini, *Phytotherapy Research* **2022**, *36*, 266-278.

[17] aL. Song, X. Hu, X. Ren, J. Liu, X. Liu, *Frontiers in Pharmacology* **2022**, *13*, bJ. I. M. Pagna, T. Awazi, P. E. Mbarga, I. M. K. Mbekou, P. Mkounga, J. Fotie, M. Frese, F. B. Fabrice, B. N. Lenta, N. Sewald, E. A. Nkengfack, *Journal of Asian Natural Products Research* **2022**, *24*, 1041-1051.

[18] aS. Kalli, C. Araya-Cloutier, J. Chapman, J.-W. Sanders, J.-P. Vincken, *Food Control* **2022**, *132*, 108434; bC. Förster, V. Handrick, Y. Ding, Y. Nakamura, C. Paetz, B. Schneider, G. Castro-Falcón, C. C. Hughes, K. Luck, S. Poosapati, G. Kunert, A. Huffaker, J. Gershenzon, E. A. Schmelz, T. G. Köllner, *Plant Physiology* **2021**, *188*, 167-190; cH. S. H. M. Ali, Y. Anwar, A. Rauf, *South African Journal of Botany* **2022**, *148*, 666-671.

[19] P. C. H. Hollman, *Pharmaceutical Biology* **2004**, *42*, 74-83.

[20] M. E. M. B. de Araújo, Y. E. Moreira Franco, T. G. Alberto, M. A. Sobreiro, M. A. Conrado, D. G. Priolli, A. C. H. Frankland Sawaya, A. L. T. G. Ruiz, J. E. de Carvalho, P. de Oliveira Carvalho, *Food Chemistry* **2013**, *141*, 266-273.

[21] C. Kornpointner, J. Scheibelreiter, H. Halbwirth, *Front Plant Sci* **2022**, *13*, 889184.

[22] Z. Wang, L.-C. Zhao, W. Li, L.-X. Zhang, J. Zhang, J. Liang, *Molecules* **2013**, *18*, 9717-9726.

[23] J.-Y. You, C. Peng, X. Liu, X.-J. Ji, J. Lu, Q. Tong, P. Wei, L. Cong, Z. Li, H. Huang, *Bioresource Technology* **2011**, *102*, 6088-6094.

[24] FAO, "Food and Agriculture Organization of the United Nations - FAOSTAT - Crops and livestock products", can be found under https://www.fao.org/faostat/en/#data/QCL/visualize,2023 (07/2023)

[25] C. A. Perussello, Z. Zhang, A. Marzocchella, B. K. Tiwari, *Compr Rev Food Sci Food Saf* **2017**, *16*, 776-796.

[26] aM. Magyar, L. da Costa Sousa, M. Jin, C. Sarks, V. Balan, *Applied Microbiology and Biotechnology* **2016**, *100*,

7349-7358; bS. Pathania, N. Sharma, S. Handa, *Biocatalysis and Biotransformation* **2017**, *35*, 450-459.

[27]   M. Hijosa-Valsero, A. I. Paniagua-García, R. Díez-Antolínez, *Applied Microbiology and Biotechnology* **2017**, *101*, 8041-8052.

[28]   V. L. Pachapur, S. J. Sarma, S. K. Brar, Y. Le Bihan, G. Buelna, M. Verma, *Bioresource Technology* **2015**, *193*, 297-306.

[29]   F. Xu, S. Zhang, G. I. N. Waterhouse, T. Zhou, Y. Du, D. Sun-Waterhouse, P. Wu, *Food Hydrocolloids* **2022**, *133*, 107945.

[30]   K. Piwowarek, E. Lipińska, E. Hać-Szymańczuk, V. Kolotylo, M. Kieliszek, *Applied Microbiology and Biotechnology* **2022**, *106*, 5433-5448.

[31]   J. Oszmiański, A. Wojdyło, J. Kolniak, *Food Chemistry* **2011**, *127*, 623-631.

[32]   aF. Dranca, E. Talón, M. Vargas, M. Oroian, *Food Hydrocolloids* **2021**, *121*, 107026; bZ. Zhang, M. M. Poojary, A. Choudhary, D. K. Rai, B. K. Tiwari, *Electrophoresis* **2018**, *39*, 1934-1945.

[33]   aL. Pollini, F. Blasi, F. Ianni, L. Grispoldi, S. Moretti, A. Di Veroli, L. Cossignani, B. T. Cenci-Goga, *Molecules* **2022**, *27*, 1933; bI. Egüés, F. Hernandez-Ramos, I. Rivilla, J. Labidi, *Molecules* **2021**, *26*, 3783.

[34]   J. Zheng, H. Li, D. Wang, R. Li, S. Wang, B. Ling, *Food Hydrocolloids* **2021**, *121*, 107031.

[35]   G. Ferrentino, K. Morozova, O. K. Mosibo, M. Ramezani, M. Scampicchio, *Journal of Cleaner Production* **2018**, *186*, 253-261.

[36]   S. Topham, A. Bazzanella, S. Schiebahn, S. Luhr, L. Zhao, A. Otto, D. Stolten, in *Ullmann's Encyclopedia of Industrial Chemistry*, Wiley-VCH Verlag GmbH & Co. KGaA, Weinheim, Germany, **2014**, pp. 1-43.

[37]   D. Prat, J. Hayler, A. Wells, *Green Chemistry* **2014**, *16*, 4546-4551.

[38]   aN. Harper, S. Barreiros, *Biotechnology Progress* **2002**, *18*, 1451-1454; bZ. Wimmer, M. Zarevucka, *Int J Mol Sci* **2010**, *11*, 233-253; cR. Melgosa, M. T. Sanz, Á. G. Solaesa, S. L. Bucio, S. Beltrán, *The Journal of Supercritical Fluids* **2015**, *97*, 51-62.

[39]   A. Vanzo, M. Jenko, U. Vrhovsek, M. Stopar, *Journal of Agricultural and Food Chemistry* **2013**, *61*, 6580-6587.

[40]   aA. Chafer, M. C. Pascual-Martí, A. Salvador, A. Berna, *Journal of Separation Science* **2005**, *28*, 2050-2056; bA. Sainz Martinez, C. Kornpointner, C. Haselmair-Gosch, M. Mikulic-Petkovsek, K. Schröder, H. Halbwirth, *LWT - Food Science and Technology* **2021**, *138*, 110633.

[41]   aC. Liu, R. Li, J. Peng, D. Qu, M. Huang, Y. Chen, *Process Biochemistry* **2019**, *86*, 80-88; bD. Wang, H. Zhao, H. Zhu, L. Wen, J. Yu, L. Li, L. Chen, Y. Geng, *Industrial Crops and Products* **2019**, *129*, 224-230; cJ. Wang, L.-L. Zhao, G.-X. Sun, Y. Liang, F.-A. Wu, Z. Chen, *African Journal of Biotechnology* **2011**, *10*, 1460-1466.

[42]   M. Hoshino, T. Suetsugu, H. Iwai, A. Takamizu, M. Tanaka, A. Quitain, M. Sasaki, M. Goto, *The Materials Research Society of Japan* **2014**, *39*, 309-311.

[43]   C. Kornpointner, A. Sainz Martinez, M. Schnürch, H. Halbwirth, K. Bica-Schröder, *Green Chemistry* **2021**, *23*, 10079-10089.

[44]   A. Schieber, P. Keller, R. Carle, *Journal of Chromatography A* **2001**, *910*, 265-273.
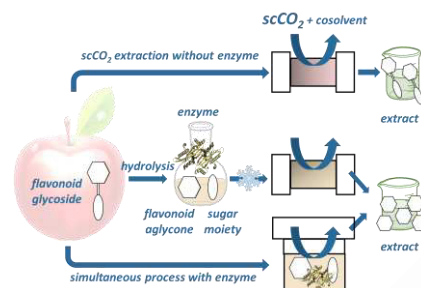
Snailase and supercritical carbon dioxide:

A powerful team for the hydrolysis of flavonoid glycosides and extraction of aglycones (quercetin, kaempferol, phloretin and 3-hydroxyphloretin) from dried and wet apple pomace in a subsequent and simultaneous process!

E Continuous Formation of Limonene Carbonates in Supercritical Carbon Dioxide

Nowadays, cyclic carbonates are produced in bulk quantities driven by the demand for their applications, for example, as electrolyte solutions in lithium-ion batteries or as building blocks for non-isocyanate polyhydroxyurethanes.[159, 160] However, they are mostly based on crude oil. Limonene, with an annual production of 43 Mt in 2020,[161] serves as an ideal bio-based feedstock to circumvent the use of a limited feedstock. Various metal catalysts and ionic liquids as co-catalysts have been studied for the batch-wise production of limonene carbonates, but only tetrabutylammonium halides were applied as single catalysts for the batch-wise production of limonene carbonates.[162-176]
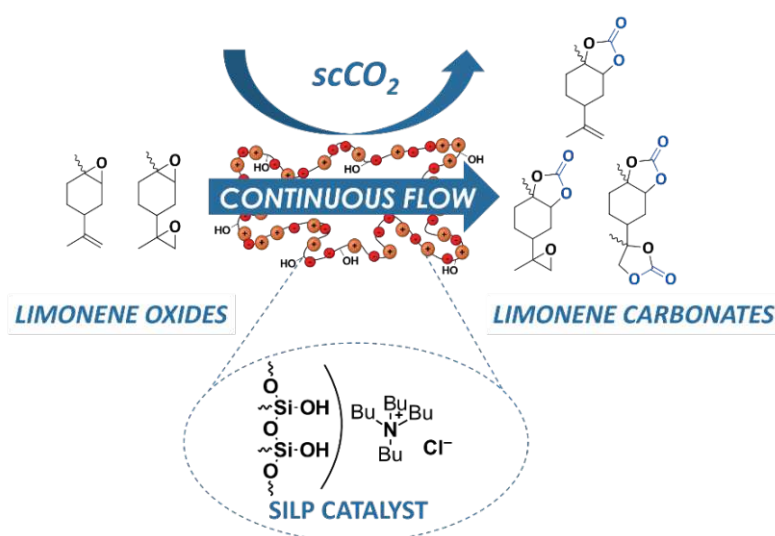
Scheme 30: Continuous formation of cyclic limonene carbonates in supercritical carbon dioxide catalyzed by tetrabutylammonium chloride immobilized on silica, serving as a supported ionic liquid phase (SILP) catalyst.

This project dealt with the continuous formation of cyclic limonene carbonates in supercritical carbon dioxide as reagent and sole solvent, starting from diastereomeric mixtures of limonene oxide and limonene dioxide as bio-based substrates (**Scheme 30**). After a screening of ammonium halides and imidazolium halides as homogeneous catalysts in batch mode, the best-performing catalyst, tetrabutylammonium chloride, was immobilized on silica. The heterogeneous SILP catalyst was characterized by nitrogen adsorption, diffuse reflectance infrared Fourier transform spectroscopy, and thermogravimetric analysis and served as heterogeneous SILP catalyst in continuous flow. After optimization of temperature, pressure, flow rates, and catalyst loading, the long-term stability was further investigated for a period of 48 h.

In the following, the below-mentioned publication is presented:

Miksovsky, P.; Horn, E. N.; Naghdi, S.; Eder, D.; Schnurch, M.; Bica-Schroder, K., Continuous Formation of Limonene Carbonates in Supercritical Carbon Dioxide. *Org Process Res Dev* **2022,** *26* (10), 2799-2810. https://doi.org/10.1021/acs.oprd.2c00143.

As the first author, I contributed to the investigation, conceptualization, methodology, visualization, writing of the original draft, and review of the manuscript.

Continuous Formation of Limonene Carbonates in Supercritical Carbon Dioxide

Philipp Mikšovsky, Elias N. Horn, Shaghayegh Naghdi, Dominik Eder, Michael Schnürch, and Katharina Bica-Schröder*

ACCESS | Metrics & More | Article Recommendations | Supporting Information

ABSTRACT: We present a continuous flow method for the conversion of bioderived limonene oxide and limonene dioxide to limonene carbonates using carbon dioxide in its supercritical state as a reagent and sole solvent. Various ammonium- and imidazolium-based ionic liquids were initially investigated in batch mode. For applying the best-performing and selective catalyst tetrabutylammonium chloride in continuous flow, the ionic liquid was physisorbed on mesoporous silica. In addition to the analysis of surface area and pore size distribution of the best-performing supported ionic liquid phase (SILP) catalysts via nitrogen physisorption, SILPs were characterized by diffuse reflectance infrared Fourier transform spectroscopy and thermogravimetric analysis and served as heterogeneous catalysts in continuous flow. Initially, the continuous flow conversion was optimized in short-term experiments resulting in the desired constant product outputs. Under these conditions, the long-term behavior of the SILP system was studied for a period of 48 h; no leaching of catalyst from the supporting material was observed in the case of limonene oxide and resulted in a yield of 16%. For limonene dioxide, just traces of leached catalysts were detected after reducing the catalyst loading from 30 to 15 wt %, thus enabling a constant product output in 17% yield over time.

KEYWORDS: continuous flow chemistry, supercritical carbon dioxide, supported ionic liquid phase, bioderived cyclic carbonates, tetrabutylammonium halide, ethyl methyl imidazolium halide

■ INTRODUCTION

The use of bioderived chemicals has attracted increasing attention in the past years in order to reduce the dependence on crude oil as limited feed stock.[1,2] In this context, cyclic carbonates with an increasing annual production provoked by applications as electrolytes in lithium ion batteries as well as aprotic polar solvents or monomeric building blocks for polyurethanes are compounds of scientific as well as industrial interest.[3,4] Suitable renewable starting materials for cyclic carbonates are oils and fatty acid,[5−9] terpenes[10] like limonene and carvone, and furfural derivatives.[11] Additionally, limonene is a feedstock of high potential displayed in a global market of approximately 314 million US$ in 2020 and a global annual production of 43 Mt of limonene.[12]

One of the most important synthetic strategies for the synthesis of cyclic carbonates is the catalytic coupling of epoxides with carbon dioxide (CO_2).[13] CO_2 is a widely and commonly used raw material of high abundance. Considering CO_2 as a greenhouse gas, it is additionally of general interest to develop techniques for CO_2 valorization. CO_2 not only is nowadays used as a C1 building block for the synthesis of bulk chemicals like methanol or formic acid but is also increasingly used for the production of higher value chemicals. However, apart from the advantageous properties of being non-flammable and non-toxic, the high stability and therefore low reactivity of CO_2 pose a challenge for the development of suitable catalytic systems. This challenge was accepted by the scientific community as well as the industry being reflected in reviews of the past years.[14−17]

In general, for the production of cyclic carbonates, derived from CO_2 and epoxide, various catalytic systems on inorganic bases like metal complexes, metal oxides, and alkali metal halides as well as organic catalysts like organic bases, hydrogen donors, or ionic liquids were investigated in the past years.[18−21]

For cyclic limonene carbonates, various metal catalysts based on aluminum,[22,23] lanthanum,[24] iron,[25] cobalt,[26] scandium and yttrium,[27] and calcium[6,28] were studied. Additionally, examples with tungstate ionic liquids[29] and ionic liquids[30−35] are published. In various publications, ionic liquids were used as co-catalysts.[23−26,36,37] However, only tetrabutyl ammonium halide-based ionic liquids were studied as single catalysts for the production of limonene mono- and biscarbonates.

In combination with supercritical CO_2 (scCO_2, T_c: 31.0 °C, p_c: 7.38 MPa),[38] ionic liquids show a particular property of high value. The high solubility of scCO_2 in ionic liquids[39] makes ionic liquids ideal candidates as reaction media in combination with scCO_2 for catalytic processes being favorable over the use of stochiometric amounts of reactants with regard to considerations of sustainability.[40,41] In contrast, ionic liquids show extremely low solubility in scCO_2, thus rendering them
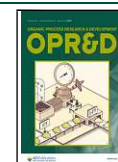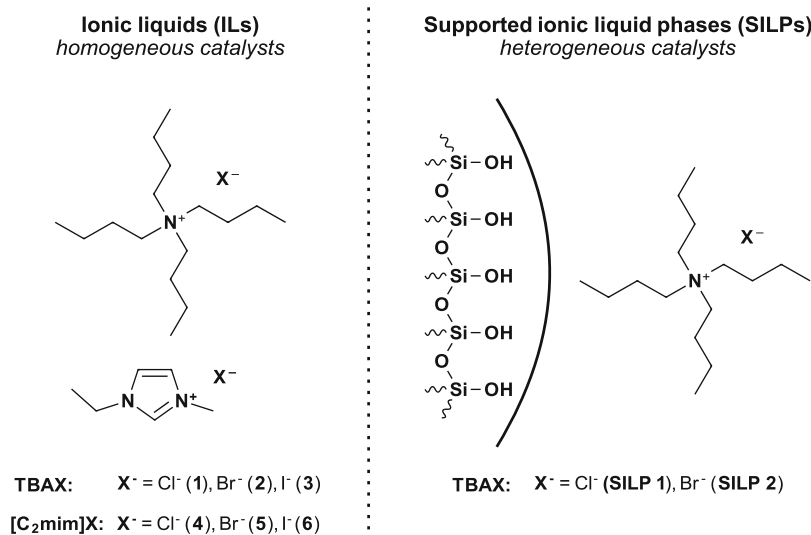
Figure 1. Catalysts: ammonium- and imidazolium-based ionic liquids served as homogeneous catalysts (left), and SILPs, where the ionic liquid was physisorbed on mesoporous silica, were applied as heterogeneous catalysts (right).

attractive for immobilized catalytic phases in heterogeneous catalysis,[42–44] where leaching of the catalyst from the supporting material can be an issue.[45] Further studies on the solubility of $scCO_2$ in ionic liquids and *vice versa* are summarized in the stated publications.[46,47]

For the immobilization of ionic liquids toward continuous flow processes, supported ionic liquid phases (SILPs) are a well-known and widely used concept for catalytic and numerous other applications.[48,49] An SILP material contains a thin film of ionic liquid on the supporting material, e.g., mesoporous silica, which offers a high surface area that is advantageous for catalytic processes and is able to overcome mass transfer limitations due to short diffusion lengths in the thin film.[50] Such mass transfer limitations can be an issue in batch mode conversions, where mostly homogeneous catalytic systems are used.

In contrast to batch mode conversions of CO_2, in continuous flow chemistry, even higher pressures can be applied under safe conditions. While reactions with normal CO_2 gas cylinders in batch are typically limited to feed pressures of 5 MPa, continuous conversions can be safely realized with pressures up to 50 MPa. In addition, flow chemistry offers a higher level of automation as well as linear scalability.[51]

Regarding the synthesis of cyclic carbonates, only a few examples of flow conversions are literature-known and summarized in a recent published review.[52] In this context, our group published in 2018 the synthesis of propylene carbonate under supercritical conditions in continuous flow.[48]

In this paper, we went one step further to a more complex, less reactive, and thus more challenging but also bioderived substrate and presented an optimized long-term conversion of bioderived limonene oxide and limonene dioxide to limonene carbonates in continuous flow. Supercritical carbon dioxide act as a reagent and sole solvent. Easily producible heterogeneous SILP catalysts were applied.

RESULTS AND DISCUSSION

Selection of Catalysts: Ionic Liquids and SILPs. So far, Morikawa et al.,[30,31] Mülhaupt et al.,[32–34] and Hintermair et

al.[35] dealt with the formation of cyclic carbonates starting from limonene oxides using tetrabutylammonium halides as sole catalysts but only under batch conditions. Based on these publications, we chose tetrabutylammonium-based halides (TBAC **1**, TBAB **2**, and TBAI **3**) for catalyst screening in batch mode followed by application in continuous flow. In addition, 1-ethyl-3-methyl imidazolium halides ([C$_2$mim]Cl **4**, [C$_2$mim]Br **5**, and [C$_2$mim]I **6**) were investigated based on our experience in continuous flow conversion of propylene oxide.[48] An overview of used catalysts is shown in Figure 1.

For the continuous production of limonene carbonates in heterogeneous mode, SILP catalysts (**SILP 1** and **2**, see Figure 1) were prepared according to a general procedure,[48] where the supporting material and ionic liquid was suspended and dissolved in dichloromethane and shaken for 1 h. After removal of the solvent, a SILP with a thin physisorbed film of ionic liquid on mesoporous silica-60 was obtained. The high surface area of the catalytically active material enables an ideal mass transfer,[50] which can be an issue in homogeneous catalysis, especially if no solvent is used, which is, on the other side, desirable with regard to sustainable chemistry.

Batch Conversion of Limonene Oxides: Catalyst Screening and Optimization. We commenced our investigation by screening catalysts and optimizing the synthesis of limonene carbonates **8** in batch mode (Figures 2 and 4).
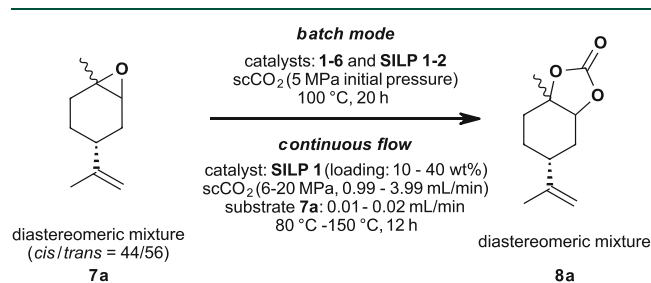
Figure 2. Limonene oxide **7a**: catalyst screening in batch mode followed by the development and optimization of the continuous flow process using heterogeneous SILP catalysts.

64

Table 1. Limonene Oxide 7a: Results of Catalyst Screening in Batch Mode

| entry | catalyst | conversion of isomer 7a (NMR) [%][a] | | | yield of 8a (NMR) [%][a] |
		cis	*trans*	sum	sum
1	TBAC **1**	43 (60[b])	94 (100[b])	72 (83[b])	68 (57[c], 50[d])
2	TBAB **2**	47	76	63	56 (32[d])
3	TBAI **3**	25	35	31	12 (7[d])
4	[C$_2$mim]Cl **4**	17	19	18	2
5	[C$_2$mim]Br **5**	6	17	13	6
6	[C$_2$mim]I **6**	11	11	11	0
7[e]	TBAC **1** + silica gel 60	48	84	68	46
8[e]	TBAB **2** + silica gel 60	71	71	71	29
9[e]	TBAI **3** + silica gel 60	69	70	70	29
10[e]	[C$_2$mim]Cl **4** + silica gel 60	12	22	17	7
11[e]	[C$_2$mim]Br **5** + silica gel 60	37	30	33	11
12[e]	[C$_2$mim]I **6** + silica gel 60	75	49	61	10
13	**SILP 1** (20 wt % TBAC **1**)	44	78	63	62
14	**SILP 2** (20 wt % TBAB **2**)	50	63	57	33

[a]Conditions: 5 MPa CO_2 (gaseous, initial pressure), 5 mmol limonene oxide **7a** (*cis/trans* = 43/57), 10 mol % catalyst **1–6**, 13 mg of naphthalene (internal standard), 100 °C, 20 h. Further information about the calculations of NMR yields are summarized in the Supplementary Information (ESI Figure S12 and Formulas S1–S6). [b]Conversions after 70 h. [c]Isolated yield after column chromatography. [d]Published values from ref 30 (conditions according to table note a except CO_2 pressure [a lower CO_2 pressure of 3 MPa and dry ice were used]). [e]Conditions according to table note a, 10 mol % catalyst **1–6** (20 wt %), and silica gel 60 (80 wt %).

Initially, we focused on the conversion of limonene oxide **7a** (Figure 2) due to a simple analysis of diastereomeric product mixtures. For the determination of yields, NMR spectroscopy with naphthalene as the internal standard was used.[30]

As shown in Table 1, during the screening of tetrabutylammonium and 1-ethyl-3-methylimidazolium halides **1–6** in batch mode, tetrabutylammonium chloride (TBAC **1**) turned out to be the most selective and highest-yielding catalyst for the conversion of diastereomeric mixture (*cis/trans* = 44/56) of limonene oxide **7a** to the corresponding limonene carbonate **8a** (entry 1). Furthermore, no byproducts were formed, as proven by NMR and GC/MS measurements.

As already shown by kinetic studies in the literature,[53] an increase in pressure of CO_2 from 3 to 5 MPa led to higher yields up to 24% as in the case of TBAB **2** (entry 2). Nevertheless, compared to TBAC **1** (entry 1), TBAB **2** (entry 2) showed a slight decrease in yield and selectivity. The order of reactivity of Cl$^-$ > Br$^-$ > I$^-$ is in accordance to the expected nucleophilicity of halides in polar aprotic reaction environments (entries 1–3). The imidazolium-based ionic liquids **4–6** were found to be catalytically less or even inactive (entries 4–6). This is in contrast to our previous studies, where imidazolium-based catalysts where identified as more suitable.[48] Regarding steric effects, the sterically more demanding *cis* isomer of limonene oxide **7a** showed in all cases a lower conversion than the *trans* isomer. After 20 h, TBAC **1** (entry 1) resulted in a conversion of 94% of the *trans* isomer and 43% of the *cis* isomer (in total 72%) and an overall yield of carbonate **8a** of 68%. Purification via column chromatography resulted in 57% isolated yield. Furthermore, after 70 h at 100 °C, the *cis* isomer showed 60% conversion, whereas the *trans* isomer indicated full conversion.

For the screening of the catalysts in the presence of silica without immobilization (entries 7–12), TBAC **1** (entry 7) and TBAB **2** (entry 8) showed a lower yield and lower selectivity. For TBAI **3** (entry 9) and the imidazolium-based catalysts **4–6** (entries 10–12), the yields increased slightly; nevertheless, the selectivities remained in the lower range.

The catalyst screening of supported ionic liquid phases (**SILP 1** and **SILP 2**) of ammonium-based ionic liquids **1–2** physisorbed on silica resulted in the same order regarding the catalytic activity than in homogeneous mode (entries 13 and 14). **SILP 1** (entry 13) with immobilized TBAC **1** gave again the highest yield and selective conversion to the desired carbonate **8a**.

Recycling studies of **SILP 1** (see ESI Table S3) revealed that the yield decreased from 62 to 50% after the first recycling step and leveled at 25% after the fourth cycle. **SILP 2** was recyclable for three times (see ESI Table S3) without a significant change in yield from 31 to 29%; after the fourth cycle, the yield slowly decreased from 29 to 23%. Nevertheless, the yield as well as selectivity (entries 13 and 14) was generally lower compared to **SILP 1**. For this reason, **SILP 1** was used for further studies.

As a general side reaction in the presence of silica, the ring opening of the epoxide[54] to limonene diol, catalyzed by the acidic hydroxy groups of silica and residual water in the silica, has to be considered. The influence of water was proven by the addition of 10 wt % of water (entry S2) to the reaction mixture where 20% of limonene diol was formed according to GC/MS. In batch mode using **SILP 1** (entry 13) as the catalyst, 5% of limonene diol was formed according to GC/MS. However, the diol was no longer formed in continuous flow, which can be explained by a shorter interaction of the substrate and supported catalyst in continuous flow than in batch mode.

Further studies on the optimization of the SILP system (see ESI Table S2) revealed that the free hydroxy groups of silica had a beneficial effect on the reaction. Upon comparing the yields of non-calcined with calcined silica, a 17% lower yield in the case of calcined silica was obtained (entries S11 and S12). This synergistic effect of surface hydroxy groups of supporting materials and ionic liquids in connection with the synthesis of cyclic carbonates is also described in the literature.[55–57]

Furthermore, a decrease in catalyst loading (entries S7–S9) from 20 to 15 or 10 wt % resulted in a drop of yield, and an increase in catalyst loading to 40 wt % (entry S10) gave only a minor increase in yield from 62 to 68%, which can be

65
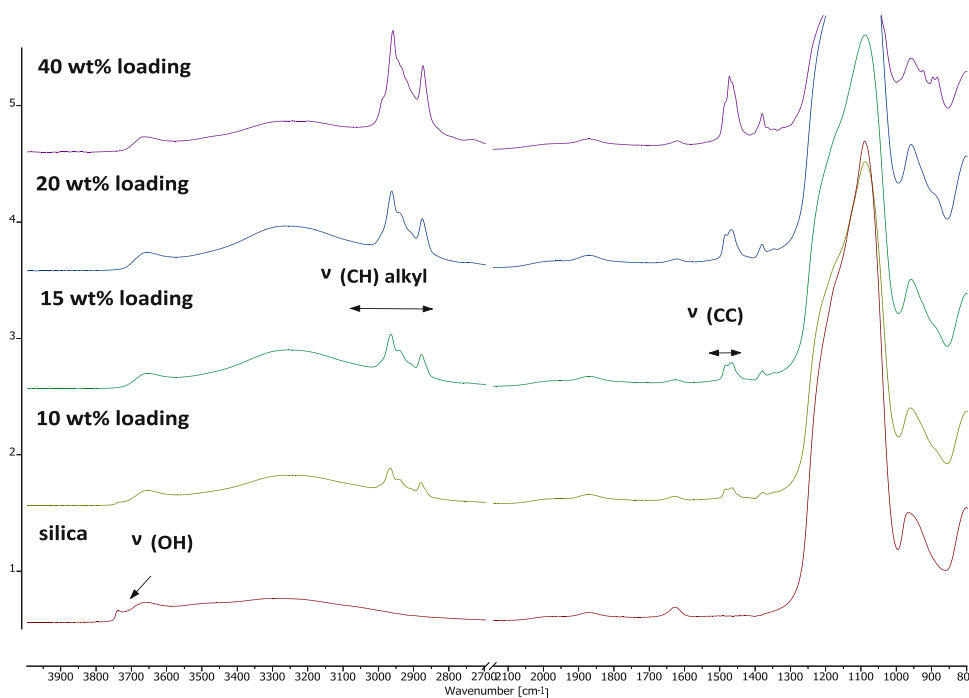
Figure 3. Different catalyst loadings of **SILP 1**: a decrease in surface hydroxy groups (3750 cm^{-1}) while increasing the loadings was observed.
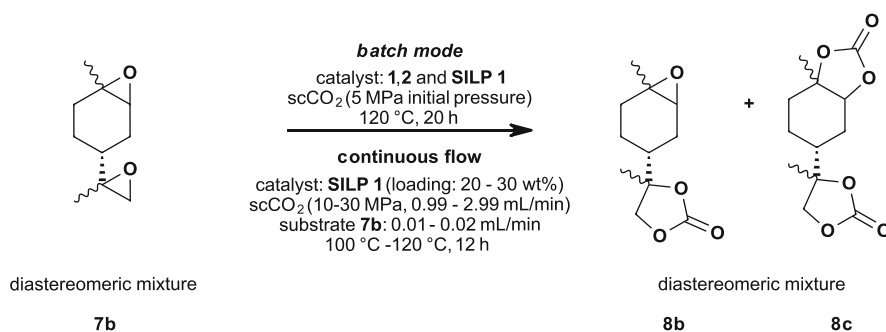
Figure 4. Limonene dioxide **7b**: catalyst screening in batch mode followed by the development and optimization of the continuous flow process using heterogeneous SILP catalysts.

explained by a fully covered surface and less hydroxy groups that exhibit the mentioned synergistic effect.[55,56]

The decrease in hydroxy groups on the surface of the material while increasing the catalyst loading from 10 to 40 wt % was also shown by DRIFT spectroscopy, where the band at 3750 cm^{-1} corresponds to the surface hydroxy groups. Apart from that, bands at around 2900 and 1550 cm^{-1} represent the CH and CC vibrations of TBAC **1** (Figure 3), respectively.

The catalyst loadings were also confirmed by TGA measurements (see ESI Figures S5 and S7), where the mass loss of the SILP materials during heating up from 25 to 450 °C with a rate of 5 °C/min was detected. The initial mass loss at around 100 °C was caused by adsorbed water in the SILP material.

Finally, 20 wt % catalyst loading as ideal conditions was chosen for further studies in continuous flow.

Based on our results of limonene oxide **7a** and the work of Mülhaupt et al.[33] we further expanded our research towards the batch conversion of limonene dioxide **7b** in homogeneous and heterogeneous mode with ammonium based ionic liquids as catalysts (Figure 4). For this reason, we selected TBAC **1**, TBAB **2**, and **SILP 1** as catalysts as they showed the highest

activity in the case of limonene oxide **7a** (Table 1, entries 1, 2, and 13).

Yields were determined via GC using octane as the internal standard since NMR analysis was not suitable due to the formation of four diastereomers of epoxycarbonate **8b** and two diastereomers of biscarbonate **8c** leading to overlapping signals.

In the case of all tested catalysts TBAC **1**, TBAB **2**, and **SILP 1** (Table 2), limonene dioxide **7b** was fully converted to carbonate **8b** or **8c**. TBAC **1** showed again the best performance regarding yield and selectivity (entry 15).

Using TBAC **1** (entry 15) as a homogeneous catalyst, a total yield of 99% was obtained after 20 h at 120 °C; hence, 30% of epoxycarbonate **8b** and 69% of biscarbonate **8c** were formed. Additionally, full conversion to biscarbonate **8c** was observed after 67 h at 120 °C.

As a side reaction in heterogeneous catalysis with **SILP 1** (entry 17), the formation of limonene diol via acid ring opening[54] of up to 13% was observed (verified via GC/MS). Nevertheless, the diol was not formed in continuous flow experiments for reasons already discussed for limonene oxide **7a**.

Table 2. Limonene Dioxide 7b: Results of Catalyst Screening in Batch Mode

		yield (GC) [%][a]		
entry	catalyst	**8b**	**8c**	sum (**8b** + **8c**)
15	TBAC **1**	30 (26[b])	69 (66[b])	99 (92[b])
16	TBAB **2**	44	35	79
17	**SILP 1** (20 wt % TBAC **1**)	36	40	76

[a]Conditions: 5 MPa CO_2 (gaseous, initial pressure), 1.07 mmol limonene dioxide **7b**, 10 mol % catalysts **1** and **2**, 120 °C, 20 h. Further information regarding the determination of GC yields is shown in the Supplementary Information (ESI Figures S17 and S18). [b]Isolated yield after column chromatography.

With this SILP system and determination of yields via GC in hand, several continuous flow experiments were conducted in the following.

Continuous Flow Conversion of Bioderived Limonene Oxides to Various Limonene Carbonates. *General Setup for Continuous Flow Reactions.* All continuous flow reactions were performed with the following reaction setup shown in Figure 5. A CO_2 cylinder with an ascending pipe served as the gas supply, CO_2 was pumped through the system with an HPLC pump. A glass vial, filled with the corresponding limonene oxide **7a** or **7b**, served as the substrate supply and was pumped through the system with an HPLC pump. Experiments with flow rates down to 0.01 mL/min were performed since lower flow rates are not recommended for reasons of accuracy of the used HPLC pumps.

As already discussed for the batch mode, no co-solvent was used, which is advantageous with regard to sustainability and leaching of the catalyst, especially in long-term experiments. CO_2 and the substrate were mixed before entering a thermostated unit where the catalyst cartridge filled with SILP materials was located. In the case of temperatures higher than 80 °C, the substrate/scCO_2 mixture was preheated in a coil to 80 °C before entering a second heating unit where the catalyst cartridge could be heated up to 150 °C. Catalyst cartridges of two different lengths were used (150 and 250 mm) during optimization, resulting in different catalyst input (1.34 and 2.22 g of SILP material). In order to perform reactions at different pressures, a back-pressure regulator was involved in the system. After passing the gas–liquid separator, the product was collected as a mixture of carbonates **8** and unreacted starting material **7** excluding any byproduct, as

verified by NMR and GC/MS measurements. Further technical details of the setup are provided in the Materials and Methods section.

Conversion and yields of the sampled product **8** were determined in the case of limonene oxide **7a** via NMR analysis[30] (internal standard: naphthalene) and in the case of limonene dioxide **7b** via GC (internal standard: octane) as described above. Further information on the determination of yields are given in the Supplementary Information (ESI sections 4.1 and 5.1). Leaching of ionic liquid from the supporting material was quantified via ^{1}H-NMR spectroscopy using naphthalene as the internal standard.

Continuous Flow Conversion of Limonene Oxide 7a. As shown in Figure 2, the optimization of the continuous flow conversion of limonene oxide **7a** to limonene carbonate **8a** included variation of flow rates for the substrate and CO_2, catalyst loading on the SILP material, pressure, and temperature.

Following the results from the batch mode experiments and our experience from a previous project with propylene oxide,[48] a flow rate of 1.99 mL/min for CO_2 and 0.01 mL/min for limonene oxide **7a**, 1.34 g of **SILP 1** (150 mm length of catalyst cartridge, residence time: 75 s) with a catalyst loading of 20 wt % TBAC **1**, and a pressure of 10 MPa were chosen as the starting point for a temperature screening (Figure 6 and Table 3, entries 18−21).

As shown in Figure 6, the reaction started after 2−3 h preliminary lead time, which is in accordance to low flow rates of limonene oxide **7a** of 0.01 mL/min. Increasing the temperature from 80 °C up to 120 °C (entries 18−20) resulted in increasing and constant outputs (maximum yield: 14%) of limonene carbonate **8a**. In contrast, at 150 °C (entry 21), Hoffmann elimination of TBAC **1** to tributylamine became an issue, resulting in a decrease in yield over time. The formation of the elimination product was confirmed via ^{1}H-NMR analysis. Additionally, the observed thermal stability is in accordance with thermogravimetric analysis data, where degradation also started at around 150 °C (see ESI Figure S6).

Besides thermal stability, preventing leaching of the catalyst from the supporting material is of high importance especially with regard to industrial applications and long-term use of the catalytic system. In this context, during the temperature screening (entries 18−21) performed at 10 MPa, either no leaching or values below 1% of leached TBAC **1** were detected via NMR spectroscopy (limit of detection: 0.5−1 mg; ≤0.2%).
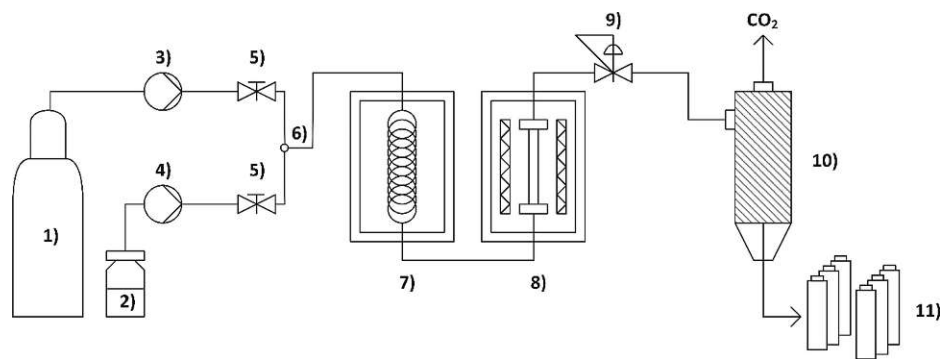
Figure 5. Schematic representation of the scCO_2 flow device: (1) liquid CO_2 supply, (2) substrate supply, (3) CO_2 pump, (4) substrate pump, (5) hand operated valve, (6) T-piece, (7) oven with preheating coil (up to 80 °C), (8) oven with catalyst cartridge (up to 150 °C), (9) back-pressure regulator, (10) gas–liquid separator, and (11) product collector.
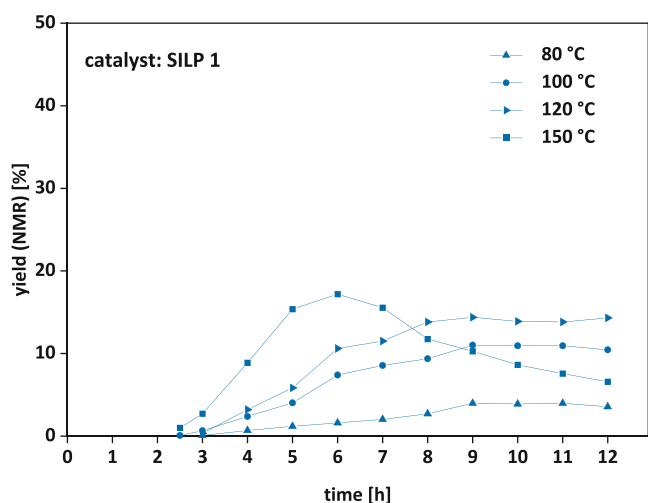
Figure 6. Limonene oxide **7a**: temperature screening in continuous flow. Detailed conditions are given in Table 3.

While screening pressures from 6 to 20 MPa (entries 22–25), it turned out that a pressure of 6 MPa (entry 22) led to leaching of 12%. In contrast, at operating pressures of 15 and 20 MPa (entries 24 and 25), no leached catalyst was detected via NMR spectroscopy. Additionally, 15 MPa (entry 24) was found to be the optimum pressure because at higher pressures, a trend to decreased yields was observed (entry 25).

In order to increase the yields, a catalyst cartridge of 250 mm (residence time: 125 s) instead of 150 mm length (residence time: 75 s) was used, resulting in a 65% higher input of SILP and equally longer residence time. With the increase in the input of SILP to 2.22 g, an increase of 60% in maximum yield from 12 to 19% was observed (entries 24 and 26). Additionally, a constant output over 12 h was achieved.

An increased catalyst loading from 20 to 30 wt % (entries 26 and 27) resulted in a slight increase in yield to 22% maximum yield and 15% overall yield paired with completely suppressed

leaching of the catalyst. However, a further increase to 40 wt % catalyst loading (entry 28) ended up in an overpressure in the system during the reaction due to a visible agglomeration and loss in the free-flowing property of the SILP material.

As a last step in optimization, the impact of different flow rates of CO_2 and substrate on the so far optimized system (entry 27; 2.22 g of SILP **1**, 30 wt % loading, 15 MPa, 120 °C) was studied (see ESI Figure S13 and Table S4).

Flow rates of CO_2 between 1.99 mL/min (residence time: 125 s, entry S15) and 2.49 mL/min (residence time: 100 s, entry S16) resulted in overall yields of 15−16% as well as no leaching of the catalyst and thus turned out to be the optimum. With a higher flow rate of 3.99 mL/min (residence time: 62 s, entry S17), lower overall yields of 12% were achieved due to a shorter residence time. In contrast, a lower flow rate of 0.99 mL/min (residence time: 250 s, entry S13) led to a blockage of the flow device and therefore a non-constant product output. This also confirmed the necessity of the solvent environment provided by $scCO_2$ as the sole solvent.

In order to further increase productivity of the process, the double flow rate of limonene oxide **7a** (0.02 mL/min, entry S18) was applied to the system. However, a higher flow rate led to leaching of the catalyst and therefore to a decrease in yield over time.

With the optimized conditions in hand (entry 27; SILP **1** (2.22 g, 30 wt % of TBAC **1**), 1.99 mL/min CO_2, 0.01 mL/min **7a**, 15 MPa, 120 °C, 250 mm catalyst cartridge), the long-term stability of our catalytic system over 48 h was further investigated (Figure 7).

The long-term stability studies of the *cis/trans* mixture of limonene oxide **7a** with SILP **1** as the catalyst over 48 h resulted in a maximum yield of 22% and an overall yield of 16%, respectively, with a production rate of 0.12 g/h of pure limonene carbonate **8a** dissolved in starting material **7a**. However, taking the ratio of the *cis* and *trans* isomer of 43/57 as well as the low reactivity of the *cis* isomer into account, the yield can be further increased by performing continuous flow

Table 3. Limonene Oxide 7a: Influence of Temperature, Pressure Catalyst Input, and Catalyst Loading in Continuous Flow Using SILP 1 as a Heterogeneous Catalyst[a]

entry	temperature [°C]	pressure [MPa]	input SILP 1 [g]	catalyst [wt %]	yield (NMR)[b] [%] maximum	yield (NMR)[b] [%] overall (12 h)	leaching[c]
18	80	10	1.34	20	4	2	n.o.
19	100				11	6	<1%
20	120				14	8	<1%
21	150				17	9	degradation[d]
22	120	6	1.34	20	12	6	12%
23		10			14	8	<1%
24		15			12	8	n.o.
25		20			11	7	n.o.
26	120	15	2.22	20	19	12	n.o.
27		15		30	22	15	n.o.
28		15		40[e]	26	16	<1%

[a]Reactions were carried out with SILP **1** using catalyst cartridges of 150 mm (1.34 g of SILP **1**, residence time: 75 s) or 250 mm length (2.22 g of SILP **1**, residence time: 125 s) under the following conditions: flow rate of limonene oxide **7a** (*cis/trans* = 43/57): 0.01 mL/min, flow rate CO_2: 1.99 mL/min, 12 h. [b]Yields are given as sum of the *cis* and *trans* isomer. Internal standard: naphthalene. Further information about the calculations of NMR yields are summarized in the Supplementary Information (ESI Figure S12 and Formulas S1−S6). [c]For determination of leaching, the integral of the signal at δ = 3.35 ppm of TBAC **1** was used (limit of detection: 0.5−1 mg; ≤0.2%). [d]The Hoffmann elimination product was obtained. [e]Inconstant product output due to overpressure during the reaction.

68
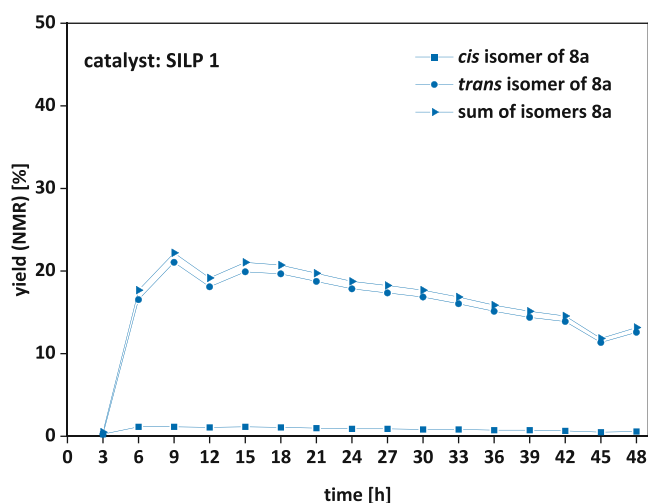
Figure 7. Limonene oxide **7a**: long-term stability of **SILP 1** over 48 h. Final optimized conditions: **SILP 1** (2.22 g, 30 wt % loading), 1.99 mL/min CO_2, 0.01 mL/min limonene oxide **7a**, 15 MPa, 120 °C, 48 h, 250 mm catalyst cartridge.

reactions exclusively with the more reactive *trans* isomer as already investigated in batch mode.[31] Nevertheless, in order to cover the reactivity of both isomers, the commercially available *cis/trans* mixture of limonene oxide **7a** was used for these purposes.

Additionally, no leaching over 48 h (Figure 7) as well as over 96 h (ESI Figure S14) was observed according to NMR analysis of the product fractions (limit of detection: 0.5−1 mg; ≤0.2%). For further studies on the catalyst stability, the recovered SILP was dried under vacuum and leached with methanol followed by NMR analysis showing no degradation of TBAC **1**.

The slight decrease in yield over time can be explained by agglomeration of the starting material, product, and intermediate on the catalytically active surface as shown by N_2 physisorption measurements (*vide infra*).

Continuous Flow Conversion of Limonene Dioxide 7b. Based on the results of the optimization of limonene oxide **7a**, we ultimately addressed the conversion of limonene dioxide **7b**, aiming for selective formation of diastereomeric mixtures of epoxycarbonate **8b** and biscarbonate **8c**. The temperature, pressure, catalyst loading, and the flow rates of CO_2 and limonene dioxide **7b** were varied (Figure 4); results of the optimization are shown in Table 4.

Independent from the used parameters (Table 4, entries 29−36), the yield of epoxycarbonate **8b** was higher than biscarbonate **8c**, which can be explained by differing steric hindrance and therefore reactivity of the epoxide groups of limonene dioxide **7b**.

During the screening, a temperature of 120 °C was found to be the optimum temperature (entry 30). Maximum yields of 30% for epoxy carbonate **8b**, 18% for biscarbonate **8c**, and an overall yield of 26% were achieved in a constant output of product over 12 h. A lower temperature of 100 °C (entry 29) resulted in a lower overall yield of 19%; higher temperatures were not suitable according to the thermal stability of **SILP 1** as already shown for limonene oxide **7a** (Figure 6).

During screening of different pressures (entries 31−34), the highest overall yield of 27% was achieved at 10 MPa (entry 31); however, pressures of 15−30 MPa (entries 32−34) resulted in a higher constancy of product output over time

Table 4. Limonene Dioxide 7b: Influence of Temperature, Pressure and, Catalyst Loading in Continuous Flow Using SILP 1 as the Heterogeneous Catalyst[a]

| | | | | yield (GC)[b] [%] | | | | |
| | | | | maximum | | overall (12 h) | | |
entry	temperature [°C]	pressure [MPa]	catalyst loading [wt %]	8b	8c	8b	8c	sum
29	100	15	30	23	10	14	5	19
30	120			30	18	18	8	26
31	120	10	30	52	22	21	6	27
32		15		30	18	18	8	26
33		20		27	14	17	8	25
34		30		22	10	15	6	22
35	120	20	20	26	7	16	4	20
36			30	27	14	17	8	25

[a]Reactions were carried out with **SILP 1** using a catalyst cartridge of 250 mm length (2.22 g of **SILP 1**, residence time: 125 s) under the following conditions: flow rate of limonene dioxide **7b**: 0.01 mL/min, flow rate of CO_2: 1.99 mL/min (2× 0.995 mL/min), 12 h. [b]Internal standard: octane. Further information regarding the determination of GC yields is shown in the Supplementary Information (ESI Figures S17 and S18).

(Figure 8), which is of higher interest in continuous flow chemistry than having high yields for a short period of time. In
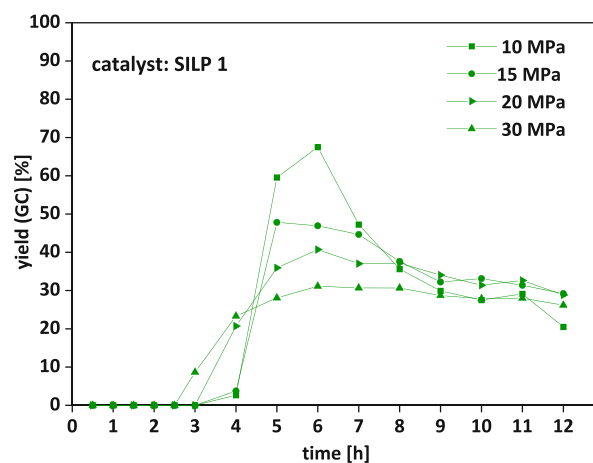
Figure 8. Limonene dioxide **7b**: pressure screening in continuous flow. Detailed conditions are given in Table 4.

terms of overall yield, 15 MPa (entry 32) and 20 MPa (entry 33) turned out to be the best conditions (Table 4).

Increasing the catalyst loading from 20 to 30 wt % (entries 35 and 36), an increase in overall yield from 20 to 25% was achieved. The increase in the maximum yield of biscarbonate **8c** from 7 to 14% has also to be mentioned at this point. A higher catalyst loading of 40 wt % was not suitable according to inconstant product outputs in the case of limonene oxide **7a** (Table 3, entry 28) being caused by visible agglomeration and loss of free-flowing property of the SILP material.

Flow rates of CO_2 (Table 5) in a range of 0.99−3.99 mL/ min (entry 37−39) resulted in constant outputs of carbonates **8b** and **8c**. However, with a flow rate of 1.99 mL/min CO_2 (entry 38), the best overall yield of 25% and maximum yields of 27% for epoxycarbonate **8b** and 14% for biscarbonate **8c** were obtained. The trends to lower yields when higher flow

69

Table 5. Limonene Dioxide 7b: Influence of Flow Rates of CO$_2$ and Substrate in Continuous Flow Using SILP 1 as the Heterogeneous Catalyst[a]

	flow rates [mL/min]			yield (GC)[b] [%]				
				maximum		overall (12 h)		
entry	CO$_2$	substrate 7b	residence time [s]	8b	8c	8b	8c	sum
37	0.99	0.01	250	31	18	17	7	24
38	1.99		125	27	14	17	8	25
39	3.99		62	21	8	13	5	17
40	1.98	0.02	125	21	7	13	4	17

[a]Reactions were carried out with **SILP 1** using a catalyst cartridge of 250 mm length (2.22 g of **SILP 1**) under the following conditions: 20 MPa, 120 °C, 12 h. [b]Internal standard: octane. Further information regarding the determination of GC yields is shown in the Supplementary Information (ESI Figures S17 and S18).

rates of CO$_2$ are applied are in accordance with a decrease in the residence time of the substrate on the catalyst.

A higher flow rate of limonene dioxide **7b** (Table 5) of 0.02 mL/min (entry 40) resulted in a drop of overall yield from 25 to 17% caused by leaching of the immobilized catalyst over time.

Hence, with the optimized conditions (Figure 9), maximum yields of 27% for epoxycarbonate **8b** and 14% for biscarbonate
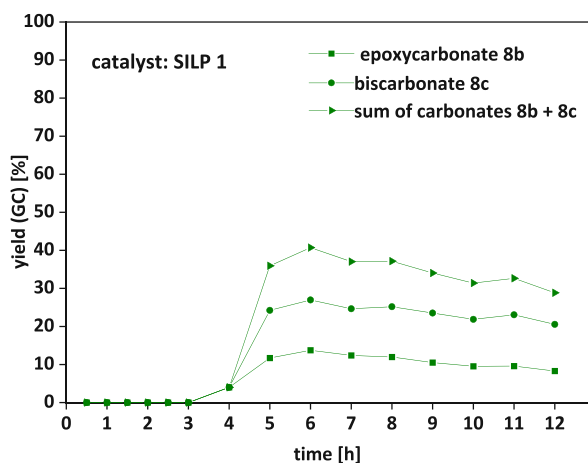
Figure 9. Limonene dioxide **7b**: optimized conditions resulted in an output of carbonates **8b** and **8c** of overall 25%. Final optimized conditions: **SILP 1** (2.22 g, 30 wt % of TBAC **1**), 1.99 mL/min CO$_2$, 0.01 mL/min limonene dioxide **7b**, 20 MPa, 120 °C, 12 h, 250 mm catalyst cartridge.

8c and an overall yield of 25% were obtained. The slight decrease in yield over time was caused by leaching of catalyst from the supporting material, which is also visible in long-term stability experiments (see ESI Figure S19).

The long-term experiment over 48 h of **SILP 1** with a catalyst loading of 30 wt % resulted in an overall yield of 16% (11% of **8b** and 5% of **8c**). However, leaching of 50% of immobilized TBAC **1**, most dominantly in the first 9 h, was observed, resulting in a decrease in yield over time.

For this reason, the catalyst loading was reduced to 15 wt %, whereas the overall yield of 17% remains unchanged. Furthermore, only traces of leached catalyst were detected

via ^{1}H-NMR spectroscopy (limit of detection: 0.5−1 mg; ≤0.2%) in the fractions of the first 27 h. After 27 h, no leaching and a constant output of carbonates **8b** and **8c** were observed, resulting in an overall yield of 17% over 48 h and a production rate of 0.13 g/h.

Overall, by reducing the catalyst loading from 30 to 15 wt %, leaching was suppressed almost completely, reflecting in a product output of 17% overall yield.

Measurements of the surface area and porosity via N$_2$ physisorption confirmed that, apart from leaching, the loss in yield was caused by the proceeding agglomeration of the starting material, product, or intermediate on the catalytically active surface over time. The characterization of the SILP catalysts via N$_2$ physisorption using the Brunauer−Emmett−Teller (BET) as well as the Barrett−Joyner−Halenda (BJH) method revealed that the surface area of the SILP catalyst dropped significantly from 451 to 231 m^2/g (reference material silica gel 60: 634 m^2/g) after 48 h of reaction time compared to the freshly prepared SILP catalyst. In addition, the decrease in pore volume from 0.57 to 0.34 cm^3/g (reference material silica gel 60: 0.91 cm^3/g) and the average pore diameter from 49.07 to 45.40 Å clearly reflected this trend (see ESI Table S1 and Figure S11).

CONCLUSIONS

We developed a continuous flow method for the selective synthesis of three different bioderived carbonates **8a−c** starting from limonene oxide **7a** and limonene dioxide **7b**. Thereby, supercritical carbon dioxide (scCO$_2$) served as the reactant and sole solvent. Ammonium- and imidazolium-based halides as ionic liquid catalysts were screened in batch mode, tetrabutylammonium chloride TBAC **1** turned out to be a high-yielding and a selective catalyst. The SILP concept (supported ionic liquid phase) was used for immobilization of ionic liquid **1** on silica followed by applying the SILP catalyst **SILP 1** in heterogeneous continuous flow mode. After optimizing the continuous flow parameters (temperature, pressure, flow rates, and catalyst loading) for both limonene oxides **7** in 12 h experiments, the catalytic system was successfully studied in long-term experiments over 48 h, eventually providing a constant product output with 16−17% yield.

Ultimately, SILPs in combination with scCO$_2$ were confirmed as an easily obtained and highly suitable combination for continuous flow chemistry, although yields in this particular example remained in the lower range. Our future studies will address the development of more reactive catalysts, focusing in particular on different cationic cores. In this regard, work is currently ongoing in our group.

As an outlook, a scaled flow process for limonene carbonates as potential bioderived bulk chemicals with production rates in the range of kilograms per hour is of particular interest. In this regard, a setup suitable for higher flow rates of carbon dioxide and limonene oxides as well as for bigger catalyst cartridges for SILP catalysts is expected to be crucial.

EXPERIMENTAL PART

Materials and Methods. More information on used materials and methods are summarized in the Supplementary Information (ESI section 1).

Continuous flow experiments were performed with a scCO$_2$ continuous flow device from Jasco (Jasco Corporation, Tokyo,

70

Japan). CO_2, provided by Messer Austria GmbH (>99.995% purity; with ascension pipe), was cooled to −7 °C by a recirculating cooler (CF 40, JULABO GmbH) and was introduced by two CO_2 pumps (PU-2086Plus) with cooled heads. An HPLC pump (PU-2089Plus) delivered substrates. Catalyst cartridges (empty 316 stainless-steel HPLC columns from Restek; 150 mm × 4.6 mm × 1/4″ OD, 2 μm frits, 2.49 mL volume, and 1.34 g of SILP catalyst and 250 mm × 4.6 mm × 1/4″ OD, 2 μm frits, 4.15 mL volume, and 2.22 g of SILP catalyst) filled with SILP catalysts (the maximum weight of packing is dependent on catalyst loading; silica gel 60 served as the reference material for the determination of weight of packing) were heated up in an HPLC column oven (CO-2060Plus, up to 80 °C; Brinkmann CH-500 HPLC column heater system, up to 150 °C). A back-pressure regulator (BP-2080Plus, temperature set to 60 °C), UV detector (UV-2075Plus), and a product collector (SCF-Vch-Bp) were also included and were all connected with 1/16″ stainless-steel tubings.

Preparation of Supported Ionic Liquid Phases on the Example of SILP 1 (30 wt % of TBAC 1). The syntheses and analytical data of the ionic liquids are summarized in the Supplementary Information (ESI section 2).

SILPs were prepared according to a modified literature procedure.[48] Tetrabutylammonium chloride 1 (7.000 g, 30 wt %), dried under high vacuum overnight, was dissolved in 100 mL of dry dichloromethane. Silica gel 60 (21.000 g, 70 wt %), dried in a vacuum oven (50 °C, 50 mbar) for 3 days, was added to the solution. The suspension was shaken for 60 min at 480 rpm. The solvent was removed *in vacuo* followed by further drying under high vacuum. TGA analysis and DRIFT spectra are given in the Supplementary Information (ESI section 3).

Conversion of Limonene Oxide 7a under Batch Conditions on the Example of TBAC 1 and SILP 1 as Catalysts. The formation of limonene carbonate 8a under batch conditions was performed according to a modified literature procedure.[30] Limonene oxide 7a (*cis/trans* = 43/57, 761 mg, 5.00 mmol, 1.00 equiv) and naphthalene as the internal standard (13 mg, 0.10 mmol) were mixed together. A ^{1}H-NMR spectrum (t = 0) was measured as the reference (see also Figure S12).

A 40 cm^3 stainless-steel autoclave was charged either with TBAC 1 (139 mg, 0.50 mmol, 10 mol % with respect to the epoxide) or with SILP 1 (695 mg, 20 wt % of TBAC 1, 0.50 mmol TBAC 1, respectively, 10 mol % TBAC 1), the previously prepared mixture, and CO_2 (5 MPa). The reaction mixture was stirred at 100 °C for 20 h. After 20 h, the autoclave was cooled to room temperature and CO_2 was released. In the case of heterogeneous catalysis, the crude mixture was diluted with 5 mL of deuterated chloroform and homogenized. For the determination of the yield, a ^{1}H-NMR spectrum (t = 20) of the crude mixture was recorded (see Figure S11). For verifying the NMR yield, the isolation was performed once via column chromatography (LP:EA = 10/1–1/1, 50 g of silica). catalyst TBAC 1: NMR yield: 68% (isolated: 57%, colorless oil); catalyst SILP 1: NMR yield: 62%, FTIR (ATR, neat): 2942 (alkyl), 1790 (C=O) cm^{-1}; ^{1}H-NMR (600 MHz, CDCl$_3$ CH$_4$Si): δ 4.74 (t, J = 1.6 Hz, *cis* 1H), 4.72 (t, J = 1.5 Hz, *trans* 1H), 4.70–4.68 (m, *cis* 1H + *trans* 1H), 4.43–4.40 (m, *cis* 1H), 4.35 (dd, J = 9.5, 7.0 Hz, *trans* 1H), 2.30–2.18 (m, *cis* 2H + *trans* 2H), 2.02–1.94 (m, *cis* 1H), 1.94–1.85 (m, *trans* 1H), 1.84–1.74 (m, *cis* 2H), 1.70

(s, *cis* 3H), 1.68 (s, *trans* 3H), 1.67−1.55 (m, *cis* 1H + *trans* 2H), 1.49−1.47 (m, *cis* 3H), 1.45−1.34 (m, *trans* 5H), 1.24−1.08 (m, *cis* 1H). ^{13}C NMR (101 MHz, CDCl$_3$, CH$_4$Si): δ 154.87 (*trans*), 154.61 (*cis*), 147.53 (*cis*), 147.42 (*trans*), 110.27 (*trans*), 110.05 (*cis*), 82.78 (*cis*), 82.24 (*trans*), 81.93 (*cis*), 80.66 (*trans*), 40.01 (*trans*), 37.42 (*cis*), 34.26 (*cis*), 34.07 (*trans*), 33.14 (*trans*), 30.66 (*cis*), 26.36 (*cis*), 26.27 (*trans*), 25.77 (*trans*), 22.35 (*cis*), 20.99 (*cis*), 20.66 (*trans*) ppm.

Conversion of Limonene Dioxide 7b under Batch Conditions on the Example of TBAC 1 and SILP 1. The batch reactions were performed according to a modified literature procedure.[33] An 8 mL glass vial, charged either with TBAC 1 (31 mg, 0.11 mmol, 10 mol %) or with SILP 1 (83 mg, 30 wt % TBAC 1 loading, 0.11 mmol TBAC 1, 10 mol % TBAC 1), limonene dioxide 7b (180 mg, 1.07 mmol, 1.00 equiv), and CO_2 (5 MPa), was placed in a 40 cm^3 stainless-steel autoclave. The reaction mixture was stirred at 120 °C for 20 h.

After 20 h, the autoclave was cooled to room temperature and CO_2 was released. For verifying the GC yield, the isolation of products was performed once via column chromatography (LP:EA = 6:4, 15 g of silica).

For the determination of the GC yield, the crude mixture was homogenized with 5 mL of ethyl acetate (36 mg limonene dioxide /mL). An aliquot of 42 μL of crude solution, 30 μL of internal standard (20 mg octane/mL ethyl acetate), and 1428 μL of ethyl acetate resulted in a 1.5 mL GC sample. The identity of the peaks was verified via GC/MS.

Catalyst TBAC 1: GC yield: 99% of carbonates 8b and 8c (8b: 30%, isolated: 26%; 8c: 69%, isolated: 66%; colorless oils), SILP 1 (30 wt % TBAC 1): GC yield: 76% (8b: 36%, 8c: 40%); epoxycarbonate 8b (diastereomeric mixture, 94:3:2:1), FTIR (ATR, neat): 2932 (alkyl), 1778 (C=O) cm^{-1}; ^{1}H-NMR (400 MHz, CDCl$_3$): δ 4.23 (dd, J = 8.5, 2.7 Hz, 1H), 4.13–3.96 (m, 1H), 3.31–3.01 (m, 1H), 2.33–2.07 (m, 1H), 2.06–1.73 (m, 3H), 1.71–1.53 (m, 2H), 1.43 (s, 3H), 1.32 (s, 3H), 1.21–1.01 (m, 1H). ^{13}C NMR (101 MHz, CDCl$_3$): δ 154.62, 154.60, 85.34, 85.37, 73.53, 73.25, 60.06, 60.04, 57.56, 57.35, 37.73, 37.53, 28.71, 28.62, 26.53, 26.31, 24.32, 24.27, 22.29, 22.12, 22.11, 21.99 ppm. Biscarbonate 8c (diastereomeric mixture, 34:66), FTIR (ATR, neat): 2983 (alkyl), 1775 (C=O) cm^{-1}; ^{1}H-NMR (400 MHz, CDCl$_3$, CH$_4$Si): δ 4.55−4.48 (m), 4.44–4.35 (m), 4.35−4.23 (m), 4.19−4.06 (m), 2.49−2.28 (m), 2.31−2.15 (m), 2.08−1.70 (m), 1.69−1.55 (m), 1.54−1.43 (m), 1.45−1.20 (m). ^{13}C NMR (101 MHz, CDCl$_3$, CH$_4$Si): δ 154.16, 84.70, 84.66, 84.51, 84.43, 82.25, 82.20, 82.02, 80.91, 80.72, 79.68, 79.55, 73.34, 73.28, 73.24, 73.06, 40.84, 40.78, 37.59, 37.58, 32.98, 32.88, 32.63, 32.55, 29.10, 29.00, 26.11, 26.10, 25.81, 25.67, 23.00, 22.91, 22.85, 22.46, 21.45, 21.06, 21.03, 20.98, 20.82, 20.66 ppm.

General Procedure for the Continuous Conversion of Limonene Oxides under Optimized Conditions over 48 h. An empty HPLC column (250 mm × 4.6 mm × 1/4″ OD) was charged with SILP 1 (2.22 g, loading: 30 wt % TBAC 1 for 7a, 15 wt % TBAC 1 for 7b), connected to the scCO$_2$ device, and put in an oven, which was heated up to 120 °C. The back-pressure regulator was set to the appropriate pressure (15 MPa for 7a, 20 MPa for 7b). A 20 mL vial filled with substrate 7 was used as the substrate supply. The flow rates of the HPLC pumps were set to 0.01 mL/min (substrate 7a and 7b) and 1.99 mL/min (CO$_2$, 2× 0.995 mL/min). The mixtures of the corresponding limonene oxide 7 and carbonate 8 were collected in 30 mL vials at different fractions. The collection

time for each flask was set to 3 h, resulting in a total collection time of 48 h.

Limonene Oxide 7a as the Substrate for Continuous Conversion: Determination of NMR Yields. For the determination of NMR yields and conversions, naphthalene as the internal standard was added to each fraction (30 min fractions: 5.0 ± 0.1 mg (12 h experiments), 1 h fractions: 10.0 ± 0.1 mg (12 h experiments), 3 h: 30.0 ± 0.1 mg (48 h experiment), and 40.0 ± 0.1 mg (96 h experiment)) and homogenized with 0.5 mL of $CDCl_3$. NMR measurements were performed with a 5–10 mg aliquot of the resulting mixtures. For the reference NMR spectrum ($t = 0$, see ESI Figure S12), 558 mg of limonene oxide **7a** (0.6 mL per 1 h, $\rho = 0.93$ g/mL) and 10 mg of naphthalene were mixed together.

Limonene Dioxide 7b as the Substrate for Continuous Conversion: Determination of GC Yields. For the determination of GC yields, the 3 h fractions were homogenized with 15 mL of ethyl acetate (ρ (**7b**) = 1.03 mg/mL; 123 mg of **7b**/mL of ethyl acetate, 12 h experiments: 5 mL of ethyl acetate). An aliquot of 12 μL of crude solution (30 min fractions: 24 μL (12 h experiments)), 30 μL of internal standard (20 mg octane/mL ethyl acetate), and 1458 μL (30 min fractions: 1446 μL (12 h experiments)) of ethyl acetate resulted in 1.5 mL of GC sample. The identity of the peaks was verified via GC/MS.

■ ASSOCIATED CONTENT

ⓢ Supporting Information

The Supporting Information is available free of charge at https://pubs.acs.org/doi/10.1021/acs.oprd.2c00143.

> Synthesis and analysis of ionic liquids; characterization of SILPs via TGA, DRIFTS, and N_2 physisorption (surface area: BET theory; porosity: BJH method); recycling studies of SILPs in batch mode; further studies and optimization works conducted in batch mode and under continuous flow; details about determination of NMR and GC yields; and analysis of products via NMR and GC (PDF)

■ AUTHOR INFORMATION

Corresponding Author

Katharina Bica-Schröder − *Institute of Applied Synthetic Chemistry (E163), TU Wien, 1060 Vienna, Austria;* ⓞ orcid.org/0000-0002-2515-9873; Email: katharina.schroeder@tuwien.ac.at

Authors

Philipp Mikšovsky − *Institute of Applied Synthetic Chemistry (E163), TU Wien, 1060 Vienna, Austria;* ⓞ orcid.org/0000-0002-8045-5667

Elias N. Horn − *Institute of Applied Synthetic Chemistry (E163), TU Wien, 1060 Vienna, Austria;* ⓞ orcid.org/0000-0003-0204-2469

Shaghayegh Naghdi − *Institute of Materials Chemistry (E165), TU Wien, 1060 Vienna, Austria;* ⓞ orcid.org/0000-0001-7738-2607

Dominik Eder − *Institute of Materials Chemistry (E165), TU Wien, 1060 Vienna, Austria;* ⓞ orcid.org/0000-0002-5395-564X

Michael Schnürch − *Institute of Applied Synthetic Chemistry (E163), TU Wien, 1060 Vienna, Austria;* ⓞ orcid.org/0000-0003-2946-9294

Complete contact information is available at:
https://pubs.acs.org/10.1021/acs.oprd.2c00143

■ ACKNOWLEDGMENTS

■ ABBREVIATIONS

[C_2mim]X, 1-ethyl-3-methyl imidazolium halide; BET, Brunauer−Emmett−Teller (surface area); BJH, Barret−Joyner−Halenda (pore size distribution); DRIFTS, diffuse reflectance infrared Fourier transform spectroscopy; GC, gas chromatography; GC/MS, gas chromatography mass spectroscopy hyphenation; HPLC, high-performance liquid chromatography; NMR, nuclear magnetic resonance (spectroscopy); $scCO_2$, supercritical CO_2; SILP, supported ionic liquid phase; TBAX, tetrabutylammonium halide; TGA, thermogravimetric analysis; UV, ultraviolet

■ REFERENCES

(1) de Jong, E.; Higson, A.; Walsh, P.; Wellisch, M. Product developments in the bio-based chemicals arena. *Biofuels, Bioprod. Biorefin.* **2012**, *6*, 606−624.

(2) Lee, S. Y.; Kim, H. U.; Chae, T. U.; Cho, J. S.; Kim, J. W.; Shin, J. H.; Kim, D. I.; Ko, Y.-S.; Jang, W. D.; Jang, Y.-S. A comprehensive metabolic map for production of bio-based chemicals. *Nat. Catal.* **2019**, *2*, 18−33.

(3) Kamphuis, A. J.; Picchioni, F.; Pescarmona, P. P. CO_2-fixation into cyclic and polymeric carbonates: principles and applications. *Green Chem.* **2019**, *21*, 406−448.

(4) Stadler, B. M.; Wulf, C.; Werner, T.; Tin, S.; de Vries, J. G. Catalytic Approaches to Monomers for Polymers Based on Renewables. *ACS Catal.* **2019**, *9*, 8012−8067.

(5) Maisonneuve, L.; More, A. S.; Foltran, S.; Alfos, C.; Robert, F.; Landais, Y.; Tassaing, T.; Grau, E.; Cramail, H. Novel green fatty acid-based bis-cyclic carbonates for the synthesis of isocyanate-free poly(hydroxyurethane amide)s. *RSC Adv.* **2014**, *4*, 25795−25803.

(6) Longwitz, L.; Steinbauer, J.; Spannenberg, A.; Werner, T. Calcium-Based Catalytic System for the Synthesis of Bio-Derived Cyclic Carbonates under Mild Conditions. *ACS Catal.* **2018**, *8*, 665−672.

(7) Martínez, J.; de la Cruz-Martínez, F.; de Sarasa Buchaca, M. M.; Caballero, M. P.; Ojeda-Amador, R. M.; Salvador, M. D.; Fregapane, G.; Tejeda, J.; Castro-Osma, J. A.; Lara-Sánchez, A. Valorization of

agricultural waste and CO_2 into bioderived cyclic carbonates. *J. Environ. Chem. Eng.* **2021**, *9*, 105464.

(8) Laprise, C. M.; Hawboldt, K. A.; Kerton, F. M.; Kozak, C. M. Synthesis of a Renewable, Waste-Derived Nonisocyanate Polyurethane from Fish Processing Discards and Cashew Nutshell-Derived Amines. *Macromol. Rapid Commun.* **2021**, *42*, 2000339.

(9) Hu, S.; Chen, X.; Torkelson, J. M. Biobased Reprocessable Polyhydroxyurethane Networks: Full Recovery of Crosslink Density with Three Concurrent Dynamic Chemistries. *ACS Sustainable Chem. Eng.* **2019**, *7*, 10025−10034.

(10) de la Cruz-Martínez, F.; Martínez de Sarasa Buchaca, M.; Martínez, J.; Fernández-Baeza, J.; Sánchez-Barba, L. F.; Rodríguez-Diéguez, A.; Castro-Osma, J. A.; Lara-Sánchez, A. Synthesis of Bio-Derived Cyclic Carbonates from Renewable Resources. *ACS Sustainable Chem. Eng.* **2019**, *7*, 20126−20138.

(11) Martínez, J.; de la Cruz-Martínez, F.; Martínez de Sarasa Buchaca, M.; Fernández-Baeza, J.; Sánchez-Barba, L. F.; North, M.; Castro-Osma, J. A.; Lara-Sánchez, A. Efficient Synthesis of Cyclic Carbonates from Unsaturated Acids and Carbon Dioxide and their Application in the Synthesis of Biobased Polyurethanes. *ChemPlusChem* **2021**, *86*, 460−468.

(12) 360ResearchReports Global Limonene Market Research Report 2020. https://www.360researchreports.com/global-limonene-market-15061488.

(13) Lopes, E. J. C.; Ribeiro, A. P. C.; Martins, L. M. D. R. S. New Trends in the Conversion of CO_2 to Cyclic Carbonates. *Catalysts* **2020**, *10*, 479.

(14) Li, J.-Y.; Song, Q.-W.; Zhang, K.; Liu, P. Catalytic Conversion of Carbon Dioxide through C-N Bond Formation. *Molecules* **2019**, *24*, 182.

(15) Cai, X.; Hu, Y. H. Advances in catalytic conversion of methane and carbon dioxide to highly valuable products. *Energy Sci Eng.* **2019**, *7*, 4−29.

(16) Maeda, C.; Miyazaki, Y.; Ema, T. Recent progress in catalytic conversions of carbon dioxide. *Catal. Sci. Technol.* **2014**, *4*, 1482−1497.

(17) Garba, M. D.; Usman, M.; Khan, S.; Shehzad, F.; Galadima, A.; Ehsan, M. F.; Ghanem, A. S.; Humayun, M. CO_2 towards fuels: A review of catalytic conversion of carbon dioxide to hydrocarbons. *J. Environ. Chem. Eng.* **2021**, *9*, 104756.

(18) Büttner, H.; Longwitz, L.; Steinbauer, J.; Wulf, C.; Werner, T. Recent Developments in the Synthesis of Cyclic Carbonates from Epoxides and CO_2. *Top. Curr. Chem.* **2017**, *375*, 50.

(19) North, M.; Pasquale, R.; Young, C. Synthesis of cyclic carbonates from epoxides and CO_2. *Green Chem.* **2010**, *12*, 1514−1539.

(20) Takaishi, K.; Okuyama, T.; Kadosaki, S.; Uchiyama, M.; Ema, T. Hemisquaramide Tweezers as Organocatalysts: Synthesis of Cyclic Carbonates from Epoxides and CO_2. *Org. Lett.* **2019**, *21*, 1397−1401.

(21) Cokoja, M.; Wilhelm, M. E.; Anthofer, M. H.; Herrmann, W. A.; Kühn, F. E. Synthesis of Cyclic Carbonates from Epoxides and Carbon Dioxide by Using Organocatalysts. *ChemSusChem* **2015**, *8*, 2436−2454.

(22) Fiorani, G.; Stuck, M.; Martin, C.; Belmonte, M. M.; Martin, E.; Escudero-Adan, E. C.; Kleij, A. W. Catalytic Coupling of Carbon Dioxide with Terpene Scaffolds: Access to Challenging Bio-Based Organic Carbonates. *ChemSusChem* **2016**, *9*, 1304−1311.

(23) Navarro, M.; Sánchez-Barba, L. F.; Garcés, A.; Fernández-Baeza, J.; Fernández, I.; Lara-Sánchez, A.; Rodríguez, A. M. Bimetallic scorpionate-based helical organoaluminum complexes for efficient carbon dioxide fixation into a variety of cyclic carbonates. *Catal. Sci. Technol.* **2020**, *10*, 3265−3278.

(24) Martínez, J.; Fernández-Baeza, J.; Sánchez-Barba, L. F.; Castro-Osma, J. A.; Lara-Sánchez, A.; Otero, A. An Efficient and Versatile Lanthanum Heteroscorpionate Catalyst for Carbon Dioxide Fixation into Cyclic Carbonates. *ChemSusChem* **2017**, *10*, 2886−2890.

(25) Kamphuis, A. J.; Milocco, F.; Koiter, L.; Pescarmona, P. P.; Otten, E. Highly Selective Single-Component Formazanate Ferrate-

(II) Catalysts for the Conversion of CO_2 into Cyclic Carbonates. *ChemSusChem* **2019**, *12*, 3635−3641.

(26) Li, C.-Y.; Su, Y.-C.; Lin, C.-H.; Huang, H.-Y.; Tsai, C.-Y.; Lee, T.-Y.; Ko, B.-T. Synthesis and characterization of trimetallic cobalt, zinc and nickel complexes containing amine-bis(benzotriazole phenolate) ligands: efficient catalysts for coupling of carbon dioxide with epoxides. *Dalton Trans.* **2017**, *46*, 15399−15406.

(27) Aomchad, V.; Cristòfol, À.; Della Monica, F.; Limburg, B.; D'Elia, V.; Kleij, A. W. Recent progress in the catalytic transformation of carbon dioxide into biosourced organic carbonates. *Green Chem.* **2021**, *23*, 1077−1113.

(28) Hu, Y.; Steinbauer, J.; Stefanow, V.; Spannenberg, A.; Werner, T. Polyethers as Complexing Agents in Calcium-Catalyzed Cyclic Carbonate Synthesis. *ACS Sustainable Chem. Eng.* **2019**, *7*, 13257−13269.

(29) Calmanti, R.; Selva, M.; Perosa, A. Tungstate ionic liquids as catalysts for CO_2 fixation into epoxides. *Mol. Catal.* **2020**, *486*, 110854.

(30) Morikawa, H.; Minamoto, M.; Gorou, Y.; Yamaguchi, J.; Morinaga, H.; Motokucho, S. Two Diastereomers of d-Limonene-Derived Cyclic Carbonates from d-Limonene Oxide and Carbon Dioxide with a Tetrabutylammonium Chloride Catalyst. *Bull. Chem. Soc. Jpn.* **2018**, *91*, 92−94.

(31) Morikawa, H.; Yamaguchi, J. I.; Sugimura, S. I.; Minamoto, M.; Gorou, Y.; Morinaga, H.; Motokucho, S. Systematic synthetic study of four diastereomerically distinct limonene-1,2-diols and their corresponding cyclic carbonates. *Beilstein J. Org. Chem.* **2019**, *15*, 130−136.

(32) Bähr, M.; Mülhaupt, R.; Ritter, B. S. CARBONATE GROUP COMPRISING TERPENE-DERIVED MONOMERS AND ISO-CYANATE-FREE POLYURETHANES. WO2012171659A1, 2012.

(33) Bähr, M.; Bitto, A.; Mülhaupt, R. Cyclic limonene dicarbonate as a new monomer for non-isocyanate oligo- and polyurethanes (NIPU) based upon terpenes. *Green Chem.* **2012**, *14*, 1447−1454.

(34) Schimpf, V.; Ritter, B. S.; Weis, P.; Parison, K.; Mülhaupt, R. High Purity Limonene Dicarbonate as Versatile Building Block for Sustainable Non-Isocyanate Polyhydroxyurethane Thermosets and Thermoplastics. *Macromolecules* **2017**, *50*, 944−955.

(35) Maltby, K. A.; Hutchby, M.; Plucinski, P.; Davidson, M. G.; Hintermair, U. Selective Catalytic Synthesis of 1,2- and 8,9-Cyclic Limonene Carbonates as Versatile Building Blocks for Novel Hydroxyurethanes. *Chem. Eur. J.* **2020**, *26*, 7405−7415.

(36) Aomchad, V.; Del Gobbo, S.; Yingcharoen, P.; Poater, A.; D'Elia, V. Exploring the potential of group III salen complexes for the conversion of CO_2 under ambient conditions. *Catal. Today* **2021**, *375*, 324−334.

(37) Sopeña, S.; Laserna, V.; Guo, W.; Martin, E.; Escudero-Adán, E. C.; Kleij, A. W. Regioselective Organocatalytic Formation of Carbamates from Substituted Cyclic Carbonates. *Adv. Synth. Catal.* **2016**, *358*, 2172−2178.

(38) Topham, S.; Bazzanella, A.; Schiebahn, S.; Luhr, S.; Zhao, L.; Otto, A.; Stolten, D., Carbon Dioxide. In *Ullmann's Encyclopedia of Industrial Chemistry*; Wiley-VCH Verlag GmbH & Co. KGaA: Weinheim, Germany, 2014; pp. 1−43, DOI: 10.1002/14356007.a05_165.pub2.

(39) Kroon, M. C.; Peters, C. J., Supercritical Fluids in Ionic Liquids. In *Ionic Liquids Further UnCOILed: Critical Expert Overviews*, Plechkova, N. V.; Seddon, K. R., Eds. John Wiley & Sons, Inc.: 2014; pp. 39−57, DOI: 10.1002/9781118839706.ch2.

(40) Lozano, P.; De Diego, T.; Vaultier, M.; Iborra, J. L., Enzyme Catalysis in Ionic Liquids and Supercritical Carbon Dioxide. In *Ionic Liquid Applications: Pharmaceuticals, Therapeutics, and Biotechnology*, Malhotra, S., Ed. American Chemical Society: Washington, DC,USA 2010; Vol. *1038*, pp. 181−196, DOI: 10.1021/bk-2010-1038.ch015.

(41) Jutz, F.; Andanson, J.-M.; Baiker, A. Ionic Liquids and Dense Carbon Dioxide: A Beneficial Biphasic System for Catalysis. *Chem. Rev.* **2011**, *111*, 322−353.

(42) Hintermair, U.; Zhao, G.; Santini, C. C.; Muldoon, M. J.; Cole-Hamilton, D. J. Supported ionic liquid phase catalysis with supercritical flow. *Chem. Commun.* **2007**, *14*, 1462−1464.

73

(43) Lozano, P.; García-Verdugo, E.; Piamtongkam, R.; Karbass, N.; De Diego, T.; Burguete, M. I.; Luis, S. V.; Iborra, J. L. Bioreactors Based on Monolith-Supported Ionic Liquid Phase for Enzyme Catalysis in Supercritical Carbon Dioxide. *Adv. Synth. Catal.* **2007**, *349*, 1077−1084.

(44) Aprile, C.; Giacalone, F.; Agrigento, P.; Liotta, L. F.; Martens, J. A.; Pescarmona, P. P.; Gruttadauria, M. Multilayered Supported Ionic Liquids as Catalysts for Chemical Fixation of Carbon Dioxide: A High-Throughput Study in Supercritical Conditions. *ChemSusChem* **2011**, *4*, 1830−1837.

(45) Kukawka, R.; Pawlowska-Zygarowicz, A.; Dzialkowska, J.; Pietrowski, M.; Maciejewski, H.; Bica, K.; Smiglak, M. Highly Effective Supported Ionic Liquid-Phase (SILP) Catalysts: Characterization and Application to the Hydrosilylation Reaction. *ACS Sustainable Chem. Eng.* **2019**, *7*, 4699−4706.

(46) Keskin, S.; Kayrak-Talay, D.; Akman, U.; Hortaçsu, Ö. A review of ionic liquids towards supercritical fluid applications. *J. Supercrit. Fluids* **2007**, *43*, 150−180.

(47) Blanchard, L. A.; Gu, Z.; Brennecke, J. F. High-Pressure Phase Behavior of Ionic Liquid/CO_2 Systems. *J. Phys. Chem. B* **2001**, *105*, 2437−2444.

(48) Sainz Martinez, A.; Hauzenberger, C.; Sahoo, A. R.; Csendes, Z.; Hoffmann, H.; Bica, K. Continuous Conversion of Carbon Dioxide to Propylene Carbonate with Supported Ionic Liquids. *ACS Sustainable Chem. Eng.* **2018**, *6*, 13131−13139.

(49) Fehér, C.; Papp, M.; Urbán, B.; Skoda-Földes, R., Chapter 17 - Catalytic Applications of Supported Ionic Liquid Phases. In *Advances in Asymmetric Autocatalysis and Related Topics*, Pályi, G.; Kurdi, R.; Zucchi, C., Eds. Academic Press: 2017; pp. 317−336, DOI: 10.1016/ B978-0-12-812824-4.00017-4.

(50) Olivier-Bourbigou, H.; Magna, L.; Morvan, D. Ionic liquids and catalysis: Recent progress from knowledge to applications. *Appl. Catal., A* **2010**, *373*, 1−56.

(51) Gambacorta, G.; Sharley, J. S.; Baxendale, I. R. A comprehensive review of flow chemistry techniques tailored to the flavours and fragrances industries. *Beilstein J. Org. Chem.* **2021**, *17*, 1181−1312.

(52) Rehman, A.; Saleem, F.; Javed, F.; Ikhlaq, A.; Ahmad, S. W.; Harvey, A. Recent advances in the synthesis of cyclic carbonates via CO_2 cycloaddition to epoxides. *J. Environ. Chem. Eng.* **2021**, *9*, 105113.

(53) Rehman, A.; López Fernández, A. M.; Gunam Resul, M. F. M.; Harvey, A. Highly selective, sustainable synthesis of limonene cyclic carbonate from bio-based limonene oxide and CO_2: A kinetic study. *Journal of CO2 Utilization* **2019**, *29*, 126−133.

(54) Costa, V. V.; da Silva Rocha, K. A.; Kozhevnikov, I. V.; Kozhevnikova, E. F.; Gusevskaya, E. V. Heteropoly acid catalysts for the synthesis of fragrance compounds from biorenewables: isomerization of limonene oxide. *Catal. Sci. Technol.* **2013**, *3*, 244−250.

(55) Takahashi, T.; Watahiki, T.; Kitazume, S.; Yasuda, H.; Sakakura, T. Synergistic hybrid catalyst for cyclic carbonate synthesis: Remarkable acceleration caused by immobilization of homogeneous catalyst on silica. *Chem. Commun.* **2006**, *15*, 1664−1666.

(56) Cao, T.; Sun, L.; Shi, Y.; Hua, L.; Zhang, R.; Guo, L.; Zhu, W.; Hou, Z. The Role of Inorganic Oxide Supports in Synthesis of Cyclic Carbonates from Carbon Dioxide and Epoxides. *Chin. J. Catal.* **2012**, *33*, 416−424.

(57) Steinbauer, J.; Longwitz, L.; Frank, M.; Epping, J.; Kragl, U.; Werner, T. Immobilized bifunctional phosphonium salts as recyclable organocatalysts in the cycloaddition of CO_2 and epoxides. *Green Chem.* **2017**, *19*, 4435−4445.

74

F   Silicon Oxycarbide (SiOC) Supported Ionic Liquids: Heterogeneous Catalysts for Cyclic Carbonate Formation

Homogeneous catalysts for the production of bio-based cyclic carbonates are elaborately studied, whereas heterogeneous systems are rarely described in literature[111, 174, 177-182]. In addition, supports are mostly based on silica. Based on our experience employing silica-immobilized ionic liquids as heterogeneous catalysts for the production of cyclic carbonates,[101, 102] the high affinity to water and the free hydroxyl groups on the surface of silica can trigger the formation of undesired byproducts, such as diols, oligomers or polymers, after the epoxide ring is opened.
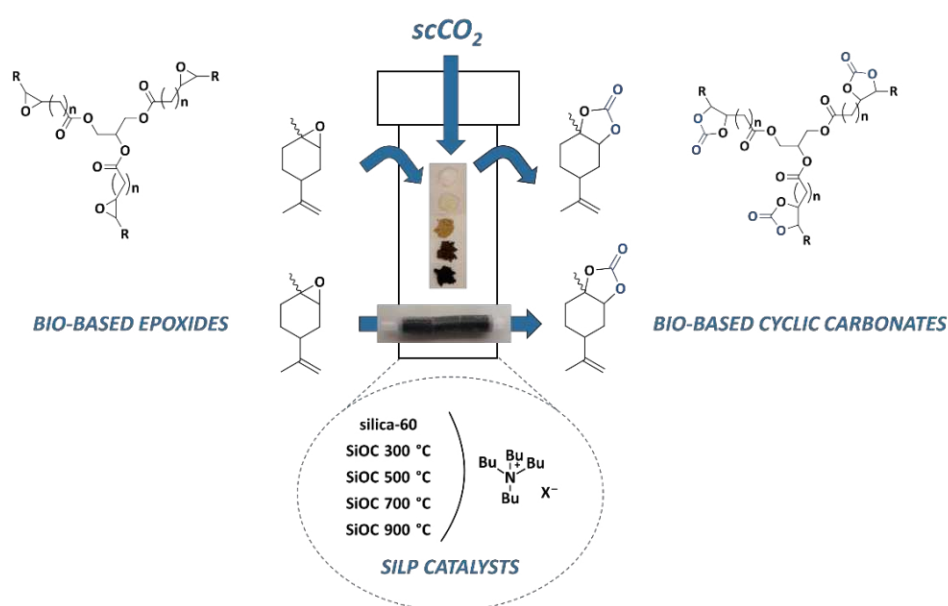
Scheme 31: Silica- and silicon oxycarbide-based SILPs for the batch-wise and continuous formation of bio-based cyclic carbonates in supercritical carbon dioxide.

Silicon oxycarbide-based SILPs were investigated for the formation of limonene- and linseed oil-derived cyclic carbonates as an alternative to commonly used silica-based SILPs (**Scheme 31**). Silicon oxycarbides were produced *via* the polymer-derived ceramics route[183] and shaped *via* photopolymerization-assisted solidification templating.[184, 185] Photopolymerized green bodies were pyrolyzed at temperatures between 300-900 °C and milled to obtain, after impregnation, with ionic liquid, silicon oxycarbide-based SILPs, which were tested in batch mode as heterogeneous catalysts. Characterization was performed *via* Fourier transform infrared spectroscopy, nitrogen adsorption, thermogravimetric analysis, and microscopy. Furthermore, solvent adsorption revealed low affinity of silicon oxycarbides to water compared to silica, which is beneficial for the selectivity of the catalytic process. Ultimately, macroporous monolithic silicon oxycarbide-based SILPs were successfully applied for the continuous production of cyclic limonene carbonates.

In the following, the below-mentioned publication is presented:

Mikšovsky, P.; Rauchenwald, K.; Naghdi, S.; Eder, D.; Konegger T.; Bica-Schröder, K., Silicon Oxycarbide (SiOC) Supported Ionic Liquids: Heterogeneous Catalysts for Cyclic Carbonate Formation. *ACS Sustainable Chem Eng* **2023** (revision submitted).

As a main author, together with Katharina Rauchenwald, I contributed to the investigation, conceptualization, methodology, visualization, writing of the original draft, and review of the manuscript.

Silicon Oxycarbide (SiOC) Supported Ionic Liquids: Heterogeneous Catalysts for Cyclic Carbonate Formation

Philipp Mikšovsky [1, †], Katharina Rauchenwald [2, †], Shaghayegh Naghdi [3], Hannah Rabl [3], Dominik Eder [3], Thomas Konegger [2,]* and Katharina Bica-Schröder [1,]*

[1]Institute of Applied Synthetic Chemistry, TU Wien, Getreidemarkt 9, 1060 Vienna, Austria.

* katharina.schroeder@tuwien.ac.at

[2]Institute of Chemical Technologies and Analytics, TU Wien, Getreidemarkt 9, 1060 Vienna, Austria.

* thomas.konegger@tuwien.ac.at

[3]Institute of Materials Chemistry, TU Wien, Getreidemarkt 9, 1060 Vienna, Austria.

† These two authors contributed equally.

ABSTRACT

Silicon oxycarbides (SiOCs) impregnated with tetrabutylammonium halides (TBAX) were investigated as an alternative to silica-based supported ionic liquid phases for the production of bio-based cyclic carbonates derived from limonene and linseed oil. The support materials and the supported ionic liquid phases (SILPs) were characterized via Fourier transform infrared spectroscopy, thermogravimetric analysis, nitrogen adsorption, X-ray photoelectron spectroscopy, microscopy and solvent adsorption. Silicon oxycarbide supports were pyrolyzed at 300-900 °C prior to coating with different tetrabutylammonium halides and further used as heterogeneous catalysts for the formation of cyclic carbonates in batch mode. Excellent selectivities of 97-100% and yields of 53-62% were obtained with tetrabutylammonium chloride supported on silicon oxycarbides. For comparison, the catalytic performance of commonly employed silica-supported ionic liquids was investigated under the same conditions. Silica-supported species triggered the formation of diol as a by-product leading to a lower selectivity of 87% and a lower yield of 48%, respectively. Ultimately, macroporous monolithic SiOC-SILPs with suitable permeability characteristics ($k_1 = 10^{-11}\,\mathrm{m}^2$) were produced via photopolymerization-assisted solidification templating and applied for the selective and continuous production of limonene carbonate in supercritical carbon dioxide as reagent and sole solvent. Constant product output over 48 h without concurrent catalyst leaching was achieved.

INTRODUCTION

The concept of supported ionic liquid phases (SILPs) describes materials where a thin layer of ionic liquid remains confined on a porous solid support, resulting in composite materials that possess unique properties.[1] The combination of the liquid-like behavior of ionic liquids with the structural integrity of solid supports lead to numerous applications that emerged over the past years, covering catalysis,[2-10] gas purification and storage,[11-14] as well as metal recovery.[15-17] Especially in catalysis, SILPs combine the properties of ionic liquids with the advantages of heterogeneous systems, such as easy catalyst separation and improved mass transfer. Furthermore, the application of SILPs circumvents the use of bulk quantities of ionic liquids which is not feasible for their application on an industrial scale.[18-20]

SILPs have also been successfully employed for the immobilization of catalysts in combination with supercritical carbon dioxide (scCO$_2$, T$_c$: 31.0 °C, p$_c$: 7.38 MPa)[21] since scCO$_2$ is highly soluble in ionic liquids, but the ionic liquid cannot dissolve in scCO$_2$. This behavior provides ideal conditions for the immobilization of catalysts, where scCO$_2$ serves either as solvent[22-25] or as reagent and solvent at the same time.[26-29] The scCO$_2$ can thus act simultaneously as C1 building block, for example in the formation of cyclic carbonates from epoxides, and as solvent for the use of SILP catalysts. The aims are to increase the catalytic activity,[30] facilitate the recyclability of the catalyst,[31] or to enable a continuous flow process for this particular reaction.[32, 33]

The use of epoxides and carbon dioxide as starting materials further benefits from particularly high atom economies of 100% since all starting materials are fully incorporated in the product. Other synthetic routes for cyclic carbonates include transesterification or phosgenation which suffer e.g., from lower atom economy and the use of toxic reagents.[34, 35]

Various ionic liquid-based heterogenous but also homogeneous catalysts are reported for the conversion of common epoxides such as propylene oxide or styrene oxide to cyclic carbonates using different supports for ionic liquids or polymerizable ionic liquid-based precursors.[36-39]

Our studies, aiming for bio-based cyclic carbonates, were motivated by the annual production of such compounds on a multi-ton scale,[40] which are used as electrolyte solutions in lithium-ion batteries[41] or as precursors for isocyanate-free polyurethanes.[42] This high demand highlights the necessity to develop synthetic routes utilizing bio-based feedstocks including terpenes, such as limonene, and vegetable oils, such as linseed oil to get independent from crude oil as limited fossil feedstock. The homogeneous catalysis of such bio-based cyclic carbonates is well established, but only a few examples of heterogeneous catalysts are literature-known.[43-48] Supports based on carboxymethyl cellulose[49] and polyethylene[50] are reported. However, silica is the most used support.[48, 51-53]

Our previous studies[26, 28] with silica-supported ionic liquids as heterogeneous catalysts for the formation of cyclic carbonates from epoxides showed a synergistic effect between ionic liquid and support material. It was also briefly mentioned that although catalytic water can be beneficial in homogenous systems[54], the free hydroxyl groups and the mildly acidic surface of the silica support as well as the high affinity to water of silica can trigger the formation of undesired byproducts. After the epoxide ring is opened, byproducts such as diols, poly- or oligomers can be formed. [26, 28] The interest in a support material versatile in terms of surface hydrophilicity and tunable in shape and porosity, as an alternative to silica, has been raised.

Advanced silicon-based inorganic compounds can be obtained by the pyrolytic conversion of preceramic polymers, such as polysiloxanes to silicon oxycarbide (SiOC) in an inert atmosphere.[55] The polymer-derived ceramics route[56] yields Si-O-C materials which typically consist of

nanodomains rich in silicon dioxide, separated by a carbon phase.[57] Functionalization of the preceramic polymer and the choice of the pyrolysis atmosphere and temperature offer room for property optimization to yield materials of high chemical and thermal resistance for various fields of applications.[55] For instance, stopping the pyrolysis process at a stage where the polymer is only partly converted provides materials with intermediate characteristics of polymers and ceramics, so-called ceramers.[58] Depending on the degree of conversion, ceramers can feature tunable surface hydrophilicity and high specific surface area, rendering them suitable adsorbents,[58, 59] also for carbon dioxide[60] if amine-functionalized.

Further, polymer-derived ceramics can be processed employing advanced shaping methods including additive manufacturing[61, 62] or solidification templating.[63-67] Solidification templating, commonly referred to as freeze-casting,[68] is a porosification technique where a ceramic slurry or a preceramic polymer solution is cast into a mold, with a subsequent controlled solidification followed by selective removal of the solvent, e.g., via freeze-drying. This technique facilitates the generation of templated pore structures.[65] By variation of the solid or polymer content, selection of the structure-directing solvent, and by the thermal gradient applied during solidification, pore characteristics such as total porosity, pore morphology, pore orientation, and pore size distribution can be adjusted straightforwardly. The removal of the structure-directing solvent prior to thermal treatment renders solidification templating a more sustainable porosification method, compared to sacrificial porogens that are burned out, to obtain monolithic catalyst supports, since the solvent can be recycled in an upscaling event.

In case of preceramic polymer solutions, the solidification process initiates the phase separation of the solvent from the preceramic polymer. However, to retain the templated shape upon removal of the solvent and during subsequent pyrolytic conversion, the preceramic polymer needs to be cross-

5

linked. Controlled polycondensation treatments have been employed to facilitate the freeze-casting of polysiloxanes,[64, 65, 69, 70] but these reactions are generally rather slow at low temperatures. Photopolymerization-assisted solidification templating, which has been shown using thiol-ene "click" reaction,[63, 66, 71] is an interesting alternative as it is feasible at low temperatures and applicable in a controlled manner.

With regard to the continuous production of cyclic carbonates, macroporous monoliths as SILP support, instead of a packed bed reactor, offer a high degree of control over the fluid flow,[72] in addition to easier catalyst handling. Examples of monolithic SILPs exist in literature[73-76] where ionic liquids are immobilized on porous cellulose monoliths[73-75] or where silane monomers serve as precursors for polymer-supported ionic liquids.[76, 77] However, to the best of our knowledge, no work has been thus far reported on the physisorption of ionic liquids on silicon oxycarbide subsequently used as a heterogeneous catalyst for the production of cyclic carbonates.

In this paper, we present the synthesis and characterization of silicon oxycarbide-based SILPs (SiOC-SILPs) and their successful application as heterogeneous catalysts for the formation of bio-based cyclic carbonates starting from limonene oxide and epoxidized linseed oil. Catalytic performance of SiOC-SILPs was compared to state-of-the-art silica-supported ionic liquids (SiO$_2$-SILPs) resulting in higher yields and higher selectivities for the developed SiOC-supported species. Ultimately, macroporous, monolithic SiOC-SILPs were successfully applied for the selective continuous production of cyclic carbonates.

82

RESULTS AND DISCUSSION

Preparation and Characterization of Silicon Oxycarbide as Support Material

For the preparation of silicon oxycarbide supports **7**, a commercially available polysilsesquioxane **1** was functionalized **A** with photoactive methacrylate groups **2** to perform photopolymerization-assisted solidification templating **B**, as illustrated in **Figure 1**. Preceramic solutions **4** with a polymer content of 20 or 30 wt.% were mixed with the radical initiator phenylbis (2,4,6-trimethylbenzoyl) phosphine oxide (BAPO **5**) and frozen at -20 °C to induce phase separation of the polymer from *tert*-butyl alcohol **3,** which acts as solvent for functionalization **A** and as structure directing agent for solidification templating **B**. Irradiation with blue light (405 nm, 30 min) was applied at -20 °C to stabilize the templated state via a radical crosslinking reaction, yielding samples of sufficient structural integrity to further remove the frozen solvent by sublimation. In a first step, silicon oxycarbide powders **7a** were prepared to perform batch experiments. Green bodies **6a** were converted to silicon oxycarbides **7a** via pyrolytic treatment **C** in argon flow employing different pyrolysis temperatures (300-900 °C), followed by ball milling and sieving (90 µm mesh size) in order to obtain particle sizes comparable to silica-60**.** In a second step, batch-wise production of cyclic carbonates was transitioned to continuous mode using optimized, monolithic silicon oxycarbide supports **7b.**

The pyrolytic conversion was studied by thermogravimetric analysis (TGA, **Figure S1**), which showed a typical conversion of crosslinked polysiloxane **6** to silicon oxycarbide **7**, undergoing two distinct mass-loss steps. First, low-molecular-weight residuals from the functionalization **A** as well as monomers not sufficiently bound to the polymeric backbone are removed between 200 and 400 °C. Interruption of the pyrolysis in this phase still yields silicone-type compounds. The main conversion from the green body **6** to silicon oxycarbide **7** occurs during the second mass-loss stage

at T > 400 °C via dehydrogenation of functional groups. In the range between approximately 500-700 °C, the evolution of volatile decomposition products usually reaches its maximum. An interruption of the conversion process in this stage yields ceramers with particularly high specific surface areas.[58] Upon reaching 800 °C, the conversion can be considered complete. Four distinct pyrolysis temperature treatments were selected to compare the polymer state (300 °C, denoted as SiOC300) with ceramer intermediate states (SiOC500 and SiOC700) and the final ceramic state (SiOC900) for the application as catalyst support for SILPs. The silicon oxycarbides **7a** show a difference in color as a result of the different degrees of carbon conversion (**Figure 1**).
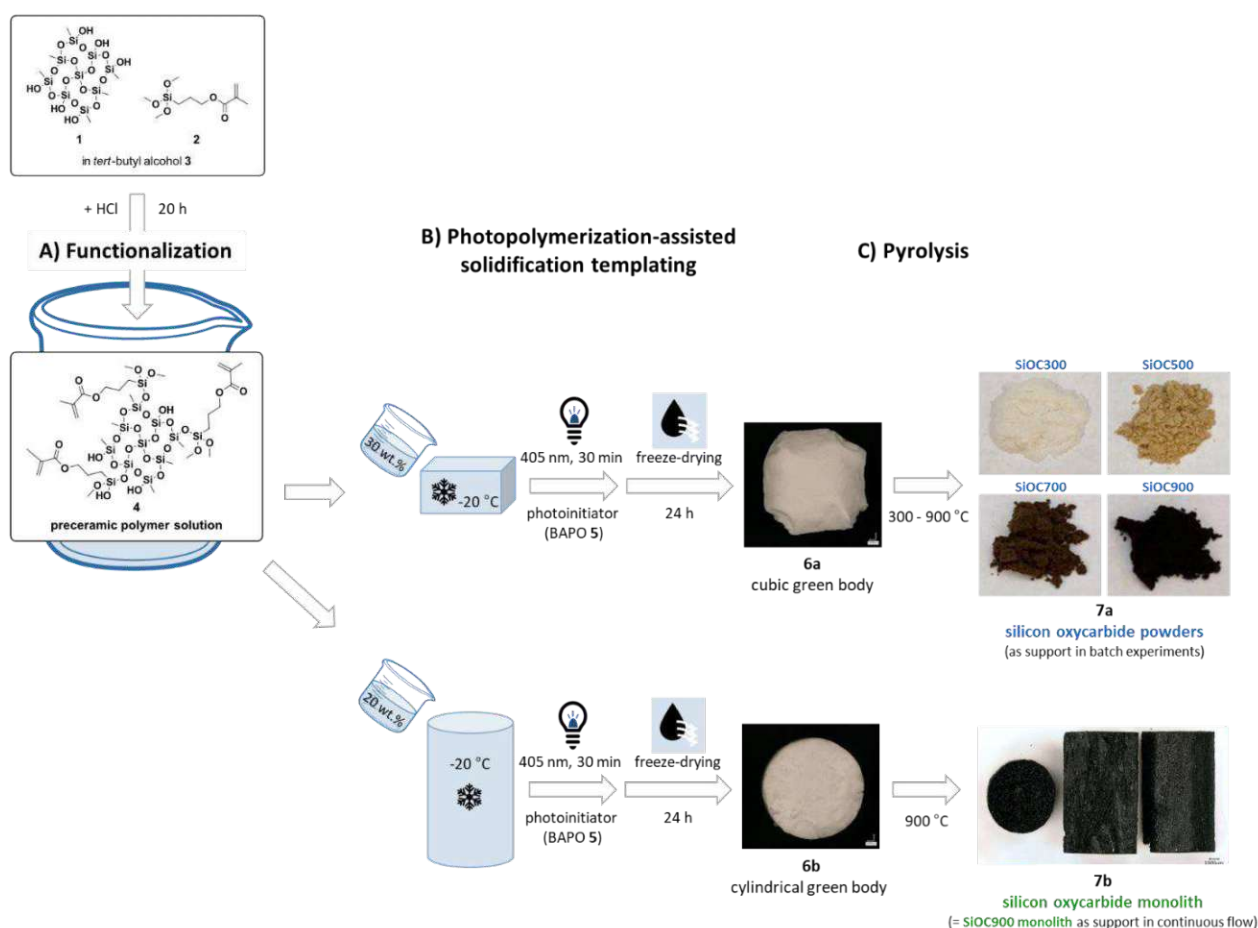
Figure 1: Functionalization **A** of polysilsesquioxane **1** to obtain a photocurable solution **4**, suitable for photopolymerization-assisted solidification templating **B** of polysiloxane-derived ceramics.

8

Fourier transform infrared spectroscopy (FTIR, **Figure 2a**) revealed that when stopping pyrolysis at 300 °C, methacrylate moieties are still present, while at 500 °C, they are completely converted (C=O band at 1728 cm^{-1}). At 700 °C, alkyl groups are almost completely converted as well (CH: 3027 – 2811 cm^{-1}; CH$_2$, CH$_3$: 1505 – 1228 cm^{-1}). Moreover, Si-CH$_3$ groups are converted successively at higher temperatures (759 cm^{-1}). At 900 °C, the preceramic polymer is fully converted to an amorphous silicon oxycarbide ceramic, preserving the Si-O-Si bands at 1214 – 901 cm^{-1}. Ionic liquid loading onto the silicon oxycarbide supports **7a** led to additional vibrations at 3023 – 2762 cm^{-1} and 1502 – 1340 cm^{-1}, indicating C-H and C-C vibrations of the tetrabutylammonium cation (**Figure S7-S8**).

Volatiles from the decomposition of methacrylate and alkyl groups, such as hydrocarbons and hydrogen,[55, 58] led to high specific surface areas (**Figure S3, Table S1**) in intermediate processing stages, with a maximum of 550 m^2 g^{-1} in microporous SiOC500. In SiOC900, transient microporosity has disappeared (indicated by a low specific surface area of 2 m^2 g^{-1}). In this case, impregnation with ionic liquid only slightly increases the specific surface area to 2 - 4 m^2 g^{-1}. At an ionic liquid loading of 20 wt.%, microporosity in SiOC500 and SiOC700 ceramers can be assumed to be filled. However, both best-performing catalysts, **SILP 5a** and **SILP 11a**, are non-micro-/mesoporous materials according to nitrogen adsorption measurements. In contrast, upon loading mesoporous silica-60 with ionic liquid, the surface area decreased but remained at a high level of 221 - 263 m^2 g^{-1}.

Furthermore, the affinity of the SiOC support materials to polar and non-polar molecules was investigated by solvent adsorption and was compared to silica-60, a commonly used support material for SILPs. Water and *n*-heptane are substances with mainly polar and non-polar interaction, respectively, and can be used to quantify the hydrophilicity of a material.[60] The amount

of solvent adsorbed was measured gravimetrically after exposure of the dried materials to saturated atmospheres, at 25 °C, for 24 h. Silica took up an exceptional amount of 57 ± 1 wt.% water and 35 ± 3 wt.% n-heptane (**Figure 2b**). The higher uptake of water compared to n-heptane is indicative of the material hydrophilicity, which is related to the oxidic surface. In contrast, silicon oxycarbides take up significantly lower amounts of solvent vapor. Further, a trend of decreasing affinity to n-heptane and increasing affinity to water was observed with increasing pyrolysis temperatures. The transition from hydrophobic to hydrophilic characteristics results from a successive loss of residual polymer functionalities, as confirmed by FTIR (**Figure 2a**). The observed transition temperature from hydrophobic to slightly hydrophilic between 500 and 700 °C is in accordance with results from a previous study.[78]
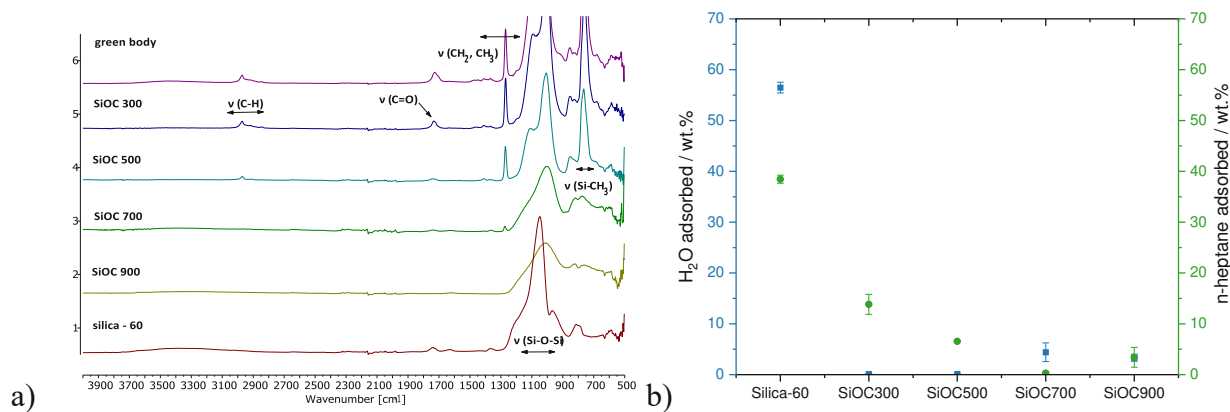
Figure 2. Characterization of surface functionalities and affinity to polar and non-polar solvents of silicon oxycarbides **7a** derived from different pyrolysis temperatures compared to silica-60 via a) FTIR-spectra and b) solvent adsorption.

In conclusion, in comparison to silica-60, carbon incorporation in silicon oxycarbide pyrolyzed at 900 °C (14.9 ± 0.5 wt.% in SiOC900, determined by combustion method) as well as lack of mesoporosity lower the affinity to water vapor, which is beneficial for the selective formation of cyclic carbonates, as shown in **Figure 4b** and discussed in detail hereinafter.

10

Based on literature procedures,[26] powdered silicon oxycarbides **7a** pyrolyzed at different temperatures (SiOC 300, SiOC500, SiOC700, SiOC900) and silica-60 (SiO$_2$) were impregnated with tetrabutylammonium chloride TBAC **8**, -bromide TBAB **9,** and -iodide TBAI **10** to generate SILPs used further as heterogeneous catalysts (**Table 1**).

Table 1. Supported ionic liquids: Powdered and monolithic supports, impregnated with ionic liquids, employed for the formation of bio-based cyclic carbonates in batch mode and in continuous flow.

SILP catalyst	support	ionic liquid (loading)
SILP 1a	SiO$_2$ (powder)	TBAC **8** (20 wt%)
SILP 2a	SiO$_2$ (powder)	TBAB **9** (20 wt%)
SILP 3a	SiO$_2$ (powder)	TBAI **10** (20 wt%)
SILP 4a	SiOC300 (powder)	TBAC **8** (20 wt%)
SILP 5a	SiOC300 (powder)	TBAB **9** (20 wt%)
SILP 6a	SiOC500 (powder)	TBAC **8** (20 wt%)
SILP 7a	SiOC500 (powder)	TBAB **9** (20 wt%)
SILP 8a	SiOC700 (powder)	TBAC **8** (20 wt%)
SILP 9a	SiOC700 (powder)	TBAB **9** (20 wt%)
SILP 10a	SiOC700 (powder)	TBAI **10** (20 wt%)
SILP 11a	SiOC900 (powder)	TBAC **8** (20 wt%)
SILP 12a	SiOC900 (powder)	TBAB **9** (20 wt%)
SILP 1b	SiOC900 (monolith)	TBAC **8** (20 wt%)
SILP 2b	SiOC900 (monolith)	TBAC **8** (35 wt%)

87

XPS spectra were recorded to determine the types of chemical bonding and functional groups present on the surface of SiOC-based SILPs compared to SiOC support materials. The survey scans revealed the existence of Si, C and O elements on the SiOC-surface and additional Cl and N for SILPs (**Figure S9** and **Table S2**). The peak assignment of high-resolution core-level spectra is based on literature[79]. The C1s fits (**Figure S11**) showed C-C bonds (sp³ hybridized) decreasing in intensity upon increasing pyrolysis temperature and increasing in intensity by addition of ionic liquid. Deconvolution of Si2p spectra (**Figure S13**) revealed various binding states, whereas peak assignment was challenging due to overlapping spin-orbit components. The N1s and Cl2p core level spectra were only present in SILPs (**Figure S12** and **Figure S14**). The O1s spectra revealed the presence of C-O, Si-O and Si-O-Si bonds (**Figure S10**). Furthermore, differences in structural behavior of SILPs and supports could be inferred especially from O1s spectra. This suggested an interaction of the catalytically active ionic liquid especially with the oxygen atoms of the SiOC support.

To investigate the stability of SILPs, thermogravimetric analyses of ionic liquids, silica, and SiOC-SILPs were conducted in air (**Figure S6**). Measurements revealed that after an initial loss of water (25-100 °C), mass loss started at around 160 °C, independently of the used supporting material or kind of ionic liquid, showing the high thermal stability of used ionic liquids. In addition, complete degradation of the ionic liquid was observed at around 230 °C for silicon oxycarbide-based SILPs, while for silica-based SILPs, the end of degradation was observed at 270 °C, most likely due to a stronger interaction of the support surface with the ionic liquid or the degradation products. Furthermore, the same thermal stabilities, with regard to the on-set of decomposition for supported and unsupported ionic liquids were observed. As expected, further conversion processes were observed for compounds previously pyrolyzed only at 300 °C (SiOC300).

Comparison of Silicon Oxycarbide- and Silica-Based Catalysts for the Formation of Bioderived

Cyclic Carbonates 15 and 18

Limonene oxide **14** was chosen as the primary bio-based feedstock since its potential as

feedstock for bulk chemicals, such as cyclic carbonates, is displayed in a global annual

production of 43 Mt and a global market of 314 million US\$ (2020).[80] SiO$_2$-SILPs for the batch

and continuous production of limonene carbonate (**Figure 3**

Figure 3) have already been studied in our group.[26] Furthermore, the production of linseed oil

carbonates **18** as promising precursors for non-isocyanate polyurethanes[51] is presented (**Figure 5**).
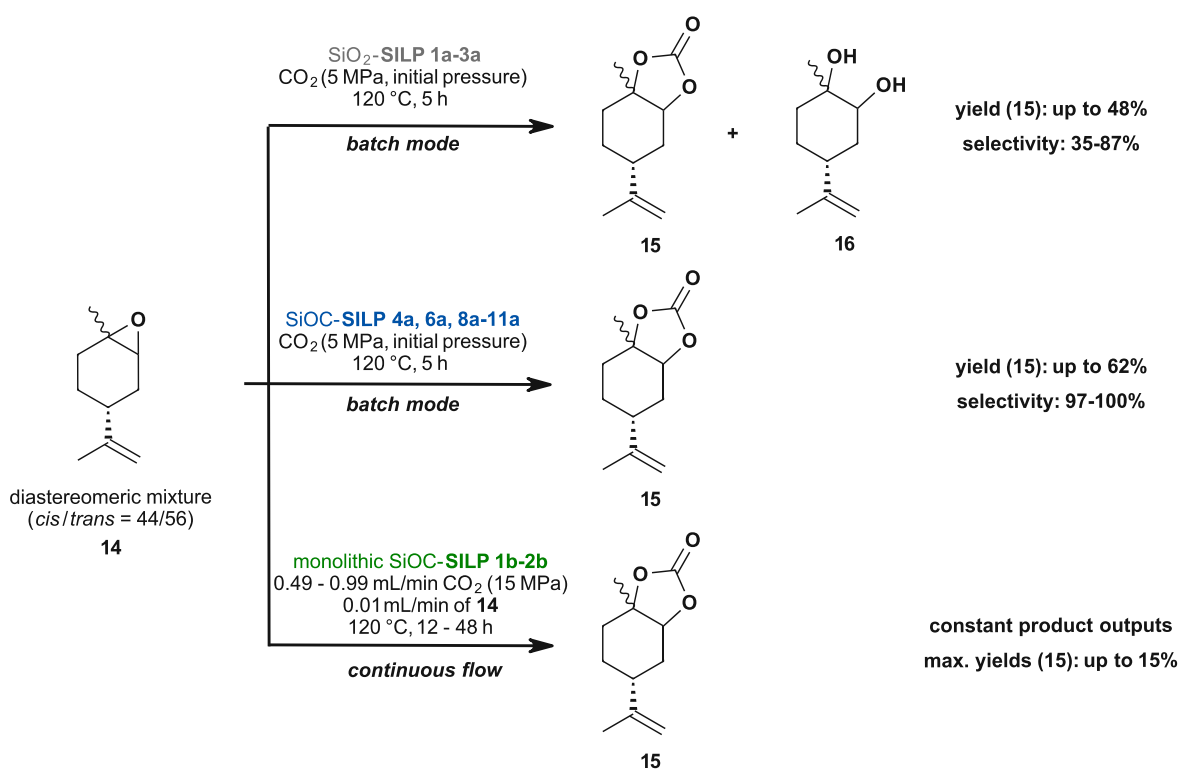
Figure 3. Limonene carbonates **15**: SiO$_2$-SILPs and SiOC-SILPs as catalysts in batch mode and

in continuous flow.

Based on reports of Morikawa *et al.*[81, 82], where tetrabutylammonium halides **8-10** were screened in batch mode for the conversion of limonene oxide **14** to limonene carbonate **15**, we expanded the scope of preliminarily tested homogeneous catalysts to imidazolium-based ionic liquids (**Table S3**) in a previous work.[26] During this screening, tetrabutylammonium halides **8-10** turned out to be suitable catalysts for the formation of limonene carbonate **15** resulting in a selective conversion of 72% and a yield of 68% (isolated yield: 57%) after 20 h at 100 °C in the case of the best candidate TBAC **8** (**Table S3,** entry S1-S3). Subsequently, TBAC **8** was physisorbed on silica as most commonly used support material for SILP catalysts and employed to the continuous production of different limonene carbonates. During the optimization of the continuous formation in the previous work, 120 °C turned out to be the optimum temperature in terms of yields, while higher temperatures lead to the degradation of catalyst. Due to higher reaction temperatures, the reaction time could be shortened from 20 h to 5 h for the catalyst screening performed in this work, resulting in a conversion of 58% of limonene oxide **14** using TBAC **8** (**Table S4**, entry S7). Furthermore, we were interested in the investigation of both isomers starting from the commercially available *cis/trans* mixture, however, the more reactive *trans* isomer (*cis*: 23%, *trans*: 85%) can be obtained via kinetic separation[83] to further increase yields.

Commonly used SiO_2-based SILPs impregnated with tetrabutylammonium halides **8-10** were employed as heterogeneous catalysts and compared to SiOC-based SILPs. Out of all tested SiO_2-based **SILPs 1a-3a (Figure 4a)**, **SILP 1a**, impregnated with TBAC **8**, performed best, which is following the nucleophilicity of halides in aprotic polar environment ($Cl^- > Br^- > I$). Nevertheless, the yield dropped from 55% to 48%, and selectivity from 95% to 87% compared to the homogeneous version (**Table S4**, entry S7). Moreover, it was observed that selectivity decreased

further to 63% and 35% when bromide and iodide served as anions in SiO_2-based **SILP 2a-3a**, respectively (**Figure 4a**).
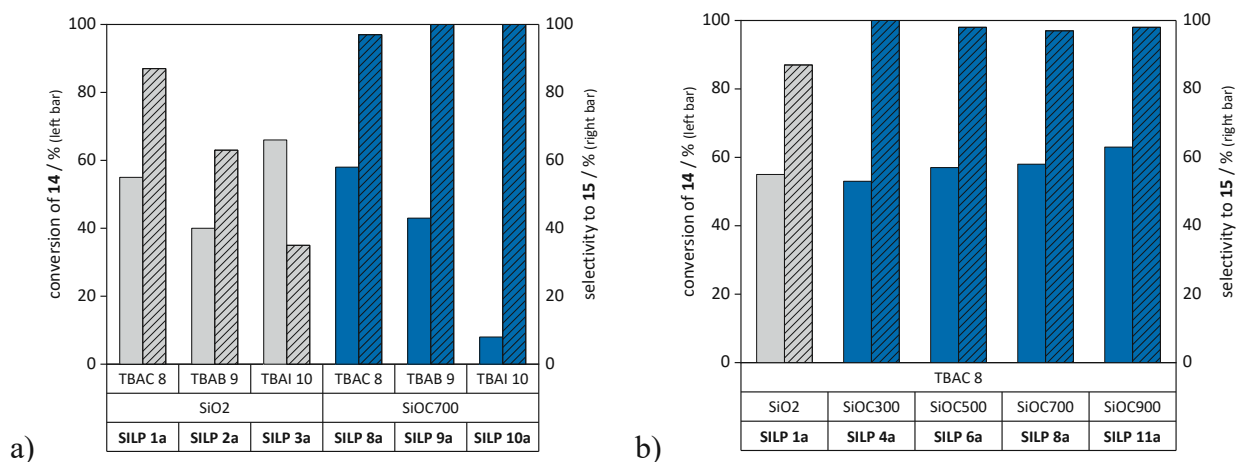
Figure 4: Catalyst screening for the formation of limonene carbonate **15** in batch mode.[a]

[a]conditions: 0.5 mmol of **14** (cis/trans = 43/57), SILP catalyst (0.05 mmol of **8-10**, catalyst loading: 20 wt%), 120 °C, 5 MPa CO_2 (gaseous, initial pressure), 5 h. Further details about the determination of conversion and selectivity (ratio of yield and conversion) is given in ESI chapter S.3.1.

Residual water and free hydroxyl groups on the surface of silica triggered the ring opening of the epoxide and the formation of diol **16** in amounts of 3-17%, determined via GC/MS. Furthermore, when 10 mol% of water was added to the reaction, generating a polar protic environment, a decrease in conversion from 55% to 50% and a selectivity of 66% were observed (**Table S3**, entry S10).

The co-catalytic effect of silica on the formation of undesired byproducts was further verified when silica was solely employed as catalyst (**Table S4,** entry S22). In this case, conversion reached 36%, 13% of diol **16** and no carbonate **15** were formed. This experiment showed the inevitable influence of the silica surface and the requirement for the development of alternative supports for the ionic liquid-catalyzed heterogeneous conversion of epoxides to cyclic carbonates to increase selectivity.

The diol was no longer formed when powdered silicon oxycarbides **7a** were employed as support materials, displayed by the obtained selectivity of 97-100 % (**Figure 4b**) and increased yields of 53-62 %. This correlates with the lower affinity of silicon oxycarbides to water as made apparent from solvent vapor adsorption experiments (**Figure 2b**). Moreover, the addition of 10 mol% of water to the reaction mixture resulted in no change of conversion and selectivity (**Table S4**, entry S21) when SiOC was employed as support. On the other hand, conversion and selectivity decreased in case of employing silica-based SILPs with catalytic amounts of water (**Table S4**, entry S10), as mentioned before. Therefore, the constantly high conversion and selectivity obtained with SiOC support suggests the involvement of the mildly acidic surface of silica on the epoxide ring opening and subsequent formation of byproduct diol **13.**

The trend of nucleophilicity (Cl$^-$ > Br$^-$ > I$^-$) was preserved with SiOC-**SILPs 8a-10a**, displayed by the obtained yields of 8-56%. Additionally, the influence of pyrolysis temperature (300 – 900 °C) of the silicon oxycarbide supports was investigated (**Figure 4b**). Yields increased from 53% to 62% with higher pyrolysis temperature, and remarkable selectivities of 97 – 100% were obtained without leaching of catalyst (limit of detection: 0.1 mg, ≤ 0.2% of total amount of TBAC **8**). Furthermore, silicon oxycarbide supports do not exert any catalytic effect (**Table S4**, entry S23-S26), in contrast to silica support (**Table S4**, entry S22).

Overall, **SILP 11a** (20 wt.% TBAC **8**, SiOC900) exhibited the highest yield and a selective formation of limonene carbonate **15** with 100% atom economy and thus was subsequently employed in continuous flow in monolithic form **7b**.

Secondly, we investigated the reaction of epoxidized linseed oil **17** catalyzed by SiO$_2$-SILPs and SiOC-SILPs (**Figure 5**). Determination of conversion was performed via ^{1}H-NMR (ESI chapter S.3.2) by quantifying the signal of the epoxide moieties (δ = 3.21 – 2.82 ppm) and using the protons

92

next to the carbonyl groups of the backbone ($\delta = 2.29$ ppm) as internal standard. Yields could not be determined due to overlapping signals in the NMR spectra (carbonate: $\delta = 5.40 - 4.06$ ppm). However, the formation of carbonate **18** was further proven via FTIR (**Figure S23**), where the appearing C=O band at 1792 cm^{-1} indicated the ongoing reaction.[51]
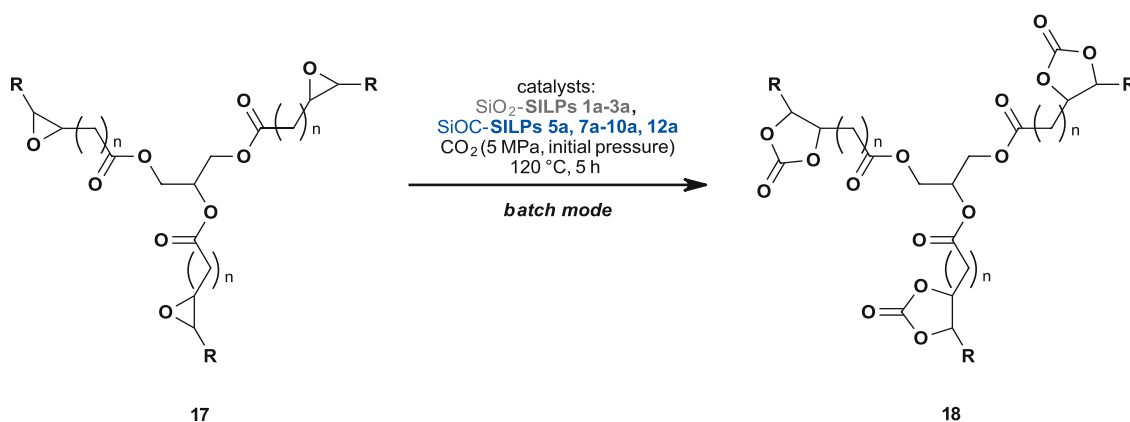
Figure 5. Linseed oil carbonates **18**: SiO$_2$-SILPs and SiOC-SILPs as catalysts in batch mode.

An extensive homogeneous catalyst screening with various ionic liquids reported by Tassaing *et al.*,[84] where the influence of halides (Cl$^-$, Br$^-$, I$^-$) and cationic cores (e.g. ammonium, phosphonium, sulfonium, imidazolium, pyridinium) on the conversion of epoxidized linseed oil **17** were investigated, revealed that different halides have the most pronounced impact on the catalytic activity. Tetrabutylammonium halides **8-10** turned out to be promising candidates, resulting in yields of 17-30% (TBAB **9** > TBAI **10** > TBAC **8**) in a 30 g scale (100 °C, 10 MPa).

Reproduction on a 220 mg scale (120 °C, 5 MPa) resulted in the same order of catalytic activity (TBAB **9** > TBAI **10** > TBAC **8**), displayed in yields of 41-56% (**Table S6**, entry S32-S34). Almost complete conversion of 97% was achieved after 20 h. The order of catalytic activity clearly shows the competition between the nucleophilicity and the size of the anion, since epoxidized linseed oil **17** is a sterically demanding substrate and smaller anions can reach the epoxide moieties easier.
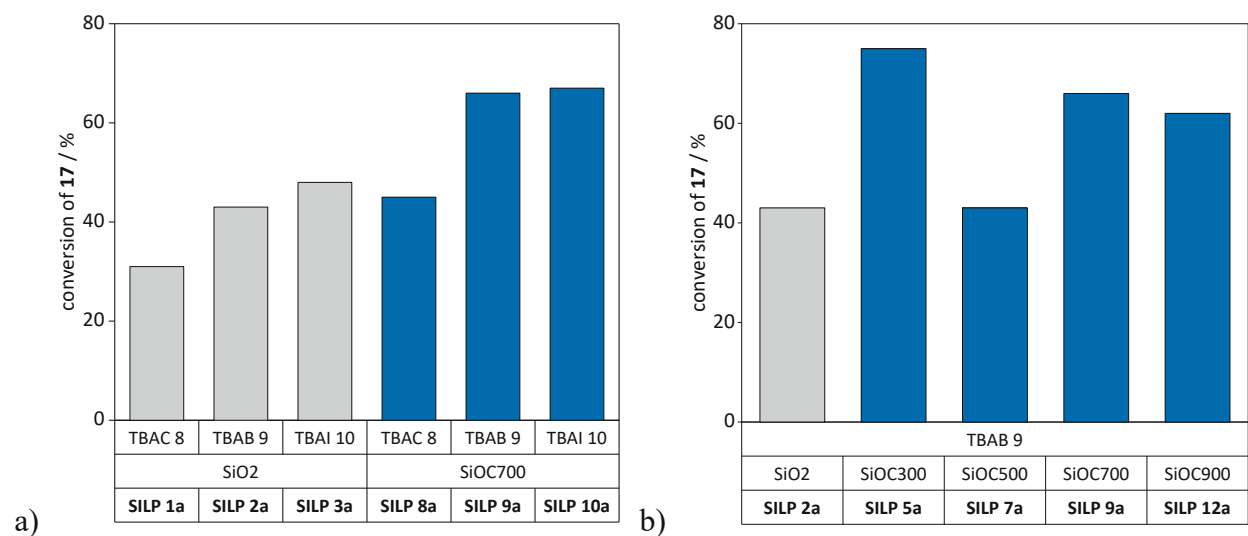
Figure 6: Catalyst screening for the formation of linseed oil carbonates **18** in batch mode.[a]

[a]conditions: 220 mg of **17**, SILP catalyst (0.02 mmol of **8-10**, catalyst loading: 20 wt%), 120 °C, 5 MPa CO_2 (gaseous, initial pressure), 5 h. Further details about the determination of conversion is given in ESI chapter S.3.2.

For SiO_2-**SILPs 1a-3a** (**Figure 6a**), impregnation with TBAI **10** resulted in the highest conversion of 48%. Conversion increased with SiOC-**SILPs 9a-10a** (**Figure 6a**) impregnated with TBAB **9** and TBAI **10** to 66-67%. Yields were further increased by employing the SiOC-SILPs prepared with silicon oxycarbide supports derived from different pyrolysis temperatures (300 – 900 °C), achieving conversions of up to 75% with **SILP 5a** using support SiOC300 (**Figure 6b**). Finally, it was proven that all supports show only low or no co-catalytic effect (**Table S6**, entry S46-S50). Leaching of catalysts **8-10** in batch experiments could not be determined due to inseparability of SILP catalyst from the highly viscous and poorly soluble reaction mixture e.g., via centrifugation or via dissolution of the reaction mixture in apolar solvents.

Moreover, the interaction behavior of SiOC support[79] with ionic liquid was further investigated via XPS as discussed before. Comparison of the O1s spectra of the supports and the SILPs (**Figure S10**) revealed different interaction behavior and, thus, an interaction of catalyst and support predominantly via the oxygen atom. This suggests that the interaction of the oxygen of SiOC

18

support with the ionic liquid is of crucial importance for the formation of cyclic carbonates using SiOC-supported ionic liquids compared to homogeneous catalysis.

Ultimately, studies in continuous flow with monolithic silicon oxycarbide-supported ionic liquids were conducted solely with limonene oxide **14** since neat epoxidized linseed oil **17** turned out to be too viscous for continuous transport; the addition of necessarily polar solvents for dissolution of epoxidized linseed oil **17** led to significant catalyst leaching (30%).

Characterization of Monolithic SiOC-SILPs 1b-2b

In **Figure 7a,** an optical microscopy image of monolithic silicon oxycarbide pyrolyzed at 900 °C **7b** cut in cross and longitudinal sections, with regard to the flow direction in the reactor for continuous experiments, is shown. The pore orientation is visualized by the color contrast of oxycarbide and epoxy resin, which appear as bright grey and dark grey, respectively, due to their difference in atomic mass, with the aid of backscattered electron detection in scanning electron microscopy (**Figure 7b,** method details given in ESI chapter S.7.1**).** Evidently, porosity generated by solidification templating in aluminum molds results in radial pore orientation in the cross-section, due to preferential nucleation of *tert*-butyl alcohol **3** on aluminum that features high thermal conductivity, thereby causing oriented crystal growth from the outside to the inside of the cylinders, as indicated by arrows. Further characterization of the monolith by mercury intrusion porosimetry revealed a broad macropore size distribution with a median pore opening diameter of 26 µm (**Figure 7c**). A fracture surface of the monolith reveals the prismatic pore morphology templated by solidified *tert*-butyl alcohol **3** (**Figure 7d**).
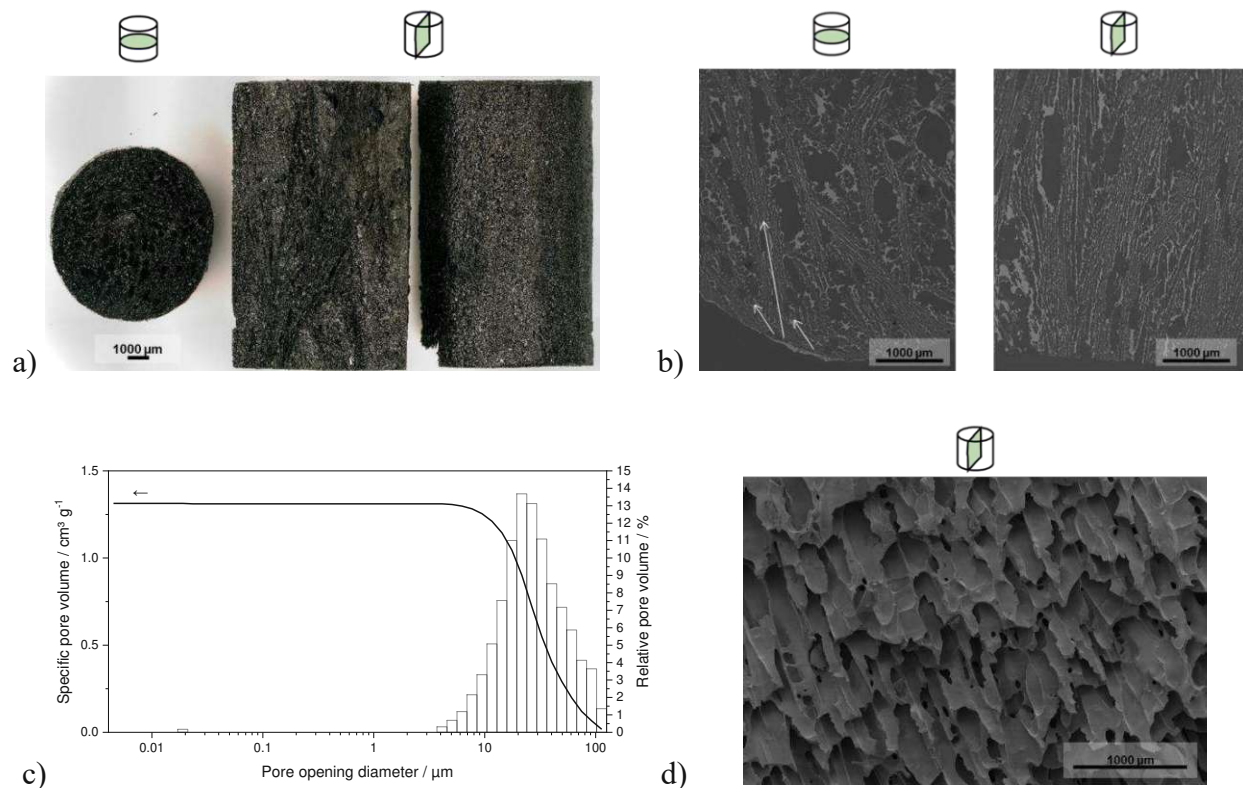
Figure 7: Characterization of monoliths **7b** for continuous experiments: a) optical microscopy images; b) scanning electron micrographs (backscattered electron detection) of sections embedded in epoxy resin, ground and polished; c) mercury intrusion porosimetry pore size distribution; d) scanning electron micrographs of a fracture surface (field emission gun – scanning electron microscopy, secondary electron detection).

Permeability of silicon oxycarbide monoliths **7b** was quantified by applying Forchheimer's equation for compressible fluids (**Formula S1**)[72] to obtain both k_1 (Darcian) and k_2 (non-Darcian) permeability constants from measured pressure drops and permeating air flow using filtered compressed air as permeating fluid (**Figure S4**). The air flow was applied in the same flow direction as in continuous carbonate production. The Darcian flow refers to a linear dependence of the fluid flow on the pressure gradient solely dependent on the fluid's dynamic viscosity. Non-Darcian permeability also considers inertial resistance, which becomes particularly relevant for

applications where fluids of high density are used. Determined permeability constants of monoliths **7b** ($k_1 = 10^{-11}\ m^2$, $k_2 = 10^{-6}\ m$) are classified in the order of honeycomb or fibrous filters.[72]

For the physisorption of amounts of 20-35 wt.% ionic liquid TBAC **8**, silicon oxycarbide monoliths **7b** were added to a methanolic solution of TBAC **8** and treated in an ultrasonic bath for efficient removal of air from the macropores. After solvent removal, surface morphologies of fractured monoliths were investigated by high-resolution field emission gun – scanning electron microscopy (FEG-SEM, method details given in ESI chapter S.7.1), which revealed that physisorbed ionic liquid causes a change in surface morphology, as shown in **Figure 8**. In comparison to the reference (monolithic silicon oxycarbide **7b**), partial coverage of the monolith's inner surface with ionic liquid was observed for lower loadings (20 wt.% TBAC **8**, **SILP 1b**) while a more uniform distribution was achieved for higher loading (35 wt.% TBAC **8**, maximal loading, **SILP 2b**) (**Figure 8**).
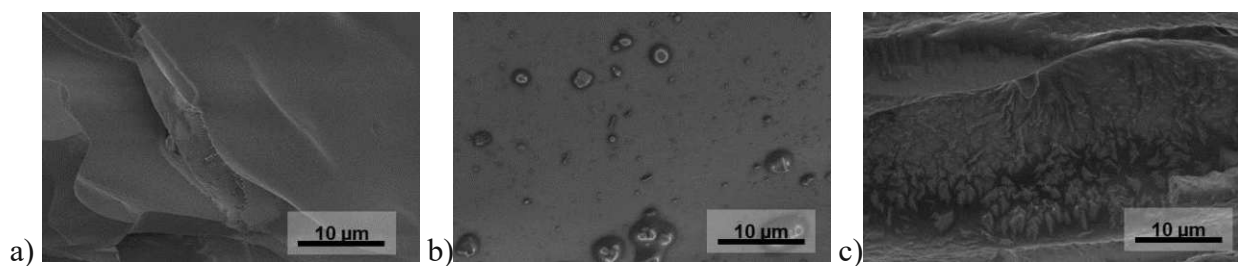

Figure 8: Scanning electron micrographs of fracture surfaces (field emission gun – scanning electron microscopy, secondary electron detection)**:** a) monolithic silicon oxycarbide **7b**; b) **SILP 1b** (20 wt.% TBAC **8**) and c) **SILP 2b** (35 wt.% TBAC **8**). Images of an additional spot and additional magnifications are given in **Figure S5**.

For continuous application, **SILPs 1b-2b** were finally inserted in a shrinking tube, which was heated carefully with a heat gun to shrink tightly onto the monolith to perfectly fit stacked monoliths into a catalyst cartridge, and thus ensure flow through the macropores of monolithic SiOC-SILPs.

Continuous Formation of Limonene Carbonate 15 with Monolithic SiOC-SILPs 1b-2b

With the monolithic SiOC-**SILPs 1b-2b** in hand, the formation of limonene carbonate **15** in continuous flow was conducted (**Figure 9**), using a device normally employed for supercritical carbon dioxide applications[26] (details are given in the experimental section and ESI chapter S.7.1). In the course of the continuous-flow experiments, the influence of the flow rate of carbon dioxide and the catalyst loading were investigated. As illustrated in **Figure 9**, all experiments resulted in a desired constant product output independent of the varied parameters.
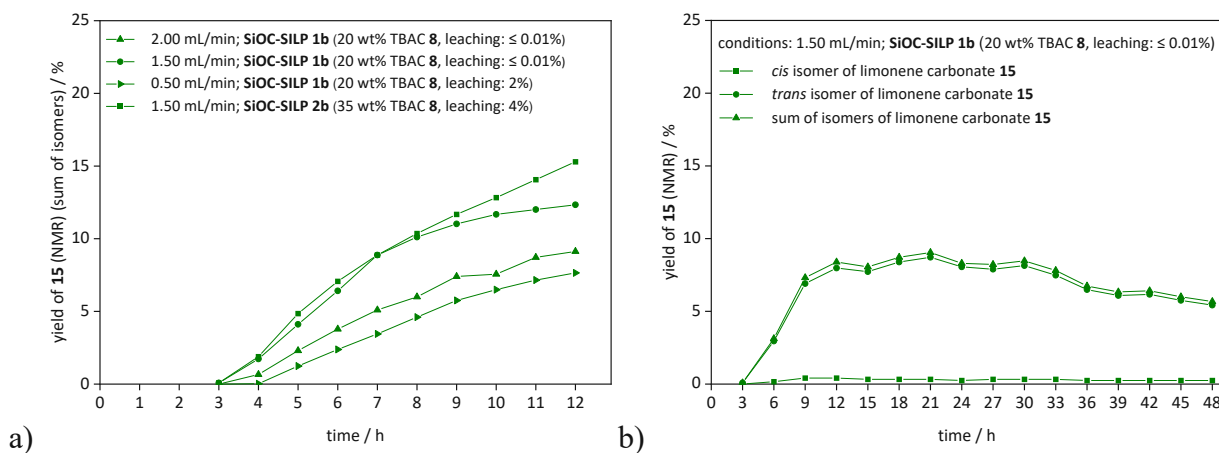
Figure 9. Continuous production of limonene carbonate **15** with monolithic SiOC-**SILPs 1b-2b**.[a] [a]conditions: 0.01 mL/min limonene oxide **14** (*cis*/*trans* = 43/57), **SILP 1b-2b** (15 – 20 mm monolith pieces, 220 mm in total), 1.99-0.49 mL/min CO_2 (15 MPa), 120 °C, a) 12 h or b) 48 h. Maximum and overall yields are depicted in **Table S5**.

An initial experiment employing a flow rate of carbon dioxide of 1.49 mL/min (total flow: 1.50 mL/min) and **SILP 1b** (**Figure 9a**) as catalyst resulted in a maximum yield of 12%. Only traces of leached catalyst (limit of detection: 0.1 mg, $\leq$ 0.1% of total amount of TBAC **8**) were observed. A higher flow rate of carbon dioxide of 1.99 mL/min (total flow: 2.00 mL/min) led to a decrease of the maximum yield to 9% (**Table S5,** entry S27) due to a shorter residence time of 7.6 min as opposed to 10.1 min at a total flow of 1.50 mL/min.

However, a lower flow rate of carbon dioxide of 0.49 mL/min (**Table S5,** entry S29; total flow: 0.50 mL/min, residence time: 30.5 min) resulted in a decrease of the maximum yield to 8% and leaching of 2%. This indicates that a minimum concentration of carbon dioxide is required for sufficient carbonate formation and a higher flow rate is beneficial to remove reacted species from the catalytically active surface.

Moreover, a higher catalyst loading of 35 wt.% (**SILP 2b**) resulted in a higher maximum yield of 15% (**Table S5,** entry S30), whereupon the maximum was not reached even after 12 h reaction time (**Figure 9a**). However, leaching of 4% of the catalyst was observed, thus a decrease of yield over time can be expected. Ultimately, a stability test over 48 h using **SILP 1b** (total flow: 1.50 mL/min) resulted in an overall yield of 7% without leaching of catalyst (limit of detection: 0.1 mg, $\leq$ 0.1% of total amount of TBAC **8**) (**Figure 9b**).

CONCLUSIONS

In this paper, we investigated SiOC-SILPs for their application as heterogeneous catalysts in the formation of bio-based cyclic carbonates **15** and **18** and compared them to the performance of commonly used silica-based SILPs. The processing benefits associated with the polymer-derived ceramic route enabled a smooth transition from batch to continuous-flow operation utilizing monolithic SiOC-SILPs. Extensive catalyst screening in batch mode revealed that excellent selectivities of 97-100% and yields of 53-62% after 5 h reaction time with SiOC-**SILPs 4a** and SiOC-**SILP 7a-9a** can be achieved for limonene carbonate **15**. In contrast, SiO_2-SILPs resulted in a low selectivity of 87% and a yield of 48% due to the formation of diol **16** as a byproduct, which was triggered by residual water and free hydroxyl groups on the surface of silica-60. For linseed oil carbonates, yields could be increased from 48% (SiO_2-**SILP 3a**) to 75% (SiOC-**SILP 5a**).

Finally, silicon oxycarbide monoliths were successfully implemented for continuous selective limonene carbonate formation, resulting in constant product outputs. Studying the long-term behavior of the monolithic catalyst over 48 h resulted in an overall yield of 7% and high selectivity, without significant leaching of ionic liquid from the monolithic silicon oxycarbide.

These results illustrate that scaleable SiOC-SILP-catalyzed continuous-flow processes are highly suitable for the formation of various cyclic carbonates. An extended ionic-liquid screening could further lead to an increase of reaction yields. Moreover, the pore orientation within the silicon oxycarbide monoliths could be improved via rotational freeze-casting[85] or by controlled unidirectional freeze-casting.[86] In conclusion, solidification-templated polymer-derived ceramics offer plenty of possibilities to tailor porosity and surface properties to host ionic liquids, rendering silicon oxycarbide-supported ionic liquids highly interesting for future applications in heterogeneous catalysis.

EXPERIMENTAL PART

Further details regarding preparation, characterization as well as materials, methods, and typical procedures can be found in the electronic supporting information (ESI).

Preparation of Silicon Oxycarbide Supports via Photopolymerization-Assisted Solidification Templating

Preparation of the photocurable polysiloxane solution **4** was performed according to a modification of procedures reported in literature[61, 62, 87] for additive manufacturing. For a typical master batch of 40 wt.% polymer content, 15 g of methyl silsesquioxane **1** were dissolved in 30 g *tert*-butyl alcohol **3** at 40 °C. 5 g of 3-(trimethoxysilyl)-propyl methacrylate **2** were added and stirred for 1 h at room temperature. One drop of concentrated HCl (37%) was added while stirring at 500 rpm. The mixture was stirred at 200 rpm for 20 h to ensure complete functionalization.

The master batch of 40 wt.% polymer content was diluted with *tert*-butyl alcohol **3** to yield 10, 20, or 30 wt.% polymer content in the preceramic solution **4**. Subsequently, phenylbis(2,4,6-trimethylbenzoyl) phosphine oxide **5** was added as a photoinitiator (1 wt.% with respect to the polymer content). The solution was homogenized (4 min, 2000 rpm) and degassed (10 min, 800 rpm) using a planetary mixer (Thinky ARE-250).

The solution was frozen at -20 °C for 24 h in polyethylene or aluminum molds to yield cubic or cylindrical samples. Solidified samples were demolded and illuminated at a wavelength of 405 nm (Sovol, 6 W) for a total of 30 min at -20 °C. Subsequently, samples were stored at -20 °C overnight. Solidified *tert*-butyl alcohol **3** was removed using a freeze-dryer (CHRIST Alpha 1-4 LDplus) for 21 h at 1 mbar, followed by 3 h at < 0.4 mbar. Pyrolytic conversion was conducted in a tube furnace (STF 166, Carbolite) under argon flow (30 L h^{-1}). The maximum pyrolysis temperature ranged from 300 to 900 °C (heating rate: 1 K min^{-1}, dwell time:1 h, cooling rate to room

temperature: 2 K min^{-1}). Linear shrinkage and ceramic yield were evaluated measuring diameter, height, and weight of the monoliths before and after pyrolysis. For batch-conversion experiments, the porous supports were ball-milled and sieved (mesh size 90 µm). For continuous-conversion experiments, cylindrically shaped monoliths were used and impregnated with ionic liquid, as further described in the supplementary material (ESI chapter S.7.3).

Formation of Limonene Carbonate 15 in Batch Mode

The synthesis was performed according to a modification of a literature procedure.[26] An 8 mL glass vial was charged with limonene oxide **14** (cis/trans = 43/57, 103 µL, ρ = 0.93 g/mL; remaining amount after sampling for ^{1}H-NMR: 82 µL, 0.5 mmol) and internal standard naphthalene (1.3 mg, 0.01 mmol). 21 µL was taken to record a ^{1}H-NMR spectrum at t = 0 (**Figure S15**). After sampling, SiOC-**SILP 11a** (preparation see ESI chapter S.7.2, 70 mg, 0.05 mmol of TBAC **8**) was added. The glass vial, equipped with a screw cap with a septum and a cannula, was placed in a 40 mL autoclave. After pressurizing with carbon dioxide (5 MPa), the reaction mixture was stirred for 5 h at 120 °C. After completion of the reaction, the autoclave was cooled to room temperature, carbon dioxide was released, and the reaction mixture was homogenized with 0.5 mL of deuterated chloroform. A ^{1}H-NMR spectrum was recorded (t = 5 h, **Figure S15**) revealing a selective conversion of 63% (62% yield).

Formation of Linseed Oil Carbonate 18 in Batch Mode

The synthesis was performed according to a modification of a literature procedure[84] and similarly to the formation of limonene carbonate **15**. 220 mg of epoxidized linseed oil **17** and SiOC-**SILP 5a** (27 mg, 0.02 mmol of TBAB **9**) were used, resulting in 75% conversion. Determination of conversion was performed via ^{1}H-NMR (see ESI chapter S.3.2).

26

Continuous Production of Limonene Carbonate 15

Monolithic SiOC-**SILP 1b-2b** (preparation see ESI chapter S.7.3, 220 mm; 15-20 mm pieces) was loaded into a shrinking tube. A heat gun was used for shrinking. The sheathed monoliths were inserted into the catalyst cartridge which was connected to a device used for supercritical carbon dioxide applications (for details see ESI chapter S.7.1 and reference[26]) The flow rates were set to 0.01 mL/min for limonene oxide **14** and 0.49-1.99 mL/min for carbon dioxide (15 MPa back pressure), and the catalyst cartridge was heated up to 120 °C. Limonene carbonate **5a** dissolved in starting material was collected in vials in different fractions for 12 h (one fraction/hour).

For the determination of NMR yields, 10.0 ± 0.1 mg of naphthalene was added to each fraction. After homogenizing with 0.5 mL of deuterated chloroform, an aliquot was taken for ^{1}H-NMR measurements. The spectrum was compared to a reference spectrum of a mixture of 558 mg of limonene oxide **14** (0.6 mL/h, $\rho = 0.93$ g/mL) and 10 mg naphthalene (see also ESI chapter S.3.1).

ASSOCIATED CONTENT

Electronic Supporting Information: preparation and analysis of supports and SILPs; determination of NMR yields and conversions; catalyst screening for SILPs; materials, methods, and typical procedures; analysis of cyclic carbonates

AUTHOR INFORMATION

Corresponding Authors

K.B.-S. * Institute of Applied Synthetic Chemistry, TU Wien, Getreidemarkt 9, 1060 Vienna, Austria. E-mail: katharina.schroeder@tuwien.ac.at, phone: +43 1 58801 163601; orcid.org/0000-0002-2515-9873

T.K. * Institute of Chemical Technologies and Analytics, TU Wien, Getreidemarkt 9, 1060 Vienna, Austria. E-mail: thomas.konegger@tuwien.ac.at, phone: +43 1 58801 16161; orcid.org/0000-0002-0454-5062

Author Contributions

P.M. – conceptualization, investigation, methodology, visualization, writing – original draft; orcid.org/0000-0002-8045-5667

K.R. – conceptualization, investigation, methodology, visualization, writing – original draft; orcid.org/0009-0009-5010-4135

S.N. – investigation, visualization; orcid.org/0000-0001-7738-2607

H.R. – investigation, visualization; orcid.org/0000-0002-1720-0223

D.E. – supervision, review & editing; orcid.org/0000-0002-5395-564X

T.K.* (corresponding author) – conceptualization, funding acquisition, supervision, writing – review & editing; orcid.org/0000-0002-0454-5062

K.B.-S.* (corresponding author) – conceptualization, funding acquisition, supervision, writing – review & editing; orcid.org/0000-0002-2515-9873

FUNDING SOURCES

NOTES

There are no conflicts of interest to declare.

ACKNOWLEDGMENT

ABBREVIATIONS

BET – Brunauer-Emmett-Teller; FEG-SEM – field emission gun – scanning electron microscopy; NMR – nuclear magnetic resonance; PSO – polysiloxane; SiO_2 – silica; SILP – supported ionic liquid phase; SiOC – silicon oxycarbide; TBAX – tetrabutylammonium halide; TGA – thermogravimetric analysis; XPS – X-ray photoelectron spectroscopy

SYNOPSIS. Silicon oxycarbide-supported ionic liquids were investigated for the formation of bio-based cyclic carbonates in batch mode and continuous flow using supercritical carbon dioxide.

REFERENCES

1.   Fehrmann, R.; Riisager, A.; Haumann, M., *Supported Ionic Liquids*. Wiley-VCH: 2014.

2.   Castro-Amoedo, R.; Csendes, Z.; Brünig, J.; Sauer, M.; Foelske-Schmitz, A.; Yigit, N.; Rupprechter, G.; Gupta, T.; Martins, A. M.; Bica, K.; Hoffmann, H.; Kirchner, K., Carbon-based SILP catalysis for the selective hydrogenation of aldehydes using a well-defined Fe(ii) PNP complex. *Catal. Sci. Technol.* **2018,** *8* (18), 4812-4820. 10.1039/C8CY00818C

3.   Blaumeiser, D.; Stepić, R.; Wolf, P.; Wick, C. R.; Haumann, M.; Wasserscheid, P.; Smith, D. M.; Smith, A.-S.; Bauer, T.; Libuda, J., Cu carbonyls enhance the performance of Ru-based SILP water–gas shift catalysts: a combined in situ DRIFTS and DFT study. *Catal. Sci. Technol.* **2020,** *10* (1), 252-262. 10.1039/C9CY01852B

4.   Wolf, P.; Wick, C. R.; Mehler, J.; Blaumeiser, D.; Schötz, S.; Bauer, T.; Libuda, J.; Smith, D.; Smith, A.-S.; Haumann, M., Improving the Performance of Supported Ionic Liquid Phase Catalysts for the Ultra-Low-Temperature Water Gas Shift Reaction Using Organic Salt Additives. *ACS Catal.* **2022,** *12* (9), 5661-5672. 10.1021/acscatal.1c05979

5.   Wolny, A.; Siewniak, A.; Zdarta, J.; Ciesielczyk, F.; Latos, P.; Jurczyk, S.; Nghiem, L. D.; Jesionowski, T.; Chrobok, A., Supported ionic liquid phase facilitated catalysis with lipase from Aspergillus oryzae for enhance enantiomeric resolution of racemic ibuprofen. *Environ Technol Innov* **2022,** *28*, 102936. 10.1016/j.eti.2022.102936

6.   Zenner, J.; Moos, G.; Luska, K. L.; Bordet, A.; Leitner, W., Rh NPs Immobilized on Phosphonium- based Supported Ionic Liquid Phases (Rh@SILPs) as Hydrogenation Catalysts. *CHIMIA* **2021,** *75* (9), 724-732. 10.2533/chimia.2021.724

7.   Kukawka, R.; Pawlowska-Zygarowicz, A.; Dzialkowska, J.; Pietrowski, M.; Maciejewski, H.; Bica, K.; Smiglak, M., Highly Effective Supported Ionic Liquid-Phase (SILP) Catalysts: Characterization and Application to the Hydrosilylation Reaction. *ACS Sustain. Chem. Eng.* **2019,** *7* (5), 4699-4706. 10.1021/acssuschemeng.8b04357

8.   Brun, N.; Hesemann, P.; Laurent, G.; Sanchez, C.; Birot, M.; Deleuze, H.; Backov, R., Macrocellular Pd@ionic liquid@organo-Si(HIPE) heterogeneous catalysts and their use for Heck coupling reactions. *New J. Chem.* **2013,** *37* (1), 157-168. 10.1039/C2NJ40527J

9.   Motos-Pérez, B.; Roeser, J.; Thomas, A.; Hesemann, P., Imidazolium-functionalized SBA-15 type silica: efficient organocatalysts for Henry and cycloaddition reactions. *Applied Organometallic Chemistry* **2013,** *27* (5), 290-299. 10.1002/aoc.2974

10.   Peris, E.; Porcar, R.; Garcia-Alvarez, J.; Burguete, M. I.; Garcia-Verdugo, E.; Luis, S. V., Divergent Multistep Continuous Synthetic Transformations of Allylic Alcohol Enabled by Catalysts Immobilized in Ionic Liquid Phases. *ChemSusChem* **2019,** *12* (8), 1684-1691. 10.1002/cssc.201900107

11.   Kohler, F. T. U.; Popp, S.; Klefer, H.; Eckle, I.; Schrage, C.; Böhringer, B.; Roth, D.; Haumann, M.; Wasserscheid, P., Supported ionic liquid phase (SILP) materials for removal of hazardous gas compounds – efficient and irreversible NH_3 adsorption. *Green Chem.* **2014,** *16* (7), 3560-3568. 10.1039/C3GC42275E

12.   Kaftan, A.; Klefer, H.; Haumann, M.; Laurin, M.; Wasserscheid, P.; Libuda, J., An operando DRIFTS-MS study of NH_3 removal by supported ionic liquid phase (SILP) materials. *Sep. Purif. Technol.* **2017,** *174*, 245-250. 10.1016/J.SEPPUR.2016.10.017

13.   Li, X. S.; Zhang, L. Q.; Zhou, D.; Liu, W. Q.; Zhu, X. Y.; Xu, Y. Q.; Zheng, Y.; Zheng, C. G., Elemental Mercury Capture from Flue Gas by a Supported Ionic Liquid Phase Adsorbent. *Energy & Fuels* **2017,** *31* (1), 714-723. 10.1021/acs.energyfuels.6b01956

14.   Thomassen, P. L.; Kunov-Kruse, A. J.; Mossin, S. L.; Kolding, H.; Kegnæs, S.; Riisager, A.; Fehrmann, R., Separation of Flue Gas Components by SILP (Supported Ionic Liquid-Phase) Absorbers. *ECS Trans.* **2013,** *50* (11), 433. 10.1149/05011.0433ecst

15.   Avdibegović, D.; Yagmurlu, B.; Dittrich, C.; Regadío, M.; Friedrich, B.; Binnemans, K., Combined multi-step precipitation and supported ionic liquid phase chromatography for the recovery of rare earths from leach solutions of bauxite residues. *Hydrometallurgy* **2018,** *180*, 229-235. 10.1016/j.hydromet.2018.07.023

16.   Lanaridi, O.; Sahoo, A. R.; Limbeck, A.; Naghdi, S.; Eder, D.; Eitenberger, E.; Csendes, Z.; Schnurch, M.; Bica-Schroder, K., Toward the Recovery of Platinum Group Metals from a Spent Automotive Catalyst with Supported Ionic Liquid Phases. *ACS Sustain. Chem. Eng.* **2021,** *9* (1), 375-386. 10.1021/acssuschemeng.0c07384

17.   Avdibegović, D.; Binnemans, K., Separation of Scandium from Hydrochloric Acid–Ethanol Leachate of Bauxite Residue by a Supported Ionic Liquid Phase. *Ind. Eng. Chem. Res.* **2020,** *59* (34), 15332-15342. 10.1021/acs.iecr.0c02943

18.   Steinrück, H.-P.; Wasserscheid, P., Ionic Liquids in Catalysis. *Catalysis Letters* **2014,** *145* (1), 380-397. 10.1007/s10562-014-1435-x

19.   Lemus, J.; Palomar, J.; Gilarranz, M. A.; Rodriguez, J. J., Characterization of Supported Ionic Liquid Phase (SILP) materials prepared from different supports. *Adsorption* **2011,** *17* (3), 561-571. 10.1007/s10450-011-9327-5

20.   Singh, S. K.; Savoy, A. W., Ionic liquids synthesis and applications: An overview. *J. Mol. Liq.* **2020,** *297*, 112038. 10.1016/j.molliq.2019.112038

21.   Topham, S.; Bazzanella, A.; Schiebahn, S.; Luhr, S.; Zhao, L.; Otto, A.; Stolten, D., Carbon Dioxide. In *Ullmann's Encyclopedia of Industrial Chemistry*, Wiley-VCH Verlag GmbH & Co. KGaA: Weinheim, Germany, 2014; pp 1-43.

22.   Lozano, P.; García-Verdugo, E.; Piamtongkam, R.; Karbass, N.; De Diego, T.; Burguete, M. I.; Luis, S. V.; Iborra, J. L., Bioreactors Based on Monolith-Supported Ionic Liquid Phase for Enzyme Catalysis in Supercritical Carbon Dioxide. *Adv. Synt. Catal.* **2007,** *349* (7), 1077-1084. 10.1002/adsc.200600554

23.   Zhang, Z. Y.; Francio, G.; Leitner, W., Continuous-Flow Asymmetric Hydrogenation of an Enol Ester by using Supercritical Carbon Dioxide: Ionic Liquids versus Supported Ionic Liquids as the Catalyst Matrix. *Chemcatchem* **2015,** *7* (13), 1961-1965. 10.1002/cctc.201500295

24.   Hintermair, U.; Höfener, T.; Pullmann, T.; Franciò, G.; Leitner, W., Continuous Enantioselective Hydrogenation with a Molecular Catalyst in Supported Ionic Liquid Phase under Supercritical CO_2 Flow. *ChemCatChem* **2010,** *2* (2), 150-154. 10.1002/cctc.200900261

25.   Hintermair, U.; Franciò, G.; Leitner, W., A Fully Integrated Continuous-Flow System for Asymmetric Catalysis: Enantioselective Hydrogenation with Supported Ionic Liquid Phase Catalysts Using Supercritical CO_2 as the Mobile Phase. *Chem. Eur. J.* **2013,** *19* (14), 4538-4547. 10.1002/chem.201204159

26.   Miksovsky, P.; Horn, E. N.; Naghdi, S.; Eder, D.; Schnurch, M.; Bica-Schroder, K., Continuous Formation of Limonene Carbonates in Supercritical Carbon Dioxide. *Org Process Res Dev* **2022,** *26* (10), 2799-2810. 10.1021/acs.oprd.2c00143

27.   Aprile, C.; Giacalone, F.; Agrigento, P.; Liotta, L. F.; Martens, J. A.; Pescarmona, P. P.; Gruttadauria, M., Multilayered supported ionic liquids as catalysts for chemical fixation of carbon dioxide: a high-throughput study in supercritical conditions. *ChemSusChem* **2011,** *4* (12), 1830-1837. 10.1002/cssc.201100446

28.   Sainz Martinez, A.; Hauzenberger, C.; Sahoo, A. R.; Csendes, Z.; Hoffmann, H.; Bica, K., Continuous Conversion of Carbon Dioxide to Propylene Carbonate with Supported Ionic Liquids. *ACS Sustainable Chemistry & Engineering* **2018,** *6* (10), 13131-13139. 10.1021/acssuschemeng.8b02627

29.   Wang, J.-Q.; Yue, X.-D.; Cai, F.; He, L.-N., Solventless synthesis of cyclic carbonates from carbon dioxide and epoxides catalyzed by silica-supported ionic liquids under supercritical conditions. *Catal. Commun.* **2007,** *8* (2), 167-172. 10.1016/j.catcom.2006.05.049

30.   Martínez-Ferraté, O.; Chacón, G.; Bernardi, F.; Grehl, T.; Brüner, P.; Dupont, J., Cycloaddition of carbon dioxide to epoxides catalysed by supported ionic liquids. *Catal. Sci. Technol.* **2018,** *8* (12), 3081-3089. 10.1039/C8CY00749G

31.   Wang, T.; Wang, W.; Lyu, Y.; Chen, X.; Li, C.; Zhang, Y.; Song, X.; Ding, Y., Highly recyclable polymer supported ionic liquids as efficient heterogeneous catalysts for batch and flow conversion of CO_2 to cyclic carbonates. *RSC Adv.* **2017,** *7* (5), 2836-2841. 10.1039/C6RA26780G

32.   Sun, J.; Li, X.; Yu, K.; Yin, J., A novel supported ionic liquid membrane reactor for catalytic CO_2 conversion. *J. CO_2 Util.* **2022,** *65*, 102216. 10.1016/j.jcou.2022.102216

33.   Li, X.; Sun, J.; Xue, M.; Yin, J., Catalytic conversion of CO_2 by supported ionic liquid prepared with supercritical fluid deposition in a continuous fixed-bed reactor. *J. CO_2 Util.* **2022,** *64*, 102168. 10.1016/j.jcou.2022.102168

34.   Guo, F.; Wang, L.; Cao, Y.; He, P.; Li, H., Efficient synthesis of ethylene carbonate via transesterification of ethylene glycol with dimethyl carbonate over $Mg_3Al_{1-x}Ce_xO$ composite oxide. *Applied Catalysis A: General* **2023,** *662*, 119273. 10.1016/j.apcata.2023.119273

35.   Shaikh, A.-A. G.; Sivaram, S., Organic Carbonates. *Chemical Reviews* **1996,** *96* (3), 951-976. 10.1021/cr950067i

36.   He, Q.; O'Brien, J. W.; Kitselman, K. A.; Tompkins, L. E.; Curtis, G. C. T.; Kerton, F. M., Synthesis of cyclic carbonates from CO_2 and epoxides using ionic liquids and related catalysts including choline chloride–metal halide mixtures. *Catal. Sci. Technol.* **2014,** *4* (6), 1513-1528. 10.1039/C3CY00998J

37.   Jia, D.; Ma, L.; Wang, Y.; Zhang, W.; Li, J.; Zhou, Y.; Wang, J., Efficient CO_2 enrichment and fixation by engineering micropores of multifunctional hypercrosslinked ionic polymers. *Chemical Engineering Journal* **2020,** *390*, 124652. 10.1016/j.cej.2020.124652

38.   Comin, E.; Aquino, A. S.; Favero, C.; Mignoni, M. L.; de Souza, R. F.; de Souza, M. O.; Pergher, S. B. C.; Campos, C. X. d. S.; Bernardo-Gusmão, K., Cyclic carbonate synthesis via cycloaddition of CO_2 and epoxides catalysed by beta zeolites containing alkyl imidazolium ionic liquids used as structure-directing agents. *Molecular Catalysis* **2022,** *530*, 112624. 10.1016/j.mcat.2022.112624

39.   Li, G.; Dong, S.; Fu, P.; Yue, Q.; Zhou, Y.; Wang, J., Synthesis of porous poly(ionic liquid)s for chemical CO_2 fixation with epoxides. *Green Chemistry* **2022,** *24* (9), 3433-3460. 10.1039/D2GC00324D

40.   Pescarmona, P. P., Cyclic carbonates synthesised from CO_2: Applications, challenges and recent research trends. *Curr. Opin. Green Sustain. Chem.* **2021,** *29*, 100457. 10.1016/j.cogsc.2021.100457

41.   Raj, A.; Panchireddy, S.; Grignard, B.; Detrembleur, C.; Gohy, J.-F., Bio-Based Solid Electrolytes Bearing Cyclic Carbonates for Solid-State Lithium Metal Batteries. *ChemSusChem* **2022,** *15* (18), e202200913. 10.1002/cssc.202200913

42. Maisonneuve, L.; More, A. S.; Foltran, S.; Alfos, C.; Robert, F.; Landais, Y.; Tassaing, T.; Grau, E.; Cramail, H., Novel green fatty acid-based bis-cyclic carbonates for the synthesis of isocyanate-free poly(hydroxyurethane amide)s. *RSC Adv.* **2014,** *4* (49), 25795-25803. 10.1039/C4RA03675A

43. Longwitz, L.; Steinhauer, J.; Spannenberg, A.; Werner, T., Calcium-Based Catalytic System for the Synthesis of Bio-Derived Cyclic Carbonates under Mild Conditions. *Acs Catalysis* **2018,** *8* (1), 665-672. 10.1021/acscatal.7b03367

44. Centeno-Pedrazo, A.; Perez-Arce, J.; Freixa, Z.; Ortiz, P.; Garcia-Suarez, E. J., Catalytic Systems for the Effective Fixation of CO_2 into Epoxidized Vegetable Oils and Derivates to Obtain Biobased Cyclic Carbonates as Precursors for Greener Polymers. *Ind. Eng. Chem. Res.* **2023,** *62* (8), 3428-3443. 10.1021/acs.iecr.2c03747

45. Fiorani, G.; Stuck, M.; Martin, C.; Belmonte, M. M.; Martin, E.; Escudero-Adan, E. C.; Kleij, A. W., Catalytic Coupling of Carbon Dioxide with Terpene Scaffolds: Access to Challenging Bio-Based Organic Carbonates. *ChemSusChem* **2016,** *9* (11), 1304-1311. 10.1002/cssc.201600238

46. de la Cruz-Martínez, F.; Martínez de Sarasa Buchaca, M.; Martínez, J.; Fernández-Baeza, J.; Sánchez-Barba, L. F.; Rodríguez-Diéguez, A.; Castro-Osma, J. A.; Lara-Sánchez, A., Synthesis of Bio-Derived Cyclic Carbonates from Renewable Resources. *ACS Sustain. Chem. Eng.* **2019,** *7* (24), 20126-20138. 10.1021/acssuschemeng.9b06016

47. Laprise, C. M.; Hawboldt, K. A.; Kerton, F. M.; Kozak, C. M., Synthesis of a Renewable, Waste-Derived Nonisocyanate Polyurethane from Fish Processing Discards and Cashew Nutshell-Derived Amines. *Macromol. Rapid Commun.* **2021,** *42* (3), 2000339. 10.1002/marc.202000339

48. Bähr, M.; Bitto, A.; Mülhaupt, R., Cyclic limonene dicarbonate as a new monomer for non-isocyanate oligo- and polyurethanes (NIPU) based upon terpenes. *Green Chem.* **2012,** *14* (5), 1447-1454. 10.1039/C2GC35099H

49. Cai, X.; Tolvanen, P.; Virtanen, P.; Eränen, K.; Rahkila, J.; Leveneur, S.; Salmi, T., Kinetic study of the carbonation of epoxidized fatty acid methyl ester catalyzed over heterogeneous catalyst HBimCl-NbCl$_5$/HCMC. *Int. J. Chem. Kinet.* **2021,** *53* (11), 1203-1219. 10.1002/kin.21526

50. Akhdar, A.; Onida, K.; Vu, N. D.; Grollier, K.; Norsic, S.; Boisson, C.; D'Agosto, F.; Duguet, N., Thermomorphic Polyethylene-Supported Organocatalysts for the Valorization of Vegetable Oils and CO_2. *Adv Sustain Syst* **2021,** *5* (2), 2000218. 10.1002/adsu.202000218

51. Bähr, M.; Mülhaupt, R., Linseed and soybean oil-based polyurethanes prepared via the non-isocyanate route and catalytic carbon dioxide conversion. *Green Chem.* **2012,** *14* (2), 483-489. 10.1039/C2GC16230J

52. Schaffner, B.; Blug, M.; Kruse, D.; Polyakov, M.; Kockritz, A.; Martin, A.; Rajagopalan, P.; Bentrup, U.; Bruckner, A.; Jung, S.; Agar, D.; Rungeler, B.; Pfennig, A.; Muller, K.; Arlt, W.; Woldt, B.; Grass, M.; Buchholz, S., Synthesis and application of carbonated fatty acid esters from carbon dioxide including a life cycle analysis. *ChemSusChem* **2014,** *7* (4), 1133-1139. 10.1002/cssc.201301115

53. Perez-Sena, W. Y.; Eränen, K.; Kumar, N.; Estel, L.; Leveneur, S.; Salmi, T., New insights into the cocatalyst-free carbonation of vegetable oil derivatives using heterogeneous catalysts. *J. CO$_2$ Util.* **2022,** *57*, 101879. 10.1016/j.jcou.2021.101879

54. Alassmy, Y. A.; Pescarmona, P. P., The Role of Water Revisited and Enhanced: A Sustainable Catalytic System for the Conversion of CO_2 into Cyclic Carbonates under Mild Conditions. *ChemSusChem* **2019,** *12* (16), 3856-3863. 10.1002/cssc.201901124

55. Stabler, C.; Ionescu, E.; Graczyk-Zajac, M.; Gonzalo-Juan, I.; Riedel, R., Silicon oxycarbide glasses and glass-ceramics:"All-Rounder" materials for advanced structural and functional applications. *J. Am. Ceram. Soc.* **2018,** *101* (11), 4817-4856. 10.1111/jace.15932

56. Colombo, P.; Mera, G.; Riedel, R.; Soraru, G. D., Polymer-derived ceramics: 40 years of research and innovation in advanced ceramics. *J. Am. Ceram. Soc.* **2010,** *93* (7), 1805-1837. 10.1111/j.1551-2916.2010.03876.x

57. Wen, Q.; Yu, Z.; Riedel, R., The fate and role of in situ formed carbon in polymer-derived ceramics. *Prog. Mat. Sci.* **2020,** *109*, 100623.

58. Wilhelm, M.; Soltmann, C.; Koch, D.; Grathwohl, G., Ceramers—functional materials for adsorption techniques. *J. Eur. Ceram. Soc.* **2005,** *25* (2-3), 271-276. 10.1016/j.jeurceramsoc.2004.08.008

59. Prenzel, T.; Wilhelm, M.; Rezwan, K., Pyrolyzed polysiloxane membranes with tailorable hydrophobicity, porosity and high specific surface area. *Microporous Mesoporous Mater.* **2013,** *169*, 160-167. 10.1016/j.micromeso.2012.10.014

60. Prenzel, T.; Guedes, T. L. M.; Schluter, F.; Wilhelm, M.; Rezwan, K., Tailoring surfaces of hybrid ceramics for gas adsorption - From alkanes to CO_2. *Sep. Purif. Technol.* **2014,** *129*, 80-89. 10.1016/j.seppur.2014.03.029

61. Essmeister, J.; Altun, A. A.; Staudacher, M.; Lube, T.; Schwentenwein, M.; Konegger, T., Stereolithography-based additive manufacturing of polymer-derived SiOC/SiC ceramic composites. *J. Eur. Ceram. Soc.* **2022,** *42* (13), 5343-5354. 10.1016/j.jeurceramsoc.2022.06.021

62. Essmeister, J.; Schachtner, L.; Szoldatits, E.; Schwarz, S.; Lichtenegger, A.; Baumann, B.; Föttinger, K.; Konegger, T., Polymer-derived Ni/SiOC materials structured by vat-based photopolymerization with catalytic activity in CO2 methanation. *Open Ceram.* **2023,** *14*, 100350. 10.1016/j.oceram.2023.100350

63. Obmann, R.; Schörpf, S.; Gorsche, C.; Liska, R.; Fey, T.; Konegger, T., Porous polysilazane-derived ceramic structures generated through photopolymerization-assisted solidification templating. *J. Eur. Ceram. Soc.* **2019,** *39* (4), 838-845. 10.1016/j.jeurceramsoc.2018.11.045

64. Naviroj, M.; Miller, S. M.; Colombo, P.; Faber, K. T., Directionally aligned macroporous SiOC via freeze casting of preceramic polymers. *J. Eur. Ceram. Soc.* **2015,** *35* (8), 2225-2232. 10.1016/j.jeurceramsoc.2015.02.013

65. Naviroj, M.; Voorhees, P. W.; Faber, K. T., Suspension- and solution-based freeze casting for porous ceramics. *J Mater Res* **2017,** *32* (17), 3372-3382. 10.1557/jmr.2017.133

66. Mikl, G.; Obmann, R.; Schorpf, S.; Liska, R.; Konegger, T., Pore Morphology Tailoring in Polymer-Derived Ceramics Generated through Photopolymerization-Assisted Solidification Templating. *Adv. Eng. Mater.* **2019,** *21* (6), 1900052. 10.1002/adem.201900052

67. Naviroj, M. Silicon-based porous ceramics via freeze casting of preceramic polymers. Ph.D. thesis, Northwestern University, 2017.

68. Deville, S., Freeze-casting of porous ceramics: A review of current achievements and issues. *Adv. Eng. Mater.* **2008,** *10* (3), 155-169. 10.1002/adem.200700270

69. Schumacher, D.; Wilhelm, M.; Rezwan, K., Modified solution based freeze casting process of polysiloxanes to adjust pore morphology and surface functions of SiOC monoliths. *Mater. Design* **2018,** *160*, 1295-1304. 10.1016/j.matdes.2018.10.048

70.   Schumacher, D.; Zimnik, D.; Wilhelm, M.; Dreyer, M.; Rezwan, K., Solution based freeze cast polymer derived ceramics for isothermal wicking-relationship between pore structure and imbibition. *Sci. Technol. Adv. Mat.* **2019,** *20* (1), 1207-1221. 10.1080/14686996.2019.1699766

71.   Wang, X. F.; Schmidt, F.; Gurlo, A., Fabrication of polymer-derived ceramics with hierarchical porosities by freeze casting assisted by thiol-ene click chemistry and HF etching. *J. Eur. Ceram. Soc.* **2020,** *40* (2), 315-323. 10.1016/j.jeurceramsoc.2019.09.038

72.   Innocentini, M. D. d. M.; Sepulveda, P.; dos Santos Ortega, F., Permeability. In *Cellular Ceramics*, 2005; pp 313-341.

73.   Lee, C.; Sandig, B.; Buchmeiser, M. R.; Haumann, M., Supported ionic liquid phase (SILP) facilitated gas-phase enzyme catalysis - CALB catalyzed transesterification of vinyl propionate. *Catal. Sci. Technol.* **2018,** *8* (9), 2460-2466. 10.1039/c8cy00089a

74.   Sandig, B.; Michalek, L.; Vlahovic, S.; Antonovici, M.; Hauer, B.; Buchmeiser, M. R., A Monolithic Hybrid Cellulose-2.5-Acetate/Polymer Bioreactor for Biocatalysis under Continuous Liquid–Liquid Conditions Using a Supported Ionic Liquid Phase. *Chem. Eur. J.* **2015,** *21* (44), 15835-15842. 10.1002/chem.201501618

75.   Sandig, B.; Buchmeiser, M. R., Highly Productive and Enantioselective Enzyme Catalysis under Continuous Supported Liquid–Liquid Conditions Using a Hybrid Monolithic Bioreactor. *ChemSusChem* **2016,** *9* (20), 2917-2921. 10.1002/cssc.201600994

76.   Autenrieth, B.; Frey, W.; Buchmeiser, M. R., A Dicationic Ruthenium Alkylidene Complex for Continuous Biphasic Metathesis Using Monolith-Supported Ionic Liquids. *Chem. Eur. J.* **2012,** *18* (44), 14069-14078. doi.org/10.1002/chem.201201199

77.   Lubbad, S.; Mayr, B.; Mayr, M.; Buchmeiser, M. In *Monolithic systems: from separation science to heterogeneous catalysis*, Macromolecular Symposia, Wiley Online Library: 2004; pp 1-9.

78.   Szoldatits, E.; Essmeister, J.; Schachtner, L.; Konegger, T.; Fottinger, K., Polymer-derived SiOC as support material for Ni-based catalysts: CO_2 methanation performance and effect of support modification with La_2O_3. *Front. Chem.* **2023,** *11*, 1163503. 10.3389/fchem.2023.1163503

79.   Jella, G.; Panda, D. K.; Sapkota, N.; Greenough, M.; Datta, S. P.; Rao, A. M.; Sujith, R.; Bordia, R. K., Electrochemical Performance of Polymer-Derived Silicon-Oxycarbide/Graphene Nanoplatelet Composites for High-Performance Li-Ion Batteries. *ACS Appl. Mater. Interfaces* **2023,** *15* (25), 30039-30051. 10.1021/acsami.3c00571

80.   360ResearchReports Global Limonene Market Research Report 2020. https://www.360researchreports.com/global-limonene-market-15061488 (accessed 08/2023).

81.   Morikawa, H.; Minamoto, M.; Gorou, Y.; Yamaguchi, J.; Morinaga, H.; Motokucho, S., Two Diastereomers of d-Limonene-Derived Cyclic Carbonates from d-Limonene Oxide and Carbon Dioxide with a Tetrabutylammonium Chloride Catalyst. *B Chem Soc Jpn* **2018,** *91* (1), 92-94. 10.1246/bcsj.20170300

82.   Morikawa, H.; Yamaguchi, J. I.; Sugimura, S. I.; Minamoto, M.; Gorou, Y.; Morinaga, H.; Motokucho, S., Systematic synthetic study of four diastereomerically distinct limonene-1,2-diols and their corresponding cyclic carbonates. *Beilstein J Org Chem* **2019,** *15*, 130-136. 10.3762/bjoc.15.13

83.   Steiner, D.; Ivison, L.; Goralski, C. T.; Appell, R. B.; Gojkovic, J. R.; Singaram, B., A facile and efficient method for the kinetic separation of commercially available cis- and trans-

limonene epoxide. *Tetrahedron: Asymmetry* **2002,** *13* (21), 2359-2363. 10.1016/S0957-4166(02)00646-8

84.   Alves, M.; Grignard, B.; Gennen, S.; Detrembleur, C.; Jerome, C.; Tassaing, T., Organocatalytic synthesis of bio-based cyclic carbonates from CO_2 and vegetable oils. *RSC Adv.* **2015,** *5* (66), 53629-53636. 10.1039/C5RA10190E

85.   Seuba, J.; Leloup, J.; Richaud, S.; Deville, S.; Guizard, C.; Stevenson, A. J., Fabrication of ice-templated tubes by rotational freezing: Microstructure, strength, and permeability. *J. Eur. Ceram. Soc.* **2017,** *37* (6), 2423-2429. 10.1016/j.jeurceramsoc.2017.01.014

86.   Deville, S., Freeze-Casting of Porous Ceramics: A Review of Current Achievements and Issues. *Advanced Engineering Materials* **2008,** *10* (3), 155-169. 10.1002/adem.200700270

87.   Zanchetta, E.; Cattaldo, M.; Franchin, G.; Schwentenwein, M.; Homa, J.; Brusatin, G.; Colombo, P., Stereolithography of SiOC Ceramic Microcomponents. *Adv. Mater.* **2016,** *28* (2), 370-6. 10.1002/adma.201503470

For Table of Contents Use Only.
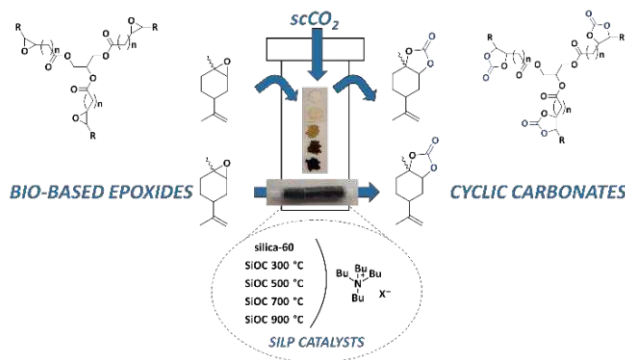
Highly selective silicon oxycarbide supported ionic liquids for the production of bio-derived cyclic carbonates were investigated in batch and in continuous flow.

G Conclusions

Supercritical carbon dioxide as non-toxic and non-flammable solvent was successfully applied for an enzyme-assisted supercritical fluid extraction. Furthermore, the neoteric solvent was combined with ionic liquids, a highly tunable compound class, to expand their application to catalysis.

In the first part of this thesis, an enzyme-assisted supercritical carbon dioxide extraction of flavonoids from apple pomace was developed, employing the enzyme mix snailase to hydrolyze the flavonoid glycosides (quercetin glycoside, kaempferol glycoside, phloridzin, 3-hydroxyphloridzin) to flavonoid aglycones (quercetin, kaempferol, phloretin, 3-hydroxyphloretin). Optimization of the enzymatic hydrolysis (amount of enzyme, pre-treatment of apple pomace, time for hydrolysis) and supercritical fluid extraction (kind and amount of cosolvent, time for extraction) in a subsequent process (**Scheme 32**) revealed that a small amount of snailase (0.25%) is already sufficient to cleave up to 96% of the sugar moieties from flavonoids after 2 h enzymatic hydrolysis. In addition, small amounts of methanol as cosolvent led to 90% of total yield extraction (0.68 µmol/g of flavonoid aglycones) already after 1 h of supercritical fluid extraction. Ultimately, the potential of snailase for a scalable industrial process, even under pressurized conditions, was demonstrated in a simultaneous process of enzymatic hydrolysis and supercritical fluid extraction. Furthermore, this snailase-assisted supercritical fluid extraction is not limited to apple pomace as raw material,[186] since snailase was already successfully employed in numerous other plant materials.
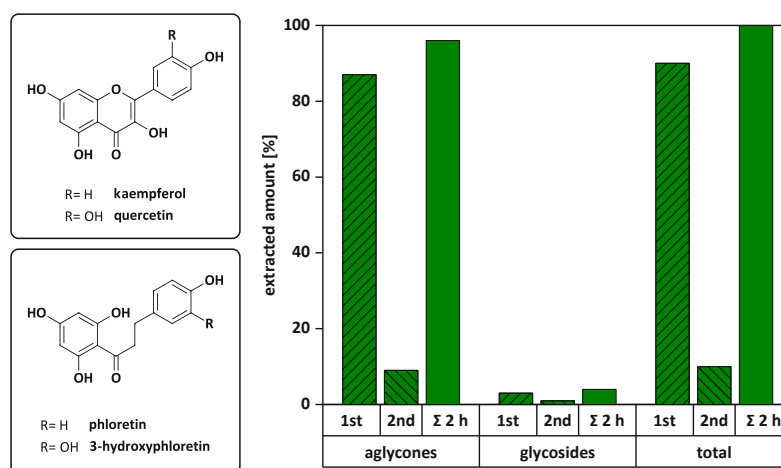
Scheme 32: Results of the snailase-assisted supercritical carbon dioxide extraction of flavonoid aglycones (left) from apple pomace.

Conditions for enzymatic hydrolysis: 3 g apple pomace (dried and ground), snailase (0.25%, 0.037 g/15 mL), 15 mL McIlvaine buffer (pH = 5.5), shaken for 2 h (37 °C, 180 rpm), lyophilized for 48 h; conditions for supercritical fluid extraction: 2 mL/min total flow, 20 v% MeOH, 60 °C, 25 MPa, 2 h. Experiments were performed in triplicate and results are reported as mean values.

Moreover, the continuous production of cyclic carbonates in supercritical carbon dioxide as reagent and sole solvent, starting from bio-based limonene oxide and limonene dioxide, was investigated (**Scheme 33**). After initial screening of ammonium- and imidazolium-based ionic liquids in homogeneous mode, the best performing ionic liquid, tetrabutylammonium chloride, was immobilized on silica and served as heterogeneous supported ionic liquid phase (SILP-) catalysts in continuous flow. Elaborate optimization in continuous flow (temperature, pressure, flow rates, catalyst loading) in 12 h experiments resulted in constant outputs when the selective SILP-catalyst (30 wt% of physisorbed ionic liquid) was applied. The long-term stability of the catalyst system was further studied for 48 h, resulting in yields of 16-17% and no or just traces of leached catalyst.
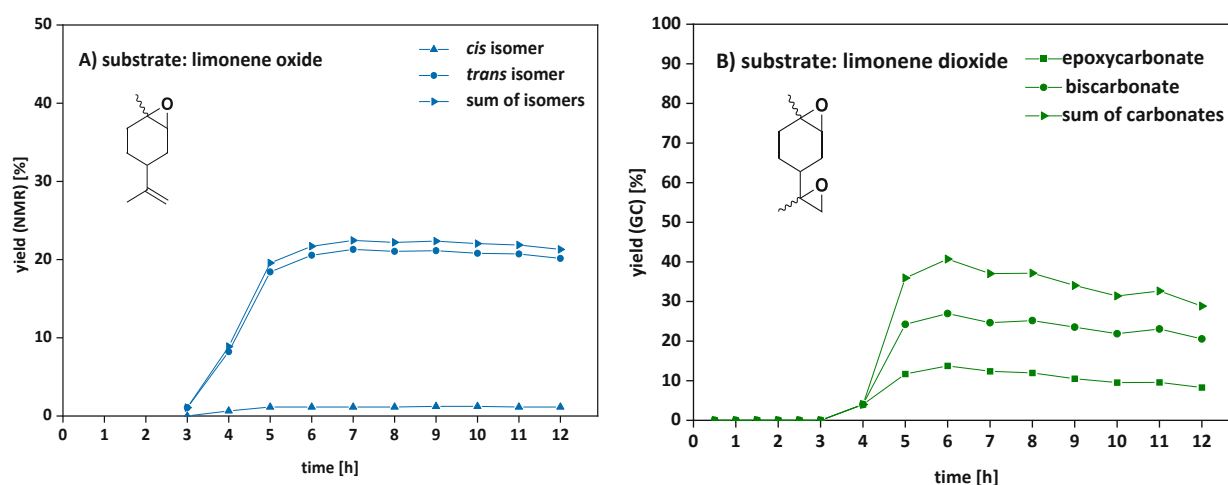
Scheme 33: Continuous production of cyclic limonene carbonates in supercritical carbon dioxide.

Conditions: SILP catalyst (30 wt% tetrabutylammonium chloride physisorbed on silica-60), 1.99 mL/min CO_2, 0.01 mL/min limonene oxide, 15 MPa (A) or 20 MPa (B), 120 °C, 12 h.

Finally, silicon oxycarbide-based SILPs for the continuous and batch-wise formation of bio-based cyclic carbonates in supercritical carbon dioxide were investigated (**Scheme 34**). Silicon oxycarbide supports were prepared by photopolymerization-assisted solidification templating and pyrolyzed at different temperatures (300 °C, 500 °C, 700 °C, 900 °C), milled, and impregnated with ionic liquid to obtain silicon oxycarbide-based SILPs. Powdered supports, silicon oxycarbide-based SILPs, and, for comparison also silica-based SILPs were characterized *via* Fourier transform infrared spectroscopy, thermogravimetric analysis, nitrogen adsorption, microscopy, X-ray photoelectron spectroscopy and solvent adsorption. They served as heterogeneous catalysts for the formation of limonene carbonates and linseed oil carbonates under batch-wise conditions, using tetrabutylammonium halide-based ionic liquids as catalytically active species. For limonene carbonate, silicon oxycarbide-based SILPs resulted in an increase of conversion of up to 15% (yield: 53-62%) after 5 h reaction time. Excellent selectivity of 97-100% was achieved compared to silica-based SILPs (48% yield, 87% selectivity). The reaction with sole silica support (no physisorbed ionic liquid) showed 16% conversion under batch-wise conditions, where the formation of diol, caused by ring opening of the epoxide, was observed as a side reaction and no carbonate as the main product was formed. For linseed oil carbonates, an increase in conversion of up to 56% (yield: 75%) was achieved after 5 h at 120 °C. Ultimately, monolithic silicon oxycarbide-based SILPs with a macroporosity of approximately 80% were employed in continuous flow and resulted in the formation of constantly 7% of limonene carbonate without leaching of catalyst for a period of 48 h.
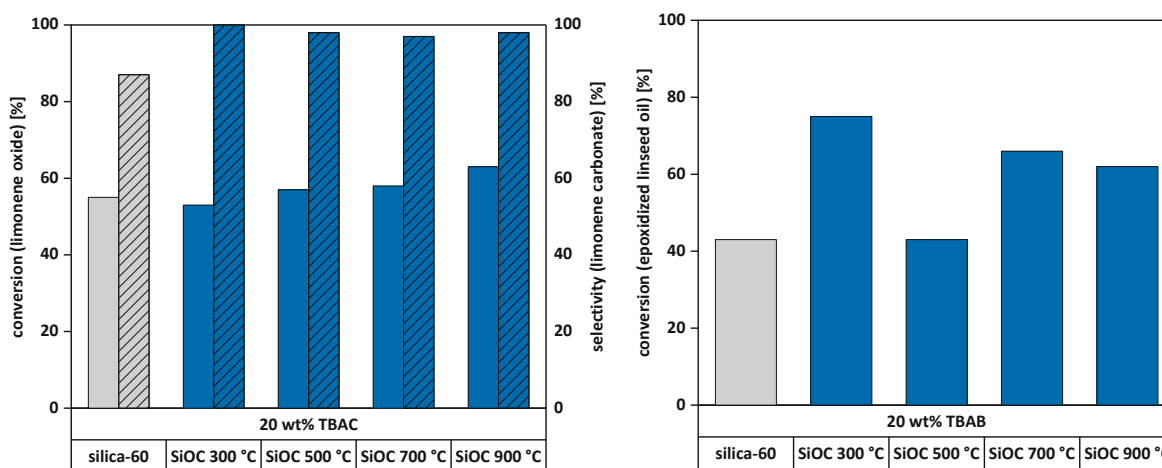
Scheme 34: Silica-based SILPs and silicon oxycarbide based-SILPs as heterogeneous catalysts for the batch-wise conversion of limonene oxide (left) and epoxidized linseed oil to cyclic carbonates (right).

Conditions: SILP catalyst (20 wt% tetrabutylammonium chloride (TBAC, 0.05 mmol) or tetrabutylammonium bromide (TBAB, 0.02 mmol) physisorbed on silica-60 or silicon oxycarbides (SiOC) pyrolyzed at different temperatures (300-900 °C)), 76 mg limonene oxide or 220 mg epoxidized linseed oil, 5 MPa CO_2 (5 MPa), 120 °C, 5 h

H   Curriculum Vitae

Dipl.-Ing. Philipp MIKŠOVSKY

address: Arnikaweg 27 | 1220 Vienna | Austria

email: philipp.miksovsky@tuwien.ac.at

                philipp_miksovsky@hotmail.com

phone: +43 (1) 58801 - 163 473

ORCID: https://orcid.org/0000-0002-8045-5667

LinkedIn: www.linkedin.com/in/philipp-miksovsky-011777288

Education:

11/2019 – present	**Doctoral Program in Engineering Sciences Technical Chemistry**
	Research Group for Sustainable Organic Synthesis and Catalysis
	TU Wien, Institute of Applied Synthetic Chemistry (E163)
03/2016 - 07/2019	**Master's Program - Technical Chemistry**
	Specialization: Synthetic Chemistry, Medicinal Chemistry
	TU Wien
01/2013 – 03/2016	**Bachelor's Program - Technical Chemistry**
	TU Wien

Professional Experience (excerpt)**:**

11/2019 – present	**University Assistant / Project Assistant**
	conduction of research incl., writing of publications, and participation in international and national conferences
	teaching of graduates and undergraduates in lab courses
	supervision of internships, and theses
	supervision of examinations
	TU Wien, Institute of Applied Synthetic Chemistry (E163)
03/2018 - 02/2019	**Student Assistant**
	teaching of undergraduates in lab courses
	TU Wien, Institute of Applied Synthetic Chemistry (E163)

Publications:

✓ **Mikšovsky, P.**; Rauchenwald, K.; Naghdi, S.; Eder, D.; Konegger T.; Bica-Schröder, K., Silicon Oxycarbide (SiOC) Supported Ionic Liquids: Heterogeneous Catalysts for Cyclic Carbonate Formation. *ACS Sustainable Chem Eng* **2023** (revision submitted).

✓ **Mikšovsky, P.**; Kornpointner, C.; Parandeh, Z.; Goessinger, M.; Bica-Schröder, K.; Halbwirth, H., Enzyme-Assisted Supercritical Fluid Extraction of Flavonoids from Apple Pomace (Malus × domestica). *ChemSusChem* **2023**, https://doi.org/10.1002/cssc.202301094.

✓ Dreier, D.; Belleza, O.; Schlögl, K.; Kickinger, S.; Hellsberg, E.; Mayer, F. P.; Sandtner, W.; **Mikšovsky, P.**; Schittmayer, M.; Hu, Y.; Jäntsch, K.; Holy, M.; Ecker, G. F.; Sitte H. H.; Mihovilovic, M. D., Careful Examination of a Novel Azobenzene Paroxetine Derivative and its Interactions with Biogenic Amine Transporters. *Commun Biol* **2023** (submitted).

✓ Anifa Mohamed Faruck, A.; Grützmacher, P. G.; Hsu, C.-J.; Dworschak, D.; Cheng, H.-W.; Valtiner, M.; Stagel, K.; **Mikšovsky, P.**; Sahoo, A. R.; Sainz Martinez, A.; Bica-Schröder, K.; Weigand, M.; Gachot, C., Applying ionic liquids as oil additives for gearboxes: Going beyond the state of the art by bridging the nano-scale and component level. **2023,** *11* (6), 1057-1078. https://doi.org/10.1007/s40544-022-0650-5.

✓ **Miksovsky, P.**; Horn, E. N.; Naghdi, S.; Eder, D.; Schnurch, M.; Bica-Schroder, K., Continuous Formation of Limonene Carbonates in Supercritical Carbon Dioxide. *Org Process Res Dev* **2022,** *26* (10), 2799-2810. https://doi.org/10.1021/acs.oprd.2c00143.

Conferences:

- ✓ **Mikšovsky, P.**; Kornpointner, C.; Lanaridi, O.; Sainz Martinez, A.; Limbeck, A.; Eder, D.; Schnürch, M.; Halbwirth H.; Bica-Schröder, K., Recovery of Valuable Compounds from Waste Materials with Alternative Solvents*, Science Days of Technical Chemistry*, Vienna (Austria), **2023**.

- ✓ **Mikšovsky**, **P.**; Rauchenwald, K.; Horn, E. N.; Naghdi, S.; Eder, D.; Konegger, T.; Schnürch, M.; Bica-Schröder, K., Continuous Formation of Bioderived Cyclic Carbonates using Supercritical Carbon Dioxide, *9th International Congress on Ionic Liquids (COIL-9)*, Lyon (France), **2023**.

- ✓ **Mikšovsky, P.**; Piotrowska, J.; Eisele, L.; Stagel, K; Bica-Schröder, K.; The ERC Project CARBOFLOW, *CO$_2$ Refinery Industry Kick-Off*, Vienna (Austria), **2022**.

- ✓ **Mikšovsky**, **P.**; Horn, E. N.; Naghdi, S.; Eder, D.; Schnürch, M.; Bica-Schröder, K., Continuous Formation of Cyclic Limonene Carbonates using Supercritical Carbon Dioxide, *9th IUPAC International Conference on Green Chemistry (9th ICGC)*, Athens (Greece), **2022**.

Theses (own and supervised):

- ✓ Parandeh, Z., Enzyme-Assisted Supercritical Carbon Dioxide Extraction of Flavonoids from Apple Pomace. **2023** (bachelor's thesis, supervision: Prof. Bica-Schröder, K.; **Mikšovsky, P.**)

- ✓ Molnar, M. M., Screening of Ionic Liquid-Based Catalysts for the Synthesis of Fatty Acid-Based Carbonates in Continuous Flow. **2023** (bachelor's thesis (ongoing), supervision: Prof. Bica-Schröder, K.; **Mikšovsky, P.**)

- ✓ Cucovic, E., Rückgewinnung wertvoller Metalle aus Flugasche von Wiens Siedlungsabfällen unter Anwendung von Grüner Chemie. **2023** (bachelor's thesis, supervision: Prof. Bica-Schröder, K.; Prof. Limbeck, A.; co-supervision: **Mikšovsky, P.**, Piotrowska, J.; Stagel, K.; Pálvölgyi, Á.M.)

- ✓ Horn, E. N., Modification of Renewables Catalyzed by Ionic Liquids: Formation of Limonene Carbonates using Supercritical Carbon Dioxide in Continuous Flow. **2021** (bachelor's thesis, supervision: Prof. Bica-Schröder, K.; **Mikšovsky, P.**)

- ✓ **Mikšovsky, P.**, Neuroscience Meets Photopharmacology: Scale-up and Optimization of the Synthesis Photoswitchable Paroxetine Based Serotonin Reuptake Inhibitors. **2019** (diploma thesis, supervision: Prof. Mihovilovic, M. D.; Dreier, D.)

I   Appendix

I.1   Supporting Information: Enzyme-Assisted Supercritical Fluid Extraction of Flavonoids from Apple Pomace (Malus × domestica)

Supporting information:

Mikšovsky, P.; Kornpointner, C.; Parandeh, Z.; Goessinger, M.; Bica-Schröder, K.; Halbwirth, H., Enzyme-Assisted Supercritical Fluid Extraction of Flavonoids from Apple Pomace (Malus × domestica). *ChemSusChem* **2023**, https://doi.org/10.1002/cssc.202301094.

Supplementary Information

Enzyme-Assisted Supercritical Fluid Extraction of Flavonoids from Apple Pomace (*Malus × domestica)*

Philipp Mikšovsky[a,†], Christoph Kornpointner[b,†], Zahra Parandeh[a], Manfred Goessinger[c]

Katharina Bica-Schröder[a,]* and Heidi Halbwirth[b,]*

[a] Institute of Applied Synthetic Chemistry (E163), TU Wien, 1060 Vienna, Austria;

Email: katharina.schroeder@tuwien.ac.at

[b] Institute of Chemical, Environmental and Bioscience Engineering (E166), TU Wien, 1060 Vienna, Austria;

Email: heidrun.halbwirth@tuwien.ac.at

[c] Department of Fruit Processing, Federal College and Institute for Viticulture and Pomology, A-3400, Klosterneuburg, Austria

Table of Contents

1   Flow Scheme of the Supercritical Fluid Extraction Set-Up for the Sequential Process
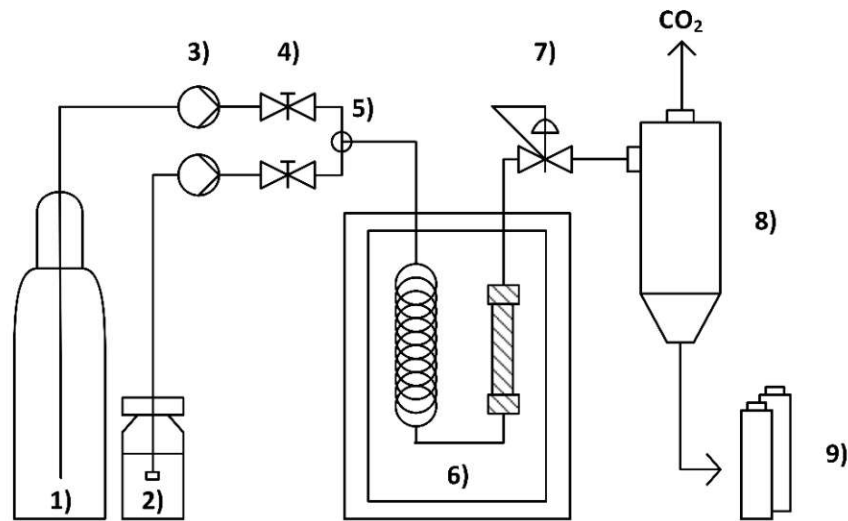
Figure S1: **Schematic representation of the SFE set-up for the sequential process.** (1) carbon dioxide cylinder with ascending pipe; (2) cosolvent supply; (3) HPLC pump; (4) hand operated valve; (5) t-piece; (6) oven with heating coil and flow extraction vessel; (7) back-pressure regulator; (8) gas-liquid separator; (9) product collector

2   Pictures of Ground and Unground Apple Pomace
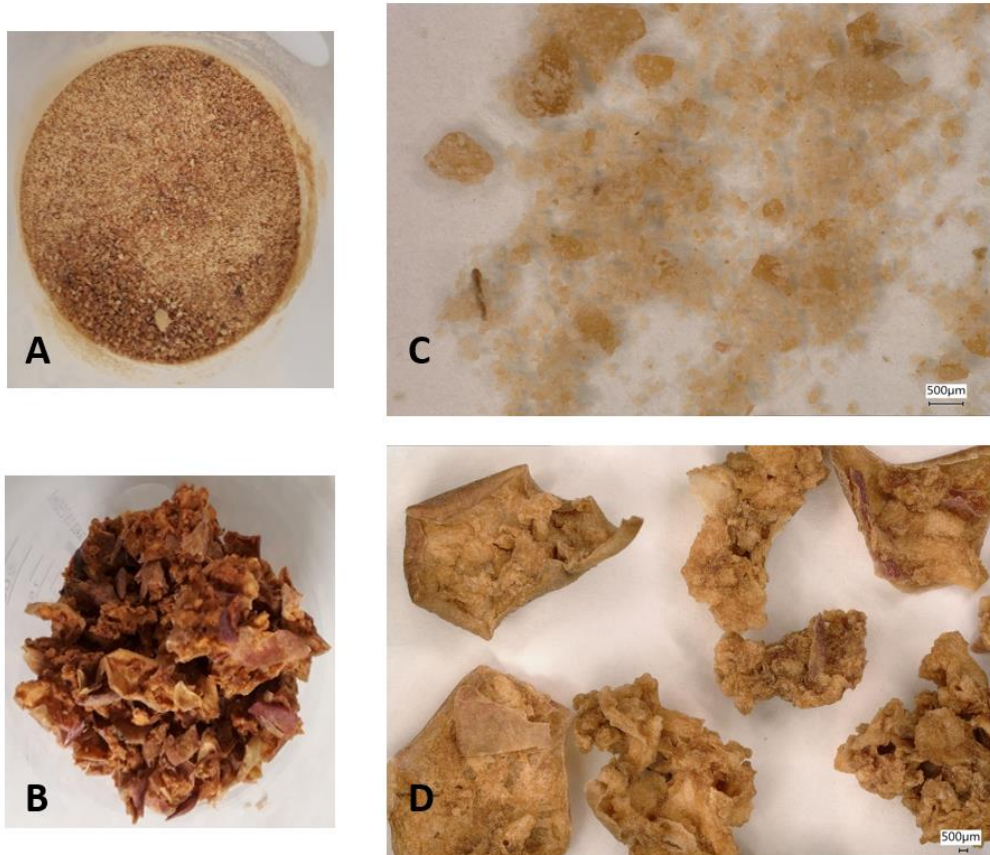
Figure S2: **Pictures of ground (A, C) and unground (B, D) apple pomace.** Topaz apples were crushed using a centrifugal grinder and pressed with a hydraulic press. The pomace was dried in a drying cabinet at 65° C for 16 h. Dry apple pomace was further ground with a Fritsch Universal Pulverisette 19 cutting mill using a 2 mm sieve and stored in a desiccator over silica gel drying agent. A digital microscope (VHX-5000, KEYENCE) was used for pictures C and D and the determination of the average particle diameters.

3 Quantification via HPLC and LC/MS

Table S1: HPLC and LC-MS data of the targeted flavonoids in apple pomace extracts.

flavonoid	t_{Ret} [min]	UV_{max} [nm]	$[M-H]^-$	$[M-H]^-_{calc.}$	fragments for identification	molecular formula
kaempferol **1a**	21.697	266/365	285.0399	285.0405	-	$C_{15}H_{10}O_6$
quercetin **1b**	19.123	255/370	301.0365	301.0354	-	$C_{15}H_{10}O_7$
phloretin **1c**	20.970	286	273.0765	273.0768	-	$C_{15}H_{14}O_5$
3-hydroxyphloretin **1d**	18.590	286	289.0712	289.0718	-	$C_{15}H_{14}O_6$
kaempferol glycoside **2a**	16.353	264/321	-	-	285.0 $[M-H-Glc]^-$	-
quercetin glycosides **2b**	13.620[a]	256/356	463.0870	463.0882	301.0 $[M-H-Glc]^-$	$C_{21}H_{20}O_{12}$
	14.293	256/358	433.0765	433.0776	301.0 $[M-H-Glc]^-$	$C_{20}H_{18}O_{11}$
	14.820	256/353	433.0768	433.0776	301.0 $[M-H-Glc]^-$	$C_{20}H_{18}O_{11}$
	14.990	256/347	447.0934	447.0933	301.0 $[M-H-Glc]^-$	$C_{21}H_{20}O_{11}$
phloridzin **2c**	15.997	285	435.1288	435.1297	273.0 $[M-H-Glc]^-$	$C_{21}H_{24}O_{10}$
3-hydroxyphloridzin **2d**	14.593	286	-	451.1246	289.0 $[M-H-Glc]^-$	$C_{21}H_{24}O_{11}$

[a]This peak refers to two different quercetin glycosides which were not separable via HPLC.
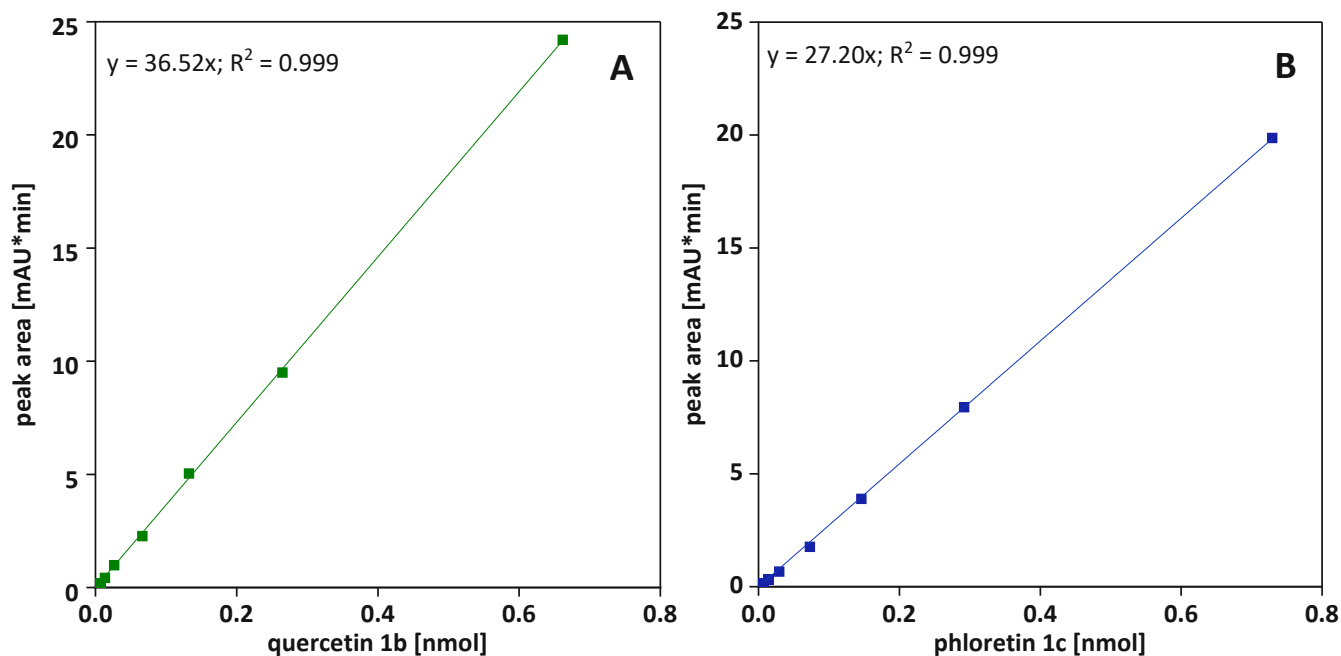
Figure S3: Calibration curve for quercetin 1b (A) and phloretin 1c (B). Further details on calibration are given in **Table S2**.

Table S2: Summary of calibration for quercetin 1b and phloretin 1c. Due to the structural similarities of flavonols **1a-b** and **2a-b,** the calibration curve of quercetin **1b** was used for the quantification of kaempferol **1a** and flavonoid glycosides **2a-b**. Accordingly, the calibration curve of the chalcone phloretin **1c** was used for the quantification of 3-hydroxyphloretin **1d** and the flavonoid glycosides phloridzin **2c** and 3-hydroxyphloridzin **2d**.[a]

flavonoid	concentration [µg/mL]	amount of substance [b] [nmol]	peak area [mAU·min]
quercetin **1b**	0.5	0.007	0.19
	1	0.013	0.43
	2	0.026	0.99
	5	0.066	2.27
	10	0.132	5.05
	20	0.265	9.50
	50	0.662	24.21
phloretin **1c**	0.5	0.007	0.14
	1	0.015	0.31
	2	0.029	0.67
	5	0.073	1.77
	10	0.146	3.89
	20	0.292	7.96
	50	0.729	19.87

[a]A stock solution of 1 mg/mL of quercetin **1b** and phloretin **1c** in 1 mL MeOH was employed to prepare 1 mL of methanolic solution for each concentration in the dilution series. An aliquot of 80 µL was taken for HPLC measurements (4 µL injection volume), quantification of quercetin **1b** was carried out at 340 nm, the quantification of phloretin **1c** at 310 nm. [b] in 4 µL injection volume

4 Snailase – Assisted Supercritical Carbon Dioxide Extraction – Summary of Results

Table S3: Extracted amounts of flavonoid aglycones 1a-d and total amounts in µmol/g after supercritical fluid extraction (n = 3 ± SD).

experiments	kaempferol 1a [µmol/g]	quercetin 1b [µmol/g]	phloretin 1c [µmol/g]	3-hydroxyphloretin 1d [µmol/g]	total amounts of flavonoid aglycones 1a-d [µmol/g]	total amounts [µmol/g]
Figure 3 – SFE of enzymatically untreated apple pomace						
entry S1 - 5 v% EtOH (SFE)	n.d.	0.0013 ± 0.0003	n.d.	n.d.	0.0013 ± 0.0003 [p]	0.0048 ± 0.0004 [l]
entry S2 - 10 v% EtOH (SFE)	n.d.	0.0048 ± 0.0002	n.d.	n.d.	0.0048 ± 0.0002 [p]	0.215 ± 0.008 [hij]
entry S3 - 20 v% EtOH (SFE)	n.d.	0.006 ± 0.001	n.d.	n.d.	0.006 ± 0.001 [p]	0.48 ± 0.02 [cde]
Figure 4 - amount of snailase						
entry S4 - 0%Sna	n.d.	0.012 ± 0.001	0.0013 ± 0.0002	n.d.	0.013 ± 0.001 [p]	0.27 ± 0.02 [gh]
entry S5 - 0.1%Sna	0.0054 ± 0.0009	0.22 ± 0.02	0.061 ± 0.004	0.061 ± 0.002	0.352 ± 0.017 [hij]	0.47 ± 0.02 [cde]
entry S6 - 0.25%Sna	0.008 ± 0.001	0.33 ± 0.06	0.054 ± 0.005	0.061 ± 0.008	0.45 ± 0.07 [defg]	0.51 ± 0.07 [bcde]
entry S7 - 0.5%Sna	0.0093 ± 0.0006	0.35 ± 0.03	0.054 ± 0.009	0.059 ± 0.006	0.47 ± 0.03 [cdef]	0.51 ± 0.04 [bcde]
entry S8 - 1%Sna	0.0107 ± 0.0001	0.37 ± 0.01	0.056 ± 0.003	0.057 ± 0.002	0.49 ± 0.01 [bcde]	0.520 ± 0.009 [bcde]
entry S9 - 5% Sna	0.0075 ± 0.0007	0.24 ± 0.03	0.036 ± 0.004	0.029 ± 0.005	0.31 ± 0.04 [hijk]	0.33 ± 0.04 [fg]
entry S10 - 10%Sna	0.0052 ± 0.0005	0.16 ± 0.01	0.032 ± 0.004	0.017 ± 0.002	0.22 ± 0.01 [lmn]	0.251 ± 0.007 [ghi]
entry S11 - 20%Sna	0.0028 ± 0.0005	0.088 ± 0.008	0.020 ± 0.002	0.0079 ± 0.0004	0.12 ± 0.01 [o]	0.13 ± 0.01 [jk]
Figure 5 - time of hydrolysis						
entry S12 - 0.25%Sna_0.5h	0.0043 ± 0.0001	0.16 ± 0.02	0.061 ± 0.004	0.042 ± 0.002	0.27 ± 0.01 [ijkl]	0.42 ± 0.03 [ef]
entry S13 - 0.5%Sna_0.5h	0.0063 ± 0.0008	0.260 ± 0.006	0.052 ± 0.003	0.046 ± 0.0003	0.365 ± 0.008 [ghi]	0.43 ± 0.01 [ef]
entry S14 - 1%Sna_0.5h	0.0073 ± 0.0006	0.28 ± 0.02	0.065 ± 0.003	0.046 ± 0.006	0.39 ± 0.02 [fgh]	0.46 ± 0.02 [de]
entry S6 - 0.25%Sna_1h	0.008 ± 0.001	0.33 ± 0.06	0.054 ± 0.005	0.061 ± 0.008	0.45 ± 0.07 [defg]	0.51 ± 0.07 [bcde]
entry S7 - 0.5%Sna_1h	0.0093 ± 0.0006	0.35 ± 0.03	0.054 ± 0.009	0.059 ± 0.006	0.47 ± 0.03 [cdef]	0.51 ± 0.04 [bcde]
entry S8 - 1%Sna_1h	0.0107 ± 0.0001	0.37 ± 0.01	0.056 ± 0.003	0.057 ± 0.002	0.49 ± 0.01 [bcde]	0.520 ± 0.009 [bcde]
entry S15 - 0.25%Sna_2h	0.012 ± 0.001	0.44 ± 0.03	0.041 ± 0.008	0.084 ± 0.008	0.58 ± 0.04 [b]	0.61 ± 0.04 [ab]
entry S16 - 0.5%Sna_2h	0.0120 ± 0.0004	0.42 ± 0.02	0.0502 ± 0.0008	0.072 ± 0.004	0.56 ± 0.02 [bc]	0.60 ± 0.03 [ab]
entry S17 - 1%Sna_2h	0.0123 ± 0.0001	0.43 ± 0.01	0.046 ± 0.003	0.071 ± 0.006	0.56 ± 0.01 [bc]	0.58 ± 0.02 [bc]

Mean values of total amounts within the same column marked with different letters (a, b etc.) are statistically different ($p < 0.05$). For ANOVA tests, entries were considered only once. n.d. not detected

Continuation of Table S3: Extracted amounts of flavonoids 1a-d and total amounts in µmol/g after supercritical fluid extraction (n = 3 ± SD).

experiments	kaempferol 1a [µmol/g]	quercetin 1b [µmol/g]	phloretin 1c [µmol/g]	3-hydroxyphloretin 1d [µmol/g]	total amounts of flavonoid aglycones 1a-d [µmol/g]	total amounts [µmol/g]
Figure 6 - cosolvent + optimum conditions						
entry S18 - 5 v% EtOH	0.0074 ± 0.0002	0.12 ± 0.02	0.020 ± 0.003	0.006 ± 0.003	0.16 ± 0.03 [mno]	0.16 ± 0.03 [ijk]
entry S19 - 10 v% EtOH	0.0093 ± 0.0001	0.301 ± 0.008	0.046 ± 0.003	0.05 ± 0.01	0.41 ± 0.02 [efgh]	0.43 ± 0.01 [ef]
entry S7 - 20 v% EtOH	0.0093 ± 0.0006	0.35 ± 0.03	0.054 ± 0.009	0.059 ± 0.006	0.47 ± 0.03 [cdef]	0.51 ± 0.04 [bcde]
entry S20 - 5 v% MeOH	0.0079 ± 0.0009	0.12 ± 0.02	0.019 ± 0.003	0.006 ± 0.002	0.152 ± 0.022 [no]	0.15 ± 0.02 [ijk]
entry S21 - 10 v% MeOH	0.011 ± 0.001	0.36 ± 0.03	0.053 ± 0.009	0.056 ± 0.002	0.48 ± 0.03 [cdef]	0.50 ± 0.03 [bcde]
entry S22 - 20 v% MeOH	0.0112 ± 0.0005	0.39 ± 0.02	0.051 ± 0.007	0.068 ± 0.009	0.52 ± 0.02 [bcd]	0.57 ± 0.02 [bcd]
entry S23 - OPTIMUM	0.0150 ± 0.0003	0.52 ± 0.02	0.060 ± 0.003	0.082 ± 0.006	0.676 ± 0.023 [a]	0.70 ± 0.02 [a]
Table 3 – ground vs. unground apple pomace						
entry S7 - ground	0.009 ± 0.0006	0.35 ± 0.03	0.054 ± 0.009	0.059 ± 0.006	0.47 ± 0.03 [cdef]	0.51 ± 0.04 [bcde]
entry S24 - unground	0.006 ± 0.001	0.22 ± 0.04	0.023 ± 0.006	0.018 ± 0.001	0.26 ± 0.04 [jkl]	0.46 ± 0.07 [de]
Table 7 – SFE employing batch extraction vessel						
entry S25 - sequential - dried pomace	0.0043 ± 0.0009	0.17 ± 0.03	0.030 ± 0.008	0.026 ± 0.005	0.25 ± 0.02 [klm]	0.34 ± 0.05 [fg]
entry S26 - sequential - wet pomace	0.0006 ± 0.001	0.05 ± 0.04	0.02 ± 0.02	0.010 ± 0.005	0.08 ± 0.04 [op]	0.15 ± 0.06 [ijk]
entry S27 - simultaneous - 5% MeOH	0.005 ± 0.007	0.05 ± 0.03	0.013 ± 0.007	0.006 ± 0.007	0.07 ± 0.04 [op]	0.09 ± 0.05 [kl]
entry S28 - simultaneous - 5% EtOH	n.d.	0.05 ± 0.04	0.03 ± 0.03	0.005 ± 0.005	0.09 ± 0.07 [op]	0.09 ± 0.07 [kl]

Mean values of total amounts within the same column marked with different letters (a, b etc.) are statistically different ($p < 0.05$). For ANOVA tests, entries were considered only once. n.d. not detected

Table S4: Extracted amounts of flavonoid glycosides 2a-d and total amounts in µmol/g after supercritical fluid extraction (n = 3 ± SD).

experiments	kaempferol glycoside 2a [µmol/g]	quercetin glycosides 2b [µmol/g]	phloridzin 2c [µmol/g]	3-hydroxyphloridzin 2d [µmol/g]	total amounts flavonoid glycosides 2a-d [µmol/g]	total amounts [µmol/g]
Figure 3 – SFE of enzymatically untreated apple pomace						
entry S1 - 5 v% EtOH (SFE)	0.00030 ± 0.00002	0.0032 ± 0.0006	n.d.	n.d.	0.0035 ± 0.0006 [i]	0.0048 ± 0.0004 [l]
entry S2 - 10 v% EtOH (SFE)	0.0072 ± 0.0003	0.183 ± 0.007	0.0191 ± 0.0008	0.0008 ± 0.0001	0.210 ± 0.007 [bc]	0.215 ± 0.008 [hij]
entry S3 - 20 v% EtOH (SFE)	0.0101 ± 0.0007	0.40 ± 0.02	0.0574 ± 0.0001	0.005 ± 0.002	0.48 ± 0.02 [a]	0.48 ± 0.02 [cde]
Figure 4 - amount of snailase						
entry S4 - 0%Sna	0.0067 ± 0.0008	0.21 ± 0.02	0.029 ± 0.002	0.019 ± 0.002	0.26 ± 0.02 [b]	0.27 ± 0.02 [gh]
entry S5 - 0.1%Sna	0.0038 ± 0.0003	0.11 ± 0.02	0.0039 ± 0.0008	0.0040 ± 0.0007	0.12 ± 0.02 [de]	0.47 ± 0.02 [cde]
entry S6 - 0.25%Sna	0.00145 ± 0.00002	0.054 ± 0.005	0.0037 ± 0.0008	0.0028 ± 0.0003	0.062 ± 0.004 [efgh]	0.51 ± 0.07 [bcde]
entry S7 - 0.5%Sna	0.0010 ± 0.0001	0.034 ± 0.002	0.0016 ± 0.0002	0.0014 ± 0.0002	0.038 ± 0.003 [fghi]	0.51 ± 0.04 [bcde]
entry S8 - 1%Sna	0.0010 ± 0.0001	0.026 ± 0.003	n.d.	0.0014 ± 0.0002	0.029 ± 0.003 [ghi]	0.520 ± 0.009 [bde]
entry S9 - 5% Sna	0.0006 ± 0.0002	0.021 ± 0.004	n.d.	n.d.	0.021 ± 0.004 [ghi]	0.33 ± 0.04 [fg]
entry S10 - 10%Sna	0.0011 ± 0.0005	0.03 ± 0.02	0.002 ± 0.002	n.d.	0.03 ± 0.02 [fghi]	0.251 ± 0.007 [ghi]
entry S11 - 20%Sna	0.0004 ± 0.0002	0.0120 ± 0.0008	n.d.	n.d.	0.012 ± 0.001 [hi]	0.13 ± 0.01 [jk]
Figure 5 - time of hydrolysis						
entry S12 - 0.25%Sna_0.5h	0.0050 ± 0.0007	0.14 ± 0.01	0.0044 ± 0.0004	0.0021 ± 0.0003	0.15 ± 0.02 [cd]	0.42 ± 0.03 [ef]
entry S13 - 0.5%Sna_0.5h	0.0020 ± 0.0007	0.07 ± 0.01	0.0033 ± 0.0005	0.0015 ± 0.0001	0.07 ± 0.01 [efg]	0.43 ± 0.01 [ef]
entry S14 - 1%Sna_0.5h	0.01 ± 0.01	0.058 ± 0.003	0.0023 ± 0.0004	0.0018 ± 0.0005	0.07 ± 0.01 [efgh]	0.46 ± 0.02 [de]
entry S6 - 0.25%Sna_1h	0.00145 ± 0.00002	0.054 ± 0.005	0.0037 ± 0.0008	0.0028 ± 0.0003	0.062 ± 0.004 [efgh]	0.51 ± 0.07 [bcde]
entry S7 - 0.5%Sna_1h	0.0010 ± 0.0001	0.034 ± 0.002	0.0016 ± 0.0002	0.0014 ± 0.0002	0.038 ± 0.003 [fghi]	0.51 ± 0.04 [bcde]
entry S8 - 1%Sna_1h	0.0010 ± 0.0001	0.026 ± 0.003	n.d.	0.0014 ± 0.0002	0.029 ± 0.003 [ghi]	0.520 ± 0.009 [bcde]
entry S15 - 0.25%Sna_2h	0.0007 ± 0.0002	0.023 ± 0.001	0.0013 ± 0.0003	0.0015 ± 0.0005	0.027 ± 0.002 [ghi]	0.61 ± 0.04 [ab]
entry S16 - 0.5%Sna_2h	0.0007 ± 0.0002	0.04 ± 0.02	0.002 ± 0.001	0.0015 ± 0.0003	0.04 ± 0.02 [fgh]	0.60 ± 0.03 [ab]
entry S17 - 1%Sna_2h	0.0006 ± 0.0001	0.019 ± 0.002	0.0011 ± 0.0002	0.0015 ± 0.0004	0.022 ± 0.002 [fghi]	0.58 ± 0.02 [bc]

Mean values of total amounts within the same column marked with different letters (a, b etc.) are statistically different ($p < 0.05$). For ANOVA tests, entries were considered only once. n.d. not detected

Continuation of Table S4: Extracted amounts of flavonoid glycosides 2a-d and total amounts in µmol/g after supercritical fluid extraction (n = 3 ± SD).

experiments	kaempferol glycoside 2a [µmol/g]	quercetin glycosides 2b [µmol/g]	phloridzin 2c [µmol/g]	3-hydroxyphloridzin 2d [µmol/g]	total amounts flavonoid glycosides 2a-d [µmol/g]	total amounts [µmol/g]
Figure 6 - cosolvent + optimum conditions						
entry S18 - 5 v% EtOH	n.d.	n.d.	n.d.	n.d.	n.d.	0.16 ± 0.03 [ijk]
entry S19 - 10 v% EtOH	0.00067 ± 0.00004	0.019 ± 0.001	0.0007 ± 0.0001	n.d.	0.020 ± 0.001 [ghi]	0.43 ± 0.01 [ef]
entry S7 - 20 v% EtOH	0.0010 ± 0.0001	0.034 ± 0.002	0.0016 ± 0.0002	0.0014 ± 0.0002	0.038 ± 0.003 [fghi]	0.51 ± 0.04 [bcde]
entry S20 - 5 v% MeOH	n.d.	n.d.	n.d.	n.d.	n.d.	0.15 ± 0.02 [ijk]
entry S21 - 10 v% MeOH	0.0008 ± 0.0002	0.017 ± 0.004	0.0004 ± 0.0001	n.d.	0.019 ± 0.004 [ghi]	0.50 ± 0.03 [bcde]
entry S22 - 20 v% MeOH	0.0013 ± 0.0002	0.038 ± 0.005	0.0023 ± 0.0004	0.0017 ± 0.0004	0.044 ± 0.005 [fghi]	0.57 ± 0.02 [bcd]
entry S23 - OPTIMUM	0.0007 ± 0.0001	0.024 ± 0.002	0.0014 ± 0.0001	0.0025 ± 0.0002	0.028 ± 0.002 [fgh]	0.70 ± 0.02 [a]
Table 3 – ground vs. unground apple pomace						
entry S7 - ground	0.0010 ± 0.0001	0.034 ± 0.002	0.0016 ± 0.0002	0.0014 ± 0.0002	0.038 ± 0.003 [ghi]	0.51 ± 0.04 [bcde]
entry S24 - unground	0.0055 ± 0.0008	0.18 ± 0.04	0.0052 ± 0.0007	0.0024 ± 0.0003	0.20 ± 0.04 [c]	0.46 ± 0.07 [de]
Table 7 – SFE employing batch extraction vessel						
entry S25 - sequential - dried pomace	n.d.	0.032 ± 0.007	0.05 ± 0.07	0.008 ± 0.005	0.09 ± 0.07 [ef]	0.34 ± 0.05 [fg]
entry S26 - sequential - wet pomace	n.d.	0.05 ± 0.02	0.014 ± 0.008	0.004 ± 0.003	0.07 ± 0.02 [efg]	0.15 ± 0.06 [ijk]
entry S27 - simultaneous – 5% MeOH	n.d.	0.01 ± 0.01	0.001 ± 0.001	0.0002 ± 0.0004	0.02 ± 0.02 [ghi]	0.09 ± 0.05 [kl]
entry S28 - simultaneous – 5% EtOH	n.d.	0.02 ± 0.01	0.02 ± 0.02	n.d.	0.004 ± 0.003 [i]	0.09 ± 0.07 [kl]

Mean values of total amounts within the same column marked with different letters (a, b etc.) are statistically different ($p < 0.05$). For ANOVA tests, entries were considered only once. n.d. not detected

I.2 Supporting Information: Continuous Formation of Limonene Carbonates in Supercritical Carbon Dioxide

Supporting information:

Miksovsky, P.; Horn, E. N.; Naghdi, S.; Eder, D.; Schnurch, M.; Bica-Schroder, K., Continuous Formation of Limonene Carbonates in Supercritical Carbon Dioxide. *Org Process Res Dev* **2022,** *26* (10), 2799-2810. https://doi.org/10.1021/acs.oprd.2c00143.

Supporting Information

Continuous Formation of Limonene Carbonates in Supercritical Carbon Dioxide

Philipp Mikšovsky [1], Elias N. Horn [1], Shaghayegh Naghdi [2], Dominik Eder [2], Michael Schnürch [1]

and Katharina Bica-Schröder [1],*

[1]Institute of Applied Synthetic Chemistry (E163), TU Wien, Getreidemarkt 9/E163, 1060 Vienna, Austria.

[2]Institute of Materials Chemistry (E165), TU Wien, Getreidemarkt 9/E165, 1060 Vienna, Austria.

* Corresponding author: Katharina Bica-Schröder,

email: katharina.schroeder@tuwien.ac.at

phone: +43 1 58801 163601

Table of Contents

1   Materials and Methods

Detailed information about the scCO$_2$ flow device is summarized in the experimental part of the main manuscript.

Unless otherwise noted, chemicals were purchased from several chemical suppliers and used without further purification. Limonene dioxide **7b** was kindly provided by Nitrochemie Aschau GmbH. 1-Methylimidazole was distilled prior to use (80 °C, 13 mbar). Dichloromethane, used for reactions which required anhydrous conditions, were pre-distilled and dried over Al$_2$O$_3$ columns (PURESOLV, Innovative Technology). TLC analysis was performed on silica gel 60 F$_{254}$ aluminium plates from Merck containing a fluorescent indicator using solvent mixtures of ethyl acetate in liquid petroleum. Spots were visualized using ultraviolet light (254 nm) or were stained with cer ammonium molybdate (0.5 g Ce(NH$_4$)$_4$(SO$_4$)$_4$ · 2H$_2$O, 12.0 g (NH$_4$)$_6$Mo$_7$O$_{24}$· 4 H$_2$O, 235 mL H$_2$O, 15 mL conc. H$_2$SO$_4$) followed by heating.

GC measurements were performed with a Thermo Scientific Trace 1310 gas chromatograph containing two capillary columns from Restek Rtx-5 (Rtx-5, 15 m x 0.25 mm x 1.00 µm) and a flame ionization detector (FID). A Thermo Trace 1300 / ISQ LT (single quadrupole MS (EI)) containing a standard capillary column from Restek (Rxi-5sil MS, 30 m x 0,25 mm x 0,25 µm) was used for GC/MS measurements (initial temperature: 100 °C (holding time 2 min); rate: 35 °C/min to 300 °C (holding time: 4 min).

^{1}H-NMR and ^{13}C-NMR spectra were recorded from CDCl$_3$ solutions on a Bruker Avance UltraShield *400/600* (^{1}H: 400, 600 MHz, ^{13}C: 101 MHz) spectrometer.

FTIR spectra (transmission mode) were recorded on a PerkinElmer Spectrum 65 FTIR spectrometer. Resolution was set to 4 cm^{-1}, 8 scans were used. Spectra were recorded from 4000 - 500 cm^{-1}. Raw data were processed with the PerkinElmer Spectrum Software.

DRIFT spectra (result spectra: Kubelka Munk) were recorded on a Bruker Vertex 80 FTIR spectrometer using a narrow band MCT detector. Resolution was set to 4 cm^{-1}, 256 scans were used. Spectra were recorded from 4000 – 800 cm^{-1} and raw data were processed with MestreNova and OPUS. Samples (40 mg / 400 mg KBr) were diluted with KBr from Sigma Aldrich (99%, FTIR grade) and dried for 4 days under high vacuum.

The physisorption measurements were carried out on an ASAP 2010 by Micromeritics GmbH. The degassing procedure was set to 120 °C for 6 hours and the isotherms were obtained using nitrogen at 77 K. BET (Brunauer-Emmett-Teller) specific surface areas were calculated based on BET equation, pore volumes were calculated based on BJH (Barret-Joyner-Halenda) equation from the desorption branch and average pore diameters were calculated based on desorption branch.

For thermogravimetric analysis (TGA), a Netzsch STA 449 F1 system was used. Temperature was increased from 25 °C to 450 °C with a rate of 5 °C/min.

2 Ionic Liquids

2.1 Synthesis of [C$_2$mim]Br 5 and [C$_2$mim]I 6

Tetrabutylammonium halides TBAX **1-3** and 1-ethyl-3-methylimidazolium chloride [C$_2$mim]Cl **4** were purchased from several suppliers and dried under high vacuum prior to use.

1-Ethyl-3-methylimidazolium bromide [C$_2$mim]Br **5** and 1-ethyl-3-methylimidazolium iodide [C$_2$mim]I **6** were synthesized according to modified literature protocols[1, 2]

Bromoethane or iodoethane (134 mmol, 1.10 equiv.) was added dropwise to freshly distilled 1-methylimidazole (10.00 g, 122 mmol, 1.00 equiv.) under argon atmosphere. For [C$_2$mim]Br **5**, the reaction mixture was heated up to 40 °C for 4.5 h, respectively to 80 °C for 30 min for [C$_2$mim]I **6**. Complete conversion was confirmed via ^{1}H-NMR spectroscopy. The reaction mixture was cooled with an ice bath whereby the product precipitated. The solid material was recrystallized (minimum amount of ACN for dissolving, ethyl acetate for precipitation). The solid material was washed with ethyl acetate (3 x 30 mL), volatiles were removed in *vacuo*. The ionic liquids **5** and **6** were dried for three days at room temperature under high vacuum. [C$_2$mim]Br **5**: 96% (22.35 g, 117 mmol, colorless crystals) ^{1}H NMR (400 MHz, CDCl$_3$, CH$_4$Si) δ = 10.28 (s, 1H, -N=C*H*-N-), 7.61 – 7.53 (m, 2H, -N-C*H*-C*H*-N-), 4.36 (q, *J* = 7.4 Hz, 2H, -N-C*H*$_2$-CH$_3$), 4.06 (s, 3H, -N-C*H*$_3$), 1.55 (t, *J* = 7.4 Hz, 3H, -N-CH$_2$-C*H*$_3$) ppm. ^{13}C NMR (101 MHz, CDCl$_3$, CH$_4$Si) δ = 137.04 (d, C2), 123.70 (d, C4), 121.97 (d, C5), 45.29 (t, *C*H$_2$-CH$_3$), 36.70 (q, N-*C*H$_3$), 15.71 (q, *C*H$_2$-*C*H$_3$) ppm. [C$_2$mim]I **6**: quant. (28.90 g, 121 mmol, pale yellow crystals) ^{1}H NMR (400 MHz, CDCl$_3$, CH$_4$Si) δ = 10.47 – 9.63 (m, 1H, -N=C*H*-N-), 7.50 (d, *J* = 1.7 Hz, 2H, -N-C*H*-C*H*-N-), 4.51 – 4.34 (m, 2H, -N-C*H*$_2$-CH$_3$), 4.11 (d, *J* = 0.6 Hz, 3H, -N-C*H*$_3$), 1.61 (t, *J* = 7.4 Hz, 3H, -N-CH$_2$-C*H*$_3$) ppm. ^{13}C NMR (101 MHz, CDCl$_3$, CH$_4$Si) δ = 136.76 (d, C2), 123.74 (d, C4), 121.99 (d, C5), 45.61 (t, *C*H$_2$-CH$_3$), 37.22 (q, N-*C*H$_3$), 15.75 (q, CH$_2$-*C*H$_3$) ppm.

2.2 NMR Spectra: 1-Ethyl-3-methylimidazolium Bromide [C$_2$mim]Br 5

Figure S1: ^{1}H-NMR spectrum of 1-ethyl-3-methylimidazolium bromide [C$_2$mim]Br 5.

Figure S2: ^{13}C-NMR spectrum of 1-ethyl-3-methylimidazolium bromide [C$_2$mim]Br 5.

Spectral data are in accordance with literature[3].

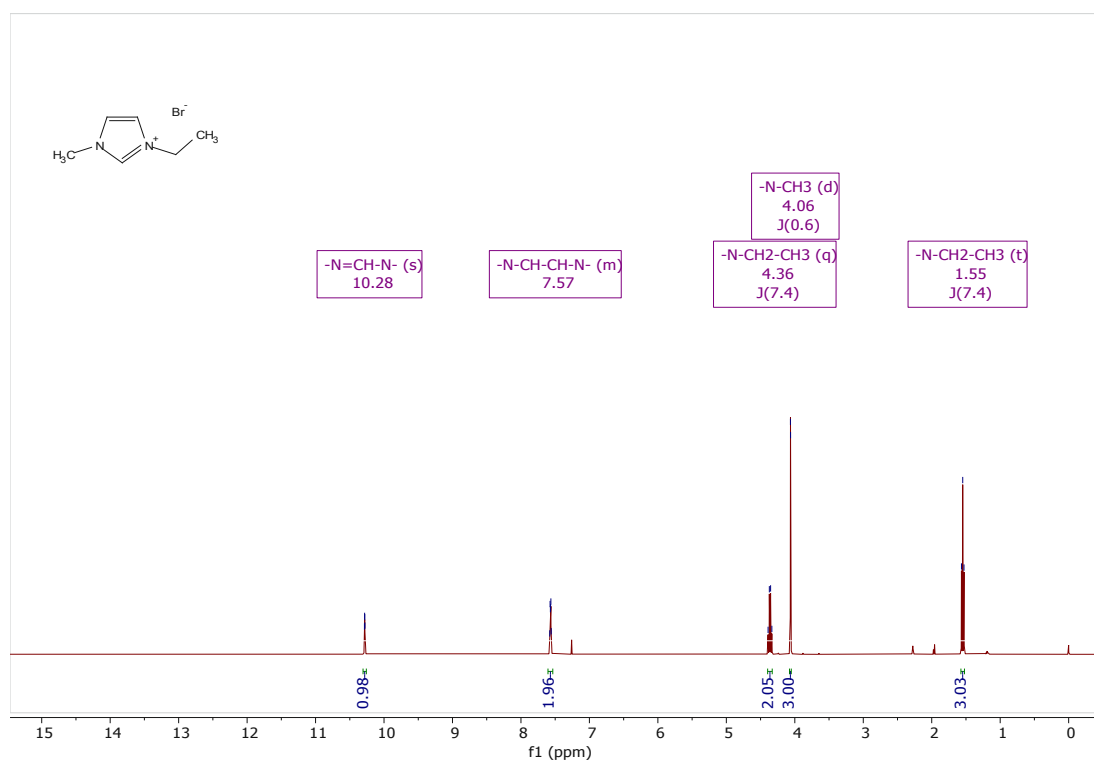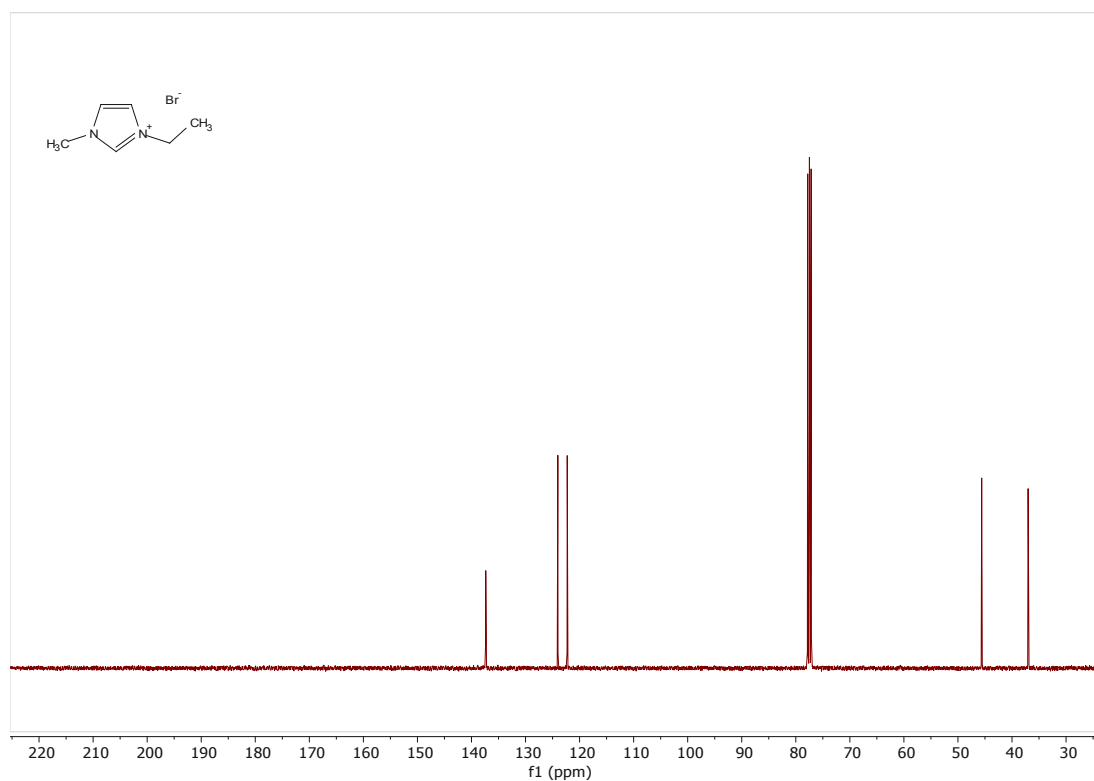## 2.3   NMR Spectra: 1-Ethyl-3-methylimidazolium Iodide [C₂mim]I 6
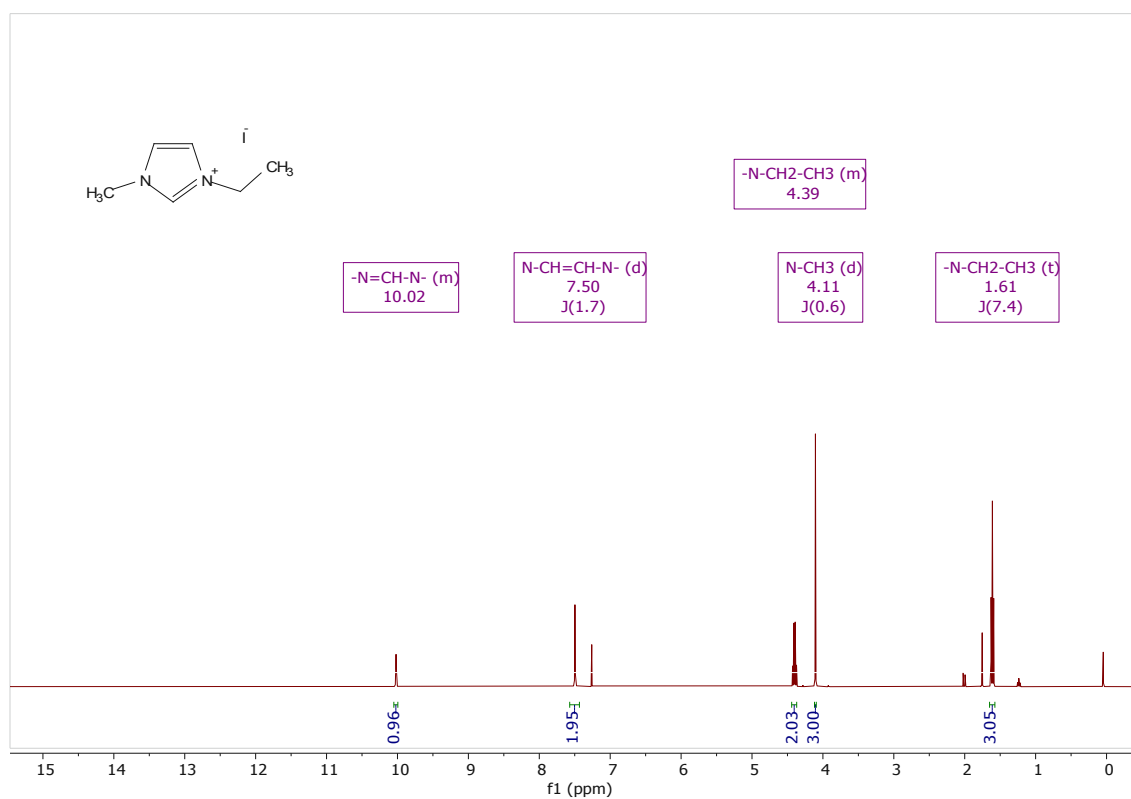
Figure S3: ¹H-NMR spectrum of 1-ethyl-3-methylimidazolium iodide [C₂mim]I 6.
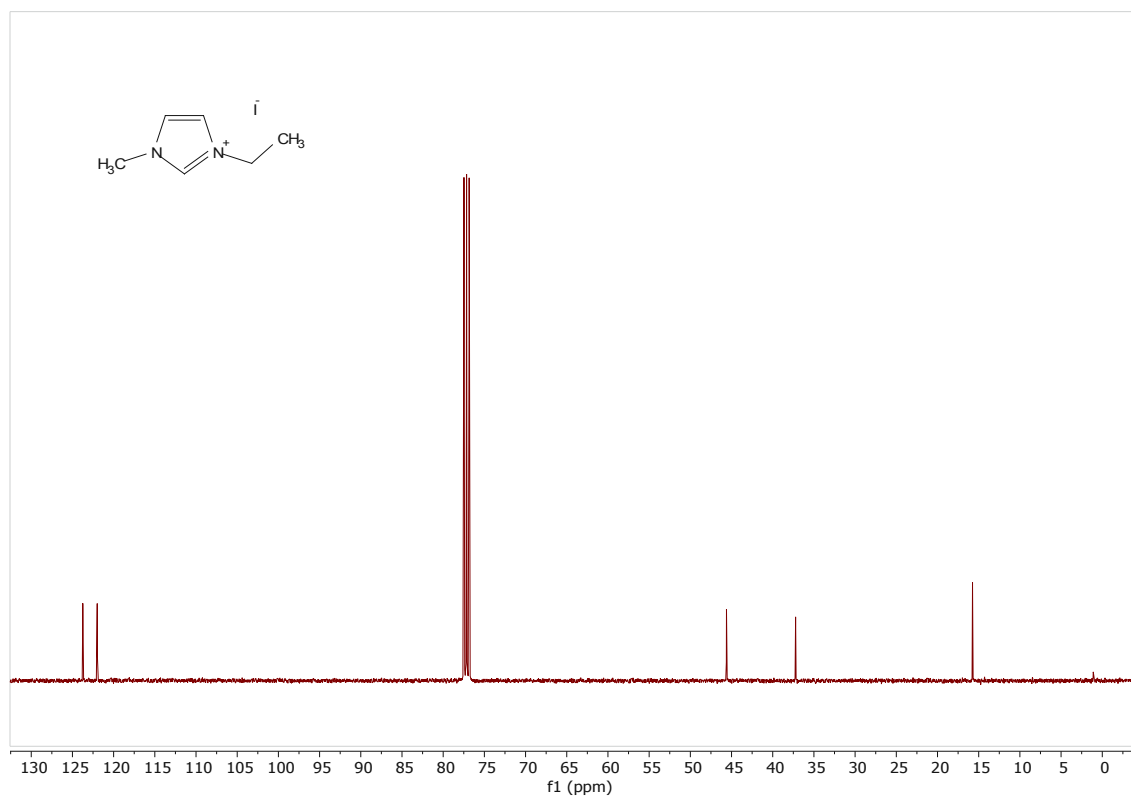
Figure S4: ¹³C-NMR spectrum of 1-ethyl-3-methylimidazolium iodide [C₂mim]I 6.

Spectral data are in accordance with literature[4].

3 Supported Ionic Liquid Phases (SILPs)

3.1 Thermogravimetric Analysis (TGA)
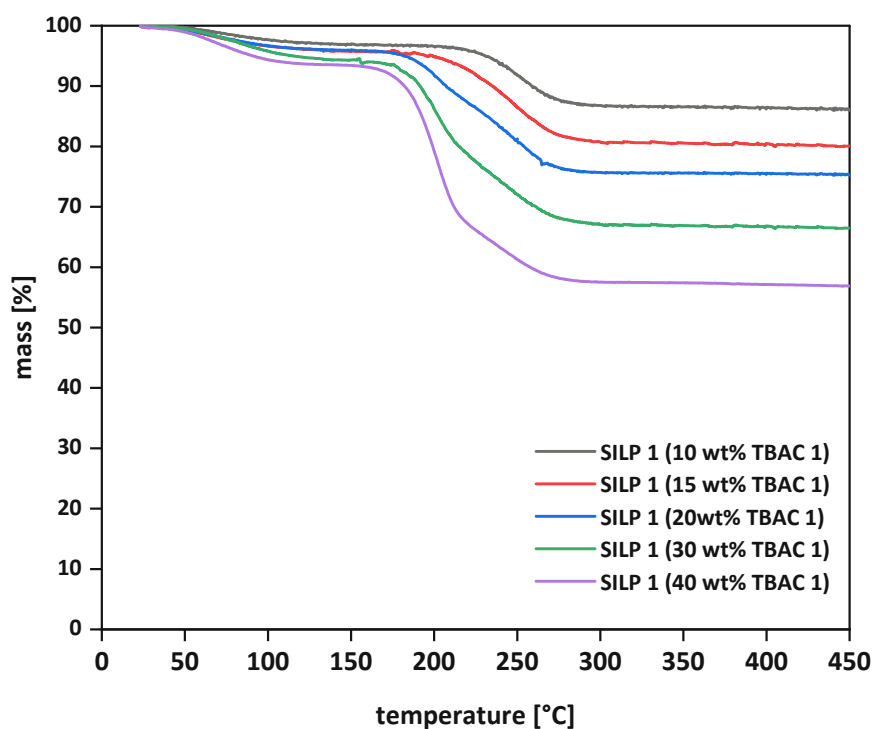
Figure S5: Catalyst loadings of SILP 1 measured via TGA.

Range: 25 °C – 450 °C (rate: 5 °C/min)
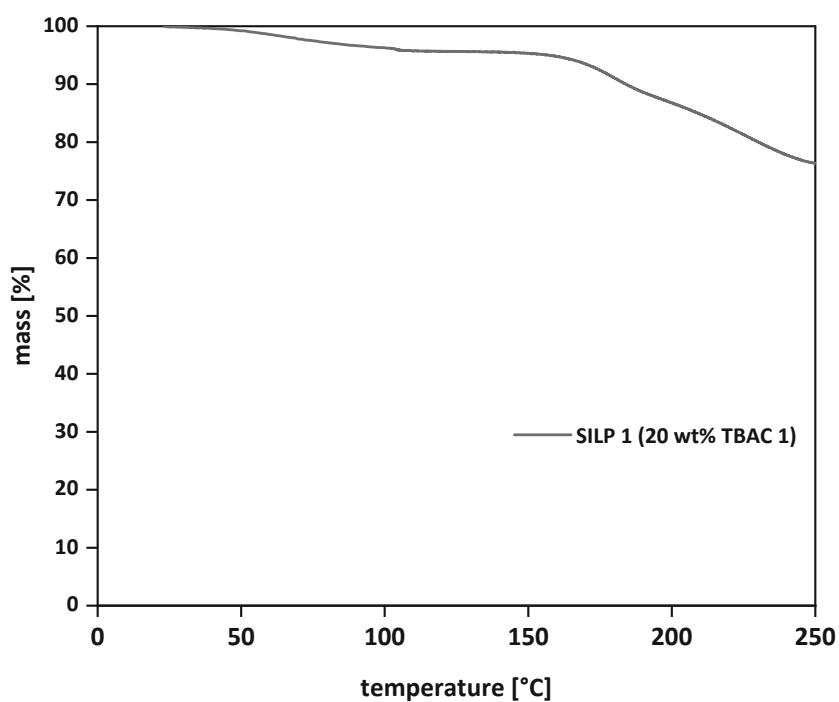
Figure S6: Thermal stability of SILP 1 (20 wt% TBAC 1) determined via TGA.

Range: 25 °C – 100 °C (rate: 5 °C/min); 100 °C – 250 °C (rate: 1 °C/min)

S8

Supported Ionic Liquid Phases (SILPs)
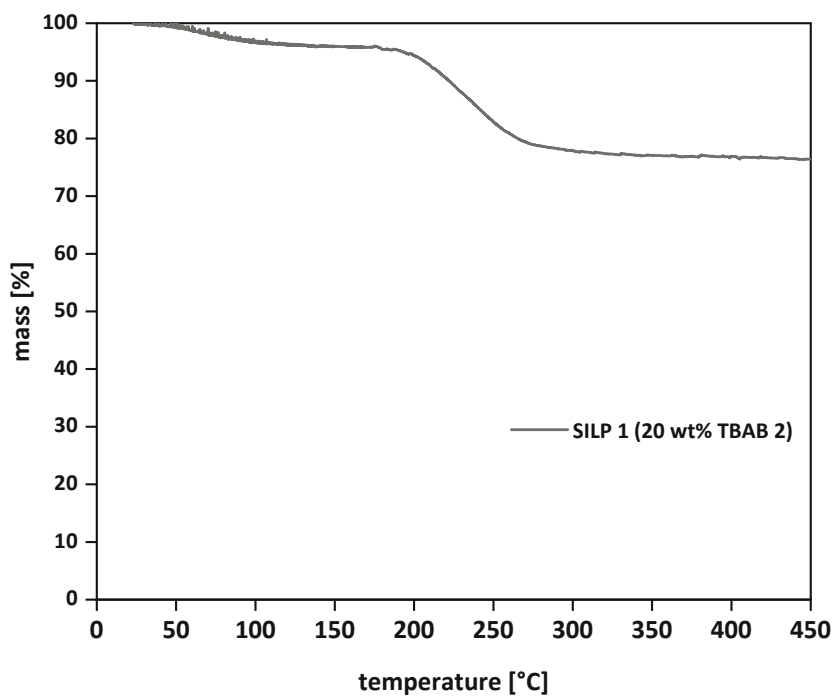
Figure S7: Catalyst loading of SILP 2 (20 wt% TBAB 2) measured via TGA.

Range: 25 °C – 500 °C (rate: 5 °C/min)

3.2   Diffuse Reflectance Infrared Fourier Transform Spectra (DRIFTS)
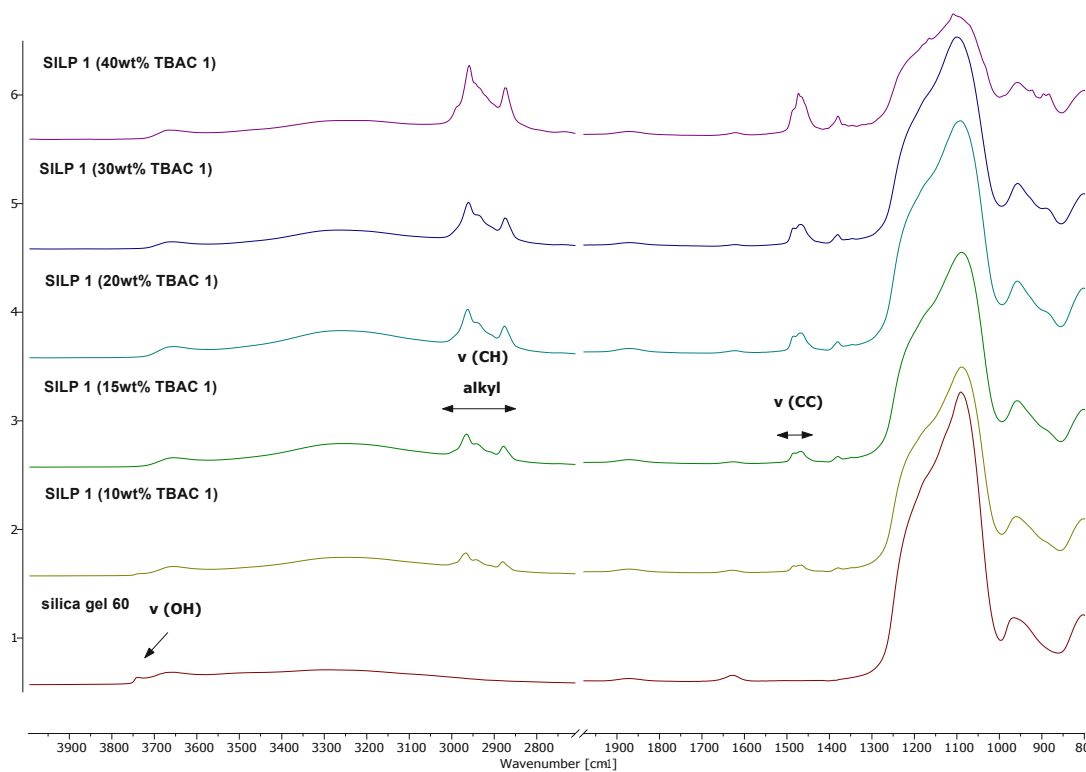
Figure S8: DRIFTS spectra of SILP 1 compared to supporting material silica gel 60
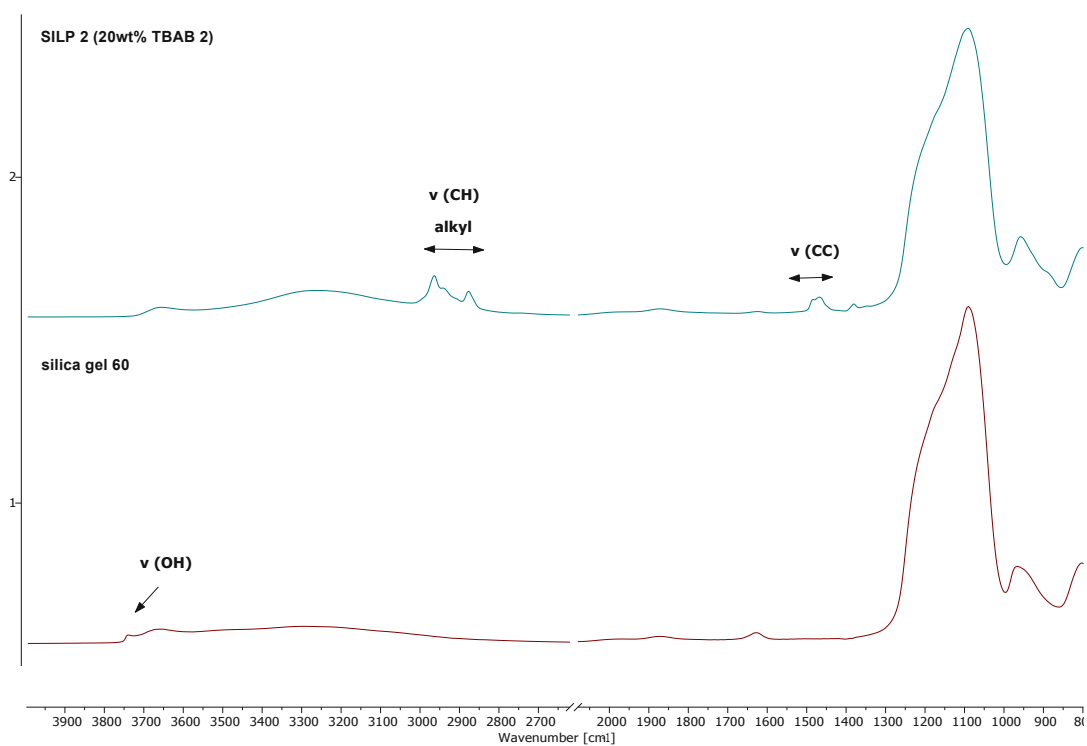
Figure S9: DRIFTS spectra of SILP 2 compared to supporting material silica gel 60
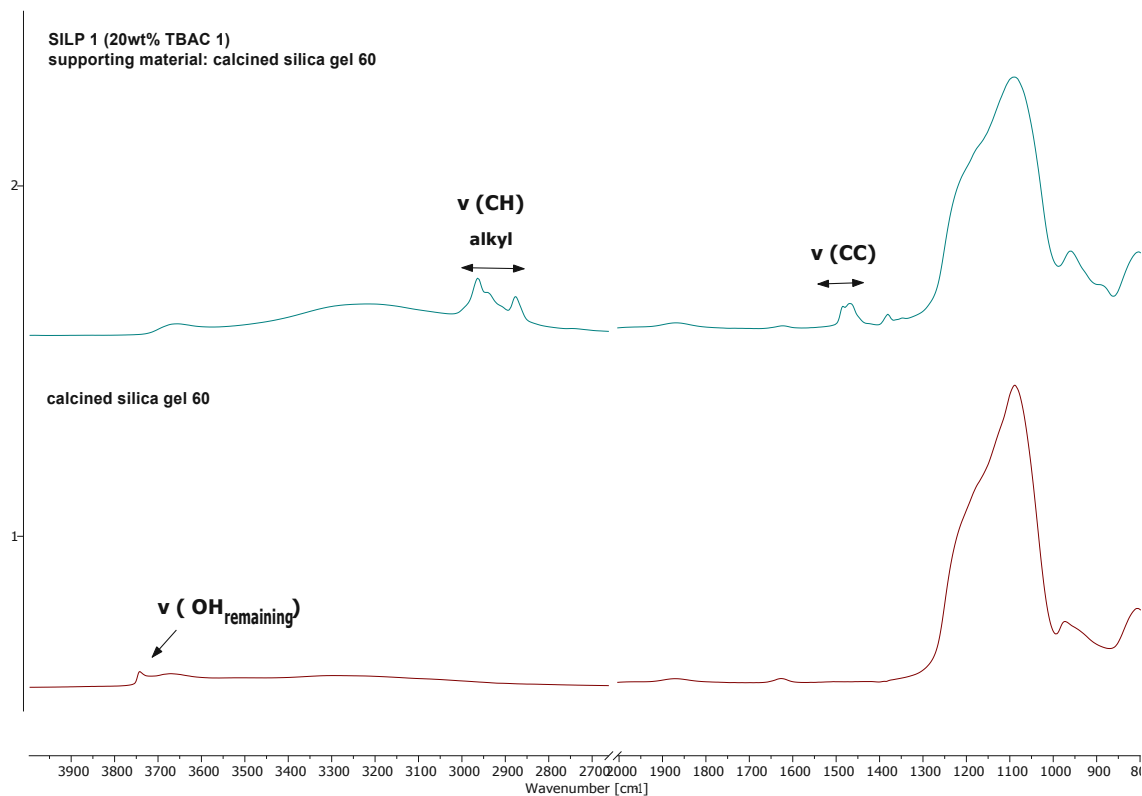
Figure S10: DRIFTS spectra of SILP 1 compared to supporting material calcined silica gel 60

3.3 Nitrogen Physisorption Measurements (BET, BJH)

Table S1: Characterization of SILP 1 (15 wt% catalyst loading) via N$_2$ physisorption

sample	BET surface area[a] [m^2/g]	pore volume[b] [cm^3/g]	average pore diameter[c] [Å]
silica gel 60 (reference)	634.37	0.91	55.38
SILP 1 (15 wt% TBAC 1 - freshly prepared)	450.93	0.57	49.07
SILP 1 (15 wt% TBAC 1 – after 48 h reaction time)	231.01	0.34	45.40

[a] calculated based on BET equation; [b] calculated based on BJH equation; determined based on desorption branch
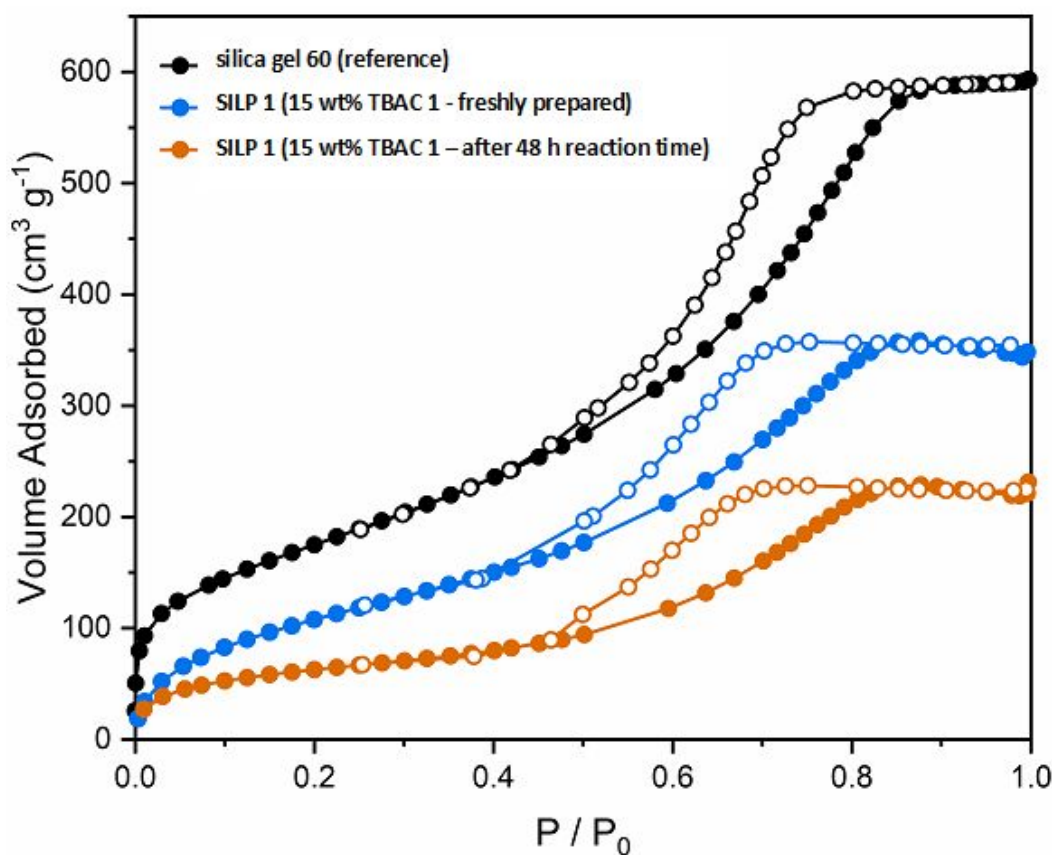
Figure S11: N$_2$ adsorption – desorption isotherms of silica gel 60 (reference material, black), freshly prepared SILP 1 catalyst (blue) and SILP 1 catalyst after 48 h reaction time (orange)

4 Conversion of Bioderived Limonene Oxide 7a

4.1 Determination of NMR Conversions and NMR Yields

On the Example of a Batch Reaction Running for 20 h

For the determination of yields and conversions, an NMR spectrum of the reaction mixture before (t=0) and after (t=20) the reaction was recorded (see Figure S11). The NMR conversions and NMR yields were determined according to formulas S1-S6 given below by comparison of the integrals of the same hydrogens of the starting material before the reaction and the product after the reaction. The integrals are always referenced to the same amount of internal standard (naphthalene, δ = 7.82 and 7.45 ppm, integral set to 1.00).

In case of the continuous flow experiments, no conversions were determined, incorrect values were determined due to partial evaporation of the volatile starting material while CO_2 was released via the back-pressure regulator.
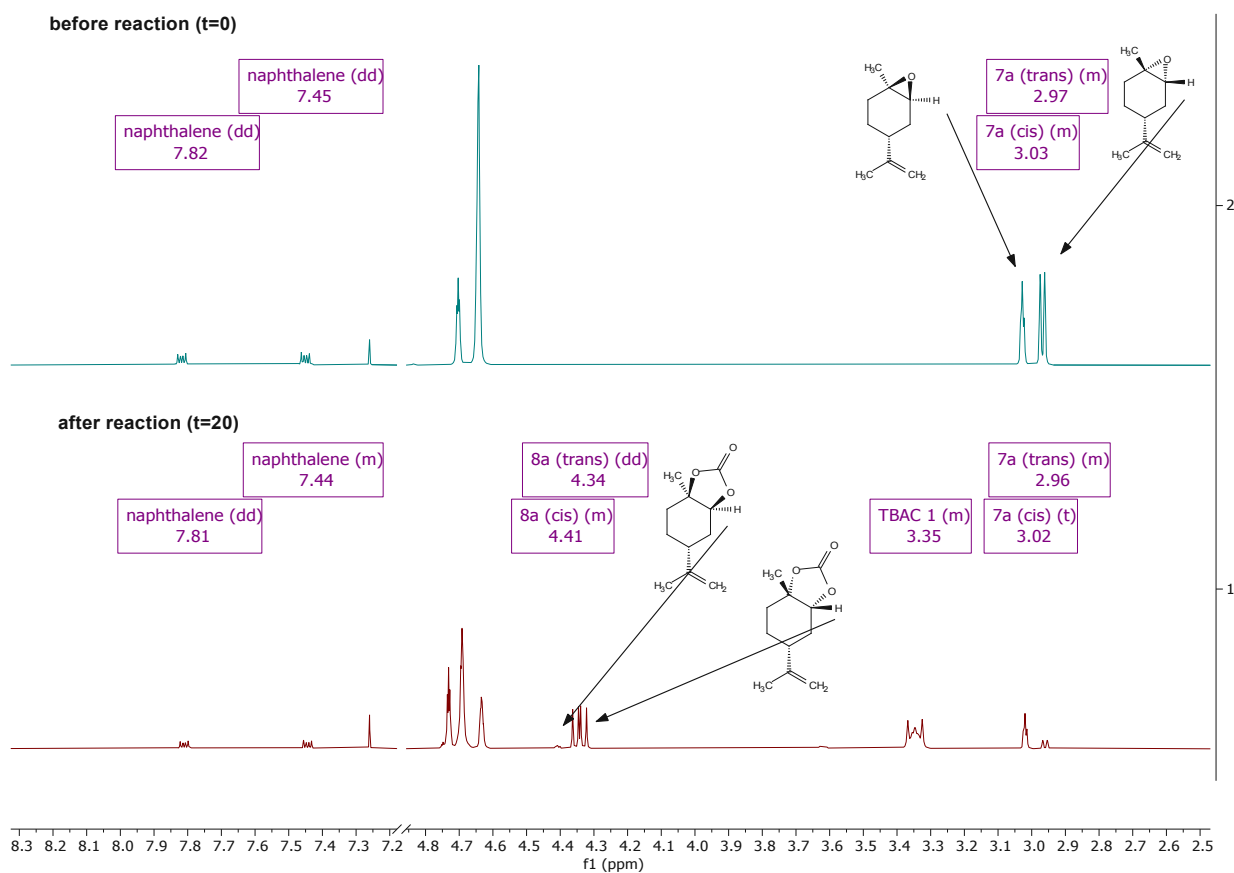
Figure S12: Limonene oxide 7a: Calculation of NMR yields via the comparison of the integrals of recorded ^{1}H-NMR spectra before and after the reaction.

$$\text{conversion } \textbf{7a} \, (\textit{cis}) \, (\%) = \frac{I_{7a\,(\textit{cis})_{t=0}} - I_{7a\,(\textit{cis})_{t=20}}}{I_{7a\,(\textit{cis})_{t=0}}} \cdot 100$$

Formula S1

$$\text{conversion } \textbf{7a} \, (\textit{trans}) \, (\%) = \frac{I_{7a\,(\textit{trans})_{t=0}} - I_{7a\,(\textit{trans})_{t=20}}}{I_{7a\,(\textit{trans})_{t=0}}} \cdot 100$$

Formula S2

$$\text{conversion } \textbf{7a} \, (\%) = \frac{(I_{7a\,(\textit{cis})_{t=0}} + I_{7a\,(\textit{trans})_{t=0}}) - (I_{7a\,(\textit{cis})_{t=20}} + I_{7a\,(\textit{trans})_{t=20}})}{I_{7a\,(\textit{cis})_{t=0}} + I_{7a\,(\textit{trans})_{t=0}}} \cdot 100$$

Formula S3

$$\text{yield } \textbf{8a} \, (\textit{cis}) \, (\%) = \frac{I_{8a\,(\text{cis})_{t=20}}}{I_{8a\,(\text{cis})_{t=0}} + I_{8a\,(\text{cis})_{t=0}}} \cdot 100$$

Formula S4

$$\text{yield } \textbf{8a} \, (\textit{trans}) \, (\%) = \frac{I_{8a\,(\textit{trans})_{t=20}}}{I_{7a\,(\textit{cis})_{t=0}} + I_{7a\,(\textit{trans})_{t=0}}} \cdot 100$$

Formula S5

$$\text{yield } \textbf{8a} \, (\%) = \frac{I_{8a\,(\textit{cis})_{t=20}} + I_{8a\,(\textit{trans})_{t=20}}}{I_{7a\,(\textit{cis})_{t=0}} + I_{7a\,(\textit{trans})_{t=0}}} \cdot 100$$

Formula S6

conversion (**7a**)	conversion of *cis* and *trans* limonene oxide **7a**
yield (**8a**)	yield of *cis* and *trans* limonene carbonate **8a**
$I_{7a\,(xxx)_{t=yy}}$	integral of *cis* or *trans* limonene oxide **7a** at t= 0 h or 20 h
$I_{8a\,(xxx)_{t=20}}$	integral of *cis* or *trans* limonene carbonate **8a** after the reaction (t=20)

4.2 Batch Conditions: Optimization Studies with SILP 1 as Catalyst

Table S2: Limonene oxide 7a: Summary of optimization studies with SILP 1. [a]

entry	solvent	temperature	catalyst loading	supporting material [b]	yield of 8a (NMR) [%]
S1	neat				62
S2	+ 10 wt% H_2O	100 °C	20 wt%	silica	31 (+20% limonene diol[c])
S3	heptane				41
S4		80 °C			42
S5	neat	100 °C	20 wt%	silica	62
S6		120 °C			60
S7			10 wt%		26
S8	neat	100 °C	15 wt%	silica	30
S9			20 wt%		62
S10			40 wt%		68
S11	neat	100 °C	20 wt%	silica	62
S12				calcined silica	45

[a] conditions: 5 MPa CO_2 (gaseous, initial pressure), 5 mmol limonene oxide **7a** (*cis*/*trans*=43/57), 10 mol% TBAC **1** immobilized as **SILP 1**, 13 mg naphthalene (internal standard), 100 °C, 20 h; Further information about the calculations of NMR yields are summarized in the supplementary information (ESI Figure S12 and Formula S1-S6); [b] supporting materials were dried in a vacuum oven (50 mbar, 50 °C, 24 h) prior to use; calcination of silica was performed at 400 °C for 3 days; [c] according to GC/MS.

4.3   Batch Conditions: Recycling Studies of SILP 1 and SILP 2

Table S3: Limonene oxide 7a: Recycling of SILPs in batch mode

cycle	catalyst	yield (NMR) [%] [a] sum
cycle 1		62
cycle 2	**SILP 1** (20 wt% TBAC **1**)	50
cycle 3		30
cycle 4		25
cycle 1		31
cycle 2	**SILP 2** (20 wt% TBAB **2**)	31
cycle 3		29
cycle 4		23

[a] Conditions: 5 MPa CO_2 (gaseous, initial pressure), 5 mmol limonene oxide **7a** (*cis/trans*=43/57), 10 mol% catalyst **1-6**, 13 mg naphthalene (internal standard), 100 °C, 20 h; work-up: separation of SILP material via suck filtration, washing with heptane and evaporation of volatiles; Conversions were not determined due to partial removal of volatile starting material during evaporation of heptane. Further information about the calculations of NMR yields are summarized in the supplementary information (ESI Figure S12 and Formula S1-S6).

4.4 Continuous Flow: Optimization of Flow Rates

Table S4: Limonene oxide 7a: Influence of flow rates of CO_2 and substrate in continuous flow using SILP 1 as heterogeneous catalyst. [a]

entry	flow rates [mL/min]		residence time [s]	yield (NMR) [b] [%]		leaching [c]
	CO_2	substrate		maximum	overall (12 h)	
S13	0.99		250 s	44	19	< 1%
S14	1.49		166 s	28	18	< 1%
S15	1.99	0.01	125 s	22	15	n. o.
S16	2.49		100 s	22	16	n. o.
S17	3.99		62 s	17	12	n. o.
S18	1.98	0.02	125 s	20	14	< 1%

[a] Conditions: **SILP 1** (2.222 g, 250 mm column), 15 MPa, 120 °C, 12 h; [b] Yields are given as sum of *cis* and *trans* isomer. internal standard: naphthalene; Further information about the calculations of NMR yields are summarized in the supplementary information (ESI Figure S12 and Formula S1-S6); [c] for determination of leaching, the integral of the signal at δ = 3.35 ppm of TBAC **1** was used.
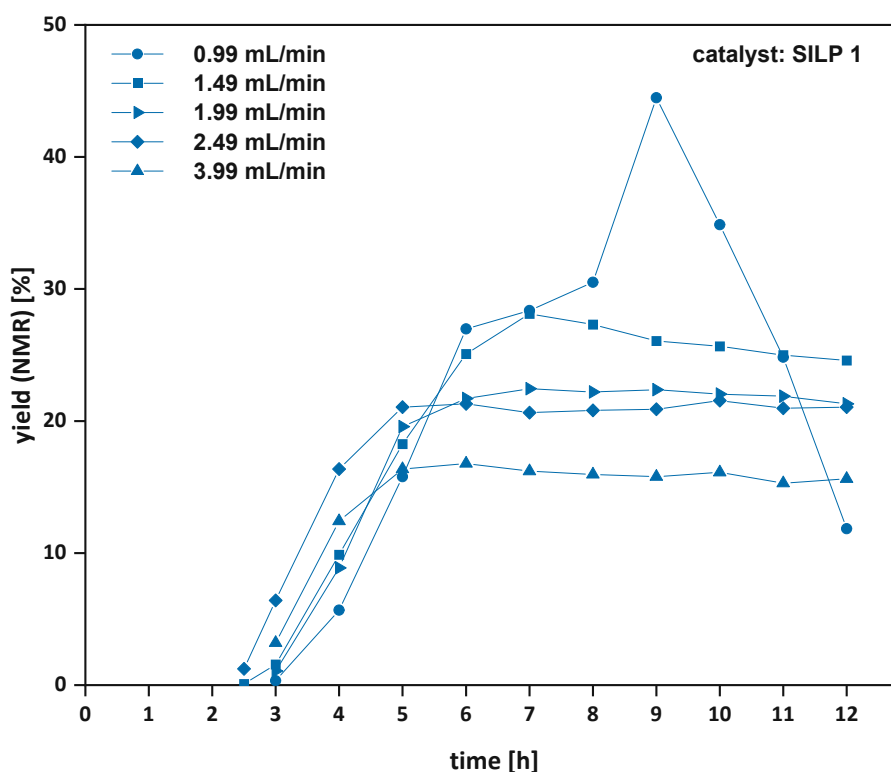
Figure S13: Limonene oxide 7a: Impact of flow rates of CO_2 in continuous flow.

4.5 Continuous Flow: Long-term Stability (96 h)
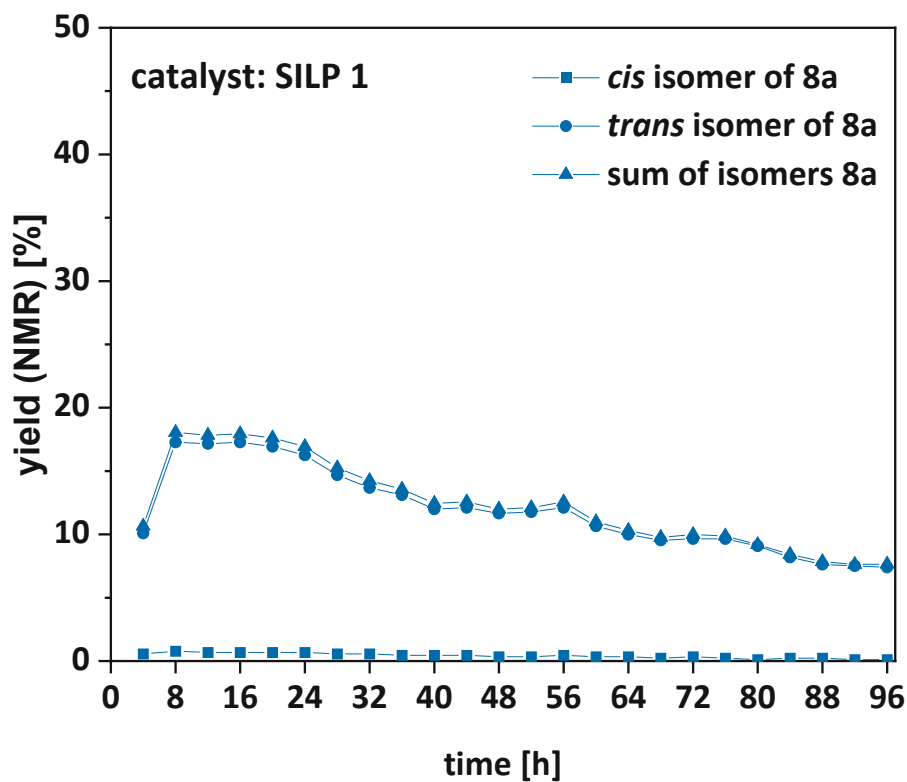
Figure S14: Limonene oxide 7a: Long-term stability of SILP 1 over 96 h. Final optimized conditions: SILP 1 (2.22 g, 30 wt% loading), 1.99 mL/min CO_2, 0.01 mL/min limonene oxide 7a, 15 MPa, 120 °C, 96 h, 250 mm catalyst cartridge

4.6 NMR Spectra: Limonene Carbonate 8a (Mixture of *cis* and *trans* Isomer)
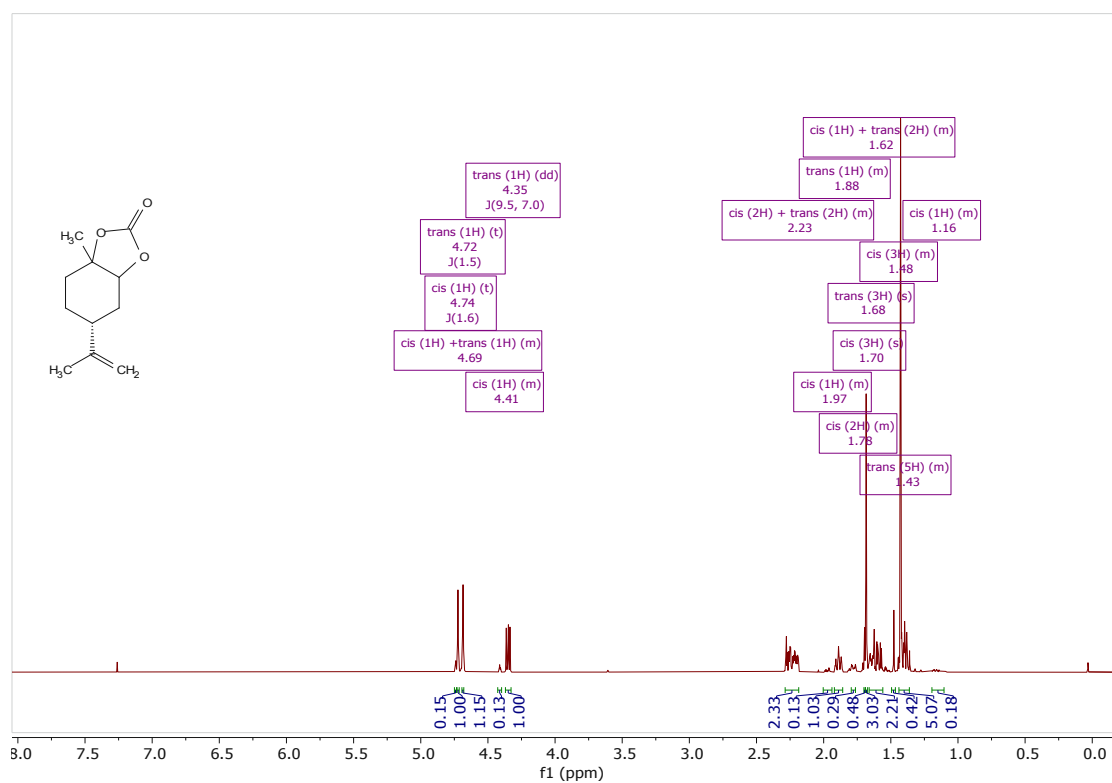
Figure S15: ^{1}H-NMR spectrum of the diastereomeric mixture of limonene carbonate 8a.
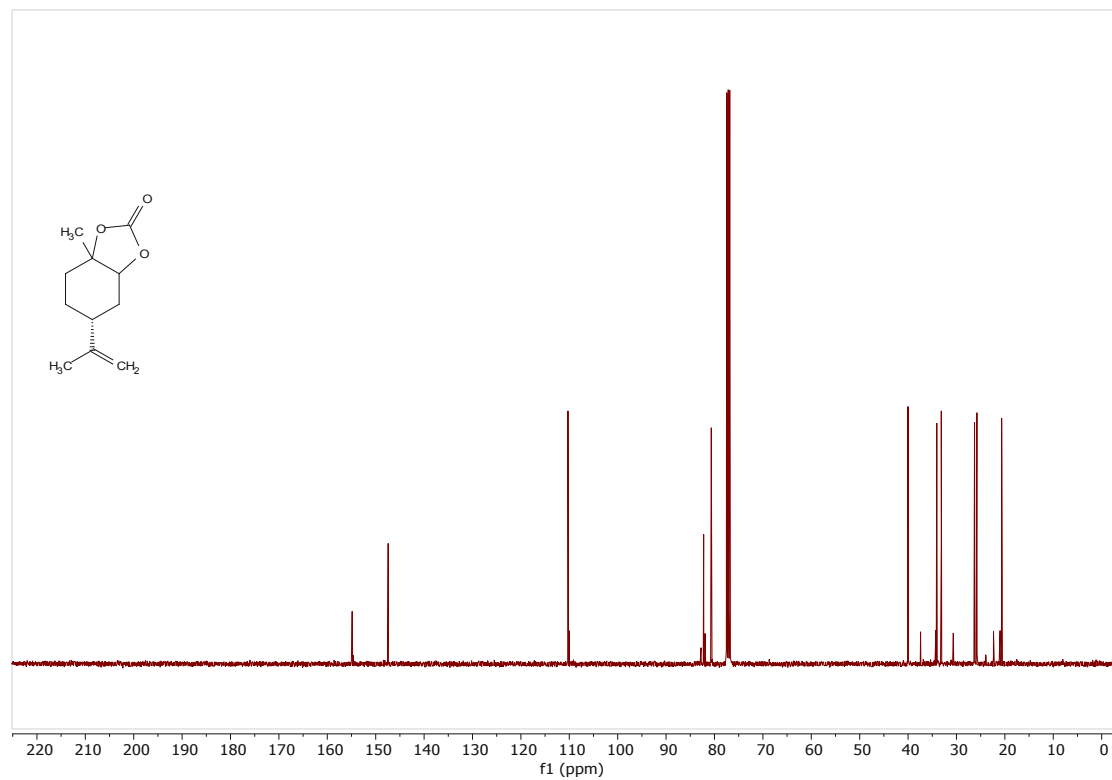
Figure S16: ^{13}C-NMR spectrum of the diastereomeric mixture of limonene carbonate 8a.

Spectral data are in accordance with literature.[5]

5 Conversion of Bioderived Limonene Dioxide 7b

5.1 Determination of GC Yields: Calibration Curves and GC Chromatogram

For the calibration curves, epoxycarbonate **8b** and biscarbonate **8c** were purified via column chromatography and a dilution series of each compound in ethyl acetate (1, 0.5, 0.25, 0.125, 0.0625 mg/mL) was prepared using octane as internal standard (0.4 mg/mL sample).
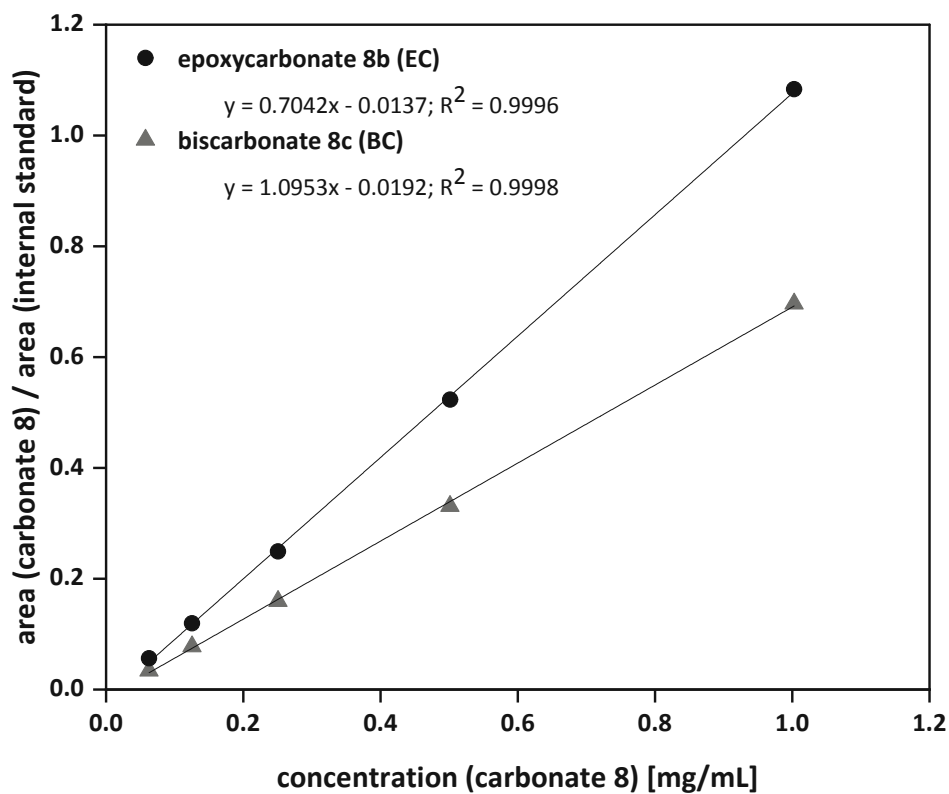
Figure S17: GC calibration curves for epoxycarbonate 8b and biscarbonate 8c.
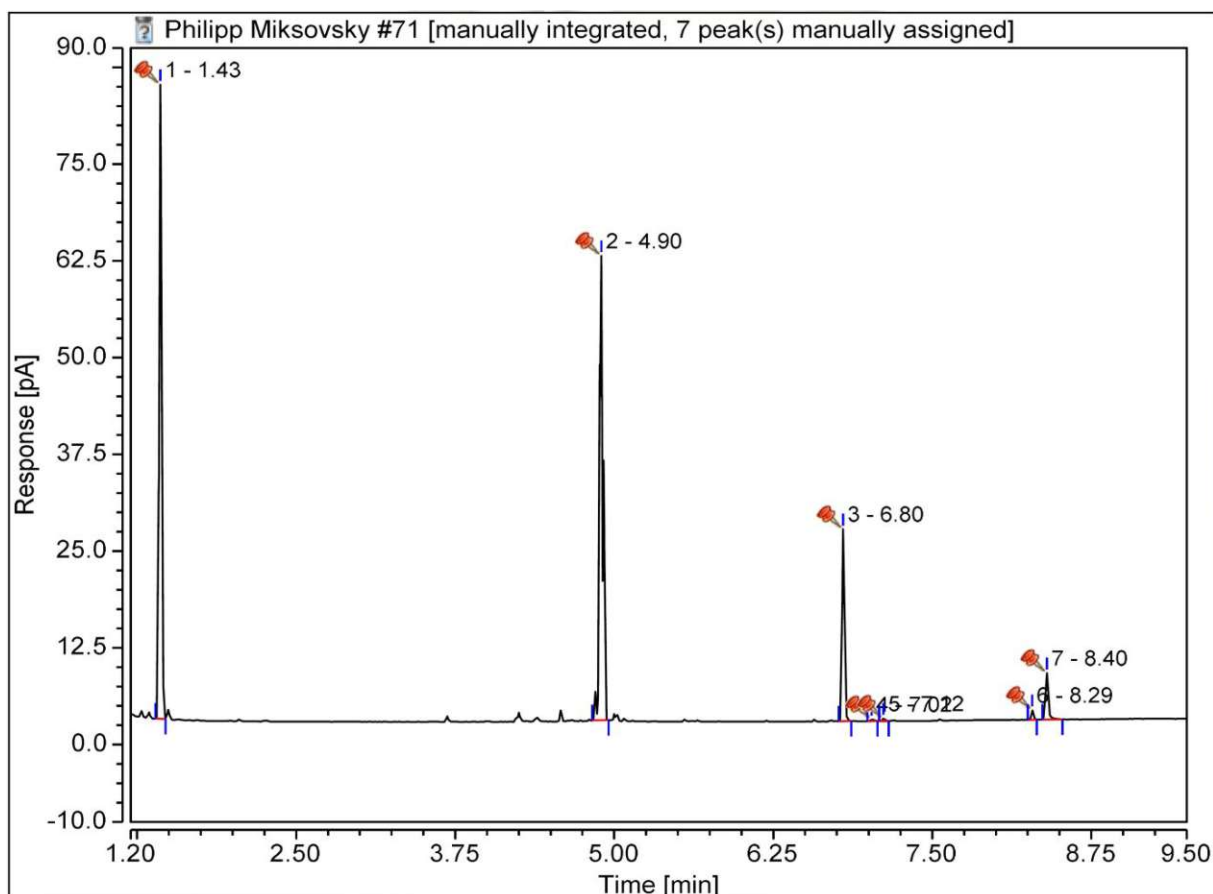
No.	Peak Name	Retention Time min	Area pA*min	Height pA	Relative Area %
1	internal standard (octane)	1.432	1.775	81.962	40.25
2	limonene dioxide	4.899	1.917	60.008	43.45
3	epoxy carbonate (EC1)	6.799	0.528	24.805	11.98
4	epoxy carbonate (EC2+3)	7.022	0.007	0.235	0.16
5	epoxy carbonate (EC4)	7.116	0.007	0.299	0.17
6	biscarbonate (BC1)	8.286	0.026	1.259	0.58
7	biscarbonate (BC2)	8.400	0.150	6.021	3.41
Total:			4.410	174.589	100.00

Figure S18: Limonene dioxide 7b: A typical gas chromatogram for the calculation of GC-yields.
The sum of isomers of epoxycarbonate **8b** (EC 1-4) and biscarbonate **8c** (BC 1-2) was used for calculations of GC yields.

5.2 Continuous Flow: Long-term Stability (48 h)
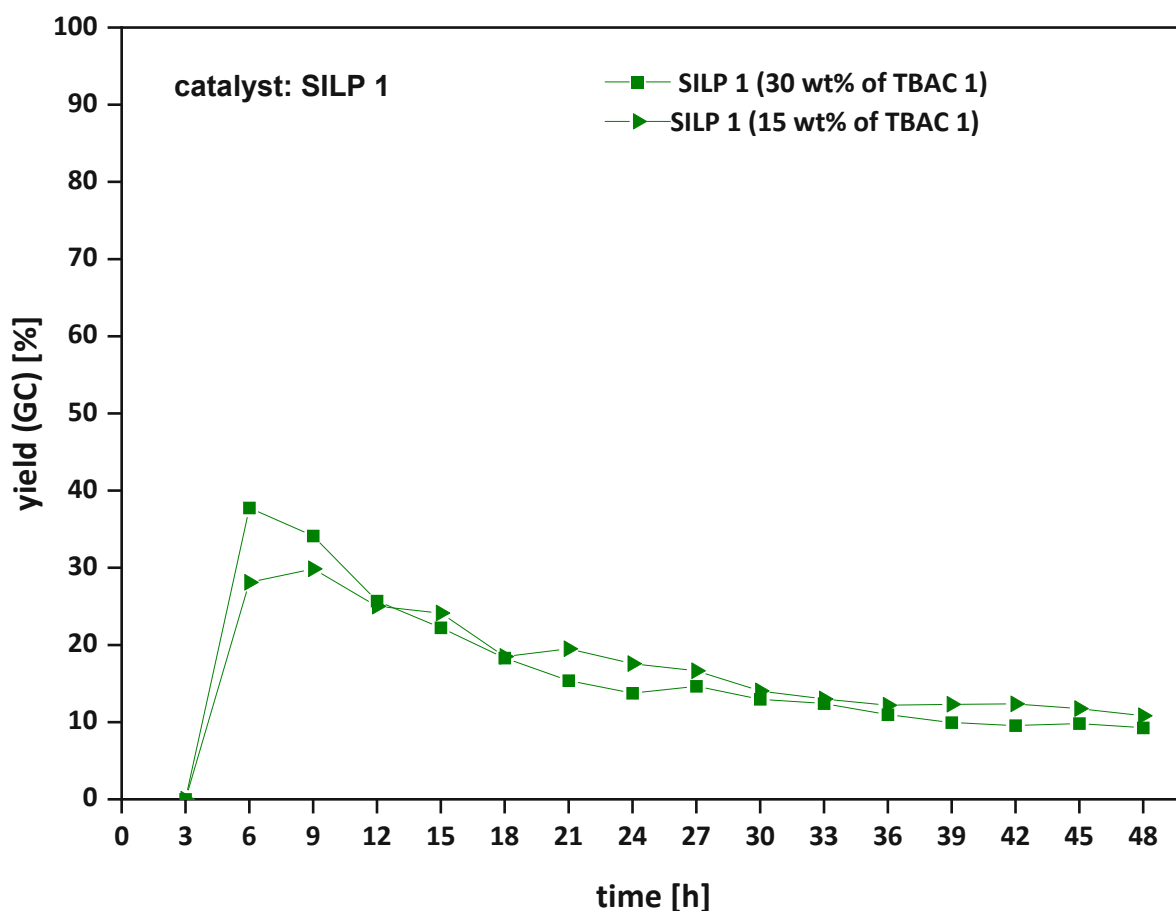
Figure S19: Limonene dioxide 7b: Long-term stability of SILP 1 using catalyst loadings of 15 wt% and 30 wt%.

Conditions: SILP 1 (2.22 g), 1.99 mL/min CO2, 0.01 mL/min limonene dioxide 7b, 20 MPa, 120 °C, 48 h; leaching of immobilized catalyst TBAC 1 was quantified via 1H-NMR spectroscopy (signal at 3.35 ppm) using naphthalene as internal standard.

5.3 NMR and GC Spectra: Epoxycarbonate 8b (Mixture of 4 Diastereomers)
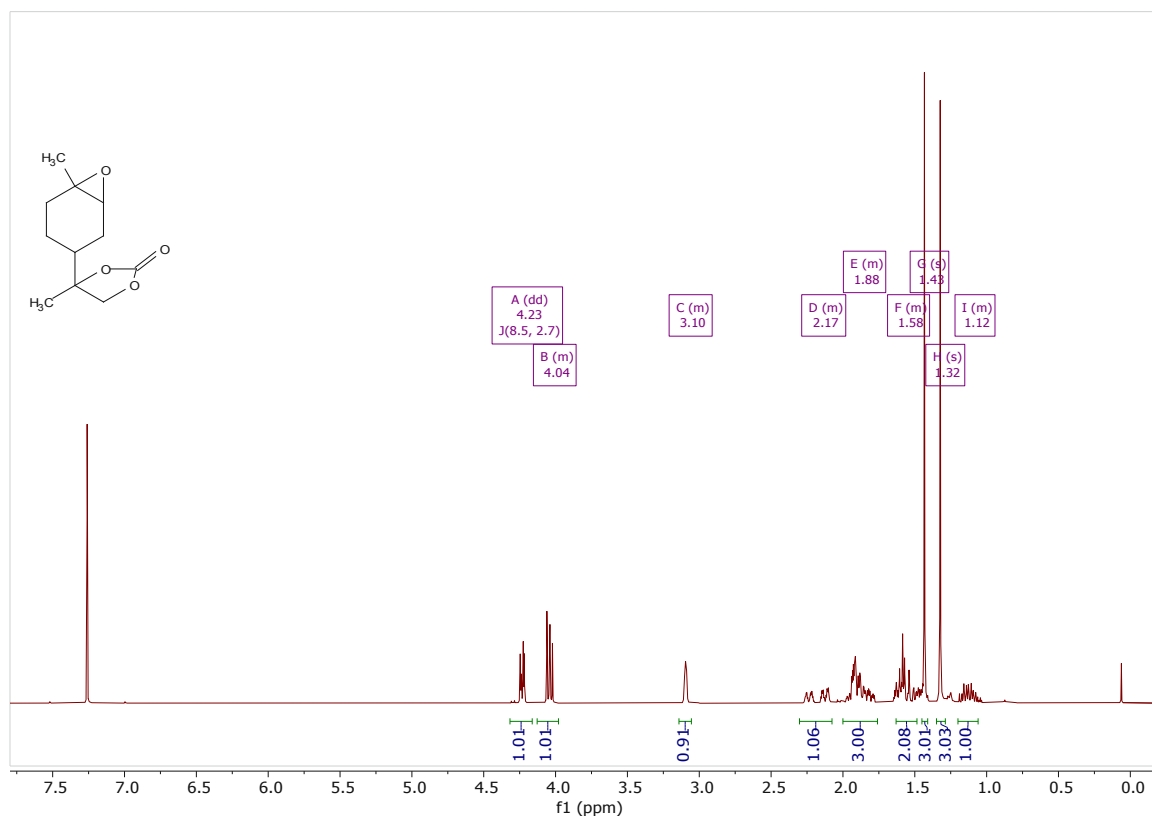
Figure S20: ^{1}H-NMR spectrum of the diastereomeric mixture of epoxycarbonate **8b**.
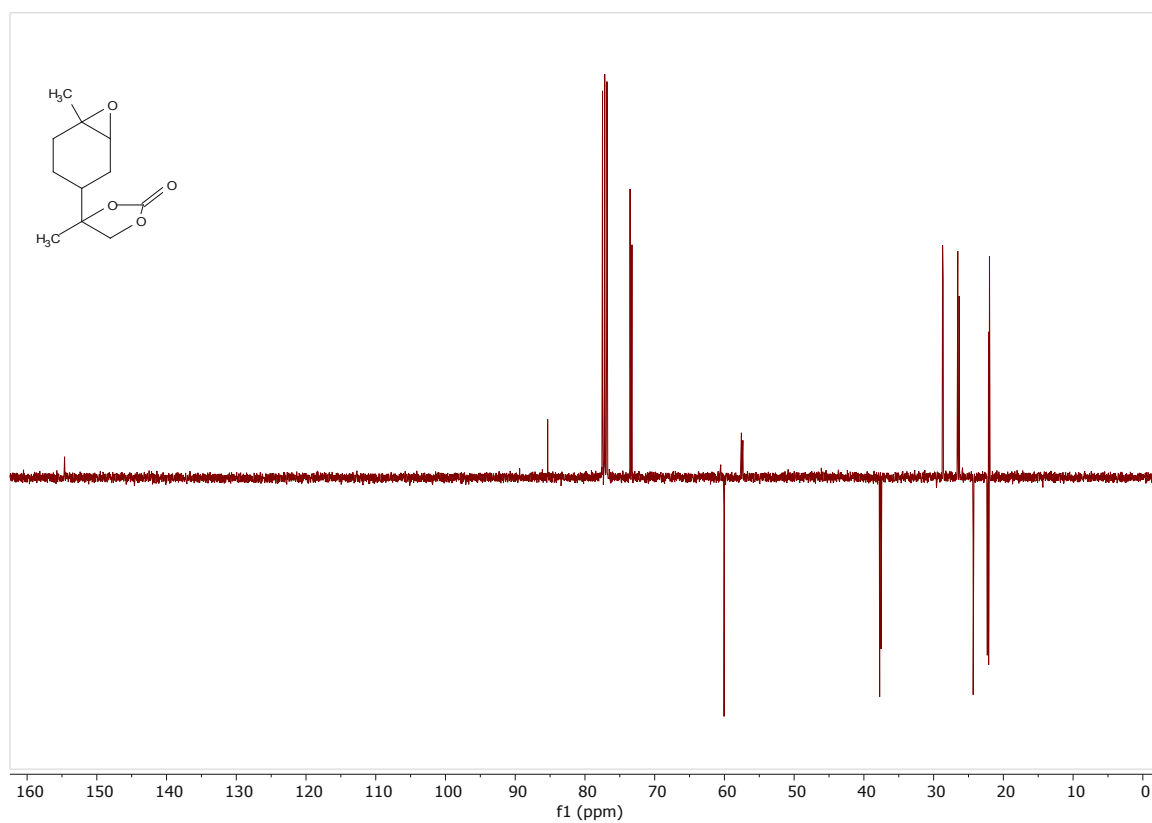
Figure S21: ^{13}C-NMR spectrum of the diastereomeric mixture of epoxycarbonate **8b**.

	RT	Scan	Type	Height	Area	Total Height %	Total Area %	Start time	End time	Fill	Label
1	6.480	1170	BB	1085208433.037	7220269514.285	89.79	93.73	6.443	6.501	None	
2	6.664	1224	BV	65671177.484	244191708.581	5.43	3.17	6.647	6.678	None	
3	6.688	1231	VB	48401694.446	182293325.820	4.00	2.37	6.678	6.712	None	
4	6.770	1255	BV	9306388.266	56760052.937	0.77	0.74	6.742	6.793	None	
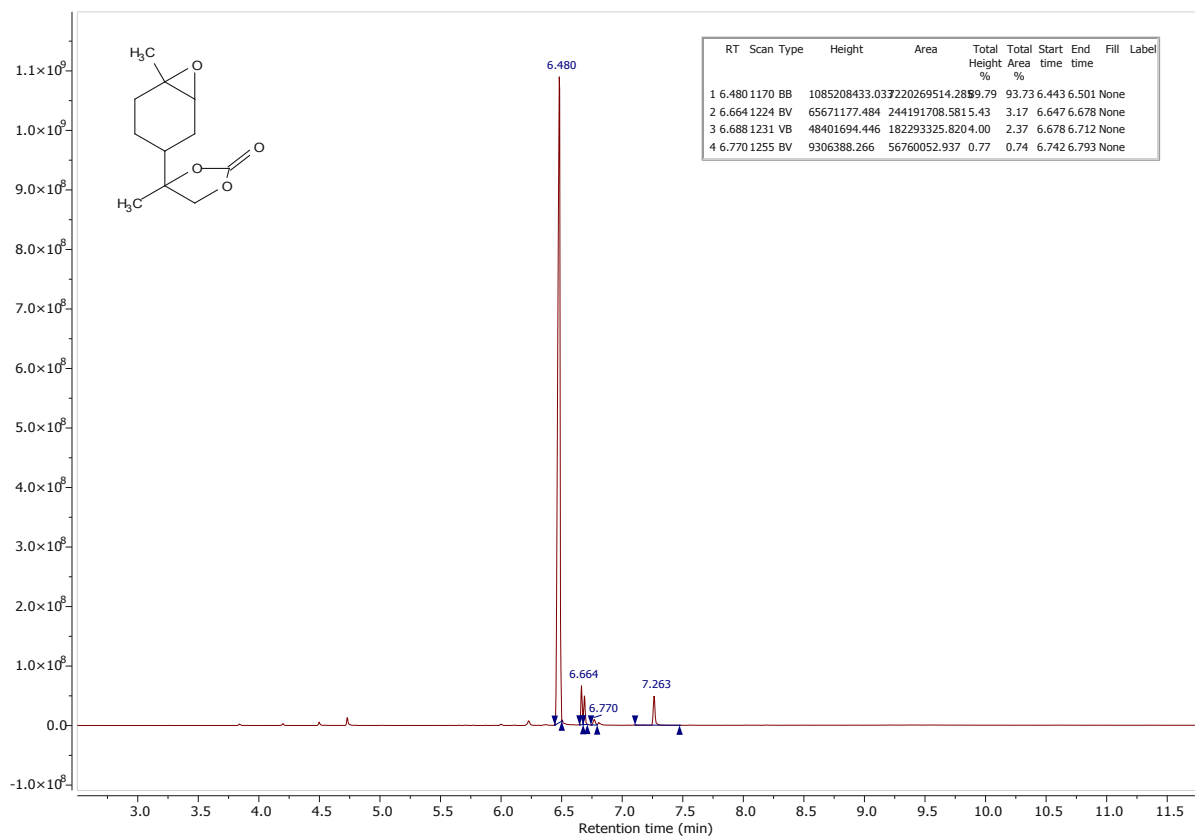
Figure S22: Gas chromatogram of the diastereomeric mixture of epoxycarbonate 8b.

5.4   NMR and GC Spectra: Biscarbonate 8c (Mixture of 2 Diasteriomers)
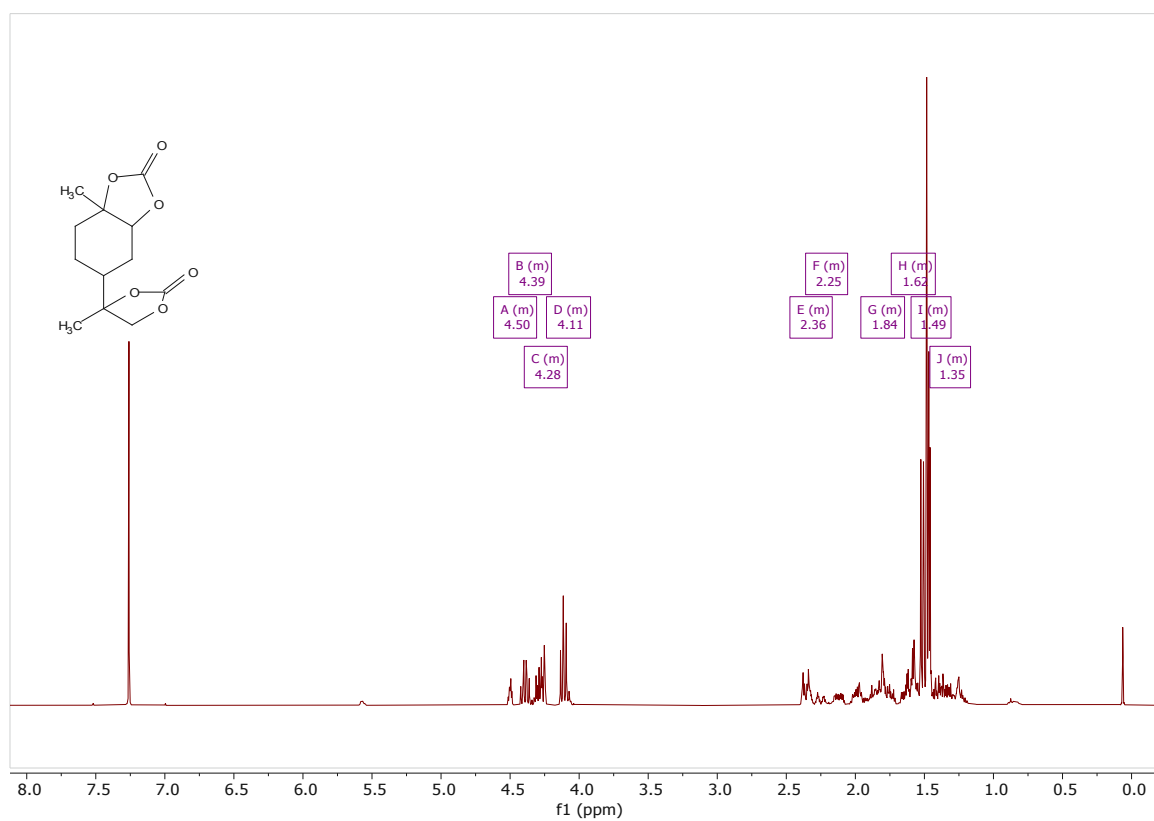
Figure S23: ¹H-NMR spectrum of the diastereomeric mixture of biscarbonate 8c.
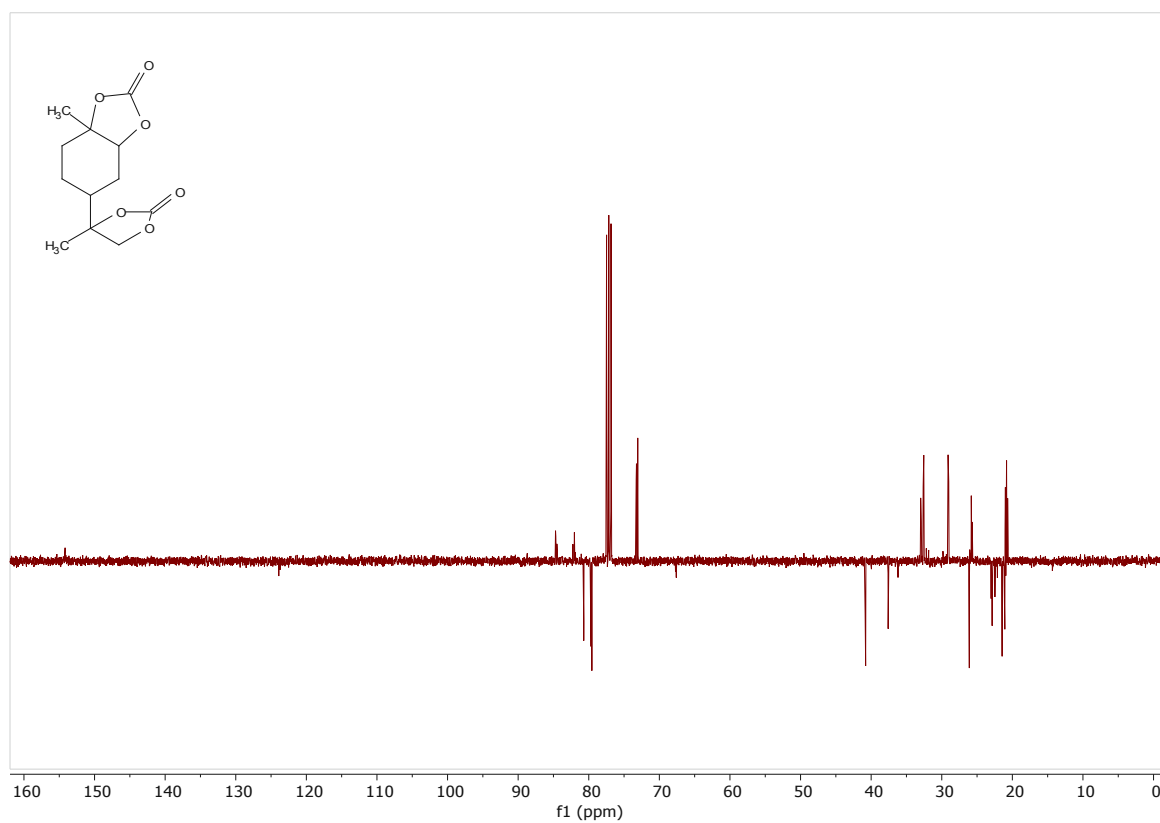
Figure S24: ¹³C-NMR spectrum of the diastereomeric mixture of biscarbonate 8c.

S25

Conversion of Bioderived Limonene Dioxide 7b

C:\Doktorat\Th...2A\PM-302Ae.raw Injection 1 {0;0} + c EI ... [50.00-550.00] TIC

RT	Scan	Type	Height	Area	Total Height %	Total Area %	Start time	End time	Fill	Label
1 7.834	1568	BB	81109775.358	363632062.703	36.60	34.34	7.813	7.871	None	
2 7.926	1595	BB	140490571.245	695351564.781	63.40	65.66	7.902	7.994	None	
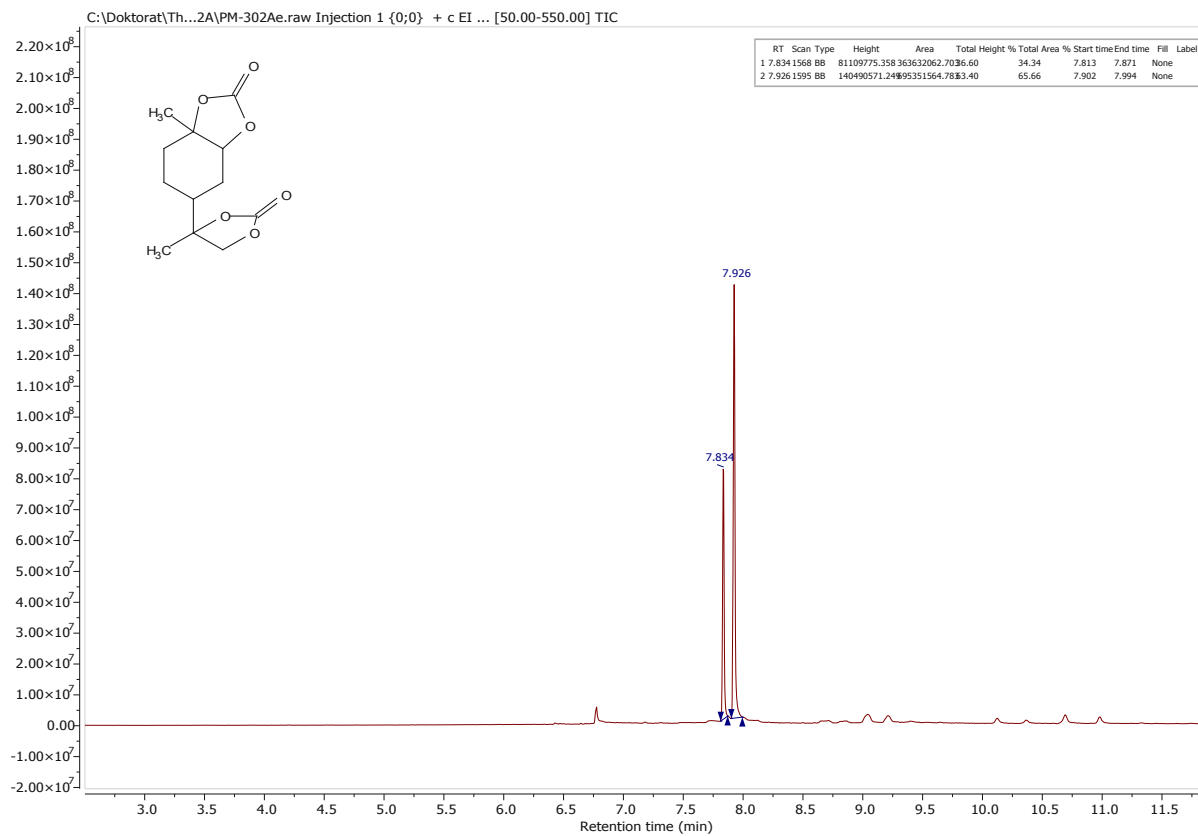
Figure S25: Gas chromatogram of the diastereomeric mixture of biscarbonate 8c.

6   List of Abbreviations

[C_2mim]Br	1-ethyl-3-methylimidazolium bromide
[C_2mim]Cl	1-ethyl-3-methylimidazolium chloride
[C_2mim]I	1-ethyl-3-methylimidazolium iodide
approx.	approximately
aqu.	aqueous
BC	(isomer of) biscarbonate **8c**
BET	Brunauer-Emmett-Teller
BJH	Barret-Joyner-Halenda
br	broad (NMR)
cat.	catalytically / catalyst / catalysis
d	doublet (NMR)
DCM	dichloromethane
dd	doublet of doublets (NMR)
dt	doublet of triplets (NMR)
EC	(isomer of) epoxycarbonate **8b**
equiv.	equivalent
EtOAc	ethyl acetate
GC/MS	gas chromatography - mass spectrometry hyphenation
J	coupling constant (NMR)
LC	limonene carbonate
LO	limonene oxide
LP	light petroleum (boiling point 40 - 60 °C)
m	multiplet (NMR)
m/z	ratio of mass to charge (GC/MS)
M^+	molecular ion (GC/MS)
Me	methyl
NMR	nuclear magnetic resonance
ppm	parts per million
R_f	retention factor (TLC)
rt	room temperature
s	singlet (NMR)
satd.	saturated
scCO_2	supercritical CO_2
SILP	supported ionic liquid phase
TBAB	tetrabutylammonium bromide
TBAC	tetrabutylammonium chloride
TBAI	tetrabutylammonium iodide
TGA	thermogravimetric analysis
TLC	thin layer chromatography
UV	ultraviolet
UV-Vis	ultraviolet-visible
wt%	weight percent
δ	chemical shift (NMR)

References

1. Bresien, J.; Ellinger, S.; Harloff, J.; Schulz, A.; Sievert, K.; Stoffers, A.; Täschler, C.; Villinger, A.; Zur Täschler, C., Tetracyanido(difluorido)phosphates M+[PF2(CN)4]−. **2015,** *54* (15), 4474-4477.

2. Shen, M.-L.; Xu, L.; Liu, B.; Jiao, H.; Kwon, Y.-U., A thermosensitive fluorescent Eu-based metal–organic framework and its polyether sulfone composite film as a thermal sensor. *Dalton Transactions* **2018,** *47* (25), 8330-8336.

3. Lin, S.-T.; Ding, M.-F.; Chang, C.-W.; Lue, S.-S., Nuclear magnetic resonance spectroscopic study on ionic liquids of 1-alkyl-3-methylimidazolium salts. *Tetrahedron* **2004,** *60* (42), 9441-9446.

4. Bartlett, P. N.; Cummings, C. Y.; Levason, W.; Pugh, D.; Reid, G., Halometallate Complexes of Germanium(II) and (IV): Probing the Role of Cation, Oxidation State and Halide on the Structural and Electrochemical Properties. **2014,** *20* (17), 5019-5027.

5. Morikawa, H.; Minamoto, M.; Gorou, Y.; Yamaguchi, J.; Morinaga, H.; Motokucho, S., Two Diastereomers of d-Limonene-Derived Cyclic Carbonates from d-Limonene Oxide and Carbon Dioxide with a Tetrabutylammonium Chloride Catalyst. *B Chem Soc Jpn* **2018,** *91* (1), 92-94.

I.3 Supporting Information: Silicon Oxycarbide (SiOC) Supported Ionic Liquids: Heterogeneous Catalysts for Cyclic Carbonate Formation

Supporting information:

Mikšovsky, P.; Rauchenwald, K.; Naghdi, S.; Eder, D.; Konegger T.; Bica-Schröder, K., Silicon Oxycarbide (SiOC) Supported Ionic Liquids: Heterogeneous Catalysts for Cyclic Carbonate Formation. *ACS Sustainable Chem Eng* **2023** (revision submitted).

Supporting Information

Silicon Oxycarbide (SiOC) Supported Ionic Liquids: Heterogeneous Catalysts for Cyclic Carbonate Formation

Philipp Mikšovsky [1, †], Katharina Rauchenwald [2, †], Shaghayegh Naghdi [3], Hannah Rabl [3], Dominik Eder [3], Thomas Konegger [2,] and Katharina Bica-Schröder [1,]*

* katharina.schroeder@tuwien.ac.at

* thomas.konegger@tuwien.ac.at

[1]Institute of Applied Synthetic Chemistry, TU Wien, Getreidemarkt 9, 1060 Vienna, Austria.

[2]Institute of Chemical Technologies and Analytics, TU Wien, Getreidemarkt 9, 1060 Vienna, Austria.

[3]Institute of Materials Chemistry, TU Wien, Getreidemarkt 9, 1060 Vienna, Austria.

[†] These two authors contributed equally.

Number of pages: 33

Number of figures: 23

Number of tables: 6

Table of Contents

S.1   Preparation of Silicon Oxycarbide Supports 7a and 7b

S.1.1 Powdered Silicon Oxycarbide Supports 7a for Batch Experiments

For batch experiments using silicon oxycarbide powder **7a**, a preceramic polymer solution **4** with 30 wt.% functionalized polysiloxane and 70 wt.% *tert*-butyl alcohol **3** was used. The ceramic yield determined after pyrolysis (N=4, heating 1 K min^{-1}, 1 h dwell time) is in reasonable agreement with the residual mass determined during thermogravimetric analysis, as shown in **Figure S1**.
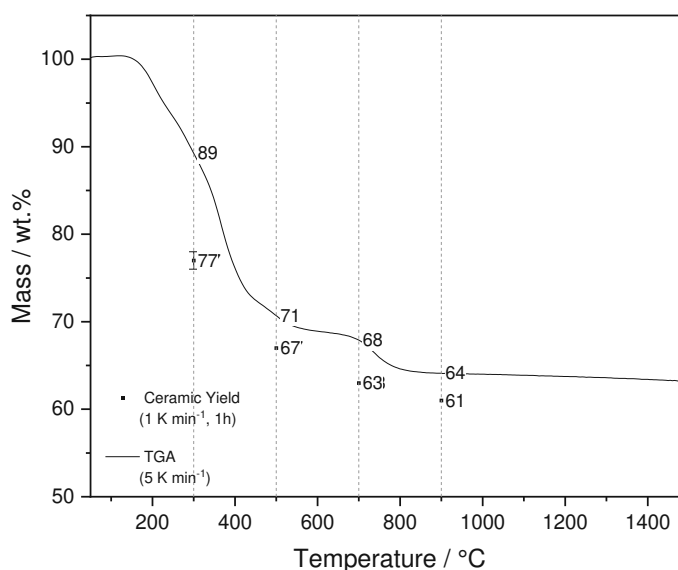
Figure S1: Thermogravimetric analysis in argon flow to study the pyrolytic conversion of the green body **6a** to silicon oxycarbide **7a** and obtained ceramic yields upon pyrolysis at 300, 500, 700, and 900 °C in argon flow.

S.1.2 Silicon Oxycarbide Monoliths 7b for Continuous-Flow Experiments

For continuous experiments using cylindrical, monolithic silicon oxycarbide **7b**, a preceramic polymer solution **4** with 20 wt.% functionalized polysiloxane and 80 wt.% *tert*-butyl alcohol **3** was chosen to combine high porosity and sufficient structural strength. As the pore structure of preliminary samples derived from a preceramic solution **4** using only 10 wt.% functionalized polysiloxane in 90 wt.% *tert*-butyl alcohol **3** collapsed upon freeze-drying and pyrolytic conversion (**Figure S2**), a polymer content of 20 wt.% in solution **4** was selected to result in monoliths of maximum porosity achievable via this method. 20 wt.% polymer content in the solution **4** was chosen for further experiments to combine high porosity and high permeability while providing enough structural strength.

Aluminum molds with an inner diameter of 12 mm were used to generate cylindrical silicon oxycarbide monoliths **7b** with a final diameter of 8.5 mm, thus seamlessly fitting in a column with a 9 mm inner diameter. The linear shrinkage during freeze-drying and pyrolytic conversion was approximately 5 % and 27-29 %, respectively (N=30). The monoliths exhibited a bulk density of 0.4 g cm^{-3} and an apparent porosity of 81 % (water immersion method, N=4).

Cylindrical samples of a length of 6 cm were obtained, a layer of 1.5 mm from the top and bottom part was removed to yield open porosity and parallel bases. The bulk was cut in specimens to stack columns of 220 mm length, requiring a total of 14 specimens. The obtained monolithic specimens had a diameter of 8.4 ± 0.1 mm (N=14).

Figure S2: Silicon oxycarbide monoliths **7b** prepared for continuous-flow experiments before cutting 15 mm pieces. Solid loadings of a) 10 b) 20 and c) 30 wt.% polysiloxane **1** in *tert*-butyl alcohol **3** were investigated, whereas b) 20 wt.% were used for all continuous-flow experiments.

S.2 Characterization of Supports and SILPs

S.2.1 Nitrogen Physisorption Measurements
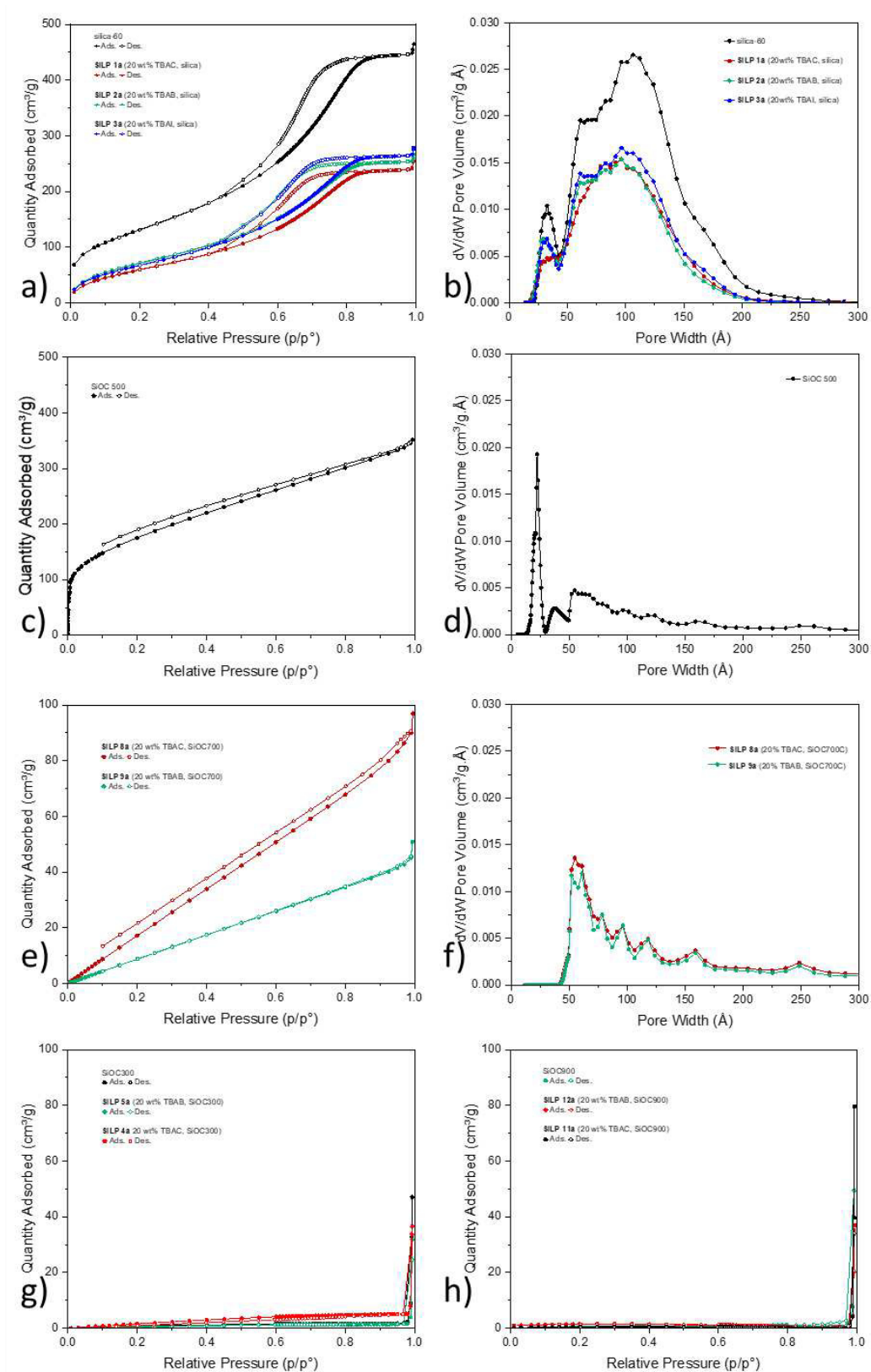
Figure S3: Nitrogen physisorption isotherms (a, c, e, g, h) and pore size distributions (b, d, f) of SILPs and supports.

Table S1: Results from nitrogen physisorption measurements of SiO_2-SILPs and SiOC-SILPs shown in **Figure S3**.

sample	surface area / $m^2\ g^{-1}$	pore volume / $cm^3\ g^{-1}$
SiO_2-60	487.54	0.70
SILP 1a	220.88	0.38
SILP 2a	262.60	0.39
SILP 3a	250.15	0.41
SiOC300	4.67	-
SILP 4a	12.58	-
SILP 5a	2.56	-
SiOC500	550.39	0.33
SILP 8a	143.28	0.15
SILP 9a	102.15	0.08
SiOC900	1.95	-
SILP 11a	2.25	-
SILP 12a	3.84	-

S.2.2 Permeability Measurement of Silicon Oxycarbide Monoliths

Measurements were performed using filtered compressed air as permeating fluid. Shrinking tubes (RS PRO) were used to seal the cylinders in flow direction, 3D printed rings were used to protect sample edges. The permeating gas flow Q was recorded as function of the pressure drop (p_1-p_2). Permeated area A and the sample height L were derived from the sample dimensions. The inlet overpressure p_1 was varied between 0.2 and 2 bar. Permeability constants (Darcian k_1, non-Darcian k_2) were determined using Forchheimer's equation for compressible fluids (**Formula S1**) using least-square fits. The viscosity of air μ was derived from the Sutherland equation (**Formula S2**) and air density ρ was derived from the ideal gas law.[1]
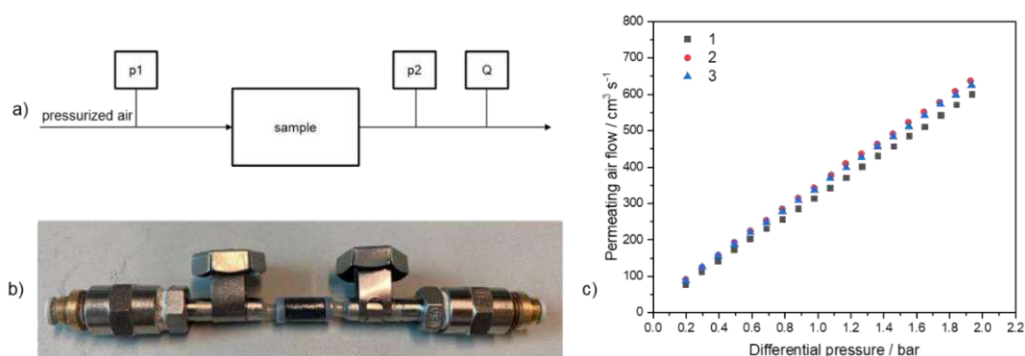
Figure S4: a) Set-up for permeability measurement, b) sample insert using shrinking tubes to seal the sample, and c) measured differential pressure and permeating air flow of SiOC900 monoliths **7b**.

Formula S1: Forchheimer's equation for compressible fluids to determine Darcian (k_1) and non-Darcian (k_2) permeability constants from the measurements shown in **Figure S4 c)**.

$$-\frac{dP}{dx} = \frac{p_{in}^2 - p_{out}^2}{2 * p_{out} * L} = \frac{\mu}{k_1}\frac{Q}{A} + \frac{\rho}{k_2}\left(\frac{Q}{A}\right)^2$$

Formula S2: Sutherland equation for calculating the viscosity of air used in **Formula S1**.

$$\mu = \mu_0 \left(\frac{T + 273}{273}\right)^{1.5}\left(\frac{273 + C_n}{T + 273 + C_n}\right)$$

dP/dx	pressure gradient along the flow direction
p_{in} , p_{out}	inlet and outlet pressure ($p_{in} = p_{atm} + p_1$; $p_{out} = p_{atm} + p_2$) with p_{atm} from *www.zamg.ac.at*
L	sample length
A	permeating area
ρ	density of the fluid (using ideal gas law and molar mass of air = 29 g mol^{-1})
μ	viscosity of the fluid from Sutherland equation (μ_0 = viscosity of air = 1.73 * 10^{-5} Pa s)
$\frac{Q}{A}$	permeating air flow per permeated area
C_n	Sutherland constant, $C_{n, air}$ = 125
T	lab temperature

S.2.3 Field Emission Gun – Scanning Electron Microscopy (FEG-SEM)
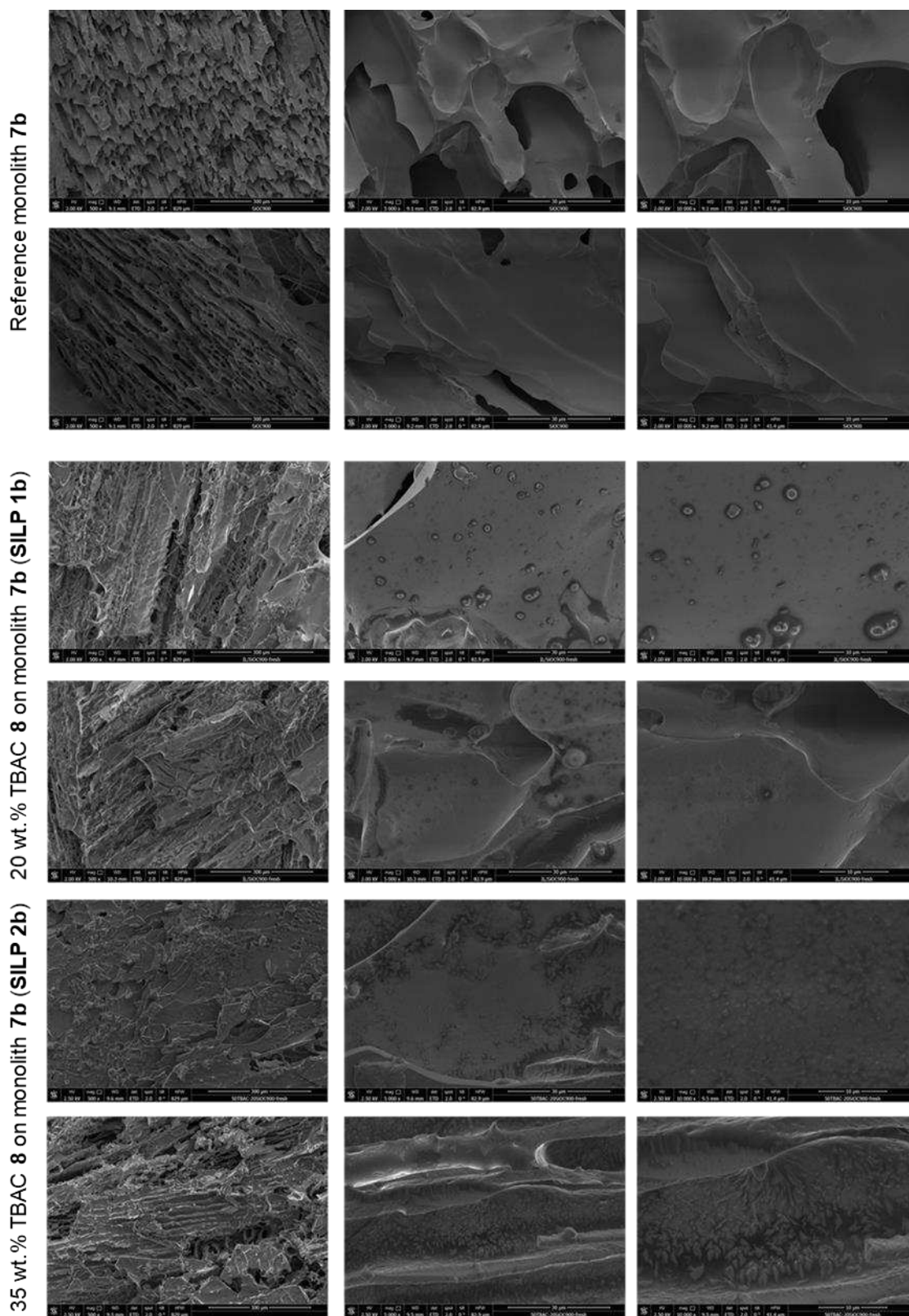
Figure S5: Longitudinal fracture surfaces of monoliths impregnated with different loadings of TBAC **8** showing differences in surface morphology revealed by secondary electron detection in low voltage FEG-SEM as described in ESI chapter S.7.1 .

S8

S.2.4 Thermogravimetric Analysis of Ionic Liquids and SILPs
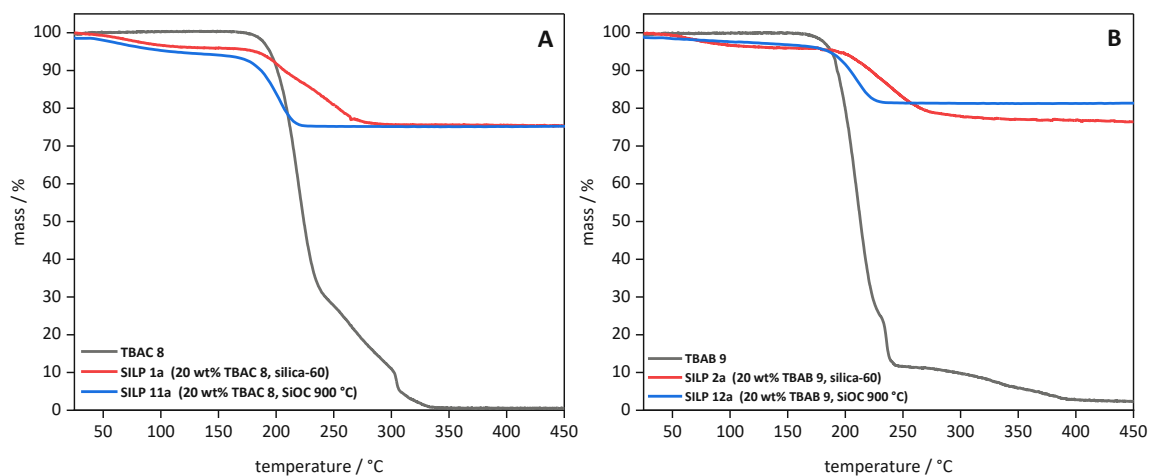
Figure S6: Thermogravimetric analysis in air of ionic liquid, silica- and silicon oxycarbide-based SILPs. (A) TBAC **8** and TBAC-based **SILP 1a** and **SILP 11a**; (B) TBAB **9** and TBAB-based **SILP 2a** and **SILP 12a.** Conditions: 25 °C to 450 °C in air (rate: 5 K min^{-1})

S.2.5 Fourier Transform Infrared Spectroscopy (FTIR)
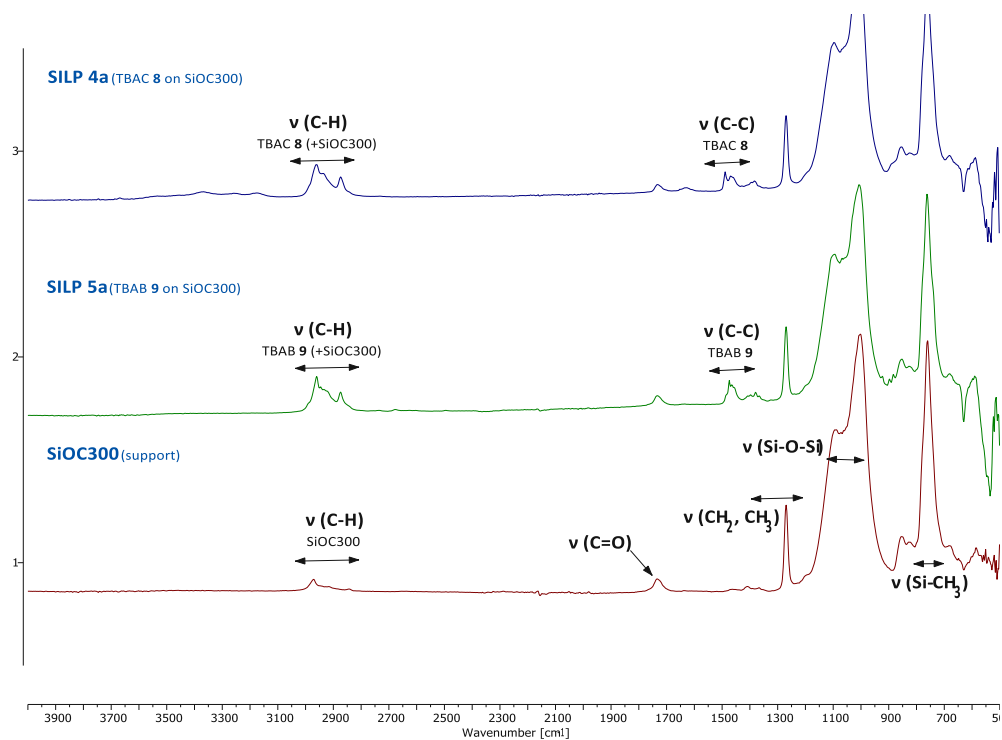
Figure S7: FTIR (ATR) spectrum of **SILP 4a**, **SILP 5a** and SiOC300.
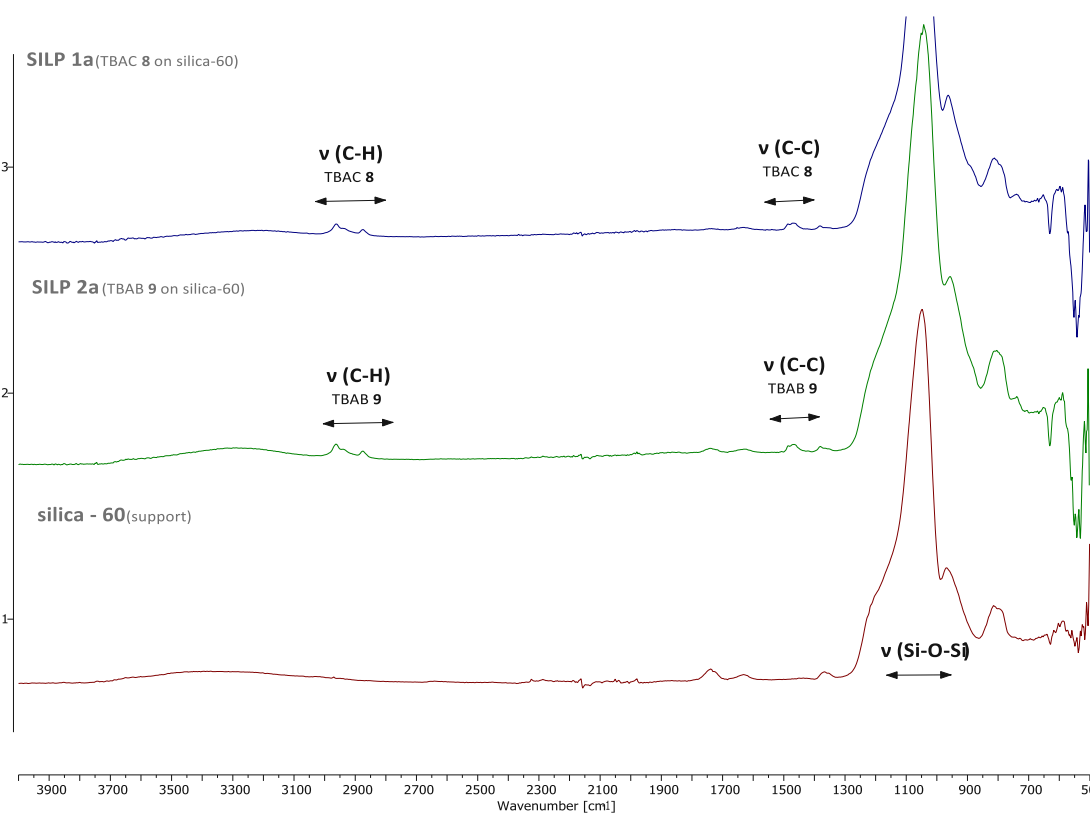
Figure S8: FTIR (ATR) spectrum of **SILP 1a**, **SILP 2a** and silica-60.

S10

S.2.6 X-Ray Photoelectron Spectroscopy (XPS)

All spectra were charge corrected to adventitious carbon at 284.8 eV according to Biesinger *et al.*[2]
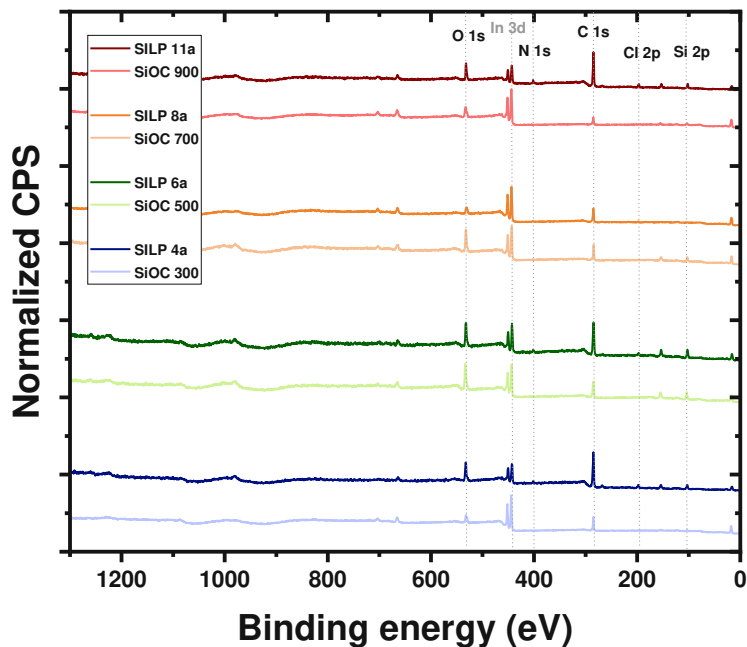
Figure S9: XPS survey of SILPs and supports.
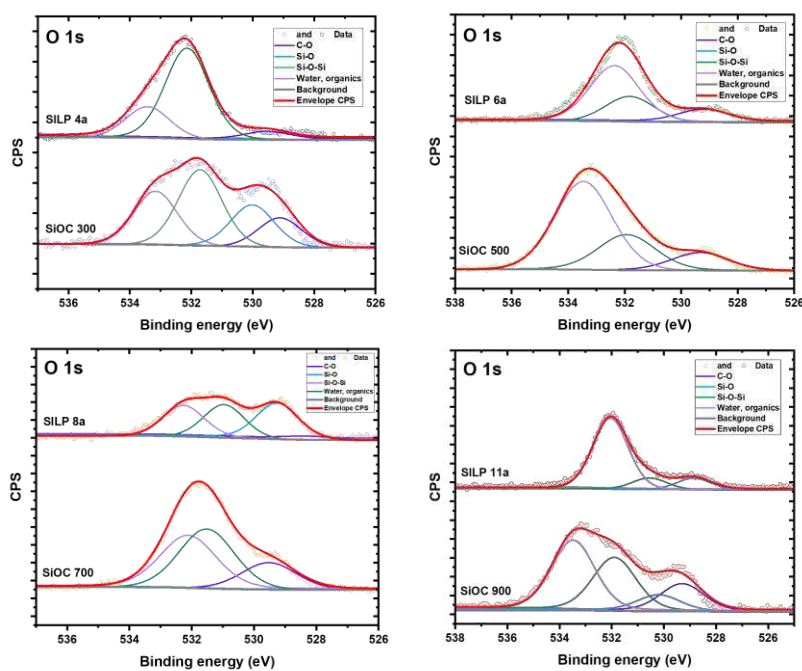
Figure S10: XPS spectra (O 1s) of SILPs and supports.
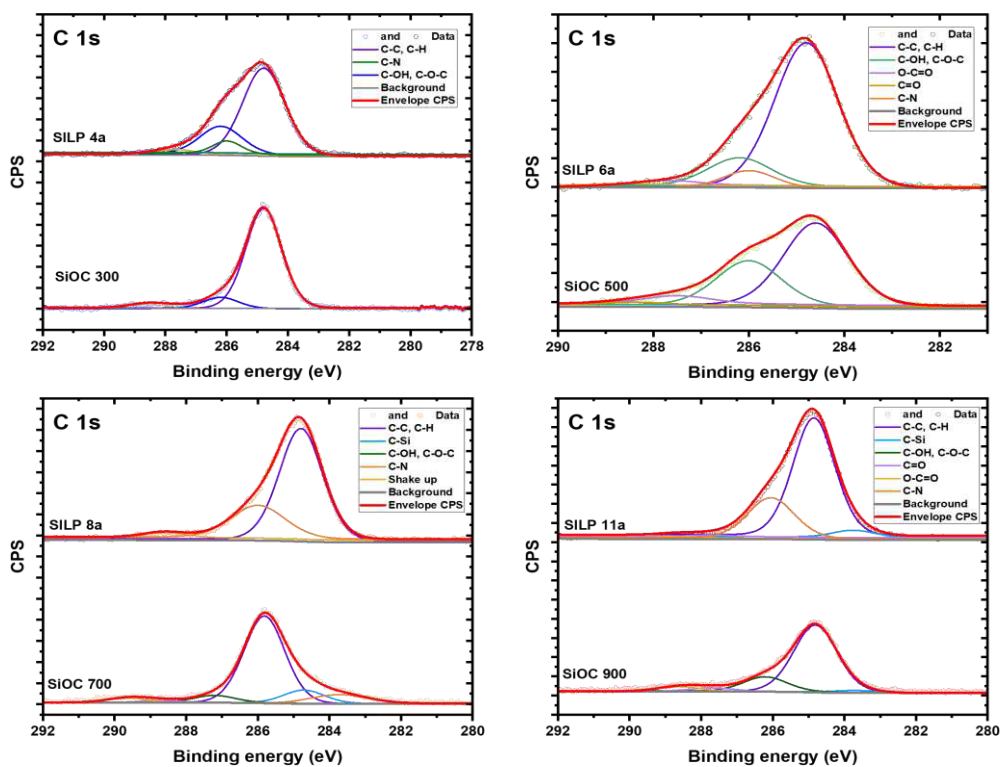
Figure S11: XPS spectra (C 1s) of SILPs and supports.
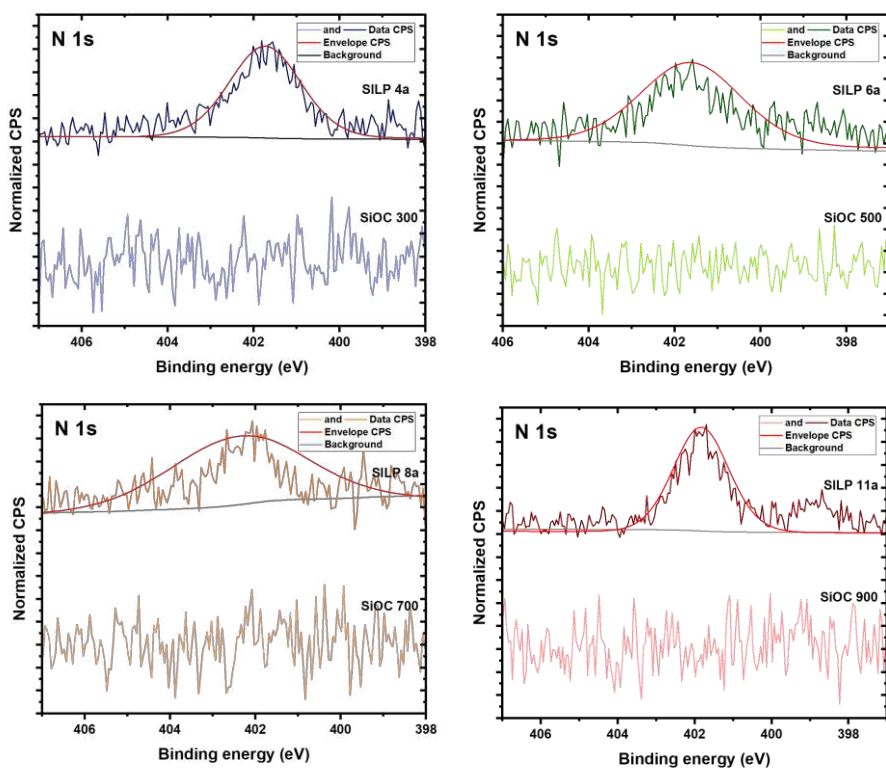
Figure S12: XPS spectra (N 1s) of SILPs and supports.
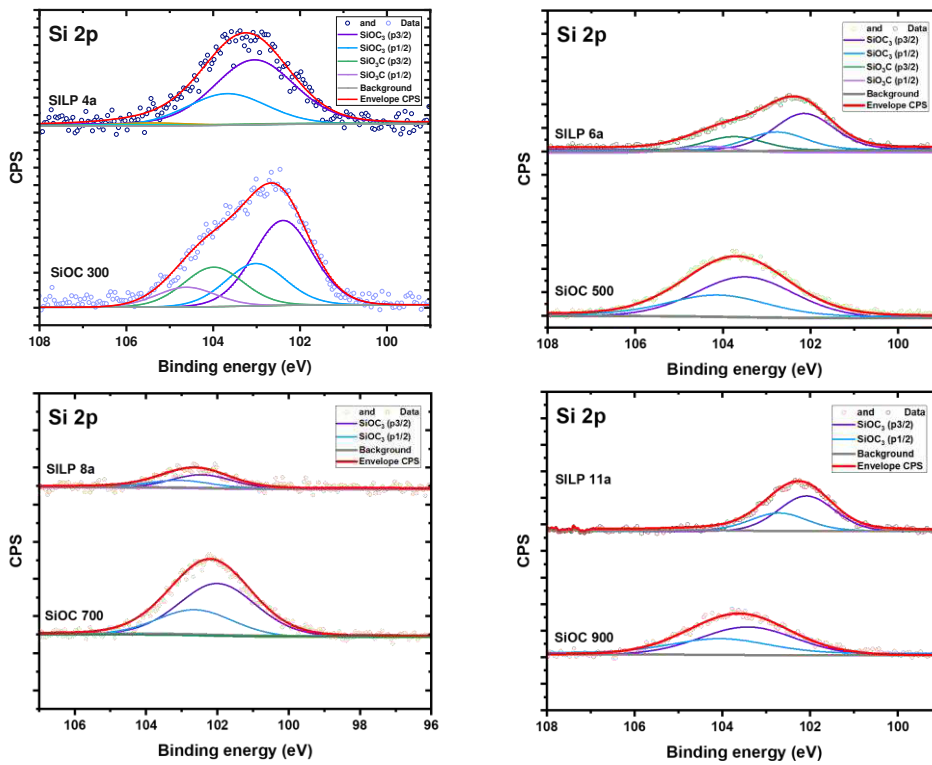
Figure S13: XPS spectra (Si 2p) of SILPs and supports.
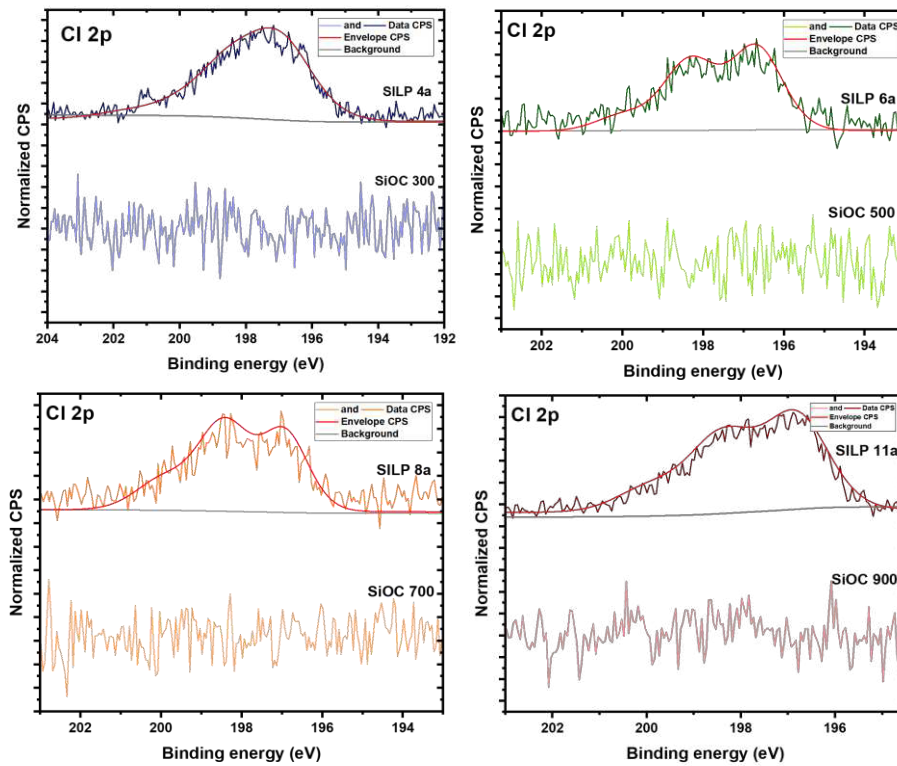
Figure S14: XPS spectra (Cl 2p) of SILPs and supports.

Table S2: Results of quantification of elements in supports and SILPs via XPS.[a]

sample	element	binding energy / eV	concentration / at%
SiOC300	O 1s	531.8	22.6
	C 1s	284.8	67.0
	N 1s	398.3	0
	Si 2p	102.8	10.3
	Cl 2p	202.3	0
SILP 4a	O 1s	532.3	14.6
	C 1s	284.8	67.8
	N 1s	401.3	2.0
	Si 2p	102.8	11.8
	Cl 2p	197.8	3.8
SiOC500	O 1s	533.8	30.2
	C 1s	284.8	44.7
	N 1s	410.8	0
	Si 2p	103.8	25.1
	Cl 2p	215.3	0
SILP 6a	O 1s	531.8	17.3
	C 1s	284.8	57.5
	N 1s	401.8	3.3
	Si 2p	102.8	19.4
	Cl 2p	197.3	2.6

Continuation of Table S2: Results of quantification of supports and SILPs via XPS. [a]

SiOC700	O 1s	532.3	33.9
	C 1s	284.8	46.9
	N 1s	406.3	0
	Si 2p	102.8	19.2
	Cl 2p	205.3	0
SILP 8a	O 1s	530.8	20.3
	C 1s	284.8	71.5
	N 1s	401.8	2.5
	Si 2p	103.3	3.6
	Cl 2p	196.8	2.1
SiOC900	O 1s	532.8	33.5
	C 1s	284.8	48.4
	N 1s	402.8	0
	Si 2p	103.8	18.1
	Cl 2p	198.3	0
SILP 11a	O 1s	531.8	12.5
	C 1s	284.8	67.0
	N 1s	401.8	5.3
	Si 2p	101.8	11.3
	Cl 2p	196.8	3.9

[a] Samples were mounted on indium foil and fixed to the stage using double sided carbon tape. Accuracy of XPS measurements falls within 10-20 at% (especially for oxygen and carbon due to adventitious carbon and oxygen) Detection limit in the recorded survey spectra used for quantification lies between 0.1-1 at%.

S.3 Determination of NMR Conversions and NMR Yields

S.3.1 Limonene Carbonate 15

NMR yields and conversions were determined according to a modification of a protocol[3] previously published by our group.

For the batch reactions running for 5 h, NMR spectra at t = 0 h (before reaction) and at t = 5 h (after reaction) were recorded (**Figure S15**). Calculations of yields and conversions were performed according to **Formulas S4-S9** based on integrals of the protons next to the epoxy and carbonate moiety. Naphthalene was used as an internal standard (δ = 7.82 and 7.45 ppm).

Conversions and, therefore, selectivities (given as ratio of yield and conversion) for flow experiments could not be determined due to the volatility of the starting material and, therefore, partial evaporation of the starting material during the release of CO_2 via the back-pressure regulator.
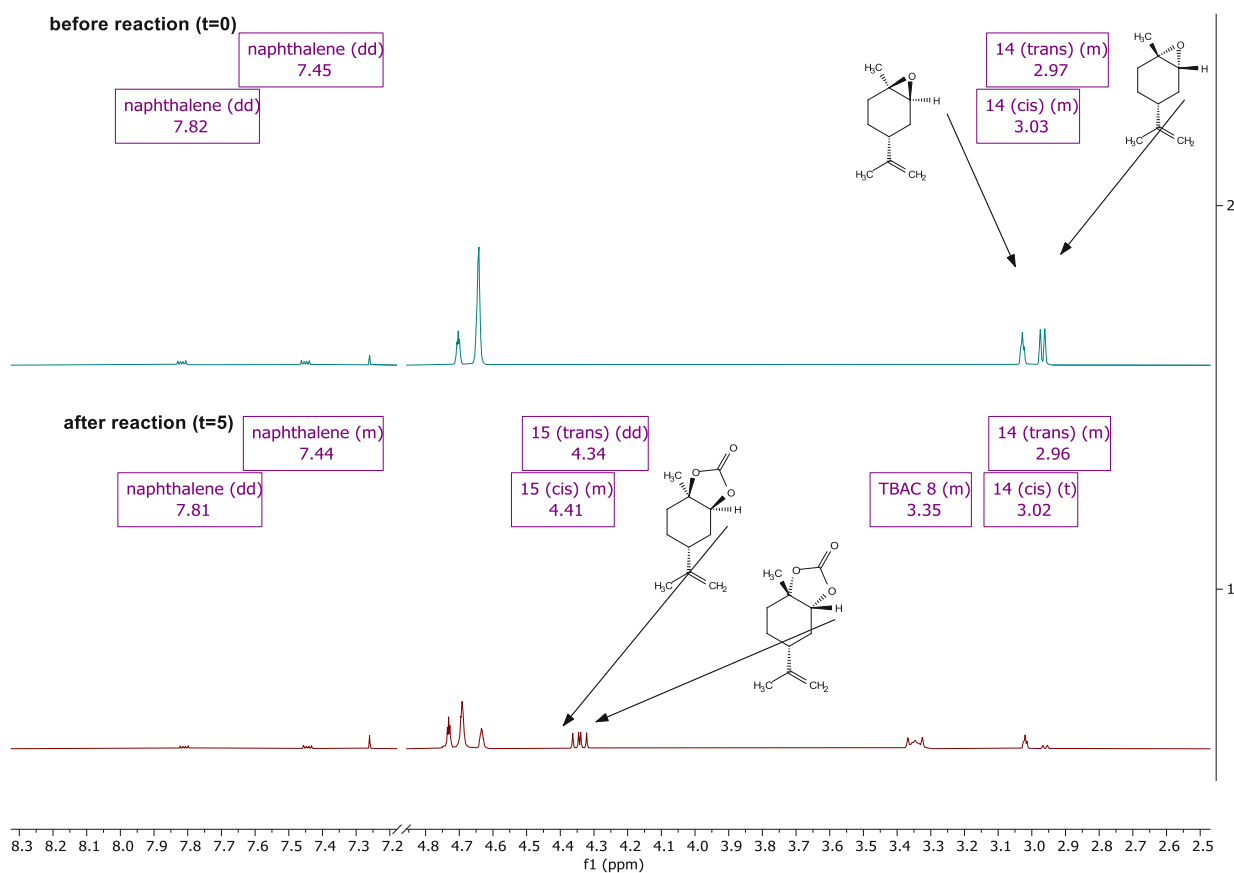
Figure S15: Determination of NMR yields of limonene carbonate **15** via the comparison of the integrals of recorded ^{1}H-NMR spectra at t = 0 h and t = 5 h.

$$\text{conversion } \mathbf{14} \ (cis) \ (\%) = \frac{I_{11 \ (cis)_{t=0}} - I_{11 \ (cis)_{t=5}}}{I_{11 \ (cis)_{t=0}}} \cdot 100$$

Formula S4

$$\text{conversion } \mathbf{14} \ (trans) \ (\%) = \frac{I_{14 \ (trans)_{t=0}} - I_{14 \ (trans)_{t=5}}}{I_{14 \ (trans)_{t=0}}} \cdot 100$$

Formula S5

$$\text{conversion } \mathbf{14} \ (\%) = \frac{(I_{14 \ (cis) \ t=0} + I_{14 \ (trans)_{t=0}}) - (I_{14 \ (cis)_{t=5}} + I_{14 \ (trans)_{t=5}})}{I_{14 \ (cis)_{t=0}} + I_{14 \ (trans)_{t=0}}} \cdot 100$$

Formula S6

$$\text{yield } \mathbf{15} \ (cis) \ (\%) = \frac{I_{15 \ (cis)_{t=5}}}{I_{14 \ (cis)_{t=0}} + I_{14 \ (trans)_{t=0}}} \cdot 100$$

Formula S7

$$\text{yield } \mathbf{15} \ (trans) \ (\%) = \frac{I_{15 \ (trans)_{t=5}}}{I_{14 \ (cis)_{t=0}} + I_{14 \ (trans)_{t=0}}} \cdot 100$$

Formula S8

$$\text{yield } \mathbf{15} \ (\%) = \frac{I_{15 \ (cis)_{t=5}} + I_{15 \ (trans)_{t=5}}}{I_{14 \ (cis)_{t=0}} + I_{14 \ (trans)_{t=0}}} \cdot 100$$

Formula S9

conversion **14**	conversion of *cis* and *trans* limonene oxide **14**
yield **15**	yield of *cis* and *trans* limonene carbonate **15**
$I_{11 \ (xxx)_{t=yy}}$	integral of *cis* or *trans* limonene oxide **14** at t= 0 h or 5 h
$I_{12 \ (xxx)_{t=5}}$	integral of *cis* or *trans* limonene carbonate **15** after the reaction (t=5 h)

S.3.2 Linseed Oil Carbonates 18

For the determination of the conversion of epoxidized linseed oil **17**, NMR spectra at t = 0 h (before reaction) and at t = 5 h (after reaction) were recorded (**Figure S16**). Calculation of the conversions was performed according to **Formula S10** based on integrals of the protons next to the epoxy moiety (δ = 3.21 – 2.82 ppm). The signal of the α-CH₂ of the carbonyl group in the backbone of linseed oil, not participating in the reaction, was used as internal standard (δ = 2.29 ppm).
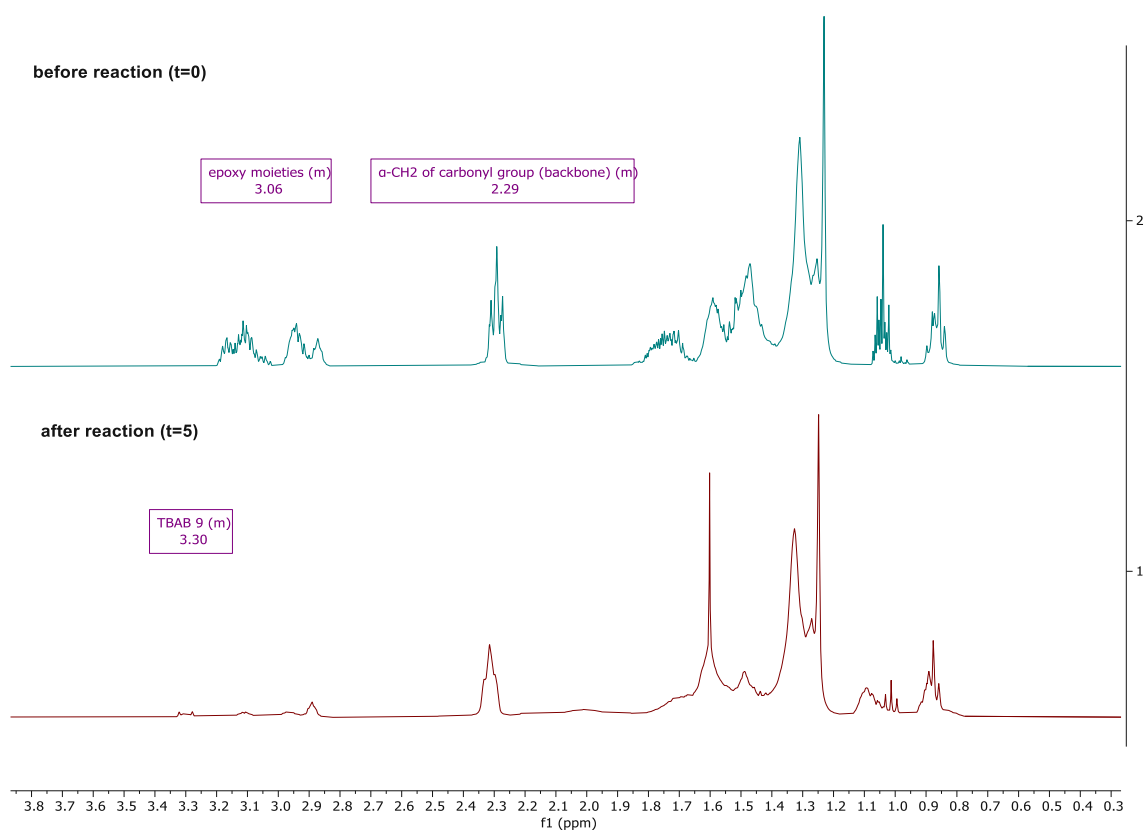
Figure S16: Determination of NMR conversions of epoxidized linseed oil **17** via the comparison of the integrals of recorded ^{1}H-NMR spectra at t = 0 h and t = 5 h.

$$\text{conversion } \mathbf{17}\ (\%) = \frac{I_{\mathbf{17}\ t=0} - I_{\mathbf{17}\ t=5}}{I_{\mathbf{17}\ t=0}} \cdot 100$$

Formula S10

conversion **17**	conversion of epoxidized linseed oil **17**
$I_{\mathbf{17}\ t=0}$	integral of epoxy moieties of epoxidized linseed oil **17** at t= 0 h
$I_{\mathbf{17}\ t=5}$	integral of epoxy moieties of epoxidized linseed oil **17** at t= 5 h

S.4   Catalyst Screenings

S.4.1 Catalyst Screening - Limonene Carbonate 15

Table S3: Homogeneous catalyst screening for limonene carbonate **15** in batch mode reported in our previous work.[3]

entry	catalyst	conversion (NMR)	yield (NMR)
S1	TBAC **8** (100 °C, 20 h)	72 (*cis*: 43, *trans*: 94)	68 (57[c])
S2	TBAB **9** (100 °C, 20 h)	63 (*cis*: 47, *trans*: 76)	56
S3	TBAI **10** (100 °C, 20 h)	31 (*cis*: 25, *trans*: 35)	12
S4	[C_2mim]Cl **11** (100 °C, 20 h)	18 (*cis*: 17, *trans*: 19)	2
S5	[C_2mim]Br **12** (100 °C, 20 h)	13 (*cis*: 6, *trans*: 17)	6
S6	[C_2mim]I **13** (100 °C, 20 h)	11 (*cis*: 11, *trans*: 11)	0

[a] conditions: 5 mmol limonene oxide **14** (cis/trans = 43/57), 13 mg naphthalene (internal standard), 10 mol % catalyst **8-10**, 5 MPa CO_2 (gaseous, initial pressure), 100 °C, 20 h. [b] conversion of more reactive trans isomer, isolated yield (column chromatography with LP:EA = 10/1– 1/1, 50 g of silica-60)

Table S4: Catalyst screening for the formation of limonene carbonate **15** in batch mode[a]

entry	catalyst	loading	support	conversion[b] (NMR)	yield[b] (NMR)	selectivity[c]
S7	TBAC **8**	-	-	58	55	95
S8	[C$_2$mim]Cl **11**	-	-	4	0	-
S9	SILP **1a**	20 wt% TBAC **8**	SiO$_2$	55	48	87
S10	SILP **1a** (+10 mol% H$_2$O)	20 wt% TBAC **8**	SiO$_2$	50	33	66
S11	SILP **2a**	20 wt% TBAB **9**	SiO$_2$	40	25	63
S12	SILP **3a**	20 wt% TBAI **10**	SiO$_2$	66	23	35
S13	SILP **8a**	20 wt% TBAC **8**	SiOC700	58	56	97
S14	SILP **9a**	20 wt% TBAB **9**	SiOC700	43	43	100
S15	SILP **10a**	20 wt% TBAI **10**	SiOC700	8	8	100
S16	SILP **4a**	20 wt% TBAC **8**	SiOC300	53	53	100
S17	SILP **6a**	20 wt% TBAC **8**	SiOC500	57	56	98
S18	SILP **8a**	20 wt% TBAC **8**	SiOC700	58	56	97
S19	SILP **11a**	20 wt% TBAC **8**	SiOC900	63	62	98
S20[d]	SILP **11a**	20 wt% TBAC **8**	SiOC900	63	61	97
S21	SILP **11a** (+10 mol% H$_2$O)	20 wt% TBAC **8**	SiOC900	62	62	100
S22[e]		-	SiO$_2$	36	0	-
S23[e]		-	SiOC300	0	0	-
S24[e]		-	SiOC500	4	0	-
S25[e]		-	SiOC700	0	0	-
S26[e]		-	SiOC900	0	0	-

[a] conditions: 0.5 mmol limonene oxide **14** (cis/trans = 43/57), 1.3 mg naphthalene (internal standard), 10 mol% of catalysts **8-10** (homogeneous or physisorbed), 5 MPa CO$_2$ (gaseous, initial pressure), 120 °C, 5 h; [b] reported as sum of *cis* and *trans* isomers, detailed information about the determination of yield and conversion is summarized in ESI chapter S.3.1 ; [c] ratio of yield (NMR) and conversion (NMR); [d] SILP was prepared using MeOH (instead of CH$_2$Cl$_2$) as solvent; [e] 56 mg of supporting material used.

S.4.2 Continuous Flow - Limonene Carbonate 15

Table S5: Continuous production of limonene carbonate **15** with monolithic SiOC-SILPs.

| entry | catalyst | loading | flowrate CO_2 [mL/min] | residence time [min] | yield (NMR) [%][c] | | leaching[d] |
					maximum	overall (12 h /48 h)	
S27[a]	SILP 1b	20 wt% PSO 20 wt% of TBAC **8**	1.99	7.6	9%	4%	≤ 0.01%
S28[a]	SILP 1b	20 wt% PSO 20 wt% of TBAC **8**	1.49	10.1	12%	7%	≤ 0.01%
S29[a]	SILP 1b	20 wt% PSO 20 wt% of TBAC **8**	0.49	30.5	8%	2%	2%
S30[a]	SILP 2b	20 wt% PSO 35 wt% of TBAC **8**	1.49	10.1	15%	7%	4%
S31[b] (48 h)	SILP 1b	20 wt% PSO 20 wt% of TBAC **8**	1.49	10.1	9%	7%	≤ 0.01%

[a] conditions: 0.01 mL/min limonene oxide **14** (cis/trans = 43/57), **SILP 1b-2b** (15 – 20 mm monolith pieces, 220 mm in total), 0.49 – 1.99 mL/min CO_2 (15 MPa), 120 °C, 12 h; [b] 48 h experiment (**Figure 9**), other conditions according to footnote a; [c] reported as sum of *cis* and *trans* isomers, detailed information about the determination of yield is summarized in ESI chapter S.3.1 and the experimental part of the main manuscript; Conversions and, therefore, selectivities (ratio of yield and conversion) could not be determined due to partial evaporation of limonene oxide **11** during the release of CO_2 via the back-pressure regulator. [d] limit of detection: 0.1 mg, ≤ 0.1% of total amount of TBAC **8**.

S.4.3 Catalyst Screening - Linseed Oil Carbonate 18

Table S6: Catalyst screening for the formation of linseed oil carbonates **18** in batch mode.[a]

entry	catalyst	loading	support	conversion (NMR)
S32	TBAC **8**		-	41%
S33	TBAB **9**		-	56% (97%)[b]
S34	TBAI **10**		-	46%
S35	[C$_2$mim]Br **12**		-	43%
S36	SILP **1a**	20 wt% TBAC **8**	SiO$_2$	31%
S37	SILP **2a**	20 wt% TBAB **9**	SiO$_2$	43%
S38	SILP **3a**	20 wt% TBAI **10**	SiO$_2$	48%
S39	SILP **8a**	20 wt% TBAC **8**	SiOC700	45%
S40	SILP **9a**	20 wt% TBAB **9**	SiOC700	66%
S41	SILP **10a**	20 wt% TBAI **10**	SiOC700	67%
S42	SILP **5a**	20 wt% TBAB **9**	SiOC300	75%
S43	SILP **7a**	20 wt% TBAB **9**	SiOC500	43%
S44	SILP **9a**	20 wt% TBAB **9**	SiOC700	66%
S45	SILP **12a**	20 wt% TBAB **9**	SiOC900	62%
S46		-	SiO$_2$	2%
S47		-	SiOC300	0%
S48		-	SiOC500	0%
S49		-	SiOC700	0%
S50		-	SiOC900	0%

[a] conditions: 220 mg of **17**, SILP catalyst (0.02 mmol of **8-10**, catalyst loading: 20 wt%), 120 °C, 5 MPa (initial pressure), 5 h. Further details about determination of conversion is given in ESI chapter S.3.2 , [b] reaction time: 20 h.

S.5   Analysis of Ionic Liquid-Based Catalysts (^{13}C-NMR)

TBAC 8

^{13}C NMR (101 MHz, CDCl$_3$) δ 58.97 (CH$_2$), 24.21 (CH$_2$), 19.87 (CH$_2$), 13.73 (CH$_3$) ppm.
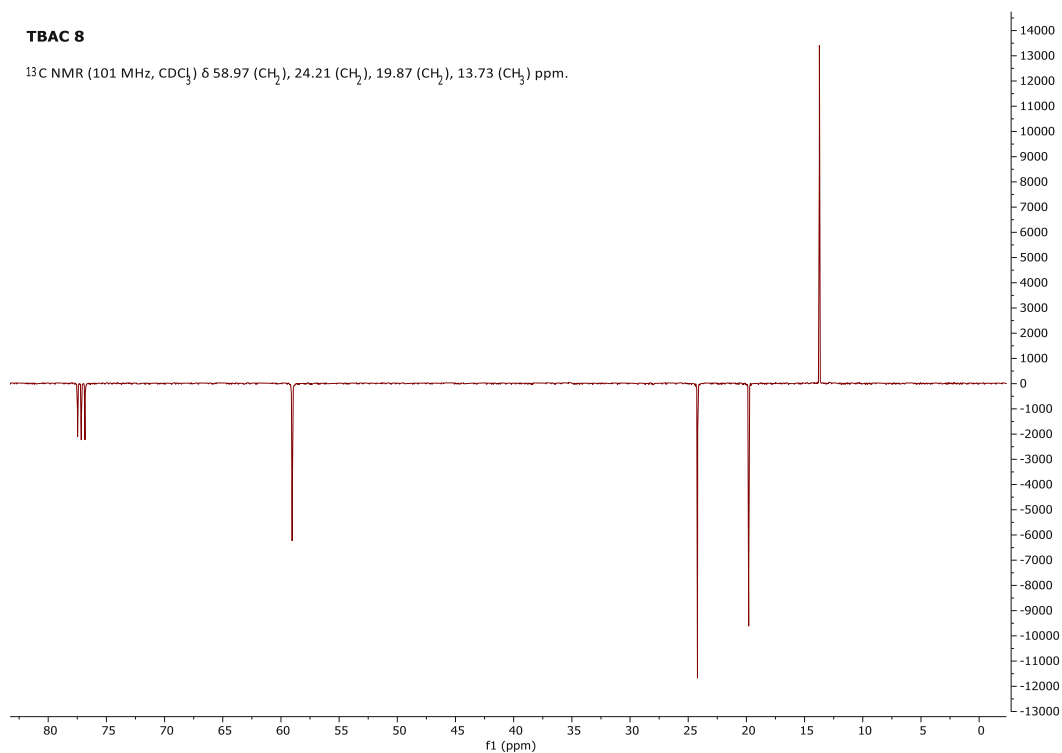
Figure S17: ^{13}C-NMR spectra of tetrabutylammonium chloride TBAC 8.

TBAB 9

^{13}C NMR (101 MHz, CDCl$_3$) δ 59.13 (CH$_2$), 24.27 (CH$_2$), 19.81 (CH$_2$), 13.75 (CH$_3$) ppm.
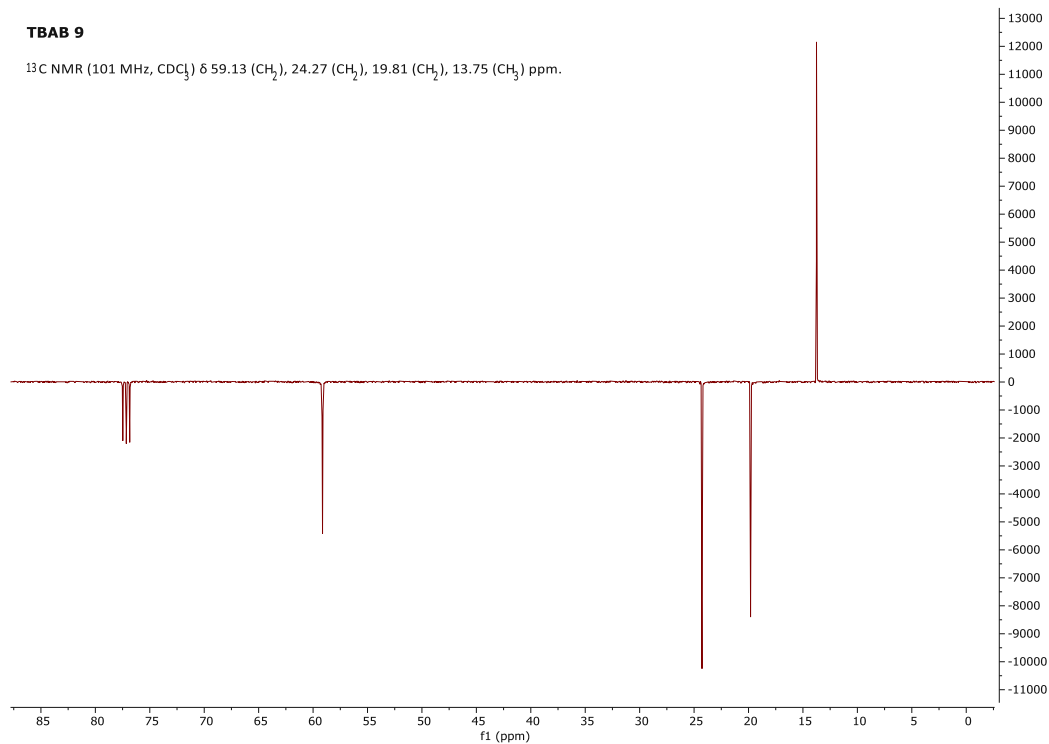
Figure S18: ^{13}C-NMR spectra of tetrabutylammonium bromide TBAB 9.

TBAI 10

^{13}C NMR (101 MHz, CDCl$_3$) δ 59.33 (CH$_2$), 24.42 (CH$_2$), 19.86 (CH$_2$), 13.82 (CH$_3$) ppm.
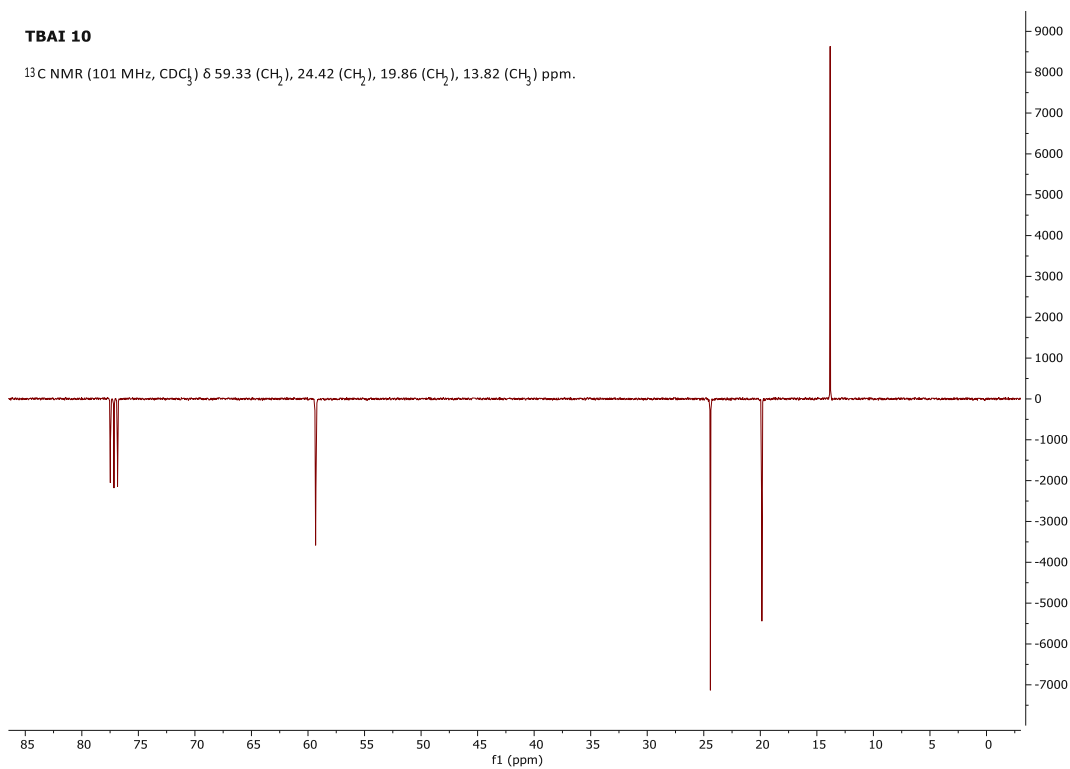
Figure S19: ^{13}C-NMR spectra of tetrabutylammonium iodide TBAI 10.

[C$_2$mim]Cl 11

^{13}C NMR (101 MHz, CDCl$_3$) δ 123.60 (CH), 121.85 (CH), 45.00 (CH$_2$), 36.34 (CH$_3$), 15.55 (CH$_3$) ppm.
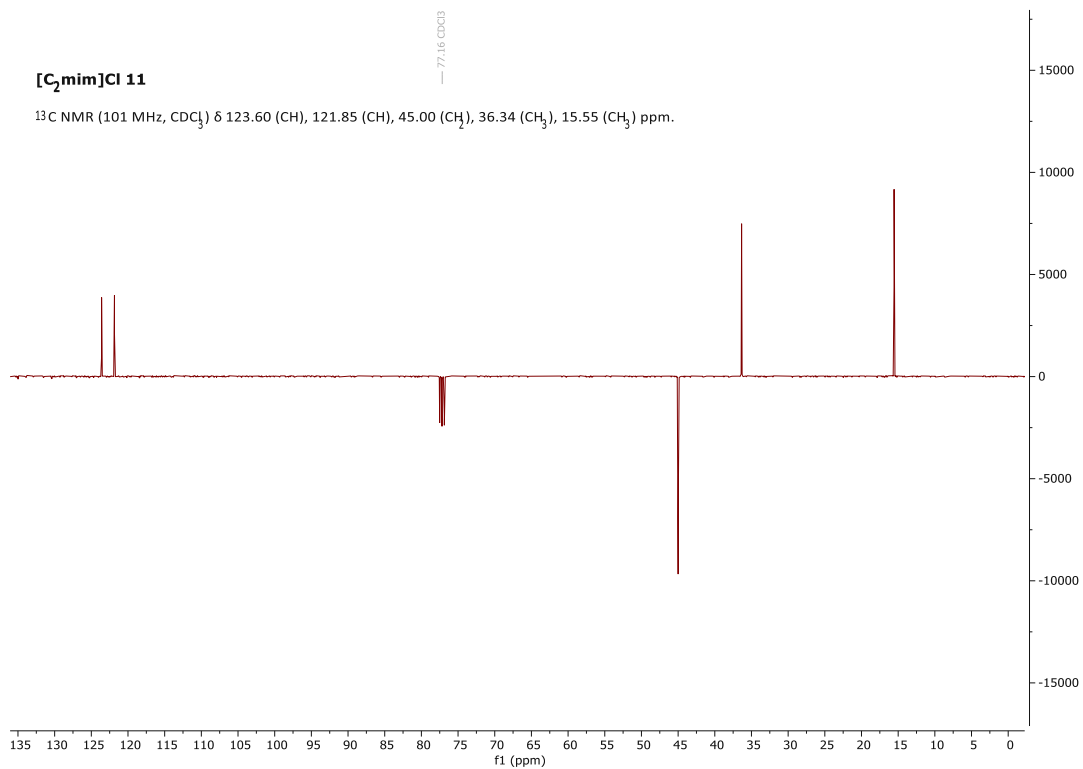
Figure S20: ^{13}C-NMR spectra of 1-ethyl-3-methyl imidazolium chloride [C₂mim]Cl 11.

[C₂mim]Br 12

¹³C NMR (101 MHz, CDCl₃) δ 123.70 (CH), 121.96 (CH), 45.30 (CH₂), 36.72 (CH₃), 15.71 (CH₃) ppm.
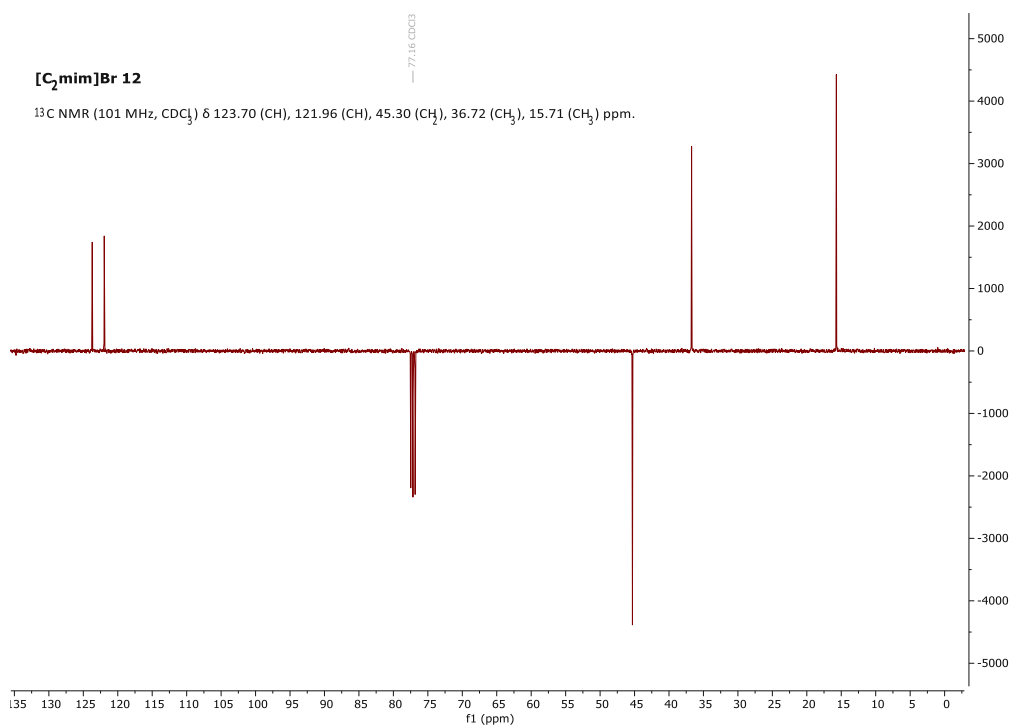
Figure S21: ¹³C-NMR spectra of 1-ethyl-3-methyl imidazolium bromide [C₂mim]Br 12.

S.6   Analysis of Cyclic Carbonates (NMR, IR)

S.6.1 Limonene Carbonate 15

Analytic data are taken from a previous work[3] published by our group and are reported as a mixture of *cis* and *trans* isomer.

FTIR (ATR, neat): 2942 (alkyl), 1790 (C=O) cm^{-1}

^{1}H-NMR (600 MHz, CDCl$_3$, CH$_4$Si): δ 4.74 (t, J = 1.6 Hz, cis 1H), 4.72 (t, J = 1.5 Hz, trans 1H), 4.70–4.68 (m, cis 1H + trans 1H), 4.43–4.40 (m, cis 1H), 4.35 (dd, J = 9.5, 7.0 Hz, trans 1H), 2.30–2.18 (m, cis 2H + trans 2H), 2.02–1.94 (m, cis 1H), 1.94–1.85 (m, trans 1H), 1.84–1.74 (m, cis 2H), 1.70 (s, cis 3H), 1.68 (s, trans 3H), 1.67–1.55 (m, cis 1H + trans 2H), 1.49–1.47 (m, cis 3H), 1.45–1.34 (m, trans 5H), 1.24–1.08 (m, cis 1H) ppm.

^{13}C-NMR (101 MHz, CDCl$_3$, CH$_4$Si): δ 154.87 (trans), 154.61 (cis), 147.53 (cis), 147.42 (trans), 110.27 (trans), 110.05 (cis), 82.78 (cis), 82.24 (trans), 81.93 (cis), 80.66 (trans), 40.01 (trans), 37.42 (cis), 34.26 (cis), 34.07 (trans), 33.14 (trans), 30.66 (cis), 26.36 (cis), 26.27 (trans), 25.77 (trans), 22.35 (cis), 20.99 (cis), 20.66 (trans) ppm.

S.6.2 Linseed Oil Carbonate 18

linseed oil carbonates 18

^{1}H NMR (400 MHz, CDCl$_3$) δ 5.40 − 4.06 (m, carbonates), 3.38 − 3.26 (m, TBAB), 3.16 − 2.83 (m, unconverted epoxides), 2.40 − 2.26 (m,α-CH$_2$ of carbonyl group (backbone)).

carbonates (m)
4.97

unconverted epoxides (m)
2.98

TBAB 9 (m)
3.30

α-CH2 of carbonyl group (backbone) (m)
2.32

epoxidized linseed oil 17 (starting material)
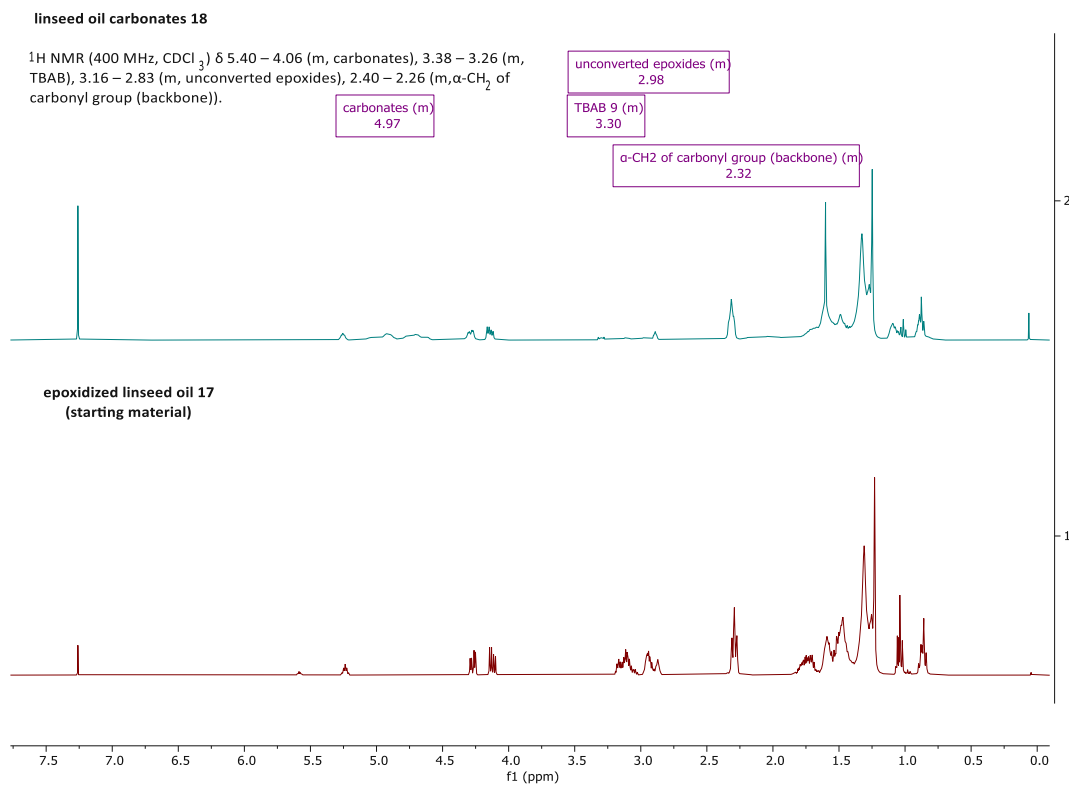
Figure S22: ^{1}H-NMR spectra of linseed oil carbonates 18 and epoxidized linseed oil 17.

linseed oil carbonates 18
FTIR (ATR, neat): 2927, 2856, 1792 (C=O, carbonate), 1737, 1174, 1047 cm^{-1}

epoxidized linseed oil 17
FTIR (ATR, neat): 2921, 2852, 1739, 1156 cm^{-1}
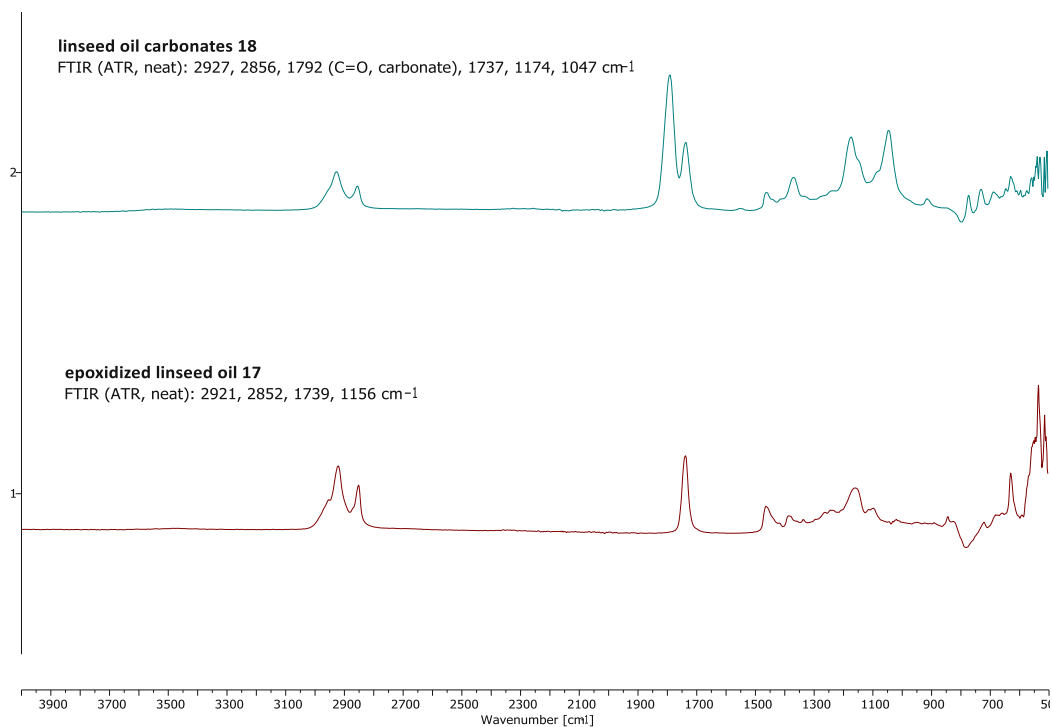
Figure S23: FTIR (ATR) spectra of linseed oil carbonates 18 and epoxidized linseed oil 17.

Spectral data are in accordance with the literature.[4]

S.7 Materials, Methods, and Typical Procedures

S.7.1 Materials and Methods

Chemicals were purchased from several chemical suppliers and used without further purification. Methylsilsesquioxane **1** (Silres, MK) was purchased from Wacker-Chemie. Radical initiator phenyl bis (2,4,6-trimethylbenzoyl) phosphine oxide **5** (Genocure*BAPO) was provided by RAHN. Epoxidized linseed oil **17** (epoxy oxygen content of 8.52 g / 100 g) was provided by HOBUM Oleochemicals. Dichloromethane and methanol were pre-distilled and dried over Al_2O_3 columns (PURESOLV, Innovative Technology).

NMR spectra were recorded from $CDCl_3$ solutions using a Bruker Avance UltraShield 400 spectrometer.

FTIR spectra were recorded on a PerkinElmer Spectrum 65 FTIR spectrometer and the resolution was set to 4 cm^{-1}, 4 scans were used. Spectra were recorded from 4000 - 500 cm^{-1} and raw data were processed with PerkinElmer Spectrum Software.

N_2 physisorption measurements were carried out at a temperature of 77 K using a 3Flex instrument by Micromeritics. Before conducting the measurements, the samples underwent vacuum outgassing at 120 °C for 10 hours. To determine the total pore volume of the samples, the amount of nitrogen adsorbed at $P/P^0 = 0.95$ was evaluated, considering the insignificance of external surface adsorption compared to adsorption within the pores.[5] The apparent surface area was calculated using the Brunauer-Emmet-Teller (BET) equation, following the recommended procedure for microporous sorbents.[6] The relevant pore size distributions were calculated from nonlocal density functional theory (NLDFT) adsorption isotherms considering a cylindrical pore model. The calculations were carried out using the Flex Version 6.01 software provided by Micromeritics Instruments.

Thermogravimetric analysis (TGA) was performed on a Netzsch STA 449 F1 system, and the temperature was gradually increased from 25 °C to 450 °C in air (rate: 5 K min^{-1}). The pyrolytic conversion of polysiloxane **6** (40 mg) to silicon oxycarbide **7** was investigated by TGA (NETZSCH STA 449 C) between 30 and 1500 °C (rate: 5 K min^{-1}) under argon flow (50 mL min^{-1}).

Microscopy was carried out using different microscopes, as follows. A digital microscope (VHX-5000, KEYENCE) was used for optical microscopy. To further investigate the microstructure, ceramographic sections of cylindric monoliths were prepared by embedding the cut monoliths in epoxy resin (EpoFix, Struers) and polished to a 1 µm diamond finish. The embedded and polished structures were observed using a scanning electron microscope (SEM, FEI Quanta 200) using backscattered electron detection. For investigating the distribution of ionic liquid on monolithic silicon oxycarbide, fracture surfaces of monoliths impregnated with 20 wt.% and 35 wt.% TBAC **8** and a reference **7b** were prepared using a razor blade, samples were dried in high vacuum overnight, mounted on graphitic tape, sputtered with Au (AGAR Sputter Coater, 30 sec) and attached to the sample holder with Ag paste to effectively remove surface charges. The fracture surfaces were investigated using a high-resolution electron microscope with a field emission gun electron source (FEG-SEM, FEI Quanta 2050 FEG) using a low acceleration voltage of 2-2.5 kV and secondary electron detection to obtain morphological contrast.

Solvent adsorption procedure is adapted from literature.[7, 8] The samples were dried for 24 h at 110 °C. 0.5 g dry sample was weighed and exposed to saturated atmosphere of H_2O or n-heptane in desiccators at 25 °C for 24 h and weighed again. The measurement was conducted in triplets.

Water immersion following DIN EN 623-2[9] for monolithic ceramics was employed to determine bulk density, apparent solid density, and apparent porosity.

Mercury intrusion porosimetry (Pascal 140/440, POROTEC) was used for the determination of pore-opening diameters and pore-size distribution.

X-ray photoelectron spectroscopy (XPS) samples were mounted on highly conductive Indium foil. XPS measurements were conducted on a custom-built SPECS XPS apparatus, featuring a monochromatized Al-Kα X-ray source (µFocus 350) with an excitation energy of 1486.6 eV (beam energy and spot size: 70 W onto 400 µm, angle: 51° to sample surface normal) and a hemispherical WAL-150 analyzer (acceptance angle: 60°). The instrument maintained a base pressure of $5 \cdot 10^{-10}$ mbar, while the pressure during measurements in the analysis chamber was $8 \cdot 10^{-9}$ mbar. Survey spectra were captured at pass energies of 100 eV, while detailed spectra utilized pass energies of 30 eV. Data analysis was performed using CasaXPS software and Scofield sensitivity factors[10]. Transmission corrections, following the instrument vendor's

specifications, were applied. For all elements Shirley backgrounds were employed[11]. Charge correction was implemented using the C 1s peak for adventitious carbon, shifting it to 284.8 eV binding energy (BE) following the methodology outlined by Biesinger *et al*[2]. Accuracy of XPS measurements falls within 10-20% of the values presented (in units of relative atomic percent (at%)), and the detection limit in survey measurements used for quantification ranges from 0.1-1 at%, varying based on the element.

Permeability measurements are described in detail in ESI chapter S.2.2 .

Autoclave experiments were carried out in a pressure vessel from Berghof (BR-40, PTFE insert 40 mL, PTFE sealing (suitable for scCO$_2$), temperature controller: BTC-3000, Manometer LEO3 from Keller).

Continuous-flow experiments were conducted with a scCO$_2$ continuous flow device from Jasco (Jasco Corporation, Tokyo, Japan). Carbon dioxide, purchased from Messer Austria GmbH (> 99.995 % purity; with ascension pipe), was cooled to -7 °C by a recirculating cooler (CF 40, JULABO GmbH) and was introduced by two CO$_2$-pumps (PU-2086Plus) with cooled heads. An HPLC pump (PU-2089Plus) delivered substrates. Empty 316 stainless steel HPLC columns from DuPont (Zorbax, bio series, GF-250; 250 mm x 9.4 mm ID x 12.7 mm OD, 2 µm frits, 17.35 mL volume) were used as catalyst cartridges. Impregnated silicon oxycarbide monoliths (220 mm; 15-20 mm pieces, 15.27 mL) were loaded into a shrinking tube (RS PRO). The shrunk monoliths were inserted into the catalyst cartridge which was heated up in an HPLC column oven (Brinkmann CH-500 HPLC column heater system, up to 150 °C). Substrates were additionally preheated to 80 °C in a preheating coil (CO-2060Plus). Carbon dioxide was released via a back-pressure regulator (BP-2080Plus, temperature set to 60 °C) and the product was collected in 30 mL glass vials with cyclones (product collector: SCF-Vch-Bp). All parts were connected with 1/16" stainless steel tubing.

S.7.2 Preparation of Powdered SILPs 1a-12a

Silicon oxycarbide cubes **7a** prepared from 30 wt.% preceramic solution **4** were milled (30 s^{-1}, 30 s, ZrO_2 inlet) using a vibrating mill (Retsch MM 40) and sieved (< 90 µm, DIN 4188) to obtain particle sizes comparable to silica-60.

For SILPs,[3] ionic liquid **8-10** (20 wt%, dried under high vacuum for 1 d) was dissolved in dry dichloromethane (silica-60: 100 mL; silicon oxycarbide: 50 mL) and silica-60 (21.000 g, 80 wt%) or silicon oxycarbide (0.800 g, 80 wt%), dried in a vacuum oven (50 °C, 50 mbar, 3 d) was added. The suspension was shaken for 1 h at 480 rpm. Solvent was removed in vacuo and SILP was further dried under high vacuum for 1 d.

S.7.3 Preparation of Monolithic SiOC-SILPs 1b-2b

For continuous-flow experiments, 1.5 mm from the bottom and top part of the cylinders (5-6 cm) was removed and the samples were cut (Struers Minitom, diamond cut-off wheel, 150 rpm) to monolith specimen **7b** of about 15-16 mm. TBAC **8** (for **SILP 1b**: 20 wt%, for **SILP 2b**: 35 wt% dried under high vacuum for 1 d) was dissolved in 100 mL of dry MeOH and monoliths (220 mm as 15 mm pieces, approx. 4.9 g, 80 wt%) were added. The suspension was treated in an ultrasonic bath for 2 h at 40 °C. Solvent was removed under vacuo and monolithic SiOC-**SILP 1b-2b** was further dried under high vacuum for 1 d. Impregnated monoliths were separated from the remaining ionic liquid and the catalyst loading was determined gravimetrically (**SILP 1b**: 20 wt% of TBAC **8**; **SILP 2b**: 35 wt% of TBAC **8**).

S.8   List of Abbreviations

[C_2mim]Cl	1-ethyl-3-methyl imidazolium chloride
[C_2mim]Br	1-ethyl-3-methyl imidazolium bromide
[C_2mim]I	1-ethyl-3-methyl imidazolium iodide
BET	Brunauer-Emmett-Teller
br	broad (NMR)
d	doublet (NMR)
DCM	dichloromethane
dd	doublet of doublets (NMR)
dt	doublet of triplets (NMR)
EtOAc	ethyl acetate
FEG	field emission gun
IR	infrared (spectroscopy)
J	coupling constant (NMR)
LP	light petroleum (boiling point 40 - 60 °C)
m	multiplet (NMR)
MeOH	methanol
NMR	nuclear magnetic resonance
NLDFT	non-local density functional theory
PDC	polymer-derived ceramic
ppm	parts per million
PSO	polysiloxane
s	singlet (NMR)
SEM	scanning electron microscopy
SILP	supported ionic liquid phase
TBAB	tetrabutylammonium bromide
TBAC	tetrabutylammonium chloride
TBAI	tetrabutylammonium iodide
TGA	thermogravimetric analysis
XPS	X-ray photoelectron spectroscopy
wt%	weight percent
δ	chemical shift (NMR)

References

1.   Innocentini, M. D. d. M.; Sepulveda, P.; dos Santos Ortega, F., Permeability. In *Cellular Ceramics*, 2005; pp 313-341.

2.   Biesinger, M. C., Accessing the robustness of adventitious carbon for charge referencing (correction) purposes in XPS analysis: Insights from a multi-user facility data review. *Applied Surface Science* **2022,** *597*, 153681.

3.   Miksovsky, P.; Horn, E. N.; Naghdi, S.; Eder, D.; Schnurch, M.; Bica-Schroder, K., Continuous Formation of Limonene Carbonates in Supercritical Carbon Dioxide. *Org Process Res Dev* **2022,** *26* (10), 2799-2810.

4.   Bähr, M.; Mülhaupt, R., Linseed and soybean oil-based polyurethanes prepared via the non-isocyanate route and catalytic carbon dioxide conversion. *Green Chem.* **2012,** *14* (2), 483-489.

5.   Aharen, T.; Habib, F.; Korobkov, I.; Burchell, T. J.; Guillet-Nicolas, R.; Kleiz, F.; Murugesu, M., Novel Co-based metal–organic frameworks and their magnetic properties using asymmetrically binding 4-(4′-carboxyphenyl)-1,2,4-triazole. *Dalton Transactions* **2013,** *42* (21), 7795-7802.

6.   Sanchez-Varretti, F. O.; Garcia, G. D.; Ramirez-Pastor, A. J.; Roma, F., A simple model for studying multilayer adsorption of noninteracting polyatomic species on homogeneous and heterogeneous surfaces. *J Chem Phys* **2009,** *130* (19), 194711.

7.   Prenzel, T.; Guedes, T.; Schlüter, F.; Wilhelm, M.; Rezwan, K., Tailoring surfaces of hybrid ceramics for gas adsorption–from alkanes to CO_2. *Separation and Purification Technology* **2014,** *129*, 80-89.

8.   Szoldatits, E.; Essmeister, J.; Schachtner, L.; Konegger, T.; Föttinger, K., Polymer-derived SiOC as support material for Ni-based catalysts: CO_2 methanation performance and effect of support modification with La_2O_3. *Frontiers in Chemistry* **2023,** *11*.

9.   DIN, Advanced technical ceramics; monolithic ceramics; general and textural properties; part 2: determination of density and porosity; German version EN 623-2:1993. 1993; pp 1-8.

10.   Scofield, J. H., Hartree-Slater subshell photoionization cross-sections at 1254 and 1487 eV. *Journal of Electron Spectroscopy and Related Phenomena* **1976,** *8* (2), 129-137.

11.   Shirley, D. A., High-Resolution X-Ray Photoemission Spectrum of the Valence Bands of Gold. *Physical Review B* **1972,** *5* (12), 4709-4714.

J   References

1.   Jessop, P. G.; Leitner, W., Volume 4: Supercritical Solvents. In *Green Solvents*, Anastas, P. T., Ed. **2010**; Vol. 4, pp 1-30.

2.   Smith, R. M., Nomenclature for Supercritical-Fluid Chromatography and Extraction (IUPAC Recommendations 1993). *Pure Appl Chem* **1993,** *65* (11), 2397-2403. https://doi.org/10.1351/pac199365112397.

3.   Guadalupe Aspromonte, S.; Andrés Piovano, F.; Alonso, E.; Viviana Boix, A., *Synthesis of Supported Mesoporous Catalysts Using Supercritical CO_2*. IntechOpen: Rijeka, **2020**. https://doi.org/10.5772/intechopen.92740.

4.   Cunico, L. P.; Turner, C., Supercritical Fluids and Gas-Expanded Liquids. In *The Application of Green Solvents in Separation Processes*, Pena-Pereira, F.; Tobiszewski, M., Eds. Elsevier: **2017**; pp 155-214. https://doi.org/10.1016/b978-0-12-805297-6.00007-3.

5.   Onyebuchi, V. E.; Kolios, A.; Hanak, D. P.; Biliyok, C.; Manovic, V., A systematic review of key challenges of CO_2 transport via pipelines. *Renew Sust Energ Rev* **2018,** *81*, 2563-2583. https://doi.org/10.1016/j.rser.2017.06.064.

6.   Blackburn, J. M.; Long, D. P.; Cabanas, A.; Watkins, J. J., Deposition of conformal copper and nickel films from supercritical carbon dioxide. *Science* **2001,** *294* (5540), 141-145. https://doi.org/10.1126/science.1064148.

7.   Humphreys, J.; Lan, R.; Tao, S., Development and Recent Progress on Ammonia Synthesis Catalysts for Haber–Bosch Process. *Adv Energy Sustain Res* **2020,** *2* (1), 2000043. https://doi.org/10.1002/aesr.202000043.

8.   BASF 1913 / First Ammonia Synthesis Plant. https://www.basf.com/global/en/who-we-are/history/chronology/1902-1924/1913.html (accessed 08/2023).

9.   Smith, C.; Hill, A. K.; Torrente-Murciano, L., Current and future role of Haber-Bosch ammonia in a carbon-free energy landscape. *Energ Environ Sci* **2020,** *13* (2), 331-344. https://doi.org/10.1039/c9ee02873k.

10.   Kyriakou, V.; Garagounis, I.; Vourros, A.; Vasileiou, E.; Stoukides, M., An Electrochemical Haber-Bosch Process. *Joule* **2020,** *4* (1), 142-158. https://doi.org/10.1016/j.joule.2019.10.006.

11.   Uwineza, P. A.; Waskiewicz, A., Recent Advances in Supercritical Fluid Extraction of Natural Bioactive Compounds from Natural Plant Materials. *Molecules* **2020,** *25* (17), 3847. https://doi.org/10.3390/molecules25173847.

12.   Pravallika, K.; Chakraborty, S.; Singhal, R. S., Supercritical drying of food products: An insightful review. *J Food Eng* **2023,** *343*, 111375. https://doi.org/10.1016/j.jfoodeng.2022.111375.

13.   Dale Spall, W.; Laintz, K. E., A Survey on the Use of Supercritical Carbon Dioxide as a Cleaning Solvent. In *Supercritical Fluid Cleaning*, McHardy, J.; Sawan, S. P., Eds. William Andrew Publishing: Westwood, NJ, **1998**; pp 162-194. https://doi.org/10.1016/b978-081551416-9.50009-4.

14.   Kang, S. M.; Levien, K. L.; Morrell, J. J., Supercritical fluid impregnation of wood with biocides using temperature reduction to induce deposition. *Wood Sci Technol* **2005,** *39* (5), 328-338. https://doi.org/10.1007/s00226-005-0295-3.

15.   Goñi, M. L.; Gañán, N. A.; Martini, R. E., Supercritical CO_2-assisted dyeing and functionalization of polymeric materials: A review of recent advances (2015–2020). *J CO2 Util* **2021,** *54*, 101760. https://doi.org/10.1016/j.jcou.2021.101760.

16.   Si-Hung, L.; Bamba, T., Current state and future perspectives of supercritical fluid chromatography. *TrAC, Trends Anal Chem* **2022,** *149*, 116550. https://doi.org/10.1016/j.trac.2022.116550.

17.   Tsai, W. C.; Wang, Y. D., Progress of supercritical fluid technology in polymerization and its applications in biomedical engineering. *Prog Polym Sci* **2019,** *98*, 101161. https://doi.org/10.1016/j.progpolymsci.2019.101161.

18.   Reverchon, E.; Adami, R., Nanomaterials and supercritical fluids. *J Supercrit Fluid* **2006,** *37* (1), 1-22. https://doi.org/10.1016/j.supflu.2005.08.003.

19.   Topham, S.; Bazzanella, A.; Schiebahn, S.; Luhr, S.; Zhao, L.; Otto, A.; Stolten, D., Carbon Dioxide. In *Ullmann's Encyclopedia of Industrial Chemistry*, Wiley-VCH Verlag GmbH & Co. KGaA: Weinheim, Germany, **2014**; pp 1-43. https://doi.org/10.1002/14356007.a05_165.pub2.

20.   Nie, S.; Zhou, J.; Yang, F.; Lan, M. Z.; Li, J. M.; Zhang, Z. Q.; Chen, Z. F.; Xu, M. F.; Li, H.; Sanjayan, J. G., Analysis of theoretical carbon dioxide emissions from cement production: Methodology and application. *J Clean Prod* **2022**, *334*, 130270. https://doi.org/10.1016/j.jclepro.2021.130270.

21.   Zosel, K. Process for recovering caffeine. US3806619 (A), 1974.

22.   Zosel, K. Process for the decoffeination of coffee. US4260639 (A), 1981.

23.   De Marco, I.; Riemma, S.; Iannone, R., Life cycle assessment of supercritical CO_2 extraction of caffeine from coffee beans. *J Supercrit Fluids* **2018,** *133*, 393-400. https://doi.org/10.1016/j.supflu.2017.11.005.

24.   Swiss Water Decaffeinated Coffee Inc. Water only Processing, How great coffee becomes great decaf, chemical-free. Swiss Water® Process. https://www.swisswater.com/ (accessed 10/2023).

25.   Lack, E.; Seidlitz, H., Commercial scale decaffeination of coffee and tea using supercritical CO_2. In *Extraction of Natural Products Using Near-Critical Solvents*, King, M. B.; Bott, T. R., Eds. Springer Netherlands: Dordrecht, **1993**; pp 101-139. https://doi.org/10.1007/978-94-011-2138-5_5.

26.   Zeković, Z.; Pfaf-Šovljanski, I.; Grujić, O., Supercritical fluid extraction of hops. *J Serb Chem Soc* **2007**, *72* (1), 81-87. https://doi.org/10.2298/JSC0701081Z.

27.   Knez, Ž.; Škerget, M.; KnezHrnčič, M., 1 - Principles of supercritical fluid extraction and applications in the food, beverage and nutraceutical industries. In *Separation, Extraction and Concentration Processes in the Food, Beverage and Nutraceutical Industries*, Rizvi, S. S. H., Ed. Woodhead Publishing: **2013**; pp 3-38. https://doi.org/10.1533/9780857090751.1.3.

28.   Sovilj, M. N.; Nikolovski, B. G.; Spasojevic, M. D., Critical Review of Supercritical Fluid Extraction of Selected Spice Plant Materials. *Maced J Chem Chem Eng* **2011,** *30* (2), 197-220. https://doi.org/10.20450/mjcce.2011.35.

29.   Magomedov, R. N.; Pripakhaylo, A. V.; Maryutina, T. A.; Shamsullin, A. I.; Ainullov, T. S., Role of Solvent Deasphalting in the Modern Oil Refining Practice and Trends in the Process Development. *Russ J Appl Chem* **2019,** *92* (12), 1634-1648. https://doi.org/10.1134/S1070427219120036.

30.   Maciel, M. R. W.; Filho, R. M.; Cárdenas, V. O. C.; Koroishi, E. T.; Rivarola, F. W. R.; Quirino, F. A. B.; Batistella, C. B.; Medina, L. C., Separating Asphaltenes from Lube Oil Through Supercritical Deasphalting Considering Experimental and Virtual Plants and Thermodynamic Analysis. In *Computer Aided Chemical Engineering*, de Brito Alves, R. M.; do Nascimento, C. A. O.; Biscaia, E. C., Eds. Elsevier: **2009**; Vol. 27, pp 771-776. https://doi.org/10.1016/S1570-7946(09)70349-9.

31.   da Silva, R. P. F. F.; Rocha-Santos, T. A. P.; Duarte, A. C., Supercritical fluid extraction of bioactive compounds. *TrAC, Trends Anal Chem* **2016**, *76*, 40-51. https://doi.org/10.1016/j.trac.2015.11.013.

32.   Herrero, M.; Mendiola, J. A.; Cifuentes, A.; Ibanez, E., Supercritical fluid extraction: Recent advances and applications. *J Chromatogr A* **2010,** *1217* (16), 2495-511. https://doi.org/10.1016/j.chroma.2009.12.019.

33.   Bimakr, M.; Rahman, R. L. A.; Taip, F. S.; Ganjloo, A.; Salleh, L. M.; Selamat, J.; Hamid, A.; Zaidul, I. S. M., Comparison of different extraction methods for the extraction of major bioactive flavonoid compounds from spearmint (Mentha spicata L.) leaves. *Food Bioprod Process* **2011,** *89* (1), 67-72. https://doi.org/10.1016/j.fbp.2010.03.002.

34.   Pasquel Reátegui, J. L.; Machado, A. P. d. F.; Barbero, G. F.; Rezende, C. A.; Martínez, J., Extraction of antioxidant compounds from blackberry (Rubus sp.) bagasse using supercritical CO_2 assisted by ultrasound. *J Supercrit Fluids* **2014**, *94*, 223-233. https://doi.org/10.1016/j.supflu.2014.07.019.

35.   Jayashankar, B.; Mishra, K. P.; Ganju, L.; Singh, S. B., Supercritical extract of Seabuckthorn Leaves (SCE200ET) inhibited endotoxemia by reducing inflammatory cytokines and nitric oxide synthase 2 expression. *Int Immunopharmacol* **2014**, *20* (1), 89-94. https://doi.org/10.1016/j.intimp.2014.02.022.

36.   Sainz Martinez, A.; Kornpointner, C.; Haselmair-Gosch, C.; Mikulic-Petkovsek, M.; Schröder, K.; Halbwirth, H., Dynamic streamlined extraction of iridoids, anthocyanins and lipids from haskap berries. *LWT - Food Sci Technol* **2021**, *138*, 110633. https://doi.org/https://doi.org/10.1016/j.lwt.2020.110633.

37. Bitencourt, R. G.; Queiroga, C. L.; Duarte, G. H. B.; Eberlin, M. N.; Kohn, L. K.; Arns, C. W.; Cabral, F. A., Sequential extraction of bioactive compounds from Melia azedarach L. in fixed bed extractor using CO_2, ethanol and water. *J Supercrit Fluid* **2014,** *95*, 355-363. https://doi.org/10.1016/j.supflu.2014.09.027.

38. Mezzomo, N.; Tenfen, L.; Farias, M. S.; Friedrich, M. T.; Pedrosa, R. C.; Ferreira, S. R. S., Evidence of anti-obesity and mixed hypolipidemic effects of extracts from pink shrimp (Penaeus brasiliensis and Penaeus paulensis) processing residue. *J Supercrit Fluid* **2015,** *96*, 252-261. https://doi.org/10.1016/j.supflu.2014.09.021.

39. Bagheri, H.; Abdul Manap, M. Y.; Solati, Z., Antioxidant activity of Piper nigrum L. essential oil extracted by supercritical CO_2 extraction and hydro-distillation. *Talanta* **2014,** *121*, 220-228. https://doi.org/10.1016/j.talanta.2014.01.007.

40. Czaikoski, K.; Mesomo, M. C.; de Paula Scheer, A.; Dalla Santa, O. R.; Queiroga, C. L.; Corazza, M. L., Kinetics, composition and biological activity of Eupatorium intermedium flower extracts obtained from scCO$_2$ and compressed propane. *J Supercrit Fluids* **2015,** *97*, 145-153. https://doi.org/10.1016/j.supflu.2014.10.008.

41. Parisotto, E. B.; Michielin, E. M. Z.; Biscaro, F.; Ferreira, S. R. S.; Filho, D. W.; Pedrosa, R. C., The antitumor activity of extracts from Cordia verbenacea D.C. obtained by supercritical fluid extraction. *J Supercrit Fluids* **2012,** *61*, 101-107. https://doi.org/10.1016/j.supflu.2011.08.016.

42. Arranz, E.; Jaime, L.; de la Hazas, M. C. L.; Vicente, G.; Reglero, G.; Santoyo, S., Supercritical sage extracts as anti-inflammatory food ingredients. *Ind Crop Prod* **2014,** *54*, 159-166. https://doi.org/10.1016/j.indcrop.2014.01.021.

43. Kornpointner, C.; Sainz Martinez, A.; Schnürch, M.; Halbwirth, H.; Bica-Schröder, K., Combined ionic liquid and supercritical carbon dioxide based dynamic extraction of six cannabinoids from Cannabis sativa L. *Green Chem* **2021,** *23* (24), 10079-10089. https://doi.org/https://doi.org/10.1039/D1GC03516A.

44. Carrara, V. S.; Filho, L. C.; Garcia, V. A. S.; Faioes, V. S.; Cunha-Junior, E. F.; Torres-Santos, E. C.; Cortez, D. A. G., Supercritical Fluid Extraction of Pyrrolidine Alkaloid from Leaves of Piper amalago L. *Evid Based Complement Alternat Med* **2017,** *2017*, 7401748. https://doi.org/10.1155/2017/7401748.

45. Falcão, M. A.; Scopel, R.; Almeida, R. N.; do Espirito Santo, A. T.; Franceschini, G.; Garcez, J. J.; Vargas, R. M. F.; Cassel, E., Supercritical fluid extraction of vinblastine from Catharanthus roseus. *J Supercrit Fluids* **2017,** *129*, 9-15. https://doi.org/10.1016/j.supflu.2017.03.018.

46. Nature Education. Plant Cells, Chloroplasts, and Cell Walls. https://www.nature.com/scitable/topicpage/plant-cells-chloroplasts-and-cell-walls-14053956/ (accessed 12/2023).

47. Patil, P. D.; Patil, S. P.; Kelkar, R. K.; Patil, N. P.; Pise, P. V.; Nadar, S. S., Enzyme-assisted supercritical fluid extraction: An integral approach to extract bioactive compounds. *Trends Food Sci Technol* **2021,** *116*, 357-369. https://doi.org/10.1016/j.tifs.2021.07.032.

48. Wimmer, Z.; Zarevucka, M., A review on the effects of supercritical carbon dioxide on enzyme activity. *Int J Mol Sci* **2010,** *11* (1), 233-253. https://doi.org/10.3390/ijms11010233.

49. Sun, N.; Rodriguez, H.; Rahman, M.; Rogers, R. D., Where are ionic liquid strategies most suited in the pursuit of chemicals and energy from lignocellulosic biomass? *Chem Commun* **2011,** *47* (5), 1405-1421. https://doi.org/10.1039/c0cc03990j.

50. Zirbs, R.; Strassl, K.; Gaertner, P.; Schröder, C.; Bica, K., Exploring ionic liquid-biomass interactions: towards the improved isolation of shikimic acid from star anise pods. *RSC Adv* **2013,** *3* (48), 26010-26016. https://doi.org/10.1039/c3ra45572f.

51. Basegmez, H. I. O.; Povilaitis, D.; Kitryte, V.; Kraujaliene, V.; Sulniute, V.; Alasalvar, C.; Venskutonis, P. R., Biorefining of blackcurrant pomace into high value functional ingredients using supercritical CO_2, pressurized liquid and enzyme assisted extractions. *J Supercrit Fluid* **2017,** *124*, 10-19. https://doi.org/10.1016/j.supflu.2017.01.003.

52. Kitrytė, V.; Povilaitis, D.; Kraujalienė, V.; Šulniūtė, V.; Pukalskas, A.; Venskutonis, P. R., Fractionation of sea buckthorn pomace and seeds into valuable components by using high pressure and enzyme-assisted extraction methods. *LWT - Food Sci Technol* **2017,** *85*, 534-538. https://doi.org/10.1016/j.lwt.2017.02.041.

53. Mushtaq, M.; Sultana, B.; Akram, S.; Anwar, F.; Adnan, A.; Rizvi, S. S. H., Enzyme-assisted supercritical fluid extraction: an alternative and green technology for non-extractable polyphenols. *Anal Bioanal Chem* **2017,** *409* (14), 3645-3655. https://doi.org/10.1007/s00216-017-0309-7.

54. Krakowska, A.; Rafinska, K.; Walczak, J.; Buszewski, B., Enzyme-assisted optimized supercritical fluid extraction to improve Medicago sativa polyphenolics isolation. *Ind Crop Prod* **2018,** *124*, 931-940. https://doi.org/10.1016/j.indcrop.2018.08.004.

55. Krakowska-Sieprawska, A.; Rafinska, K.; Walczak-Skierska, J.; Kielbasa, A.; Buszewski, B., Promising Green Technology in Obtaining Functional Plant Preparations: Combined Enzyme-Assisted Supercritical Fluid Extraction of Flavonoids Isolation from Medicago Sativa Leaves. *Materials* **2021,** *14* (11), 2724. https://doi.org/10.3390/ma14112724.

56. Mushtaq, M.; Sultana, B.; Anwar, F.; Adnan, A.; Rizvi, S. S. H., Enzyme-assisted supercritical fluid extraction of phenolic antioxidants from pomegranate peel. *J Supercrit Fluid* **2015,** *104*, 122-131. https://doi.org/10.1016/j.supflu.2015.05.020.

57. Santana, A. L.; Queiros, L. D.; Martinez, J.; Macedo, G. A., Pressurized liquid- and supercritical fluid extraction of crude and waste seeds of guarana (Paullinia cupana): Obtaining of bioactive compounds and mathematical modeling. *Food Bioprod Process* **2019,** *117*, 194-202. https://doi.org/10.1016/j.fbp.2019.07.007.

58. Lenucci, M. S.; De Caroli, M.; Marrese, P. P.; Iurlaro, A.; Rescio, L.; Bohm, V.; Dalessandro, G.; Piro, G., Enzyme-aided extraction of lycopene from high-pigment tomato cultivars by supercritical carbon dioxide. *Food Chem* **2015,** *170*, 193-202. https://doi.org/10.1016/j.foodchem.2014.08.081.

59. Wang, Q.; Huang, J.; Shao, H.; Zhou, Y.; Xia, K.; Huang, F.; Zhang, H.; Yang, X., Chemical Profile, Quality and Antioxidant Properties of Palmitoleic Acid Rich Oil from Decaisnea insignis Seeds by Different Extraction Techniques. *Food Sci Technol Res* **2019,** *25* (6), 755-763. https://doi.org/10.3136/fstr.25.755.

60. Antunes-Ricardo, M.; Mendiola, J. A.; Garcia-Cayuela, T.; Ibanez, E.; Gutierrez-Uribe, J. A.; Cano, M. P.; Guajardo-Flores, D., Enzyme-assisted supercritical fluid extraction of antioxidant isorhamnetin conjugates from Opuntia ficus-indica (L.) Mill. *J Supercrit Fluid* **2020,** *158*, 104713. https://doi.org/10.1016/j.supflu.2019.104713.

61. Dutta, S.; Bhattacharjee, P., Nanoliposomal encapsulates of piperine-rich black pepper extract obtained by enzyme-assisted supercritical carbon dioxide extraction. *J Food Eng* **2017,** *201*, 49-56. https://doi.org/10.1016/j.jfoodeng.2017.01.006.

62. Dutta, S.; Bhattacharjee, P., Microencapsulation of enzyme-assisted supercritical carbon dioxide extract of small cardamom by spray drying. *J Food Meas Charact* **2017,** *11* (1), 310-319. https://doi.org/10.1007/s11694-016-9398-9.

63. Rusznyak, S. T.; Szent-Györgyi, A., Vitamin P: Flavonols as Vitamins. *Nature* **1936,** *138*, 27-27. https://doi.org/10.1038/138027a0.

64. Juca, M. M.; Cysne Filho, F. M. S.; de Almeida, J. C.; Mesquita, D. D. S.; Barriga, J. R. M.; Dias, K. C. F.; Barbosa, T. M.; Vasconcelos, L. C.; Leal, L.; Ribeiro, J. E.; Vasconcelos, S. M. M., Flavonoids: biological activities and therapeutic potential. *Nat Prod Res* **2020,** *34* (5), 692-705. https://doi.org/10.1080/14786419.2018.1493588.

65. Falcone Ferreyra, M. L.; Rius, S. P.; Casati, P., Flavonoids: biosynthesis, biological functions, and biotechnological applications. *Front Plant Sci* **2012,** *3*, 222. https://doi.org/10.3389/fpls.2012.00222.

66. Davies, K. M.; Jibran, R.; Zhou, Y.; Albert, N. W.; Brummell, D. A.; Jordan, B. R.; Bowman, J. L.; Schwinn, K. E., The Evolution of Flavonoid Biosynthesis: A Bryophyte Perspective. *Front Plant Sci* **2020,** *11*, 7. https://doi.org/10.3389/fpls.2020.00007.

67. Hollman, P. C. H., Absorption, bioavailability, and metabolism of flavonoids. *Pharm Biol* **2004,** *42*, 74-83. https://doi.org/10.3109/13880200490893492.

68. Clark, J. H.; Tavener, S. J., Alternative solvents: Shades of Green. *Org Process Res Dev* **2007,** *11* (1), 149-155. https://doi.org/10.1021/op060160g.

69. Kunz, W.; Gores, H. J., Ionic Liquids. In *Encyclopedia of Applied Electrochemistry*, Kreysa, G.; Ota, K.-i.; Savinell, R. F., Eds. Springer: New York, **2014**; pp 1106-1111. https://doi.org/10.1007/978-1-4419-6996-5_17.

70. Gabriel, S.; Weiner, J., Ueber einige Abkömmlinge des Propylamins. *Ber Dtsch Chem Ges* **2006,** *21* (2), 2669-2679. https://doi.org/10.1002/cber.18880210288.

71. Walden, P., Ueber die Molekulargrösse und elektrische Leitfähigkeit einiger geschmolzenen Salze. *Bull Acad Imp Sci* **1914,** *8* (6), 405-422.

72. Aschenbrenner, O.; Supasitmongkol, S.; Taylor, M.; Styring, P., Measurement of vapour pressures of ionic liquids and other low vapour pressure solvents. *Green Chem* **2009,** *11* (8), 1217-1221. https://doi.org/10.1039/b904407h.

73. Weber, M.; Pompetzki, W.; Bonmann, R.; Weber, M., Acetone. In *Ullmann's Encyclopedia of Industrial Chemistry*, pp 1-19. https://doi.org/https://doi.org/10.1002/14356007.a01_079.pub4.

74. Singh, S. K.; Savoy, A. W., Ionic liquids synthesis and applications: An overview. *J Mol Liq* **2020,** *297*, 112038. https://doi.org/10.1016/j.molliq.2019.112038.

75. Deetlefs, M.; Seddon, K. R., Green Solvents. In *Volume 6 Ionic Liquids*, Anastas, P. T., Ed. pp 1-38.

76. Ratti, R., Ionic Liquids: Synthesis and Applications in Catalysis. *Adv Chem* **2014,** *2014*, 1-16. https://doi.org/10.1155/2014/729842.

77. Maase, M., Industrial Applications of Ionic Liquids. In *Ionic Liquids in Synthesis*, **2007**; pp 663-687. https://doi.org/10.1002/9783527621194.ch9.

78. Maase, M.; Massonne, K.; Vagt, U. BASIL™—BASF's Processes Based on Ionic Liquids. https://www.sigmaaldrich.com/AT/de/technical-documents/technical-article/chemistry-and-synthesis/reaction-design-and-optimization/basil-basf-s-processes (accessed 08/2023).

79. Welton, T., Ionic liquids in catalysis. *Coord Chem Rev* **2004,** *248* (21-24), 2459-2477. https://doi.org/10.1016/j.ccr.2004.04.015.

80. Fehrmann, R.; Riisager, A.; Haumann, M., *Supported Ionic Liquids*. Wiley-VCH: **2014**. https://doi.org/10.1002/9783527654789.

81. Castro-Amoedo, R.; Csendes, Z.; Brünig, J.; Sauer, M.; Foelske-Schmitz, A.; Yigit, N.; Rupprechter, G.; Gupta, T.; Martins, A. M.; Bica, K.; Hoffmann, H.; Kirchner, K., Carbon-based SILP catalysis for the selective hydrogenation of aldehydes using a well-defined Fe(ii) PNP complex. *Catal Sci Technol* **2018,** *8* (18), 4812-4820. https://doi.org/10.1039/C8CY00818C.

82. Blaumeiser, D.; Stepić, R.; Wolf, P.; Wick, C. R.; Haumann, M.; Wasserscheid, P.; Smith, D. M.; Smith, A.-S.; Bauer, T.; Libuda, J., Cu carbonyls enhance the performance of Ru-based SILP water–gas shift catalysts: a combined in situ DRIFTS and DFT study. *Catal Sci Technol* **2020,** *10* (1), 252-262. https://doi.org/10.1039/C9CY01852B.

83. Wolf, P.; Wick, C. R.; Mehler, J.; Blaumeiser, D.; Schötz, S.; Bauer, T.; Libuda, J.; Smith, D.; Smith, A.-S.; Haumann, M., Improving the Performance of Supported Ionic Liquid Phase Catalysts for the Ultra-Low-Temperature Water Gas Shift Reaction Using Organic Salt Additives. *ACS Catal* **2022,** *12* (9), 5661-5672. https://doi.org/10.1021/acscatal.1c05979.

84. Wolny, A.; Siewniak, A.; Zdarta, J.; Ciesielczyk, F.; Latos, P.; Jurczyk, S.; Nghiem, L. D.; Jesionowski, T.; Chrobok, A., Supported ionic liquid phase facilitated catalysis with lipase from Aspergillus oryzae for enhance enantiomeric resolution of racemic ibuprofen. *Environ Technol Innov* **2022,** *28*, 102936. https://doi.org/10.1016/j.eti.2022.102936.

85. Zenner, J.; Moos, G.; Luska, K. L.; Bordet, A.; Leitner, W., Rh NPs Immobilized on Phosphonium- based Supported Ionic Liquid Phases (Rh@SILPs) as Hydrogenation Catalysts. *CHIMIA* **2021,** *75* (9), 724-732. https://doi.org/10.2533/chimia.2021.724.

86. Kukawka, R.; Pawlowska-Zygarowicz, A.; Dzialkowska, J.; Pietrowski, M.; Maciejewski, H.; Bica, K.; Smiglak, M., Highly Effective Supported Ionic Liquid-Phase (SILP) Catalysts: Characterization and Application to the Hydrosilylation Reaction. *ACS Sustain Chem Eng* **2019,** *7* (5), 4699-4706. https://doi.org/10.1021/acssuschemeng.8b04357.

87. Brun, N.; Hesemann, P.; Laurent, G.; Sanchez, C.; Birot, M.; Deleuze, H.; Backov, R., Macrocellular Pd@ionic liquid@organo-Si(HIPE) heterogeneous catalysts and their use for Heck coupling reactions. *New J Chem* **2013,** *37* (1), 157-168. https://doi.org/10.1039/C2NJ40527J.

88. Kohler, F. T. U.; Popp, S.; Klefer, H.; Eckle, I.; Schrage, C.; Böhringer, B.; Roth, D.; Haumann, M.; Wasserscheid, P., Supported ionic liquid phase (SILP) materials for removal of hazardous gas compounds – efficient and irreversible NH₃ adsorption. *Green Chem* **2014,** *16* (7), 3560-3568. https://doi.org/10.1039/C3GC42275E.

89. Kaftan, A.; Klefer, H.; Haumann, M.; Laurin, M.; Wasserscheid, P.; Libuda, J., An operando DRIFTS-MS study of NH₃ removal by supported ionic liquid phase (SILP) materials. *Sep Purif Technol* **2017,** *174*, 245-250. https://doi.org/10.1016/J.SEPPUR.2016.10.017.

90. Li, X. S.; Zhang, L. Q.; Zhou, D.; Liu, W. Q.; Zhu, X. Y.; Xu, Y. Q.; Zheng, Y.; Zheng, C. G., Elemental Mercury Capture from Flue Gas by a Supported Ionic Liquid Phase Adsorbent. *Energ Fuel* **2017,** *31* (1), 714-723. https://doi.org/10.1021/acs.energyfuels.6b01956.

91. Thomassen, P. L.; Kunov-Kruse, A. J.; Mossin, S. L.; Kolding, H.; Kegnæs, S.; Riisager, A.; Fehrmann, R., Separation of Flue Gas Components by SILP (Supported Ionic Liquid-Phase) Absorbers. *ECS Trans* **2013,** *50* (11), 433. https://doi.org/10.1149/05011.0433ecst.

92. Avdibegović, D.; Yagmurlu, B.; Dittrich, C.; Regadío, M.; Friedrich, B.; Binnemans, K., Combined multi-step precipitation and supported ionic liquid phase chromatography for the recovery of rare earths from leach solutions of bauxite residues. *Hydrometallurgy* **2018,** *180*, 229-235. https://doi.org/10.1016/j.hydromet.2018.07.023.

93. Lanaridi, O.; Sahoo, A. R.; Limbeck, A.; Naghdi, S.; Eder, D.; Eitenberger, E.; Csendes, Z.; Schnurch, M.; Bica-Schroder, K., Toward the Recovery of Platinum Group Metals from a Spent Automotive Catalyst with Supported Ionic Liquid Phases. *ACS Sustain Chem Eng* **2021,** *9* (1), 375-386. https://doi.org/10.1021/acssuschemeng.0c07384.

94. Avdibegović, D.; Binnemans, K., Separation of Scandium from Hydrochloric Acid–Ethanol Leachate of Bauxite Residue by a Supported Ionic Liquid Phase. *Ind Eng Chem Res* **2020,** *59* (34), 15332-15342. https://doi.org/10.1021/acs.iecr.0c02943.

95. Steinrück, H.-P.; Wasserscheid, P., Ionic Liquids in Catalysis. *Catal Lett* **2014,** *145* (1), 380-397. https://doi.org/10.1007/s10562-014-1435-x.

96. Migowski, P.; Lozano, P.; Dupont, J., Imidazolium based ionic liquid-phase green catalytic reactions. *Green Chem* **2023,** *25* (4), 1237-1260. https://doi.org/10.1039/d2gc04749g.

97. Bordet, A.; Moos, G.; Welsh, C.; Licence, P.; Luska, K. L.; Leitner, W., Molecular Control of the Catalytic Properties of Rhodium Nanoparticles in Supported Ionic Liquid Phase (SILP) Systems. *ACS Catal* **2020,** *10* (23), 13904-13912. https://doi.org/10.1021/acscatal.0c03559.

98. Motos-Pérez, B.; Roeser, J.; Thomas, A.; Hesemann, P., Imidazolium-functionalized SBA-15 type silica: efficient organocatalysts for Henry and cycloaddition reactions. *Appl Organomet Chem* **2013,** *27* (5), 290-299. https://doi.org/10.1002/aoc.2974.

99. Gruttadauria, M.; Liotta, L. F.; Salvo, A. M. P.; Giacalone, F.; La Parola, V.; Aprile, C.; Noto, R., Multi-Layered, Covalently Supported Ionic Liquid Phase (mlc-SILP) as Highly Cross-Linked Support for Recyclable Palladium Catalysts for the Suzuki Reaction in Aqueous Medium. *Adv Synth Catal* **2011,** *353* (11-12), 2119-2130. https://doi.org/10.1002/adsc.201100186.

100. Agrigento, P.; Al-Amsyar, S. M.; Soree, B.; Taherimehr, M.; Gruttadauria, M.; Aprile, C.; Pescarmona, P. P., Synthesis and high-throughput testing of multilayered supported ionic liquid catalysts for the conversion of CO₂ and epoxides into cyclic carbonates. *Catal Sci Technol* **2014,** *4* (6), 1598-1607. https://doi.org/10.1039/c3cy01000g.

101. Sainz Martinez, A.; Hauzenberger, C.; Sahoo, A. R.; Csendes, Z.; Hoffmann, H.; Bica, K., Continuous Conversion of Carbon Dioxide to Propylene Carbonate with Supported Ionic Liquids. *ACS Sustain Chem Eng* **2018,** *6* (10), 13131-13139. https://doi.org/10.1021/acssuschemeng.8b02627.

102. Miksovsky, P.; Horn, E. N.; Naghdi, S.; Eder, D.; Schnurch, M.; Bica-Schroder, K., Continuous Formation of Limonene Carbonates in Supercritical Carbon Dioxide. *Org Process Res Dev* **2022,** *26* (10), 2799-2810. https://doi.org/10.1021/acs.oprd.2c00143.

103. Riisager, A.; Jorgensen, B.; Wasserscheid, P.; Fehrmann, R., First application of supported ionic liquid phase (SILP) catalysis for continuous methanol carbonylation. *Chem Commun* **2006,** (9), 994-996. https://doi.org/10.1039/b516314e.

104. Luska, K. L.; Julis, J.; Stavitski, E.; Zakharov, D. N.; Adams, A.; Leitner, W., Bifunctional nanoparticle-SILP catalysts (NPs@SILP) for the selective deoxygenation of biomass substrates. *Chem Sci* **2014,** *5* (12), 4895-4905. https://doi.org/10.1039/c4sc02033b.

105. Mehnert, C. P., Supported ionic liquid catalysis. *Chemistry* **2004,** *11* (1), 50-56. https://doi.org/10.1002/chem.200400683.

106. Aprile, C.; Giacalone, F.; Agrigento, P.; Liotta, L. F.; Martens, J. A.; Pescarmona, P. P.; Gruttadauria, M., Multilayered supported ionic liquids as catalysts for chemical fixation of carbon dioxide: a high-throughput study in supercritical conditions. *ChemSusChem* **2011,** *4* (12), 1830-1837. https://doi.org/10.1002/cssc.201100446.

107. Haumann, M.; Jakuttis, M.; Franke, R.; Schonweiz, A.; Wasserscheid, P., Continuous Gas-Phase Hydroformylation of a Highly Diluted Technical C4 Feed using Supported Ionic Liquid Phase Catalysts. *ChemCatChem* **2011,** *3* (11), 1822-1827. https://doi.org/10.1002/cctc.201100117.

108. Jakuttis, M.; Schonweiz, A.; Werner, S.; Franke, R.; Wiese, K. D.; Haumann, M.; Wasserscheid, P., Rhodium-phosphite SILP catalysis for the highly selective hydroformylation of mixed C$_4$ feedstocks. *Angew Chem Int Ed* **2011,** *50* (19), 4492-4495. https://doi.org/10.1002/anie.201007164.

109. Latos, P.; Wolny, A.; Zdarta, J.; Ciesielczyk, F.; Jurczyk, S.; Jesionowski, T.; Chrobok, A., Highly stable Lewis acidic trifloaluminate ionic liquid supported on silica and metallosilicates as an efficient catalyst for continuous flow aminolysis of epoxides. *Environ Technol Innov* **2023,** *31*, 103164. https://doi.org/10.1016/j.eti.2023.103164.

110. Logemann, M.; Wolf, P.; Loipersbock, J.; Schrade, A.; Wessling, M.; Haumann, M., Ultra-low temperature water-gas shift reaction catalyzed by homogeneous Ru-complexes in a membrane reactor - membrane development and proof of concept. *Catal Sci Technol* **2021,** *11* (4), 1558-1570. https://doi.org/10.1039/d0cy02111c.

111. Akhdar, A.; Onida, K.; Vu, N. D.; Grollier, K.; Norsic, S.; Boisson, C.; D'Agosto, F.; Duguet, N., Thermomorphic Polyethylene-Supported Organocatalysts for the Valorization of Vegetable Oils and CO$_2$. *Adv Sustain Syst* **2021,** *5* (2), 2000218. https://doi.org/10.1002/adsu.202000218.

112. Lin, Y.; Wang, F.; Zhang, Z. Q.; Yang, J.; Wei, Y., Polymer-supported ionic liquids: Synthesis, characterization and application in fuel desulfurization. *Fuel* **2014,** *116*, 273-280. https://doi.org/10.1016/j.fuel.2013.08.014.

113. Werner, S.; Szesni, N.; Kaiser, M.; Fischer, R. W.; Haumann, M.; Wasserscheid, P., Ultra-Low-Temperature Water-Gas Shift Catalysis using Supported Ionic Liquid Phase (SILP) Materials. *ChemCatChem* **2010,** *2* (11), 1399-1402. https://doi.org/10.1002/cctc.201000245.

114. Bauer, T.; Stepic, R.; Wolf, P.; Kollhoff, F.; Karawacka, W.; Wick, C. R.; Haumann, M.; Wasserscheid, P.; Smith, D. M.; Smith, A.-S.; Libuda, J., Dynamic equilibria in supported ionic liquid phase (SILP) catalysis: in situ IR spectroscopy identifies [Ru(CO)$_x$Cl$_y$]$_n$ species in water gas shift catalysis. *Catal Sci Technol* **2018,** *8* (1), 344-357. https://doi.org/10.1039/c7cy02199b.

115. Gholinejad, M.; Esmailoghli, H.; Khosravi, F.; Sansano, J. M., Ionic liquid modified carbon nanotube supported palladium nanoparticles for efficient Sonogashira-Hagihara reaction. *J Organomet Chem* **2022,** *963*, 122295. https://doi.org/10.1016/j.jorganchem.2022.122295.

116. Zarnegar, Z.; Safari, J., Magnetic carbon nanotube-supported imidazolium cation-based ionic liquid as a highly stable nanocatalyst for the synthesis of 2-aminothiazoles. *Appl Organomet Chem* **2016,** *30* (12), 1043-1049. https://doi.org/10.1002/aoc.3540.

117. Zarnegar, Z.; Safari, J., Heterogenization of an imidazolium ionic liquid based on magnetic carbon nanotubes as a novel organocatalyst for the synthesis of 2-amino-chromenes via a microwave-assisted multicomponent strategy. *New J Chem* **2016,** *40* (9), 7986-7995. https://doi.org/10.1039/c6nj01631f.

118. Mayank; Billing, B. K.; Agnihotri, P. K.; Kaur, N.; Singh, N.; Jang, D. O., Ionic Liquid-Coated Carbon Nanotubes as Efficient Metal-Free Catalysts for the Synthesis of Chromene Derivatives. *ACS Sustain Chem Eng* **2018,** *6* (3), 3714-3722. https://doi.org/10.1021/acssuschemeng.7b04048.

119. Zheng, X.; Luo, S.; Zhang, L.; Cheng, J.-P., Magnetic nanoparticle supported ionic liquid catalysts for CO_2 cycloaddition reactions. *Green Chem* **2009,** *11* (4), 455-458. https://doi.org/10.1039/b823123k.

120. Sadjadi, S., Magnetic (poly) ionic liquids: A promising platform for green chemistry. *J Mol Liq* **2021,** *323*, 114994. https://doi.org/10.1016/j.molliq.2020.114994.

121. Sun, J.; Wang, J. Q.; Cheng, W. G.; Zhang, J. X.; Li, X. H.; Zhang, S. J.; She, Y. B., Chitosan functionalized ionic liquid as a recyclable biopolymer-supported catalyst for cycloaddition of CO_2. *Green Chem* **2012,** *14* (3), 654-660. https://doi.org/10.1039/c2gc16335g.

122. Noorani, N.; Mehrdad, A., CO_2 adsorption onto 1-butyl-3-vinylimidazolium based poly(ionic liquid)s: experimental and theoretical studies. *J Polym Res* **2021,** *28* (9), 346. https://doi.org/10.1007/s10965-021-02695-8.

123. Yuan, J. Y.; Antonietti, M., Poly(ionic liquid) Latexes Prepared by Dispersion Polymerization of Ionic Liquid Monomers. *Macromolecules* **2011,** *44* (4), 744-750. https://doi.org/10.1021/ma102858b.

124. Sengupta, A.; Ethirajan, S. K.; Kamaz, M.; Jebur, M.; Wickramasinghe, R., Synthesis and characterization of antibacterial poly ionic liquid membranes with tunable performance. *Sep Purif Technol* **2019,** *212*, 307-315. https://doi.org/10.1016/j.seppur.2018.11.027.

125. Kuzmicz, D.; Coupillaud, P.; Men, Y.; Vignolle, J.; Vendraminetto, G.; Ambrogi, M.; Taton, D.; Yuan, J. Y., Functional mesoporous poly(ionic liquid)-based copolymer monoliths: From synthesis to catalysis and microporous carbon production. *Polymer* **2014,** *55* (16), 3423-3430. https://doi.org/10.1016/j.polymer.2014.04.032.

126. Coupillaud, P.; Pinaud, J.; Guidolin, N.; Vignolle, J.; Fevre, M.; Veaudecrenne, E.; Mecerreyes, D.; Taton, D., Poly(ionic liquid)s Based on Imidazolium Hydrogen Carbonate Monomer Units as Recyclable Polymer-Supported N-Heterocyclic Carbenes: Use in Organocatalysis. *J Polym Sci Pol Chem* **2013,** *51* (21), 4530-4540. https://doi.org/10.1002/pola.26869.

127. Wang, X.; Zhou, Y.; Guo, Z.; Chen, G.; Li, J.; Shi, Y.; Liu, Y.; Wang, J., Heterogeneous conversion of CO_2 into cyclic carbonates at ambient pressure catalyzed by ionothermal-derived meso-macroporous hierarchical poly(ionic liquid)s. *Chem Sci* **2015,** *6* (12), 6916-6924. https://doi.org/10.1039/c5sc02050f.

128. Hemp, S. T.; Zhang, M. Q.; Allen, M. H.; Cheng, S. J.; Moore, R. B.; Long, T. E., Comparing Ammonium and Phosphonium Polymerized Ionic Liquids: Thermal Analysis, Conductivity, and Morphology. *Macromol Chem Phys* **2013,** *214* (18), 2099-2107. https://doi.org/10.1002/macp.201300322.

129. Kroon, M. C.; Peters, C. J., Supercritical Fluids in Ionic Liquids. In *Ionic Liquids Further UnCOILed*, Plechkova, N. V.; Seddon, K. R., Eds. John Wiley & Sons, Inc.: **2014**; pp 39-57. https://doi.org/10.1002/9781118839706.ch2.

130. Keskin, S.; Kayrak-Talay, D.; Akman, U.; Hortaçsu, Ö., A review of ionic liquids towards supercritical fluid applications. *J Supercrit Fluid* **2007,** *43* (1), 150-180. https://doi.org/10.1016/j.supflu.2007.05.013.

131. Blanchard, L. A.; Hancu, D.; Beckman, E. J.; Brennecke, J. F., Green processing using ionic liquids and CO_2. *Nature* **1999,** *399*, 28-29. https://doi.org/10.1038/19887.

132. Blanchard, L. A.; Gu, Z. Y.; Brennecke, J. F., High-pressure phase behavior of ionic liquid/CO_2 systems. *J Phys Chem B* **2001,** *105* (12), 2437-2444. https://doi.org/10.1021/jp003309d.

133. Aki, S. N. V. K.; Mellein, B. R.; Saurer, E. M.; Brennecke, J. F., High-pressure phase behavior of carbon dioxide with imidazolium-based ionic liquids. *J Phys Chem B* **2004,** *108* (52), 20355-20365. https://doi.org/10.1021/jp046895.

134. Shariati, A.; Peters, C. J., High-pressure phase behavior of systems with ionic liquids: II. The binary system carbon dioxide+1-ethyl-3-methylimidazolium hexafluorophosphate. *J Supercrit Fluid* **2004,** *29* (1-2), 43-48. https://doi.org/10.1016/S0896-8446(03)00032-9.

135. Blanchard, L. A.; Brennecke, J. F., Recovery of organic products from ionic liquids using supercritical carbon dioxide. *Ind Eng Chem Res* **2001,** *40* (1), 287-292. https://doi.org/10.1021/ie000710d.

136. Li, Y.; Wang, J.; Liu, X.; Zhang, S., Towards a molecular understanding of cellulose dissolution in ionic liquids: anion/cation effect, synergistic mechanism and physicochemical aspects. *Chem Sci* **2018,** *9* (17), 4027-4043. https://doi.org/10.1039/c7sc05392d.

137. Wu, W.; Zhang, J.; Han, B.; Chen, J.; Liu, Z.; Jiang, T.; He, J.; Li, W., Solubility of room-temperature ionic liquid in supercritical CO_2 with and without organic compounds. *Chem Commun* **2003,** (12), 1412-1413. https://doi.org/10.1039/b302311g.

138. Wu, W. Z.; Li, W. J.; Han, B. X.; Jiang, T.; Shen, D.; Zhang, Z. F.; Sun, D. H.; Wang, B., Effect of organic cosolvents on the solubility of ionic liquids in supercritical CO_2. *J Chem Eng Data* **2004,** *49* (6), 1597-1601. https://doi.org/10.1021/je034286+.

139. Shi, J. W.; Kang, X.; Mao, L. H.; Jiang, Y. Z.; Zhao, S. Y.; Liu, Y. B.; Zhai, B. J.; Jin, H.; Guo, L. J., Supercritical CO_2-applied equipment for chemical synthesis and transformation: Current status and perspectives. *Chem Eng J* **2023,** *459*, 141608. https://doi.org/10.1016/j.cej.2023.141608.

140. Hintermair, U.; Roosen, C.; Kaever, M.; Kronenberg, H.; Thelen, R.; Aey, S.; Leitner, W.; Greiner, L., A Versatile Lab to Pilot Scale Continuous Reaction System for Supercritical Fluid Processing. *Org Process Res Dev* **2011,** *15* (6), 1275-1280. https://doi.org/10.1021/op200053w.

141. Han, X.; Poliakoff, M., Continuous reactions in supercritical carbon dioxide: problems, solutions and possible ways forward. *Chem Soc Rev* **2012,** *41* (4), 1428-1436. https://doi.org/10.1039/c2cs15314a.

142. Theyssen, N.; Scovell, K.; Poliakoff, M., Volume 4: Supercritical Solvents. In *Green Solvents*, Anastas, P. T., Ed. **2010**; Vol. 4, pp 31-75.

143. García-Verdugo, E.; Altava, B.; Burguete, M. I.; Lozano, P.; Luis, S. V., Ionic liquids and continuous flow processes: a good marriage to design sustainable processes. *Green Chem* **2015,** *17* (5), 2693-2713. https://doi.org/10.1039/c4gc02388a.

144. Walsh, B.; Hyde, J. R.; Licence, P.; Poliakoff, M., The automation of continuous reactions in supercritical CO_2: the acid-catalysed etherification of short chain alcohols. *Green Chem* **2005,** *7* (6), 456-463. https://doi.org/10.1039/b413890b.

145. Guo, W.; Li, B.; Chi, H. J.; Jiang, Z. L.; Wei, L. Q.; Ramsey, E. D., On-line SFC-UV/Vis-MS using flow selection interfaces to monitor continuous flow single and sequential stage organic reactions in supercritical carbon dioxide. *J Supercrit Fluid* **2023,** *199*, 105957. https://doi.org/10.1016/j.supflu.2023.105957.

146. Hintermair, U.; Höfener, T.; Pullmann, T.; Franciò, G.; Leitner, W., Continuous Enantioselective Hydrogenation with a Molecular Catalyst in Supported Ionic Liquid Phase under Supercritical CO_2 Flow. *ChemCatChem* **2010,** *2* (2), 150-154. https://doi.org/10.1002/cctc.200900261.

147. Hintermair, U.; Franciò, G.; Leitner, W., A Fully Integrated Continuous-Flow System for Asymmetric Catalysis: Enantioselective Hydrogenation with Supported Ionic Liquid Phase Catalysts Using Supercritical CO_2 as the Mobile Phase. *Chem Eur J* **2013,** *19* (14), 4538-4547. https://doi.org/10.1002/chem.201204159.

148. Zhang, Z. Y.; Francio, G.; Leitner, W., Continuous-Flow Asymmetric Hydrogenation of an Enol Ester by using Supercritical Carbon Dioxide: Ionic Liquids versus Supported Ionic Liquids as the Catalyst Matrix. *ChemCatChem* **2015,** *7* (13), 1961-1965. https://doi.org/10.1002/cctc.201500295.

149. Geier, D.; Schrnitz, P.; Walkowiak, J.; Leitner, W.; Francio, G., Continuous Flow Asymmetric Hydrogenation with Supported Ionic Liquid Phase Catalysts Using Modified CO_2 as the Mobile Phase: from Model Substrate to an Active Pharmaceutical Ingredient. *ACS Catal* **2018,** *8* (4), 3297-3303. https://doi.org/10.1021/acscatal.8b00216.

150. Sans, V.; Gelat, F.; Karbass, N.; Burguete, M. I.; Garcia-Verdugo, E.; Luis, S. V., Polymer Cocktail: A Multitask Supported Ionic Liquid-Like Species to Facilitate Multiple and Consecutive C-C Coupling Reactions. *Adv Synth Catal* **2010,** *352* (17), 3013-3021. https://doi.org/10.1002/adsc.201000528.

151. Lozano, P.; De Diego, T.; Sauer, T.; Vaultier, M.; Gmouh, S.; Iborra, J. L., On the importance of the supporting Candida antarctica lipase B in material for activity of immobilized ionic liquid/hexane and ionic liquid/supercritical carbon dioxide biphasic media. *J Supercrit Fluid* **2007,** *40* (1), 93-100. https://doi.org/10.1016/j.supflu.2006.03.025.

152.   Lozano, P.; De Diego, T.; Mira, C.; Montague, K.; Vaultier, M.; Iborra, J. L., Long term continuous chemoenzymatic dynamic kinetic resolution of rac-1-phenylethanol using ionic liquids and supercritical carbon dioxide. *Green Chem* **2009,** *11* (4), 538-542. https://doi.org/10.1039/b821623a.

153.   Lozano, P.; De Diego, T.; Larnicol, M.; Vaultier, M.; Iborra, J. L., Chemoenzymatic dynamic kinetic resolution of rac-1-phenylethanol in ionic liquids and ionic liquids/supercritical carbon dioxide systems. *Biotechnol Lett* **2006,** *28* (19), 1559-65. https://doi.org/10.1007/s10529-006-9130-7.

154.   Lozano, P.; García-Verdugo, E.; Karbass, N.; Montague, K.; De Diego, T.; Burguete, M. I.; Luis, S. V., Supported Ionic Liquid-Like Phases (SILLPs) for enzymatic processes: Continuous KR and DKR in SILLP–scCO₂ systems. *Green Chem* **2010,** *12* (10), 1803-1810. https://doi.org/10.1039/c0gc00076k.

155.   Lozano, P.; García-Verdugo, E.; Piamtongkam, R.; Karbass, N.; De Diego, T.; Burguete, M. I.; Luis, S. V.; Iborra, J. L., Bioreactors Based on Monolith-Supported Ionic Liquid Phase for Enzyme Catalysis in Supercritical Carbon Dioxide. *Adv Synt Catal* **2007,** *349* (7), 1077-1084. https://doi.org/10.1002/adsc.200600554.

156.   Lozano, P.; Garcia-Verdugo, E.; Bernal, J. M.; Izquierdo, D. F.; Burguete, M. I.; Sanchez-Gomez, G.; Luis, S. V., Immobilised lipase on structured supports containing covalently attached ionic liquids for the continuous synthesis of biodiesel in scCO₂. *ChemSusChem* **2012,** *5* (4), 790-798. https://doi.org/10.1002/cssc.201100692.

157.   Villa, R.; Alvarez, E.; Nieto, S.; Donaire, A.; Garcia-Verdugo, E.; Luis, S. V.; Lozano, P., Chemo-enzymatic production of omega-3 monoacylglycerides using sponge-like ionic liquids and supercritical carbon dioxide. *Green Chem* **2020,** *22* (17), 5701-5710. https://doi.org/10.1039/d0gc02033h.

158.   Perussello, C. A.; Zhang, Z.; Marzocchella, A.; Tiwari, B. K., Valorization of Apple Pomace by Extraction of Valuable Compounds. *Compr Rev Food Sci Food Saf* **2017,** *16* (5), 776-796. https://doi.org/10.1111/1541-4337.12290.

159.   Kamphuis, A. J.; Picchioni, F.; Pescarmona, P. P., CO₂-fixation into cyclic and polymeric carbonates: principles and applications. *Green Chem* **2019,** *21* (3), 406-448. https://doi.org/10.1039/c8gc03086c.

160.   Stadler, B. M.; Wulf, C.; Werner, T.; Tin, S.; de Vries, J. G., Catalytic Approaches to Monomers for Polymers Based on Renewables. *ACS Catal* **2019,** *9* (9), 8012-8067. https://doi.org/10.1021/acscatal.9b01665.

161.   360ResearchReports Global Limonene Market Research Report 2020. https://www.360researchreports.com/global-limonene-market-15061488 (accessed 08/2023).

162.   Fiorani, G.; Stuck, M.; Martin, C.; Belmonte, M. M.; Martin, E.; Escudero-Adan, E. C.; Kleij, A. W., Catalytic Coupling of Carbon Dioxide with Terpene Scaffolds: Access to Challenging Bio-Based Organic Carbonates. *ChemSusChem* **2016,** *9* (11), 1304-1311. https://doi.org/10.1002/cssc.201600238.

163.   Navarro, M.; Sanchez-Barba, L. F.; Garces, A.; Fernandez-Baeza, J.; Fernandez, I.; Lara-Sanchez, A.; Rodriguez, A. M., Bimetallic scorpionate-based helical organoaluminum complexes for efficient carbon dioxide fixation into a variety of cyclic carbonates. *Catal Sci Technol* **2020,** *10* (10), 3265-3278. https://doi.org/10.1039/d0cy00593b.

164.   Martinez, J.; Fernandez-Baeza, J.; Sanchez-Barba, L. F.; Castro-Osma, J. A.; Lara-Sanchez, A.; Otero, A., An Efficient and Versatile Lanthanum Heteroscorpionate Catalyst for Carbon Dioxide Fixation into Cyclic Carbonates. *ChemSusChem* **2017,** *10* (14), 2886-2890. https://doi.org/10.1002/cssc.201700898.

165.   Kamphuis, A. J.; Milocco, F.; Koiter, L.; Pescarmona, P. P.; Otten, E., Highly Selective Single-Component Formazanate Ferrate(II) Catalysts for the Conversion of CO₂ into Cyclic Carbonates. *ChemSusChem* **2019,** *12* (15), 3635-3641. https://doi.org/10.1002/cssc.201900740.

166.   Li, C. Y.; Su, Y. C.; Lin, C. H.; Huang, H. Y.; Tsai, C. Y.; Lee, T. Y.; Ko, B. T., Synthesis and characterization of trimetallic cobalt, zinc and nickel complexes containing amine-bis(benzotriazole phenolate) ligands: efficient catalysts for coupling of carbon dioxide with epoxides. *Dalton Trans* **2017,** *46* (44), 15399-15406. https://doi.org/10.1039/c7dt02841e.

167.   Aomchad, V.; Cristofol, A.; Della Monica, F.; Limburg, B.; D'Elia, V.; Kleij, A. W., Recent progress in the catalytic transformation of carbon dioxide into biosourced organic carbonates. *Green Chem* **2021,** *23* (3), 1077-1113. https://doi.org/10.1039/d0gc03824e.

168.   Hu, Y. Y.; Steinbauer, J.; Stefanow, V.; Spannenberg, A.; Werner, T., Polyethers as Complexing Agents in Calcium-Catalyzed Cyclic Carbonate Synthesis. *ACS Sustain Chem Eng* **2019,** *7* (15), 13257-13269. https://doi.org/10.1021/acssuschemeng.9b02502.

169.   Longwitz, L.; Steinhauer, J.; Spannenberg, A.; Werner, T., Calcium-Based Catalytic System for the Synthesis of Bio-Derived Cyclic Carbonates under Mild Conditions. *ACS Catal* **2018,** *8* (1), 665-672. https://doi.org/10.1021/acscatal.7b03367.

170.   Aomchad, V.; Gobbo, S. D.; Yingcharoen, P.; Poater, A.; D'Elia, V., Exploring the potential of group III salen complexes for the conversion of CO_2 under ambient conditions. *Catal Today* **2021,** *375*, 324-334. https://doi.org/10.1016/j.cattod.2020.01.021.

171.   Sopeña, S.; Laserna, V.; Guo, W.; Martin, E.; Escudero-Adán, E. C.; Kleij, A. W., Regioselective Organocatalytic Formation of Carbamates from Substituted Cyclic Carbonates. *Adv Synth Catal* **2016,** *358* (13), 2172-2178. https://doi.org/10.1002/adsc.201600290.

172.   Morikawa, H.; Minamoto, M.; Gorou, Y.; Yamaguchi, J.; Morinaga, H.; Motokucho, S., Two Diastereomers of d-Limonene-Derived Cyclic Carbonates from d-Limonene Oxide and Carbon Dioxide with a Tetrabutylammonium Chloride Catalyst. *B Chem Soc Jpn* **2018,** *91* (1), 92-94. https://doi.org/10.1246/bcsj.20170300.

173.   Morikawa, H.; Yamaguchi, J. I.; Sugimura, S. I.; Minamoto, M.; Gorou, Y.; Morinaga, H.; Motokucho, S., Systematic synthetic study of four diastereomerically distinct limonene-1,2-diols and their corresponding cyclic carbonates. *Beilstein J Org Chem* **2019,** *15*, 130-136. https://doi.org/10.3762/bjoc.15.13.

174.   Bähr, M.; Bitto, A.; Mülhaupt, R., Cyclic limonene dicarbonate as a new monomer for non-isocyanate oligo- and polyurethanes (NIPU) based upon terpenes. *Green Chem* **2012,** *14* (5), 1447-1454. https://doi.org/10.1039/C2GC35099H.

175.   Schimpf, V.; Ritter, B. S.; Weis, P.; Parison, K.; Mulhaupt, R., High Purity Limonene Dicarbonate as Versatile Building Block for Sustainable Non-Isocyanate Polyhydroxyurethane Thermosets and Thermoplastics. *Macromolecules* **2017,** *50* (3), 944-955. https://doi.org/10.1021/acs.macromol.6b02460.

176.   Maltby, K. A.; Hutchby, M.; Plucinski, P.; Davidson, M. G.; Hintermair, U., Selective Catalytic Synthesis of 1,2- and 8,9-Cyclic Limonene Carbonates as Versatile Building Blocks for Novel Hydroxyurethanes. *Chem Eur J* **2020,** *26* (33), 7405-7415. https://doi.org/10.1002/chem.201905561.

177.   Centeno-Pedrazo, A.; Perez-Arce, J.; Freixa, Z.; Ortiz, P.; Garcia-Suarez, E. J., Catalytic Systems for the Effective Fixation of CO_2 into Epoxidized Vegetable Oils and Derivates to Obtain Biobased Cyclic Carbonates as Precursors for Greener Polymers. *Ind Eng Chem Res* **2023,** *62* (8), 3428-3443. https://doi.org/10.1021/acs.iecr.2c03747.

178.   Laprise, C. M.; Hawboldt, K. A.; Kerton, F. M.; Kozak, C. M., Synthesis of a Renewable, Waste-Derived Nonisocyanate Polyurethane from Fish Processing Discards and Cashew Nutshell-Derived Amines. *Macromol Rapid Commun* **2021,** *42* (3), 2000339. https://doi.org/10.1002/marc.202000339.

179.   Bähr, M.; Mülhaupt, R., Linseed and soybean oil-based polyurethanes prepared via the non-isocyanate route and catalytic carbon dioxide conversion. *Green Chem* **2012,** *14* (2), 483-489. https://doi.org/10.1039/C2GC16230J.

180.   Cai, X.; Tolvanen, P.; Virtanen, P.; Eränen, K.; Rahkila, J.; Leveneur, S.; Salmi, T., Kinetic study of the carbonation of epoxidized fatty acid methyl ester catalyzed over heterogeneous catalyst HBimCl-NbCl5/HCMC. *Int J Chem Kinet* **2021,** *53* (11), 1203-1219. https://doi.org/10.1002/kin.21526.

181.   Schaffner, B.; Blug, M.; Kruse, D.; Polyakov, M.; Kockritz, A.; Martin, A.; Rajagopalan, P.; Bentrup, U.; Bruckner, A.; Jung, S.; Agar, D.; Rungeler, B.; Pfennig, A.; Muller, K.; Arlt, W.; Woldt, B.; Grass, M.; Buchholz, S., Synthesis and application of carbonated fatty acid esters from carbon dioxide including a life cycle analysis. *ChemSusChem* **2014,** *7* (4), 1133-1139. https://doi.org/10.1002/cssc.201301115.

182.   Perez-Sena, W. Y.; Eränen, K.; Kumar, N.; Estel, L.; Leveneur, S.; Salmi, T., New insights into the cocatalyst-free carbonation of vegetable oil derivatives using heterogeneous catalysts. *J CO2 Util* **2022,** *57*, 101879. https://doi.org/10.1016/j.jcou.2021.101879.

183.   Colombo, P.; Mera, G.; Riedel, R.; Sorarù, G. D., Polymer-Derived Ceramics: 40 Years of Research and Innovation in Advanced Ceramics. *J Am Ceram Soc* **2010,** *93* (7), 1805-1837. https://doi.org/10.1111/j.1551-2916.2010.03876.x.

184.   Obmann, R.; Schörpf, S.; Gorsche, C.; Liska, R.; Fey, T.; Konegger, T., Porous polysilazane-derived ceramic structures generated through photopolymerization-assisted solidification templating. *J Eur Ceram Soc* **2019,** *39* (4), 838-845. https://doi.org/10.1016/j.jeurceramsoc.2018.11.045.

185.   Mikl, G.; Obmann, R.; Schorpf, S.; Liska, R.; Konegger, T., Pore Morphology Tailoring in Polymer-Derived Ceramics Generated through Photopolymerization-Assisted Solidification Templating. *Adv Eng Mater* **2019,** *21* (6), 1900052. https://doi.org/10.1002/adem.201900052.

186.   Kornpointner, C.; Scheibelreiter, J.; Halbwirth, H., Snailase: A Promising Tool for the Enzymatic Hydrolysis of Flavonoid Glycosides From Plant Extracts. *Front Plant Sci* **2022,** *13*, 889184. https://doi.org/10.3389/fpls.2022.889184.